



NANOPARTICULATE OF SILVER-MODIFIED POLY(8-ANILINO-1-NAPHTHALENE SULPHONIC ACID) NANOBIOSENSOR SYSTEMS FOR THE DETERMINATION OF TUBERCULOSIS TREATMENT DRUGS

By

RACHEL FANELWA NGECE

MSc (*Cum laude*)

A thesis Submitted in fulfillment of the requirement for the Degree of

Doctor Philosophiae in Chemistry

University of the Western Cape

Supervisor

Prof. Emmanuel I. Iwuoha

Co-supervisor

Prof. Priscilla G. L. Baker

DATE SUBMITTED: JUNE 2011

Abstract:

Tuberculosis (TB) is a disease that results from infection by *Mycobacterium tuberculosis* which is the most common infecting organism. The Directly Observed Treatment Short Course (DOTS) regime which is a combination of the drugs (isoniazid, ethambutol, pyrazinamide and rifampicin) has contributed significantly towards the decrease in the number of incidences of this disease. However, incomplete implementation of the DOTS campaign has been a major cause of the high occurrences of the drug resistant strains of *Mycobacterium tuberculosis* coupled with the spread of HIV/Aids in tuberculosis-endemic regions. This results from the fact that fully susceptible tuberculosis develops secondary resistance during therapy due to inappropriate dosing of treatment, inadequate treatment, non-adherence to the prescribed regimen or using low quality medication. A fast and reliable detection method, such as biosensing, for the determination of the TB drugs metabolic profile is, therefore, essential for the appropriate dosing of these drugs. In this thesis, nanobiosensors for the determination of the biotransformation of TB drugs were developed with cytochrome P450-2E1 (CYP2E1) isoenzyme electrodeposited on gold electrodes derivatised with silver nanoparticulate/poly(8-anilino-1-naphthalene sulphonic acid) (PVP-AgNPs/PANSA). This study firstly reports the development and characterization of PVP-AgNPs, PANSA and PVP-AgNPs/PANSA nanocomposite on gold. AFM and TEM analyses revealed highly electroactive nanocomposites whose morphology and properties were essential for the immobilization of CYP2E1. Secondly, the development and characterization of Au/PVP-AgNPs/PANSA/CYP2E1, Au/PVP-AgNPs/PANSA/SA-CYP2E1 and Au/PVP-AgNPs/PANSA/EG-CYP2E1 nanobiosensors are reported. AFM studies displayed globular morphologies with large roughness for the enzyme modified electrodes as opposed to those electrodes without enzymes. Finally, the biotransformation of standard solutions of TB drugs (isoniazid, ethambutol, pyrazinamide and rifampicin) in pH 7.4, 0.1 M phosphate buffer

solution is reported. The biotransformations of the TB drugs were successfully studied using cyclic voltammetry (CV), square wave voltammetry (SWV), differential voltammetry (DPV) and steady state amperometry under aerobic conditions. Very good detection limits were obtained for the standard solutions of TB drugs and were found to be in the micromolar range. The detection limit values for the individual TB drugs were 0.55 μM (isoniazid), 0.7 μM (ethambutol), 0.054 μM (pyrazinamide) and 0.05 μM (rifampicin). The detection limit results showed that the nanobiosensors were more sensitive and suitable for the determination of the respective drugs in plasma and serum.



Keywords:

Tuberculosis

DOTS regime

Mycobacterium tuberculosis

Isoniazid

Ethambutol

Pyrazinamide

Rifampicin

Poly(8-anilino-1-naphthalene sulphonic acid)

Silver nanoparticles

Cytochrome P450-2E1



Declaration:

I declare that

**‘Nanoparticulate of silver-modified poly(8-anilino-1-naphthalene sulphonic acid)
nanobiosensor systems for the determination of Tuberculosis treatment drugs’**

is my own work, that it has not been submitted for any degree or examination in any other

university and that all the resources I have used or quoted have been indicated and

acknowledged by means of complete references.



Rachel Fanelwa Ngece

Signed: _____

Acknowledgements:

I thank God Almighty for giving me the strength and resilience to complete this work.

To my **Supervisors and Mentors**; Prof. Emmanuel Iwuoha, Prof. Priscilla Baker Dr Mangaka Matoetoe and Dr Nazeem Jahed. Thank you so much for all your encouragements, support and always believing in my abilities to complete this work.

I thank my **Colleagues**; Prof. Green, Prof. Ameer, Prof. Mabusela, Prof. Petrik, Dr Onani, Dr Wallace, Dr Titinchi, Mr Mohammad, Mr Timothy Lesch, Mr Bongani Makhoba, Mr Andile Mantyi, Mr Benjamin de Wet and Mrs Jackson for always creating a positive atmosphere at the Chemistry Department and always motivating me to complete this study.

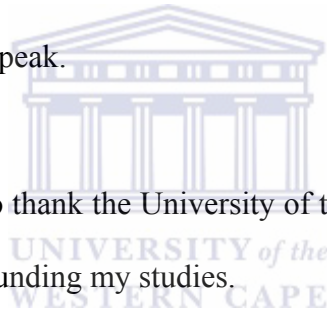
SensorLab Research group colleagues; Dr Faiza Jan Iftikhar, Dr Tesfaye Waryo, Dr Jasmina Martinovic, Dr Zelo Mangombo, Peter Ndangili, Stephen Mailu, Abogile Jijana, Euodia Hess, Godfrey Fuku, Vivian van Wyk, Rasaq Wale Olowu, Nicolette Hendricks, Abdu Baleg, Chinwe Ikpo, Njagi Njomo, Masikini Milua, Lundi Ngqongwa, Nolubabalo Matinise, Khumo Maiko, Busiswa Matyholo, Khotso Tlhomelang, Chandre Willemse, Natasha West, Noluthando Mayedwa, Sibusiso Qweshu, Mawethu Bilibana, Abebaw Tsegaye, Heidi Richards, Gcineka Mbambisa, Kereleng Molapo, Robert Siebritz and Ismarelda Fillis. I appreciate all the contribution and assistance you have made in my work. Thank you very much for always being available to me and creating a positive working environment.

Family: I am very grateful to my mother, siblings and the extended family for the continued support and believing in me throughout my studies. Ndiyabulela ngako konkhe. Olumide and Sherry Ajayi, thank you for always caring for me and my family. Thank you to my beloved

husband Olagoke for standing by me throughout this journey. I appreciate the love and support you have given to me. I am very grateful for always encouraging me and believing in my abilities and also understanding the long hours spent in the laboratory. To my baby girl Olufunmilola, thank you for being you and making me a better person. I promise to spend more time with you. Uyakuthanda umama.

Friends: Busiwa Dyan, Nothando Mungwe, Zukelwa Lothe, Babalwa Chikwendu, Nosipho Obikezi, Nyameka Ojugo, Phumeza Thomson, Anothando Daniso, S'bongile Botha, Kagiso Keatimilwe, Dr Sarah Maoela, Dr Munkombwe Muchindu, Clive Mketsu, Dr Joseph Owino, Dr Siphon Mavundla and Dr Omotayo Arotiba. Thank you for motivating me and just making me happy everytime we meet or speak.

Sponsorship: I would also like to thank the University of the Western Cape and the National Research Foundation (NRF) for funding my studies.



Dedication:

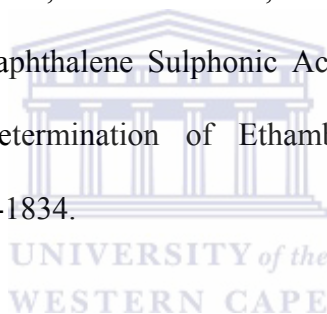
This work is dedicated to my **mother** Nomawaka Rona Ngece and my late **father** Malayipheli Jackson Sojada; **my parents' in-laws** Solomon and Olayinka Ajayi; my **siblings**, Bradley Mawandiswa Ngece, Thuliswa Irene Ngece, Anele Annabell Ngece and my **husband and daughter**; Olagoke Akinfemi Ajayi and Olufunmilola Ongezwa Ajayi.



List of Publications:

Rachel Ngece, Nicolette Hendricks, Natasha West, Peter M. Ndangili, Abongile Jijana, Stephen Mailu, Tesfaye Waryo, Priscilla Baker, Emmanuel Iwuoha. A silver nanoparticles-poly(8-anilino-1-naphthalene sulphonic acid) bioelectrochemical sensor system for the analytical determination of ethambutol, In V. Rajendra, B. Hillbrands, P. Prabu and K.E. Geckeler (eds.): *Biomedical Applications of Nanostructured Materials*, Macmillan Publishers India Limited, 2010, Pages 269-274.

Rachel F Ngece, Natasha West, Peter M Ndangili, Rasaan Olowu, Avril Williams, Nicolette Hendricks, Stephen Mailu, Priscilla Baker, Emmanuel Iwuoha (2011) ‘A silver Nanoparticle/Poly(8-Anilino-1-Naphthalene Sulphonic Acid) Bioelectrochemical Biosensor System for the Analytical Determination of Ethambutol’ *International Journal of Electrochemical Science*, 6, 1820-1834.



T. T. Waryo, E. A. Songa, M. C. Matoetoe, **R. F. Ngece**, M. Muchindu, P. M. Ndangili, A. Al-Ahmed, N. M. Jahed, P. G.L. Baker, E. I. Iwuoha. Functionalisation of polyaniline nanomaterials for amperometric biosensing: In Yogeswaran Umasankar; S. Ashok Kumar; Shen-Ming Chen (Eds). *Nanostructured Materials for Electrochemical Biosensors* Nova Science Publishers, Inc. Hauppauge, New Jersey, USA, 2009, Chapter 2, pp. 39-63.

TABLE OF CONTENTS

NANOPARTICULATE OF SILVER-MODIFIED POLY(8-ANILINO-1-NAPHTHALENE SULPHONIC ACID) NANOBIOSENSOR SYSTEMS FOR THE DETERMINATION OF TUBERCULOSIS TREATMENT DRUGS

ABSTRACT	ii
KEYWORDS	iv
DECLARATION	v
ACKNOWLEDGMENTS	vi
DEDICATION	viv
LIST OF PUBLICATIONS	ix
TABLE OF CONTENTS	x
List of Abbreviations	xvii
List of Tables	xix
List of Figures	xx
List of Schemes	xxiv



CHAPTER 1: Introduction	1
<i>Summary</i>	1
1.1 Background	2
1.2 Research Aims	6
1.3 Rationale and Motivation	7
1.4 Thesis Layout	8
1.5 References	9
CHAPTER 2: Literature Review	12
<i>Summary</i>	12
2.1 Biosensors	13

2.1.1	Biocomponents	14
	2.1.1.1 Enzymes	18
	2.1.1.2 Characteristics of Immobilised Enzymes	18
2.2	Transducers	20
	2.2.1 Optical biosensors	21
	2.2.2 Resonant biosensors	21
	2.2.3 Ion-selective biosensors	21
	2.2.4 Thermal biosensors	22
	2.2.5 Electrochemical biosensors	22
	2.2.5.1 Conductimetric electrochemical biosensors	23
	2.2.5.2 Amperometric electrochemical biosensors	23
	2.2.5.3 Potentiometric electrochemical biosensors	24
2.3	Cytochrome P450 Enzymes	25
	2.3.1 Occurrences of P450 enzymes	25
	2.3.2 Kinetic reactions of Cytochrome P450 enzymes	25
	2.3.3 Kinetics of Catalytic Reactions	27
	2.3.4 Classification of Cytochrome P450 enzymes	29
	2.3.5 Cytochrome P450-2E1 (CYP 2E1)	30
2.4	Application of Cytochrome P450 enzymes in biosensors	32
2.5	Enzyme Kinetics	36
	2.5.1 Enzyme Inhibition	39
	2.5.1.1 Reversible Inhibition	39
	2.5.1.2 Irreversible Inhibition	43
2.6	Metal nanoparticles and Conducting polymers in biosensors	43
	2.6.1 Silver nanoparticles	45

2.6.2 Gold nanoparticles	46
2.6.3 Copper nanoparticles	47
2.6.4 Polymers	49
2.6.4.1 Conducting polymers	49
2.6.4.2 Synthesis of conducting polymers	50
2.6.6 Types of conducting polymers	52
2.6.6.1 Polyaniline	52
2.6.6.2 Polypyrrole	53
2.6.6.3 Polyindole	54
2.6.6.4 Polycarbozole	55
2.6.6.5 Poly(8-anilino-1-naphthalene sulphonic acid)	56
2.7 Tuberculosis	57
2.7.1 The bacterial cell	57
2.7.2 Principles of Anti-tuberculous Therapy	59
2.7.3 Isoniazid	63
2.7.3.1 Mechanism of action and basis of resistance	63
2.7.3.2 Pharmacokinetics	64
2.7.3.3 Clinical uses	65
2.7.3.4 Adverse Reactions	65
2.7.3.5 Allergic Reactions	66
2.7.3.6 Direct Toxicity	66
2.7.4 Rifampicin	67
2.7.4.1 Mechanism of action and basis of resistance	67
2.7.4.2 Mycobacterial Infections	68
2.7.4.3 Other Indications	68

2.7.4.4 Adverse Reactions	69
2.7.5 Ethambutol	69
2.7.5.1 Mechanism of action and basis of resistance	69
2.7.5.2 Clinical used	71
2.7.5.3 Adverse Reactions	71
2.7.6 Pyrazinamide	71
2.7.6.1 Clinical used	71
2.7.6.2 Adverse Reactions	71
2.8 Detection of Tuberculosis treatment drugs	72
2.9 Electrochemical techniques	73
2.9.1 Sweep techniques	76
2.9.2 Pulse voltammetry	79
2.9.3 Square wave voltammetry (SWV)	80
2.9.4 Electrochemical Impedance Spectroscopy (EIS)	82
2.10 Other characterization techniques	84
2.10.1 Ultraviolet Visible Spectroscopy (UV/Vis)	84
2.10.2 Transmission Electron Microscopy (TEM)	88
2.10.3 Atomic Force Microscopy (AFM)	89
2.11 References	90
CHAPTER 3: Experimental Method	99
<i>Summary</i>	99
3.1 Reagents	100
3.2 Apparatus and measurements	102
3.3 Synthesis of Silver nanoparticles (PVP-AgNPs)	103

3.4 Synthesis of Poly(8-anilino-1-naphthalene sulphonic acid)	104
3.5 Preparation of Au/PANSA/PVP-AgNPs/CYP2E1 nanobiosensor	104
3.5.1 Modification of CYP2E1	104
3.5.2 Preparation of Au/PANSA/PVP-AgNP/CYP 2E1 nanobiosensors	105
3.5.3 Application of PANSA/PVP-AgNP/CYP2E1 modified gold electrodes as Amperometric TB drug nanobiosensors	105
3.6 Stability, reproducibility and interference studies	106
 CHAPTER 4: Results and Discussion. Part One	 107
<i>Summary</i>	107
4.1 Morphology characterization of PANSA, PVP-AgNPs and PANSA/PVP-AgNPs	108
4.1.1 PVP-AgNPs	108
4.1.2 PANSA	112
4.1.3 PANSA/PVP-AgNPs	115
4.1.4 EIS analysis	118
4.1.4.1 Nyquist plot characterization	118
4.1.4.2 Bode plot characterization	120
4.1.4.3 AFM analysis	123
4.2. CV characterization of PANSA	126
4.3 CV characterization of PVP-AgNP and PANSA/PVP-AgNPs	134
4.4 References	138
 CHAPTER 5: Results and Discussion: Part Two	 140
<i>Summary</i>	139
5.1 Morphology characterization of PANSA/PVP-AgNPs/CYP2E1 nanobioelectrode	141

5.1.1 TEM analysis	141
5.1.2 Uv-Visible spectroscopic analysis	143
5.1.3 EIS analysis	145
5.1.3.1 Nyquist plot characterization	145
5.1.3.2 Bode plot characterization	146
5.1.3.3 AFM analysis	149
5.1.4 Amperometric characterization of PANSA/PVP-AgNPs/CYP2E1 Nanobioelectrode	151
5.2 References	160
CHAPTER 6: Results and Discussion: Part Three	163
<i>Summary</i>	163
6.1 PANSA/PVP-AgNPs -mediated electrocatalytic reduction of TB drugs	164
6.1.1 Electrocatalytic reduction of Isoniazid and Ethambutol using PANSA/PVP- AgNPs/CYP2E1 nanobiosensors	165
6.1.1.1 Electrocatalytic reduction of Ethambutol (ETH)	165
6.1.1.2 Electrocatalytic reduction of Isoniazid (INH)	173
6.1.1.3 Electrocatalytic reduction of Pyrazinamide (PYR)	178
6.1.1.4 Electrocatalytic reduction of Rifampicin (RIF)	183
6.2 Stability and reproducibility of the modified electrode	189
6.3 Interference studies of the modified electrode	190
6.4 References	191
Chapter 7: Conclusions and Recommendations	193
<i>Summary</i>	193

7.1 Conclusions	193
7.2 Recommendations for future work	194



List of Abbreviations:

AFM	- Atomic Force Microscopy
CO ₂	- Carbon Dioxide
CV	- Cyclic Voltammetry
CYP101	- Cytochrome P450, family 1, subfamily O, polypeptide 1
CYP102	- Cytochrome P450, family 1, subfamily O, polypeptide 2
CYP2B4	- Cytochrome P450, family 2, subfamily B, polypeptide 4
CYP2D6	- Cytochrome P450, family 2, subfamily D, polypeptide 6
CYP2E1	- Cytochrome P450, family 2, subfamily E, polypeptide 1
CYP3A4	- Cytochrome P450, family 3, subfamily A, polypeptide 4
DAB-BSA	- 3,3'-Diaminobenzidine/Bovine Serum Albumin
DDAB	- Didodecyldimethylammonium bromide
DOTS	- Directly Observed Treatment Short Course
DNA	- Deoxyribonucleic acid
DPV	- Differential Pulse Voltammetry
DDT	- 1-Dodecanethiol
EDX	- Energy Dispersive X-ray Spectrum
EIS	- Electrochemical Impedance Spectroscopy
EG-NHS	- Ethylene glycol bis (succinic acid N-hydroxysuccinimide ester)
ENFET	- Enzyme Field Effect Transistors
ETH	- Ethambutol
FAD	- Flavoadenine
FET	- Field Effect Transistors
FFTCCV	- Fast Fourier Transformation Continuous Cyclic Voltammetry
H ₂ O ₂	- Hydrogen Peroxide
HIV/Aids	- Human Immunodeficiency Virus/Acquired Immunodeficiency Syndrome
HRP	- Horseradish Peroxidase
LiCl ₄	- Lithium Perchlorate
INH	- Isoniazid
MDR-TB	- Multidrug Resistant Tuberculosis
NADH	- Nicotinamide Adenine Dinucleotide
NADPH	- Nicotinamide Adenine Dinucleotide Phosphate

NCE	- Sodium Calcium Exchanger
NPV	- Normal Pulse Voltammetry
O ₂	- Oxygen
PANI	- Polyaniline
PANSA	- Poly (8-anilino-1-naphthalene sulphonic acid)
PCZ	- Polycarbazole
PND	- Polyindole
PPY-	- Polypyrrole
PVP-AgNPs/PANSA	- Silver nanoparticulate/Poly (8-anilino-1-naphthalene sulphonic acid)
PYR	- Pyrazinamide
RIF	- Rifampicin
SA-NHS	- Suberic acid (N-hydroxysuccinimideester)
SCE	- Standard Calomel Electrode
SFET	- Ion Selective Field Effect Transistors
TEM	- Transmission Electron Microscopy
TB	- Tuberculosis
TYR	- Tyrosinase
UV-vis	- Ultraviolet Visible Spectroscopy
XRD-TB	- Extensively Drug Resistant Tuberculosis

List of Tables:

Table 2.1: Conventional Immobilization methods.

Table 2.2: Some tissues used in biosensor construction and their respective analytes.

Table 2.3: Biological components and transduction methods used in biosensor design.

Table 2.4: Substrates, inducers and inhibitors of CYP 2E1.

Table 2.5: List of CYP biosensors based on direct transfer.

Table 2.6: List of CYP biosensors based on mediated direct transfer.

Table 2.7: List of first and second-line anti-microbials used in the treatment of tuberculosis.

Table 4.1: EIS parameters attained from the circuit fitting of plots in Figure 4.15 for bare Au, PANSA, PVP-AgNPs and PANSA/PVP-AgNP modified Au electrode.

Table 4.2: Results for time constant, exchange current and homogeneous rate constant for bare Au, PANSA, PVP-AgNPs and PANSA/PVP-AgNPs modified Au electrode.

Table 5.1: EIS parameters attained from the circuit fitting of plots in Figure 4.15 for PANSA, PVP-AgNPs and PANSA/PVP-AgNPs and PANSA/PVP-AgNPs/CY2E1 modified Au electrode.

Table 5.2: Results for time constant, exchange current and homogeneous rate constant bare PANSA, PVP-AgNPs and PANSA/PVP-AgNPs and PANSA/PVP-AgNPs/CYP2E1 modified Au electrode

Table 6.1: Compounds and their respective nanobiosensor analyses

List of Figures:

Figure 2.1: Components of a biosensor.

Figure 2.2: Distal face of CYP2E1 rainbow coloured N terminus (blue) to C terminus (red) showing the active site of CYP2E1.

Figure 2.3: Illustration of Michaelis - Menten Kinetics.

Figure 2.4: Illustration of Competitive and Non-Competitive Inhibition.

Figure 2.5: Structure of Polyaniline.

Figure 2.6: Structure of Polypyrrole.

Figure 2.7: Structure of Polyindole.

Figure 2.8: Structure of Polycarbozole.

Figure 2.9: Structure of Poly(8-anilino-1-naphthalene sulphonic acid).

Figure 2.10: Structures of (A) bacterial cells and (B) animal.

Figure 2.11: Structure of Isoniazid.

Figure 2.12: Structure of Rifampicin.

Figure 2.13: Structure of Ethambutol.

Figure 2.14: structure of Pyrazinamide.

Figure 2.15: Linear sweep voltammogram for the reduction $O + ne^- \rightarrow R$ at a solid electrode shown as a function of the scan rate.

Figure 2.16: Schematic cyclic voltammogram for the reduction of an analyte at a solid electrode.

Figure 2.17: Potential wave form for Normal and Differential Pulse Voltammetry.

Figure 2.18: Potential wave form for Square Wave Voltammetry.

Figure 2.19: An electrified interface in which the electrode is negatively charged and where counter anions are aligned along the surface. Below that are the electrical circuit corresponding to each interface component.

Figure 2.20: Illustration of how a UV-vis spectrometer functions.

Figure 2.21: (A) Schematic presentation of transmission electron microscope (TEM) and (b) An example of a TEM image.

Figure 2.22: (A) An illustration of AFM probing a sample surface with a sharp tip (B) An example off an AFM image showing sharp, randomly-orientated peaks.

Figure 4.1: TEM images (A) indicating spherical and polydispersed PVP-AgNPs (B) Layer by layer orientation of some nanoparticles.

Figure 4.2: Energy dispersive X-ray spectrum of PVP-AgNPs.

Figure 4.3: UV-vis spectrum of silver nanoparticles.

Figure 4.4: TEM image of PANSA.

Figure 4.5: Energy dispersive X-ray spectrum of PANSA.

Figure 4.6: SEM image of electropolymerized PANSA.

Figure 4.7: UV-vis spectrum of PANSA.

Figure 4.8: TEM image of PANSA/PVP-AgNPs nanocomposite.

Figure 4.9: Energy dispersive X-ray spectrum of PANSA/PVP-AgNPs.

Figure 4.10: UV-vis spectrum of PANSA/PVP-AgNPs.

Figure 4.11: EIS Nyquist plot of bare, PANSA, PVP-AgNPs and PANSA/PVP-AgNPs.

Figure 4.12: Bode plot of bare, PANSA, PVP-AgNPs and PANSA/PVP-AgNPs.

Figure 4.13: AFM images of (A) bare SPAuE (B) SPAuE/PVP-AgNPs (C) SPAuE/PANSA (D) SPAuE/PANSA/PVP-AgNPs.

Figure 4.14: Cyclic voltammograms of (A) electrochemical synthesis of PANSA at 50 mV/s and (B) electrochemical behaviour of (C) square wave voltammogram of Au/ PANSA electrode in 0.5 M H₂SO₄ at different scan rates.

Figure 4.15: Plot of log scan rate versus log current.

Figure 4.16: (A) CVs of Au/PVP-AgNPs electrodes, (B) CVs of Au/PANSA/PVP-AgNPs and (C) square wave voltammograms of Au/PANSA/PVP-AgNPs at different scan rates in pH 7.4, 0.1 M phosphate buffer.

Figure 5.1: TEM images of (A) PANSA/PVP-AgNPs/CYP2E1 (B) PANSA/PVP-AgNPs/EG-CYP2E1 and (C) PANSA/PVP-AgNPs/SA-CYP2E1.

Figure 5.2: Energy dispersive X-ray spectrum of PANSA/PVP-AgNPs/CYP2E1.

Figure 5.3: UV - visible spectra of (A) CYP2E1 (B) PVP-AgNPs/ CYP2E1 (C) PANSA/PVP-AgNPs composite and (D) PANSA/PVP-AgNPs/CYP2E1.

Figure 5.4: Nyquist plots of PANSA, PVP-AgNPs, and PANSA/PVP-AgNP composite and PANSA/PVP-AgNPs/CYP2E1 nanobiosensors.

Figure 5.5: Bode plots of PANSA, PVP-AgNPs, and PANSA/PVP-AgNP composite and PANSA/PVP-AgNPs/CYP2E1 nanobiosensors.

Figure 5.6: 1D and 3D AFM images of (A) SPAuE/PANSA/PVP-AgNPs and (B) SPAuE/PANSA/PVP-AgNPs/CYP2E1.

Figure 5.7: CV characterization of (A) PANSA/PVP-AgNPs/CYP2E1, PANSA/PVP-AgNPs/EG-CYP2E1 and (C) PANSA/PVP-AgNPs/SA-CYP2E1 in pH 7.4, 0.1M phosphate buffer at 10, 20, 30, 40, 60, 80 and 100 mV/s.

Figure 5.8: DPV characterization of PANSA/PVP-AgNPs/CYP2E1 pH 7.4. 0.1 M phosphate buffer, pH 7.0 at 10, 20, 30, 40, 60, 80 and 100 mV/s.

Figure 5.9: SWV characterization of PANSA/PVP-AgNPs/CYP2E1 in pH 7.4, 0.1 M phosphate buffer, pH 7.0 at 10, 20, 30, 40, 60, 80 and 100 mV/s.

Figure 5.10: CVs of (A) bare Au electrode (green line) (B) of Au/PANSA/PVP-AgNPs (black line) and (C) Au/PANSA/PVP-Ag after CYP2E1 immobilization (red line) and (D) of PANSA at 50 mV/s in pH 7.4, 0.1 M phosphate buffer.

Figure 5.11: Plot of $I_{p,c}$ versus v plot used to calculate n , the number of electrons transferred in the reaction.

Figure 5.12: Plot of E_p versus $\log v$ used to calculate α , electron transfer coefficient.

Figure 6.1: Steady state responses at applied potential of -250 mV with response time of 20 s.

Figure 6.2: (A) CV and (B) DPV responses at different ethambutol concentrations for the Au/PVP-AgNPs/PANSA/CYP2E1 nanobiosensor.

Figure 6.3: Calibration curve of ethambutol showing the linear range (inset) for the Au/PVP-AgNPs/PANSA/CYP2E1 nanobiosensor.

Figure 6.4: Steady state responses of ethambutol at applied potential of -250 mV with response time of 20 s.

Figure 6.5: (A) CV and (B) DPV responses at different ethambutol concentrations for the Au/PVP-AgNPs/PANSA/CYP2E1 nanobiosensor.

Figure 6.6: Calibration curve of isoniazid showing the linear range (inset) for the Au/PVP-AgNPs/PANSA/CYP2E1 nanobiosensor.

Figure 6.7: (A) CV and (B) DPV responses at different pyrazinamide concentrations for the Au/PVP-AgNPs/PANSA/SA-CYP2E1 nanobiosensor.

Figure 6.8: Steady state responses of pyrazinamide at applied potential of -250 mV with response time of 25 s.

Figure 6.9: Calibration curve of pyrazinamide for the Au/PVP-AgNPs/PANSA/SA-CYP2E1 nanobiosensor.

Figure 6.10: (A) CV and (B) DPV responses at different rifampicin concentrations for the Au/PVP-AgNPs/PANSA/EG-CYP2E1 nanobiosensor.

Figure 6.11: Steady state responses of rifampicin at applied potential of -250 mV with response time of 25 s.

Figure 6.12: Calibration curve of rifampicin for the Au/PVP-AgNPs/PANSA/EG-CYP2E1 nanobiosensor

List of Schemes:

Scheme 2.1: Mechanism pathway of CYP enzymes.

Scheme 2.2: Mechanism of Competitive Inhibition.

Scheme 2.3: Mechanism of Non-competitive Inhibition.

Scheme 2.4: Mechanism of Mixed Inhibition.

Scheme 2.5: Mechanism of Uncompetitive Inhibition.

Scheme 2.6: Mechanism of Irreversible Inhibition.

Scheme 4.1: Schematic representation of ANSA polymerization on Au electrode to produce PANSA.

Scheme 4.2: Schematic representation of PANSA on Au electrode and the illustration of the immobilization of PVP-AgNPs and CYP2E1.

Scheme 6.1: Reaction scheme showing the metabolism of ethambutol using the Au/PANSA/PVP-AgNPs/CYP2E1 nanobiosensor.

Scheme 6.2: Reaction scheme showing the metabolism of isoniazid using the Au/PANSA/PVP-AgNPs/CYP2E1 nanobiosensor.

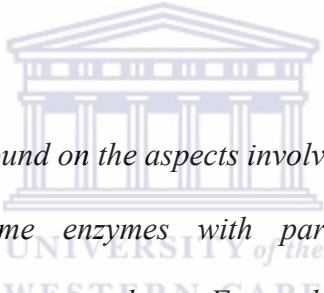
Scheme 6.3: Reaction scheme showing the metabolism of pyrazinamide using the Au/PANSA/PVP-AgNPs/EG-CYP2E1 nanobiosensor.

Scheme 6.4: Reaction scheme showing the metabolism of rifampicin using the Au/PANSA/PVP-AgNPs/SA-CYP2E1 nanobiosensor.

CHAPTER ONE

Introduction

Summary



This chapter gives a brief background on the aspects involved in this project namely; sensors, conducting polymers, cytochrome enzymes with particular emphasis on CYP2E1, Tuberculosis and Tuberculosis treatments drugs. Focused in this chapter is the relationship between these aspects and their contribution towards the success of this study. Also included in this chapter are the project's rationale and motivation, the aim and specific objectives of the study as well as the thesis outline.

1.1 Background:

Mycobacterial infections are among the most difficult of all bacterial infections to treat, let alone to cure. Mycobacteria are slow growing organisms making them relatively resistant to antibiotics, an activity of which tends to depend on how rapidly the cells are dividing. At times mycobacterial cells can be dormant thus making them completely resistant to many drugs, or at times are slowly killed by drugs that are active. A substantial proportion of mycobacterial cells are intracellular, residing within macrophages making them inaccessible to drugs that struggle to penetrate. These are organisms notorious for developing resistance to any single drug therefore, combination drug therapy is usually required to overcome these obstacles and prevent the emergence of resistance during the course of therapy. Chemotherapy is another route for the eradication of mycobacteria but is a slow means of therapy, in which treatment can go on for months to years depending on the drugs used.

One of the main subjects of this study is tuberculosis, which is a disease resultant from infection by *Mycobacterium tuberculosis* the most common infecting organism. There are however other mycobacteria such as *Mycobacterium bovis*, which is uncommon due to the virtual eradication of bovine tuberculosis from cattle and *Mycobacterium africanum*, which is found in certain areas of Africa. After the initial infection by *Mycobacterium tuberculosis*, which in most cases passes without being noticed, the disease can follow a variety of clinical courses sometimes lying dormant for months or years before being reactivated. The disease is chiefly associated with the lungs but can occur in many other organs. There is a clear distinction between tuberculosis infection and tuberculosis disease. In the latter, one or more body parts indicate bacteriological, clinical and radiographic evidence

of the disease; while in the former the tubercle bacilli are established in the host, but there are no symptoms or detectable evidence of the disease.

Of great interest is the fact that over the last century, there has been a steady decline in both these incidences and death rate probably as a result of improved social conditions, better nutrition and less overcrowding. The last few decades have seen a rapid decline through vaccination and case-finding programmes such that tuberculosis has now become less of a public health problem. However in undeveloped countries and developing countries such as South Africa, tuberculosis continues to remain a problem especially with the emergence of drug resistant strains and the high rates of HIV/Aids. Incidences of tuberculosis are dependent on a variety of factors such as age, race, geography and social conditions. In developing countries incidences can only be estimated, while in developed countries such as the America and the United Kingdom, tuberculosis is a notifiable disease.

The most recent global estimates of tuberculosis indicate that one third of the world's population has been infected with *Mycobacterium tuberculosis*, and new infections are occurring at a rate of one per second (Castagnolo *et al.* 2009). According to the World Health Organization, there are an estimated 2 billion people infected with tuberculosis (Hernandez *et al.* 2008) with an estimated 8-9 million new cases reported annually and an estimated 3 million human deaths occurring mostly in Africa and Asia where infections are stabilizing or slowly falling in some regions (Eoh *et al.* 2009; Castagnolo *et al.* 2009). The continuing high levels of tuberculosis risks in these countries is thought to be attributed to deteriorating public infrastructure and in large by the compromised immune systems of individuals as a result of HIV/Aids (Castagnolo *et al.* 2009; Wang *et al.* 2009; Eoh *et al.* 2009; Schweon *et al.* 2009). Although the directly observed treatment short course; (DOTS) regime has contributed significantly towards the falling incidences of tuberculosis, incomplete implementation of the campaign has also been a major cause of the high occurrences of the drug resistant strains of

Mycobacterium tuberculosis coupled with the spread of HIV/Aids in tuberculosis-endemic regions (Wallis *et al.* 2009; Zvavamwe *et al.* 2009). This stems from the fact that patients with fully susceptible tuberculosis develop secondary resistance during therapy as a result of inappropriate dosing of treatment, inadequate treatment, not taking the prescribed regimen appropriately or using low quality medication. Multidrug-resistant TB (MDR-TB) and extensively drug resistant TB (XRD-TB) are more difficult to treat than sensitive tuberculosis since they require the administration of expensive and less effective second line drugs for longer treatment durations than first line drugs (Eoh *et al.* 2009; Orenstein *et al.* 2009). It is therefore acknowledged that new approaches are required in order to promptly address the issue of patients falling ill as a result of inappropriate dosing of treatment and inadequate treatment administration.

To achieve that, a device with a fast response time coupled with enhanced performance and increased sensitivity is essential (Popovtzer *et al.* 2006). This form of device can only be obtained by miniaturizing bulky laboratory equipment and integrating them onto single microchips. Miniaturization is highly important because of convenience, portability, low costs, high resolution results, ease of operation, rapidity of analyses, handling reduced amounts of chemical or sample consumption (Grudpan *et al.* 2009; Popovtzer *et al.* 2006; Chikkaveeraiah *et al.* 2009). One of the most popular and elegant miniaturization methods is the incorporation of chemical process techniques and procedures into electrochemical nanobiosensors. An electrochemical nanobiosensor consists of one part where the requisite chemical or physical processes are performed and another part for information acquisition (Muchindu *et al.* 2010). These nanobiosensors can be constructed if the sensing materials are modified with biological elements such as DNA and enzymes. Electrochemical nanobiosensors possess bioactive substances which are responsible for the determination of the sensitivity of the sensor and transducers which provide the sensitivity

and also convert the recognition event into measurable signals (Nyholm *et al.* 2005; Mathebe *et al.* 2004). By replacing classical sensor materials with conducting polymers has achieved better selectivity and fast responses in electrochemical nanobiosensors by exploiting either the intrinsic or extrinsic functions of polymers. This has given polymers tremendous recognition in the field of artificial sensors for mimicking natural sensing organs due to their ease of coating onto electrode surfaces (Xia *et al.* 2010; Gerard *et al.* 2002; Adhikari *et al.* 2004). Immobilizing metal nanoparticles onto conducting polymers allow for even better responses and better functioning of biological compounds.

The present study was focused on the development of an electrochemical nanobiosensor system, which was suitable for the appropriate dosing of clinically, diagnosed patients by the measurement of tuberculosis treatment drugs namely; Isoniazid (INH), Rifampin (RIF), Pyrazinamide (PYR) and Ethambutol (ETH). When constructed this device was tailored to match the individual demands of the specified drugs.

Current literature suggests that each of the above mentioned drugs are metabolised in the liver individually by different enzymes. Isoniazid is an arylamine and is metabolised via acetylation by the important Phase II enzyme, *N*-acetyltransferase (Chen *et al.* 2009). There is however some literature which suggests CYP2E1 to be involved in the metabolism of isoniazid. Pyrazinamide is metabolised to 5-hydroxypyrazinamide by the molybdenum iron-sulphur flavin hydroxylase enzyme, xanthine oxidase/xanthine dehydrogenase (Yamamoto *et al.* 1991; Rasoulzadeh *et al.* 2009). Even though these enzymes are known for the metabolism of these two compounds, our study has introduced a new biotransformation method by studying the metabolism of these drugs; including RIF and EMB using the enzyme Cytochrome P450-2E1 (CYP2E1) coupled to a nanocomposite of poly(8-anilino-1-naphthalene sulphonic acid) PANSA and silver nanoparticles (PVP-AgNPs).

The techniques currently available for quantifying the levels of INH, RIF, PYR and ETH and their metabolites in urine and plasma are high performance liquid chromatography, thin layer chromatography and gas chromatography methods. These are accurate and well established techniques however production of results is time consuming and substantial sample preparation is required (Owino *et al.* 2008; Arotiba *et al.* 2007). These factors pose a problem when dealing with cases of drug resistance and severe side effects among tuberculosis diagnosed patients, since the level of drugs in their systems cannot be promptly studied to allow for the appropriate assistance to be delivered. Therefore, electrochemical nanobiosensors were established which have reduced sample preparation time allowing for point of care analyses.

In this study, the electrochemical interaction between Cytochrome P450-2E1 (CYP2E1) and INH, RIF, PYR and ETH mediated by poly(8-anilino-1-naphthalene sulphonic acid modified with silver nanoparticles) was investigated.

The following section illustrates the aims and objectives of the study.

1.2 Research Aims:

The aim of this study was to develop silver modified nanobiosensors for profiling the drug biotransformation of TB treatment drug. This was based on nanobiosensors developed from gold electrodes using cytochrome P450 (CYP2E1) and nanostructured poly(8-anilino-1-naphthalene sulphonic acid) composites modified with silver nanoparticles. The study had the following objectives:

1. Synthesis of poly(8-anilino-1-naphthalene sulphonic acid) (PANSAs).
2. Synthesis of silver nanoparticles (PVP-AgNPs).
3. Preparation of PANSAs-PVP-AgNPs nanocomposite.

-
4. Characterization of the PANSA, PVP-AgNPs, PANSA/PVP-AgNPs nanocomposite using TEM, UV-Vis, AFM, CV, DPV, SWV.
 5. Fabrication of nanobiosensors with genetically engineered enzyme namely; cytochrome P450 2E1 (CYP2E1) on gold electrodes.
 6. Determining the amperometric responses of the CYP2E1 nanobiosensors to Isoniazid, Rifampin, Pyrazinamide and Ethambutol.
 7. Development of kinetic models for the reactivities of the TB treatment drug (INH, RIF, PYR and ETH) metabolism biosensors.
 8. Parameter optimisation and calibration of the nanobiosensors systems.

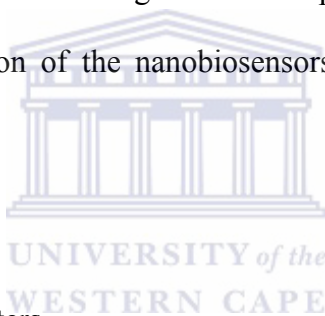
1.3 Rationale and Motivation:

This study sought to combine the bioelectronics and bioelectrochemistry of enzyme isoforms with the electron mediating ability and conductivity of electroactive nanopolymers coupled with metal nanomaterials, for the electrochemical study and modelling of TB treatment drug metabolism. The materials of interest in this study are PANSA (synthesized from a derivative of naphthalene sulphonic acid, 8-anilino-1-naphthalene sulfonic acid (ANSA) and PVP-AgNPs (synthesized from polyvinylpyrrolidone and AgNO₃).

The specific application of the proposed nanosensor system for the elucidation of the metabolism of TB treatment drugs namely; Isoniazid, Rifampin, Pyrazinamide and Ethambutol is being proposed. The feasibility of this study is borne from that fact that a number of studies have suggested *N*-acetyltransferase to be the major enzyme catalysing INH (Martins *et al.* 2008; Chen *et al.* 2009) and xanthine oxidase/xanthine dehydrogenase towards the metabolism of PYR to 5-hydroxypyrazinamide (Yamamoto *et al.* 1991; Rasoulzadeh *et al.* 2009). However a new approach has been established in this study through the use of CYP2E1 for the biotransformation of these TB drugs including RIF and ETH. The design of

the resultant device is to eliminate the need for N-transferase and xanthine oxidase physiological or artificial co-factors in the biocatalysis of the metabolism of TB treatments drugs, by combining the use of genetically engineered CYP2E1 and cathodic polarization of the enzyme immobilized in the PANSA/PVP-AgNPs nanocomposite as the source of the requisite electrons.

Clinically it is important to determine the CYP2E1 profile of patients before and after the administration of Isoniazid, Rifampin, Pyrazinamide and Ethambutol in order to provide the adequate treatment and appropriate dosing of treatment. The status of the metabolism of the TB drugs in patients would be evaluated by the use of the nanobiosensor systems consisting of PANSA modified with PVP-AgNPs and samples of plasma and urine. This will allow on-site real time application of the nanobiosensors and point of care diagnosis for patients.



1.4 Thesis lay-out:

This thesis consists of seven chapters.

Chapter 1 presents a brief background on the project, rationale and motivation, as well as the research aim and objectives.

Chapter 2 provides a detailed literature review.

Chapter 3 consists of detailed procedures used for the success of this work. Also included in this chapter are the lists of materials and instruments used.

Chapter 4 provides the morphological and amperometric results obtained from the nanomaterials; PANSA, PVP-AgNPs and PANSA/PVP-AgNPs synthesized in this work while

Chapter 5 illustrates the morphological and amperometric results for the developed PANSA/PVP-AgNPs/CYP2E1 nanobiosensors.

Chapter 6 consist of results on INH, ETH, PYR and RIF detection.

Chapter 7 is the general conclusion, recommendations and future work.

The following chapter provides the literature review.



1.5 References:

Adhikari B.; Majumdar S., 'Polymers in sensor applications' (2004) *Progress in Polymer Science* **29** pg 699-766.

Arotiba, O. A.; Ignaszak, A.; Malgas, R.; Al-Ahmed, A.; Baker, P. G. L.; Iwuoha, E. I., 'An electrochemical DNA biosensor developed on novel multinuclear nickel (II) salicylaldimine metallodendrimer platform' (2007) *Electrochimica Acta* **53** pg 1689-1696.

Castagnolo D.; Radi M.; Botta M., 'Synthesis and biological evaluation of new enantiomerically pure azole derivatives as inhibitors of *Mycobacterium tuberculosis*' (2009) *Bioorganic & Medicinal Chemistry Letter* **19** pg 2203-2205.

Chen B.; Cai W.; Cao X., 'Estimating N-transferase metabolic activity and pharmacokinetics parameters of isonizid from genotypes in Chinese subjects' (2009), *Clinica Chimica Acta* **405** pg 25-29.

Chikkaveeraiah B.V.; Liu H., 'A microfluidic electrochemical device for high sensitivity biosensing: Detection of nanomolar hydrogen peroxide' (2009) *Electrochemistry Communications* **11** pg 819-820.

Eoh H.; Brennan P.J., 'The *Mycobacterium tuberculosis* MEP (2C-methyl-D-erythritol 4-phosphate) pathway as a new drug target' (2009) *Tuberculosis* **89** pg 1-2.

Gerard M.; Chaubey A.; Malhotra B. D., 'Application of conducting polymers to biosensors' (2002) *Biosensors and Bioelectronics* **17** pg 345-359.

Hernandez C.; Cetner A., 'Tuberculosis in the age of biologic therapy' (2008) *Journal of American Academy of Dermatology* **59** No 3 pg 363-364.

Mathebe N. G. R.; Morrin A.; Iwuoha E. I., 'Electrochemistry and scanning electron microscopy of polyaniline/peroxidase-based biosensor' (2004) *Talanta* **64** pg 115-120.

Muchindu M.; Waryo T.; Arotiba, O.; Baker, P. G. L.; Iwuoha, E. I., 'Electrochemical nitrite nanosensor developed with amine- and sulphate-functionalised polystyrene latex beads self-assembled on polyaniline' (2010) *Electrochimica Acta* **55** pg 4274-4280.

Nyholm L., 'Electrochemical techniques for lab-on-a-chip application' (2005) *Analyst* **130** pg 599-600.

Orenstein E.; Basu S., 'Treatment outcomes among patients with multidrug-resistant tuberculosis: systematic review and meta-analysis' (2009) *Lancet Infectious Disease* **9** pg 153-154.

Owino J.H.O.; Arotiba O.A., 'Electrochemical Immunosensor Based on Polythionine/Gold nanoparticles for the Determination of Aflatoxin B₁' (2008) *Sensors* **8** pg 8263-8264.

Popovtzer R.; Neufeld T., 'Electrochemical detection of biological reactions using novel nano-bio-chip array' (2006) *Sensors and Actuators B* **119** pg 664-665.

Rasoulzadeh F.; Jabary H.N., 'Fluorescence quenching study of quercetin interaction with bovine milk xanthine oxidase' (2009) *Spectrochimica Acta Part A: Molecular and Biomolecular Spectroscopy* **72** pg 190-191.

Schweon S.J., 'Tuberculosis Update' (2009) *Journal of Radiology and Nursing* **28** pg 12-14.

Xia, L.; Wei, Z.; Wan, M., 'Conducting polymer nanostructures and their application in biosensors' (2010) *Journal of Colloid and Interface Science* **341** pg 1-11.

Yamamoto T.; Kario K., 'A case of Xanthinuria: A study on the Metabolism of Pyrazinamide and Allopurinol' (1991) *Japan Journal of Medicine* **30** pg 430-431.



CHAPTER 2

Literature Review

Summary

Electroanalytical Chemistry has played an important role in the ever changing panorama of diversified and extremely different scientific and industrial research. Electroanalysis is a major part involving the application of one or more electrochemical techniques to monitor and study measurements of specific interest. Therefore, the implementation of measurement systems affordable to most analysts has been assumed by scientists as a clear demand, in such a way that new developments have to be cost-effective, possess fully integrated systems, be capable of carrying out in situ, real-time and flow-monitoring studies such as biosensor systems. Over the past four decades, there has been a tremendous activity and widespread interest in the area of biosensors. Analyte recognition is among the major processes involved in any biosensor system. As a result of their speed, portability, specificity and low cost, biosensors have found a wide range of application; ranging from point-of-care testing (physicians office), bedside monitoring, home self testing and emergency-room screening. This chapter focuses on the background of the study through the description of various aspects involved in the study such as Biosensors, Enzymes, and Tuberculosis etc.

2.1 Biosensors:

Interest in the development and exploitation of analytical devices for quantification, detection and monitoring of specific chemical species and reactions has led to the emergence of biosensors. With biosensors representing an emerging new trend in diagnostic technology, metabolites such as urea, cholesterol, glucose and lactate in whole blood have been estimated (Gerard *et al.* 2002). There are various definitions attributed to biosensors depending on the field of application involved. These devices are sometimes known as optrodes, immunosensors, resonant mirrors, biochips etc. The most common definition of a biosensor is; an analytical device which incorporates intimate and deliberate combination of a specific biological compound and a physical entity. The role of the biological compound is to create a recognition event while the physical entity transduces the recognition event (Paddle *et al.* 1996). These features are clearly indicated in Figure 2.1.

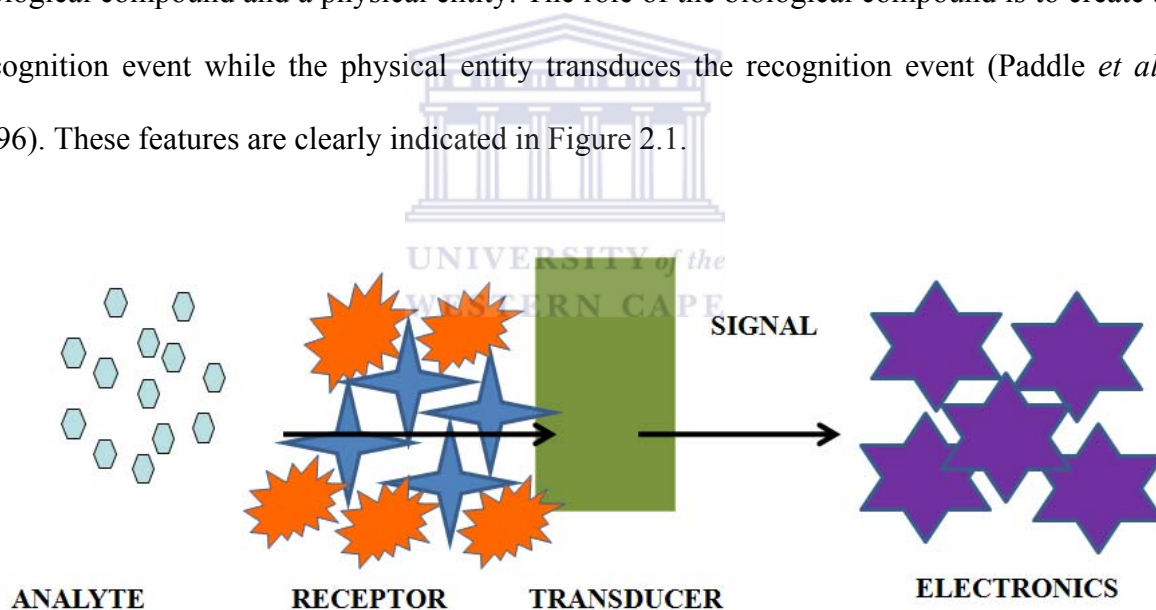
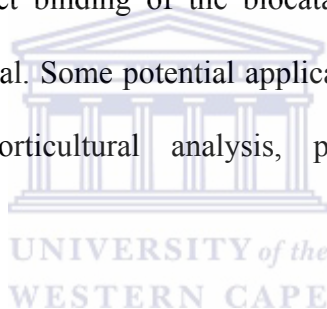


Figure 2.1: Components of a biosensor

A successful biosensor possesses some beneficial features such as; the bioactive substance should be highly specific for the purpose of the analyses. The reaction, which takes place, should be independent of physical parameters such as stirring, pH and temperature as

this would allow minimal pre-treatment of samples prior to analysis. The obtained response after analysis should be accurate, precise, reproducible and linear over the useful analytical range and should be free from electrical noise. Most importantly, the complete biosensor should be cheap, small, portable and capable of being operated by semi-skilled operators (Ryan-Byrne *et al.* 1997).

Biosensors can be divided into three generations depending on their level of integration. The first generation comprises of a biocatalyst that is either bound or entrapped in a membrane. The second generation of biosensors involves the adsorption of the biological components to the transducer surface thereby eliminating semi-permeable membranes. In the third generation, there is a direct binding of the biocatalyst to an electronic device that transduces and amplifies the signal. Some potential applications of biosensors are in clinical diagnosis, agricultural and horticultural analysis, pollution, water and microbial contamination analysis.



2.1.1 Biocomponents:

In biosensors, biocomponents also known as receptors, biological components or bioactive materials are compounds or materials that give biosensors their selectivity characteristics. In most cases these biocomponents undergo reactions with their respective analytes which is denoted by an end signal. Various biocomponents have been employed in sensor construction. Within a biosensor the recognition biocomponent incorporated possess some level of sensitivity although it may be vulnerable to extreme conditions such as pH, ionic strength and temperature. Most of these biocomponents including antibodies, enzymes and cells have very short lifetimes in solution and have to be fixed in a suitable matrix. Therefore, immobilization of these compounds is of critical importance to allow their stability although their activities are sometimes reduced (Gerard *et al.* 2002). A number of

techniques such as cross-linking, physical adsorption, gel entrapment, covalent binding etc. have been used to assist immobilization of biocomponents in various matrices as shown in Table 2.1.

The following section gives indication of a few commonly used biocomponents. Plant tissues as well as some sections of mammals have been employed in the construction of biosensors resulting in sensor systems with greater selectivity's when compared to those constructed with bacterial cells. This is due to the fact that plants and animals are not metabolically versatile. Each type of tissue slice functions the best when the appropriate analyte is present. Different types of tissues and their corresponding analytes are shown in Table 2.2 (D'Orazio *et al.* 2003).



Table 2.1: Conventional immobilization methods

Method	Advantage	Disadvantage	Example	Reference
Physical adsorption	<p>Method is low cost.</p> <p>No modification of the biocomponent.</p> <p>Underlying matrix can be regenerated.</p>	<p>High diffusion barrier.</p> <p>Binding forces are susceptible to changes in pH, temperature and ionic strength.</p>	<p>Adsorption of horseradish peroxidase (HRP) on totally cinnamoylated derivatives of D-glucosome and D-Manitol in the form of glassy beads for hydrogen peroxide detection.</p>	<p>Gerard <i>et al.</i> 2002</p>
Entrapment	<p>Method is low cost.</p> <p>Only physical contact of biocomponent near transducer.</p>	<p>High diffusion barrier.</p>	<p>Entrapment of D-fructose-5-dehydrogenase onto a platinum electrode to produce a biosensor, which was used for the fructose detection.</p>	<p>Gerard <i>et al.</i> 2002</p>

<p>Cross-linking</p>	<p>Moderate cost. Minimum loss of biocomponent.</p>	<p>Harsh treatment of biocomponent by toxic chemicals</p>	<p>Linking the enzyme tyrosinase (Tyr) in the presence of the mediator NQS for the determination of dichlorvos organophosphate pesticides.</p>	<p>Gerard <i>et al.</i> 2002</p>
<p>Covalent bonding</p>	<p>Very stable under adverse conditions. Low diffusional resistance.</p>	<p>Matrix is not regenerable. Harsh treatment of toxic chemicals.</p>	<p>Binding of oxalate oxidase and horse radish peroxidase and incorporated into carbon paste modified electrode with silica gel coated with titanium oxide containing toluidine blue for the detection of oxalate.</p>	<p>Gerard <i>et al.</i> 2002</p>

Table 2.2: Some tissues used in biosensor construction and their respective analytes

Tissue	Analyte	Reference
Mouse intestinal mucosa	Adenosine	D'Orazio <i>et al.</i> 2003
Cucumber leaf	Cysteine	D'Orazio <i>et al.</i> 2003
Banana pulp	Dopamine	D'Orazio <i>et al.</i> 2003
Yellow squash	Glutamate	D'Orazio <i>et al.</i> 2003
Bovine liver	H ₂ O ₂	D'Orazio <i>et al.</i> 2003
Corn kernel	Pyruvate	D'Orazio <i>et al.</i> 2003
Sugar beet	Tyrosine	D'Orazio <i>et al.</i> 2003

Whole microbial cells are also widely utilized in the study of biosensors and are often used when the desired enzyme is either unstable or difficult to purify. A slight disadvantage associated with these biosensors is that they have a slow response time and require frequent calibration. These biosensors have been constructed to analyse ammonia, antibiotics, enzyme activities, sugars, peptides, vitamins, nitrates, alcohols, biological oxygen demand and organic acids (Conn *et al.* 1987).

2.1.1.1 Enzymes:

Of all biocomponents, enzymes are the most widely used and research has shown that most enzymes have been successfully used in the construction of biosensors. These components are unique since they are a combination of selectivity and sensitivity and they allow for a wide selection of transducers to be used (Conn *et al.* 1987). An enzyme sensor can be considered as a combination of transducer and a thin enzymatic layer, which is responsible for measuring the concentration of the substrate. In close proximity to the enzyme, is the sensitive surface of the transducer with the assumption that there is no mass

transfer across the interface. The external surface of the biocomponent is kept immersed in solution containing the substrate of interest. In doing so, the substrate migrates towards the interior of the enzyme and is converted into products when it reacts with the immobilized enzyme (Adhikari *et al.* 2004). Signals of enzyme sensors are strongly influenced towards their application by inhibition, temperature and pH dependence (D’Orazio *et al.* 2003) which in turn affects the reaction between the immobilized enzyme and the substrate.

In this study cytochrome P450-2E1 was employed in the construction of a nanobiosensor used for the determination of tuberculosis treatment drugs.

2.1.1.2 Characteristics of Immobilized Enzymes:

Immobilized enzymes are significantly affected by factors such as activity and stability therefore, it is of importance that the percentage of immobilized enzyme together with enzyme activity remaining after immobilization should always be included, along with the experimental conditions which are well suited for the determination of interest. Enzyme activity which is the most important factor especially towards the comparison of immobilization techniques is often unavailable. It is important that one knows the amount of enzyme immobilized onto a support and this is usually achieved by measuring the amount of enzyme remaining in the supernatant after immobilization and then subtracting this from the amount which was originally present. A fraction of difficulty usually arises in the determination of the absolute activity of the enzyme on the support after immobilization. Measuring this factor therefore involves the mass transfer as well as diffusional restrictions in the experimental method being used (Worsfold *et al.* 1995).

The stability of the immobilized enzyme with respect to time, temperature, storage conditions and at times experimental variables are critical performance indicators that should be noted. This issue can be addressed through various methods; however the most popular

and highly recommended is the storage of enzyme under normal operating conditions in an appropriate buffer solution. After a fixed time period the activity of the enzyme is monitored following the same procedure as that for the determination of the enzyme activity after immobilization. Because each enzyme has its own lifetime and maximum analyses strength, to account for the efficiency of a particular enzyme, the effect of introducing synthetic standards, reference material, as well as samples at predefined intervals and frequencies should be determined prior. During the procedure, special attention should be placed to aspects such as pH, temperature, ionic strength and the incorporation of impurities as they have an effect on the enzyme during immobilization. Prior knowledge of the details of the experiment should be noted since the immobilization can affect the optimum pH, oxidation and reduction working range and the apparent Michaelis-Menten constant for the appropriate substrate of an immobilized enzyme (Worsfold *et al.* 1995).



2.2 Transducers:

The role of transducers in biosensor construction is to convert a biochemical signal to an electronic signal. Transducers allow biosensors to be more specific and more selective. Depending on the nature of the biocomponents interaction with the analyte of interest, suitable transducing systems can be adapted in the biosensor construction.

Table 2.3: Biological components and transduction methods used in biosensor designs

Biological Compounds	Transducer	Reference
Organisms	Potentiometric	Worsfold <i>et al.</i> 1995
Tissues slices	Amperometric	Worsfold <i>et al.</i> 1995
Whole microbial Cells	Conductometric	Worsfold <i>et al.</i> 1995
Organelles	Impedimetric	Worsfold <i>et al.</i> 1995
Membranes	Optical	Worsfold <i>et al.</i> 1995
Enzymes	Calorimetric	Worsfold <i>et al.</i> 1995
Enzyme components	Acoustic	Worsfold <i>et al.</i> 1995
Receptors	Mechanical	Worsfold <i>et al.</i> 1995
Antibodies	Molecular electronic	Worsfold <i>et al.</i> 1995

Thus, depending on the transduction mechanism used, biosensors can be of different types such as; Optical, Resonant, Ion-Selective, Thermal and Electrochemical. Table 2.3 illustrates some biological compounds along with their respective transduction systems.

2.2.1 Optical Biosensors:

For this type of biosensor, the transduction output measured is light which is either based on electrochemiluminescence or optical diffraction. In these types of biosensors, a silicon wafer is coated with a protein through covalent bonds and is later exposed to UV light through a photo-mask, thus inactivating the exposed antibodies. However, when the diced wafer chips are incubated in an analyte, the antigen (analyte molecule) - antibody (biological element) bindings are formed in the active regions, a diffracting grating is created. The result of this grating effect is a diffraction signal when illuminated with a light source such as laser. Therefore the resultant signal can be measured or amplified before measuring for improved

sensitivity. Optical biosensors have been used for the detection of O₂, CO₂ and pH etc (Gerard *et al.* 2002).

2.2.2 Resonant Biosensors:

Resonant biosensors couple acoustic wave transducers with antibodies. Attachment of the analyte molecule with the membrane changes the mass of the membrane thus changing the resonant frequency of the transducer which can then be measured (Paddle *et al.* 1996).

2.3.3 Ion-selective Biosensors:

These are semiconductor field effect transistors (FET) possessing ion-selective surfaces which undergo electrical changes once the ions and the semiconductor interact, and the potential change can be subsequently measured. By covering the sensor electrode with a polymer layer, an Ion Sensitive Field Effect Transistor (SFET) can be constructed. The polymeric layer is selectively permeable to analyte ions, since they diffuse through the polymeric layer, thus causing a change in the potential of the FET surface. This type of biosensor is also known as Enzyme Field Effect Transistor (ENFET) and is primarily used for pH detection (Paddle *et al.* 1996).

2.2.4 Thermal Biosensors:

These types of biosensors are developed by combining immobilized enzymes with temperature sensors. When the analyte of interest comes into contact with the enzyme, the heat reaction of the enzyme is measured and calibrated against the analyte concentration. The total heat absorbed or produced has been found to be proportional to the molar enthalpy as well as the total number of molecules involved in the reaction. The measurement of temperature is accomplished through the use of a thermistor, also known as an enzyme

thermistor. Thermistors are quite applicable in these types of applications as they are highly sensitive to thermal changes. The advantage associated with these types of biosensors is that they do not require recalibration and are insensitive to the optical and electrochemical properties of the sample. Thermal biosensors have found application towards the detection of pesticides and pathogenic bacteria (Paddle *et al.* 1996).

2.2.5 Electrochemical Biosensors:

The underlying principle governing this class of biosensors is that many chemicals produce or consume ions or electrons which result in changes in electrical properties of solutions which can be sensed and later used as measuring parameters. Therefore, the name electrochemical biosensor is applied to a molecular sensing device which couples biological recognition elements such as enzymes, antibodies, bacteria or tissues (Adhikari *et al.* 2004) to electrode transducers (Wang *et al.* 2006; Brennan *et al.* 1996; D 'Orazio *et al.* 2003). The biological recognition element is immobilized in close proximity to a transducer that relays the interaction of the analyte and the bioactive substance into a measurable response which is often an electronic signal. This signal can result from the uptake and release of gases, the change in proton concentration or absorption light emission brought about by the metabolism of the target compound by the bioactive compound. This biological signal is then converted into a measurable response such as potential, current or absorption of light through electrochemical or optical means (Brennan *et al.* 1996; D 'Orazio *et al.* 2003). Electrochemical biosensors can be classified based on their individual measuring parameters namely; Conductrimetric, Amperometric and Potentiometric.

2.2.5.1 Conductimetric Electrochemical Biosensors:

Electric conductance or resistance is measured by these biosensors. This occurs when an electrochemical system either produces ions or electrons, during which the overall conductivity or resistivity changes. The observed change is measured and calibrated to a proper scale where it has been observed to have a relatively low sensitivity. A typical example of this type of biosensor was observed through the work by Chouteau *et al.* 2005 where a conductrimetric biosensor was constructed for the detection of heavy metal ions and pesticides in water samples using immobilized *Chlorella vulgaris* microalgae as bioreceptors. The redox potential or pH changes associated with the microenvironment in the polymer matrix allowed changes in electronic conductivity to be effectively monitored.

2.2.5.2 Amperometric Electrochemical Biosensors:

This biosensor type is driven by an external constant potential, during which an electrochemical reaction takes place, and the resultant current is measured (Malhotra *et al.* 2006; Chaubey *et al.* 2002). Most importantly, the function of amperometric biosensors is affected by the electron transfer between catalytic molecules and the electrode surface involving a mediation material. These types of biosensors commonly employ conducting polymers as their means of mediation is usually with enzymes either trapped within the polymer or covalently bound to functional groups (Gerard *et al.* 2002). An example of an amperometric biosensor can be observed in the work conducted by Yang *et al.* 2004 where horseradish peroxidase was self-assembled on hydroquinone during which the current response was measured at a fixed potential range.

2.2.5.3 Potentiometric Electrochemical Biosensors:

These biosensors are based on ion-selective or gas sensing electrodes where a movement of ions into a membrane at a zero current allows for the monitoring of the cell potential (Malhotra *et al.* 2006; Chaubey *et al.* 2002). Potentiometry is rarely used in biosensing methods especially with enzymes immobilized on electrodeposited conducting polymers in which pH sensitivity of the conducting polymer is used. This interaction is clearly illustrated by Shin *et al.* 1998; where a thin hydrophilic polyurethane polymer film was combined with the enzyme urease for the determination of urea by monitoring changes in potential.

2.3 Cytochrome P450 Enzymes:

The main focus of this study was to employ Cytochrome P450-2E1 (abbreviated CYP2E1, EC 1.14.14.1), towards the construction of a biosensor responsible for the biotransformation of tuberculosis drugs. This section outlines the background on cytochrome enzymes with particular emphasis on CYP2E1.

2.3.1 Occurrence of Cytochrome P450 Enzymes:

Cytochrome P450 enzymes also known as Iron Porphyrin enzymes were first investigated by Warburg and at that time they were referred to as cell pigments. He discovered that in the dark carbon monoxide had an inhibitory factor on respiration cells, however upon illumination, respiration was resumed. Knowing this fact, Warburg then suggested that in respiration a compound of iron was involved. Upon a close examination of the photo effect, it was discovered that a specific wavelength was involved with a characteristic absorption wavelength of iron hema-chromogen containing porphyrins. Warburg then came to the conclusion that the respiratory pigments were similar to these

compounds (Key *et al.* 1966). It was Keilen who revisited the work MacMunn continued from Warburg who discovered that at specific wavelengths a pigment was absorbed in several cells hence giving them the name cytochrome. Thereafter, all examined cells containing this pigment, could be readily observed on reduction due to a change in light absorption (Key *et al.* 1966; Hermeryck *et al.* 2002).

2.3.2 Kinetic Reactions of Cytochrome P450 Enzymes:

Cytochrome P450 enzymes belong to a multigene family of heme enzymes which catalyse the NADPH – dependant monooxygenase and reactions of different exobiotic and endobiotic lipophilic substrates. The unique ability of these enzymes is based on the fact that they can hydroxylate non-activated carbon atoms (C-H bonds). Metabolism of substrates produces products which serve as regulators in cells or are excreted from organisms. These enzymes are capable of metabolizing over 1,000,000 chemicals and involve about 60 distinct classes of biotransformation reactions; N-, O-, or S-, demethylation, dealkylation, S- oxidation, epoxidation, aliphatic oxidation, reductive dehalogenation and sulfoxide formation (Shumyanteva *et al.* 2005; Bistolas *et al.* 2005). They are also involved in mono-oxygenation reactions which are very useful as they are responsible for the hydroxylation of a number of compounds including steroids, fatty acids, drugs, food additives, fungi, bacteria, (Harris *et al.* 2001) alkanes and polyaromatic and polychlorinated hydrocarbons.

In man most of the cytochrome P450 enzymes are found in the liver with a remarkable amount also found in the small intestine, around the microsomal part of the cytoplasm, in the endoplasmic reticulum as well as in the mitochondria. Enzymes isolated from the mitochondria are known as steroidogenic cytochrome enzymes since they are situated in single cell organisms and are phylogenetically older. Usually they consist of an iron-sulphur protein, NADPH and NADH-dependant reductase (on FAD-type flavoprotein)

and cytochrome P450 enzyme. Steroidogenic enzymes are responsible for steroid synthesis as well as other substances which are required for maintaining the cell wall integrity. Another form of these enzymes evolved from steroidogenic enzymes over one billion years ago are known as xenobiotic enzymes. Xenobiotic enzymes are located in the smooth endoplasmic reticulum of cells, while some studies indicate that they have evolved during the period of plant-animal differentiation. They are constituted by NADPH: P450 reductase (FAD-and FMN- containing flavoprotein) and cytochrome P450 enzyme (Iwuoha *et al.* 2003). The strength of these enzymes lies in their ability to metabolise foreign biological substances.

2.3.3 Kinetics of Catalytic Reaction:

Cytochrome P450 enzymes consist of iron-protoporphyrin IX active sites with axial thiolate of cysteine residues as fifth ligands. Resting cytochrome P450 enzymes are in the ferric form (Fe^{3+}), one electron reduction of a ferric form leads to a ferrous state (Fe^{2+}). In most cases, these enzymes are octahedral and because of unpaired electrons in their 3d orbitals, they are practically all paramagnetic. Due to the presence of protoporphyrin IX, heme enzymes exhibit characteristic visible absorption spectra however, their spectra differ according to the identities of the lower axial ligands donated by the protein and the oxidation state of the iron, while the identities of the upper axial ligands are donated by the substrates (Harris *et al.* 2001). The source of electrons in this type of system is from flavoproteins, ferredoxin like proteins, NADPH (Lewis *et al.* 2002), the mediator or an electrode.

The mechanism for substrate hydroxylation by cytochrome enzymes, involves the following steps although there are still several details that still remain unsolved.

- **Step 1:** When the substrate binds to the hexa-coordinated low-spin ferric enzyme, water is excluded from the active site resulting in a change in the 5-coordinate low

spin state. This causes a decrease in polarity which is accompanied by a positive shift (Bistolos *et al.* 2005) or lowering of the redox potential by 110 mV to 130 mV which makes the first electron transfer step thermodynamically favourable, from its redox partner NADH or NADPH (Shumyanteva *et al.* 2005).

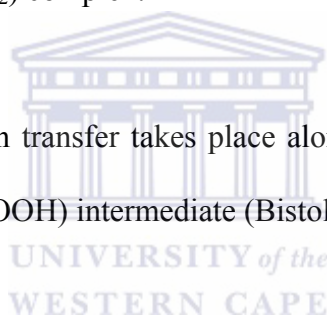
- **Step 2:** The transfer of the first electron from one of the redox partners reduces the ferric iron to the ferrous enzyme and this process is called reduction.

- **Step 3:** This form of the enzyme can now bind molecular oxygen resulting in a ferrous-dioxygen ($\text{Fe}^{2+} - \text{O}_2$) complex.

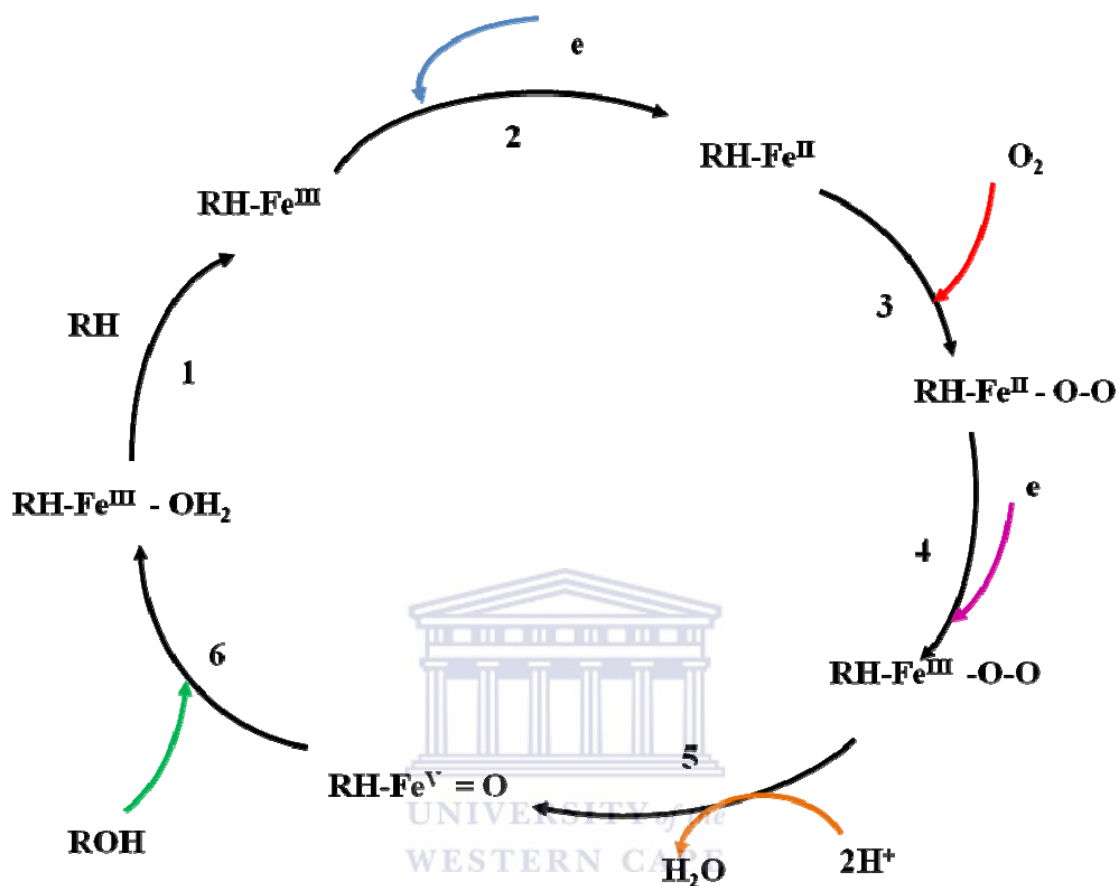
- **Step 4:** A second electron transfer takes place along with a proton gain forming an iron-hydroperoxo ($\text{Fe}^{3+} - \text{OOH}$) intermediate (Bistolos *et al.* 2005).

- **Step 5:** The O_2^{2-} reacts with two protons from the surrounding solvent, breaking the O-O bond to release a water molecule and a highly active iron-oxoferryl intermediate. One hydrogen atom is abstracted from the substrate by the intermediate to produce a one electron reduced ferryl species ($\text{Fe}^{\text{IV}} - \text{OH}$) and a substrate radical. On the other hand, the ferryl species reacts with the C – H bond of the substrate in a concerted reaction without the radical intermediate formation.

- **Step 6:** The final step of the process is the formation of the enzyme product complex and the release of the product. The low-spin state of the enzyme is then regenerated (Bistolos *et al.* 2005).



The reaction mechanism of these enzymes is illustrated in the following scheme:



Scheme 2.1: Mechanism pathway of CYP enzymes

2.3.4 Classification of Cytochrome P450 Enzymes:

The classification system of enzymes was developed based on certain similarities amongst different enzymes such as amino acid sequence homology. This system is based on the principle that the more similar the structure of the enzymes, the more closely are they both phylogenetically and functionally. Cytochrome P450 enzymes are grouped into families represented by the first number; example in cytochrome P450-2E1 (CYP2E1) the first number represented is 2. The idea behind this grouping is based on the fact that all the enzymes in the same family have at least 40% amino acid sequence homology. Furthermore,

these families are further grouped into subfamilies where at least 55% of the amino acid sequences are homologous among the enzymes. The subfamilies are denoted by an alphabetical letter which in cytochrome P450-2E1 (CYP2E1) is E. The last number which is 1 represents the gene that codes for the enzyme (Ghosal *et al.* 2005).

2.3.5 Cytochrome P450-2E1 (CYP 2E1):

As a member of the cytochrome P450 mixed-function oxidase system, CYP2E1 is involved in the metabolism of xenobiotics in the human body. While it is involved in the oxidative metabolism of a small range of substrates, solvents and anesthetics there are many important drug interactions mediated by CYP2E1. The size of the active site is the smallest observed for a human cytochrome enzyme and is therefore consistent with the low molecular weights of the many substrates of CYP2E1. Either directly or by facilitated excretion, CYP 2E1 is able to deactivate most drugs or bioactive many substances to form active compounds (Spracklin *et al.* 1997).

Among the available cytochrome P450 enzymes, CYP2E1 is notable for resulting in toxicity greatly affecting the liver. This is due to the fact that CYP2E1 comprises over 50 % of the hepatic cytochrome P450 mRNA and 7 % of the hepatic cytochrome P450 protein. On the other hand, CYP2E1 is expressed at lower levels in a variety of extra-hepatic tissues where it is thought to play a role in the metabolism of certain endogenous molecules. Levels of CYP2E1 together with resulting toxicity vary respectively in response to diabetes, alcohol consumption, fasting and obesity. Therefore, the action and behavior of CYP2E1 can have either a positive or negative influence on human health and drug metabolism (Porubsky *et al.* 2008; de Groot *et al.* 2002). Table 2.4 indicates substrates, inducers and inhibitors of CYP2E1 while the structure of CYP 2E1 is illustrated in Figure 2.2 (Porubsky *et al.* 2008).

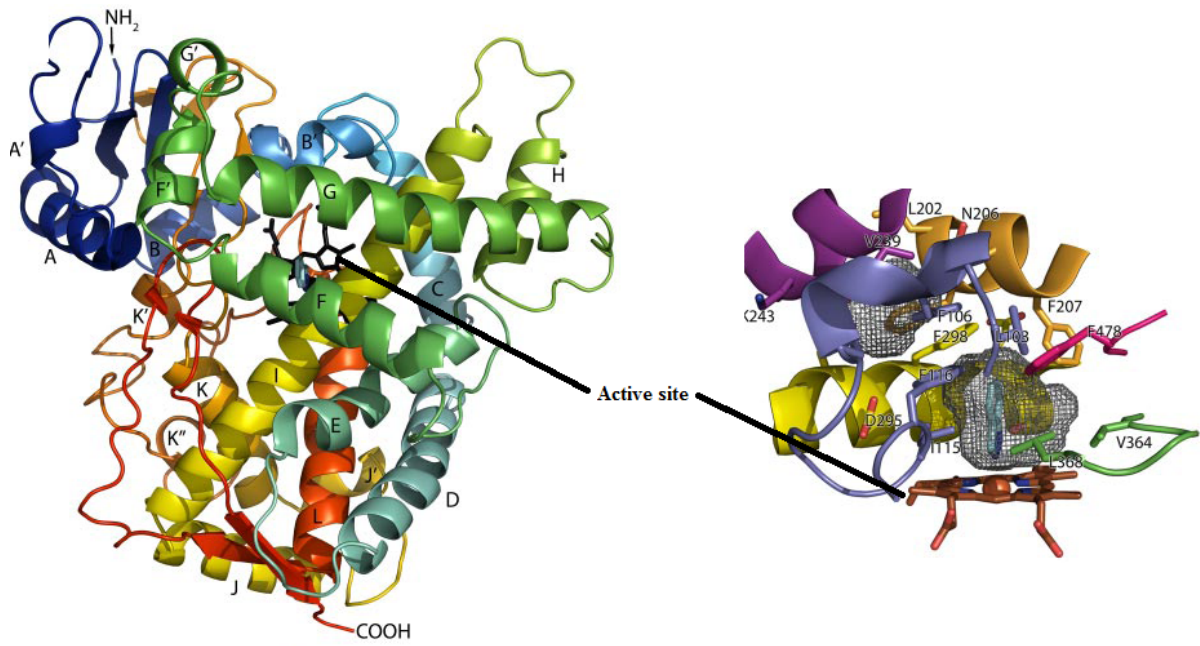



Figure 2.2: Distal face of CYP2E1 rainbow colored from N terminus (blue) to C terminus (red) also showing the active site of CYP2E1 (Porubsky et al. 2008)



Table 2.4: Substrates, inducers and inhibitors of CYP2E1

Substrates	Inhibitors	Inducers
<p>Anaesthetics:</p> <ul style="list-style-type: none"> ➤ Halothane ➤ Enflurane ➤ Isoflurane 	<p>Strong:</p> <ul style="list-style-type: none"> ○ diethyldithiocarbamate 	<ul style="list-style-type: none"> • acetone • ethanol • isoniazid
<p>Other:</p> <ul style="list-style-type: none"> ✓ paracetamol ✓ dapsone ✓ theophylline ✓ ethanol ✓ chlorzoxazone ✓ toluene ✓ Isoniazid 	<p>Unspecified:</p> <ul style="list-style-type: none"> ❖ cimetidine ❖ disulfiram 	

2.4 Application of Cytochrome P450 Enzymes in Biosensors:

Cytochrome P450 enzymes play a key role in detoxication of bioactive compounds and hydrophobic xenobiotics coming from both outside (drugs, medicines, environment pollutants and food supplements) and those formed inside cells (steroids, prostaglandins, cholesterol, saturated and unsaturated fatty acids and others) in living organisms. Computer assisted processes or enzymatic experimental systems are used to predict metabolic transformations of physiological active substances and to investigate possible metabolic pathways. As a result electrochemical systems based on recombinant forms of cytochrome P450 appear to be the most popular as they enable standardization of analysis formats

(Shumyantseva *et al.* 2007). Therefore, characterization of cytochrome P450 enzymes is a key issue in pharmacokinetics, toxicokinetics and in the regulation of some endogenous metabolic pathways.

Currently, the activity of cytochrome P450 enzymes is determined from the rates of formation of metabolites while the metabolic concentration requires development and maintenance of methods for each metabolic pathway studied. Another possible applicable method irrespective of the substrate of interest and the individual cytochrome P450 enzyme under study is to measure the consumption of reaction co-factors such as oxygen and NADPH. These co-factors however need to be available in excess to avoid any influence on enzyme activity. Redox properties of cytochrome P450 enzymes have allowed the development of amperometric biosensors allowing individuals to follow their catalytic cycles and monitor electron transfers to the enzymes. This is resultant from the fact that electrochemical systems execute dual functions; by serving as a source of electrons and have the ability to substitute partner proteins. The success of an amperometric biosensor relies on the electrical communication between an electrode and an enzyme; however in most cases the bulk nature of the protein may impede the redox site from direct electron transfer. In addition to this, macromolecular impurities and enzyme denaturing may also impede electron transfer. On the other hand, specifically binding the enzyme to the electrode surface may overcome these problems. While various immobilization techniques have been reported to establish electrical communication in enzyme-electrode construction, methods must often be designed empirically for the specific enzyme under study (Joseph *et al.* 2003; Shumyantseva *et al.* 2007; Bistolos *et al.* 2005). The ultimate approach is the direct or mediatorless electron transfer from the redox electrode to the redox active group of the CYP enzyme. Table 2.5 illustrates a list of sensors based on direct electron transfer.

Table 2.5: A list of CYP biosensors based on direct transfer

CYP Species	Electrode	Substrate tested	Reference
CYP102	DDAB-EPG electrode.	Catalysis with O ₂ and H ₂ O ₂ .	Shumyantseva <i>et al.</i> 2007
CYP2E1	Bare, thiol, DDAB-GC, Au.	Catalysis with p-nitrophenol.	Shumyantseva <i>et al.</i> 2007
CYP101	DMPC-PG, DDAB-PG.	Catalysis seen with O ₂ and TCA.	Shumyantseva <i>et al.</i> 2007
Recombinant CYP101	EPG.	Binding of camphor.	Shumyantseva <i>et al.</i> 2007
CYP101	DAB-BSA-glutaraldehyde-GCE.	Catalysis with camphor, adamantanone and fenchone.	Shumyantseva <i>et al.</i> 2007

Alternatively to this approach, cytochrome enzymes are attached to electrodes by introducing electroactive bridges; also known as mediators covalently coupled to the enzyme. Such redox relays have been bound at specifically selected sites generated by protein engineering or randomly. Table 2.6 presents a list of cytochrome biosensors based on mediated electron transfers. These approaches are relevant since cytochrome P450 and enzyme based electrodes may be used as biosensors in patient point-of-care diagnostics, the investigation of drug interferences and high-throughput screening.

This is clearly demonstrated by the study reported herein where CYP2E1 was used as a bioactive component coupled to a nanostructured silver nanoparticles-poly (8-anilino-1-naphthalene sulphonic acid) nanocomposite. This nanobiosensor was successfully used in the determination of tuberculosis treatment drugs.

Table 2.6: List of CYP biosensors based on mediated direct transfer

CYP species	Electrode	Substrate tested	Reference
CYP2D6	Polyaniline doped GCE.	Catalysis with fluoxetine.	Shumyantseva <i>et al.</i> 2007
CYP2B4	Clay/detergent-GCE.	Catalysis with aminopyrine, benzphetamine.	Shumyantseva <i>et al.</i> 2007
CYP101	PEI multilayers-rough PG electrode.	Catalysis with O ₂ and H ₂ O ₂ .	Shumyantseva <i>et al.</i> 2007
CYP3A4	Au-MPS-PDDA multilayers.	Catalysis with verapamil and medazolam.	Shumyantseva <i>et al.</i> 2007
CYP101	Au-MPS-PDDA multilayers, DDAB, multilayers carbon cloth.	Catalysis with styrene and <i>cis</i> - β -methylstyrene.	Shumyantseva <i>et al.</i> 2007
CYP101	Nano-crystalline Sb-doped tin oxide electrode.	Catalysis with styrene and camphor.	Shumyantseva <i>et al.</i> 2007

2.5 Enzyme Kinetics:

Enzymes are positive catalysts that dramatically increase the rate of a given reaction. Enzyme kinetics is principally concerned with the measurement and mathematical description of this reaction rate and its associated constants. The Michaelis–Menten equation as presented by Michaelis and Menten and further developed by Briggs and Haldane is fundamentally important to enzyme kinetics. Although derived from a simple, single-substrate, irreversible reaction, the Michaelis–Menten equation also remains valid for more complex reactions. Since enzyme-catalyzed reactions reach saturation, their rate of catalysis does not show a linear response to increasing substrate. If the initial rate of the reaction is measured over a range of substrate concentrations (denoted as $[S]$), the reaction rate (V) increases as $[S]$ increases, as illustrated in Figure 2.3. However, as $[S]$ increases, the enzyme becomes saturated with substrate and the rate reaches V_{MAX} , which is the enzyme's maximum rate (Fersht *et al.* 1984).

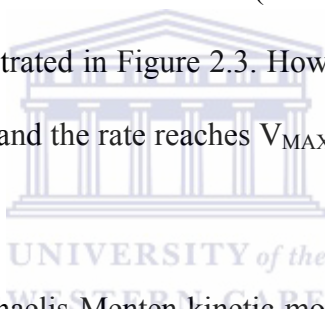


Figure 2.3 shows the Michaelis-Menten kinetic model for a single-substrate reaction. Initially there is indication of a bimolecular reaction between the enzyme $[E]$ and $[S]$ to form the enzyme-substrate complex $[ES]$. Although the enzymatic mechanism is a uni-molecular reaction; Equation 2.1 can be quite complex. There is typically one rate-determining enzymatic step that allows this reaction to be modeled as a single catalytic step with an apparent uni-molecular rate constant K_{CAT} . However, if the reaction path proceeds over one or several intermediates, K_{CAT} will be a function of several elementary rate constants, whereas in the simplest case of a single elementary reaction (a reaction absent from intermediates) it will be identical to the elementary uni-molecular rate constant k_2 . The apparent uni-molecular rate constant, K_{CAT} is also known as the turnover number and denotes the maximum number of enzymatic reactions catalysed per second (Fersht *et al.* 1984).

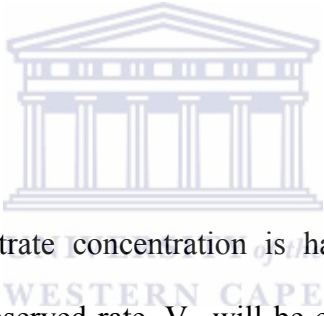


The Michaelis-Menten Equation is as follows (Equation 2.2) and it describes how the initial reaction rate v_0 depends on the position of the substrate-binding equilibrium and the rate constant k_2 .

$$V_i = \frac{V_{MAX} [S]}{K_M + [S]} \quad \text{Equ. (2.2)}$$

The above equation illustrates that the substrate concentration that produces exactly half of the maximum rate, the substrate concentration is equal to K_M . The equation can be rearranged as follows:

$$K_M = [S] \left\{ \left[\frac{V_{MAX}}{V_i} \right] - 1 \right\} \quad \text{Equ. (2.3)}$$



Therefore since the substrate concentration is half that required to enhance the maximum rate of reaction, the observed rate, V_i , will be equal to V_{MAX} divided by two. At this substrate concentration V_{MAX}/V_i will be equal to two, with the result that $[S] (1) = K_M$. A graphical representation of reaction rate (V_i) versus concentration $[S]$ produces a hyperbolic rate plot as shown in Figure 2.3 (Fersht *et al.* 1984). Figure 2.3 has key features denoted as points A, B, and C. At high substrate concentrations, the rate of reaction denoted C is almost equal to V_{MAX} with the difference almost negligible in nearby substrate concentrations. Extrapolating the plot at infinitely high substrate concentrations indicates the extrapolated rate being equal to V_{MAX} . On the other hand, the rate of reaction becomes independent of the concentration of the substrate, and the rate is said to be zero order. The substrate concentration has a very small difference in reaction velocity around point C, meaning that at

these concentrations, almost all of the enzyme molecules are bound to the substrate and the rate is not dependent on the substrate (Duggleby *et al.* 1994).

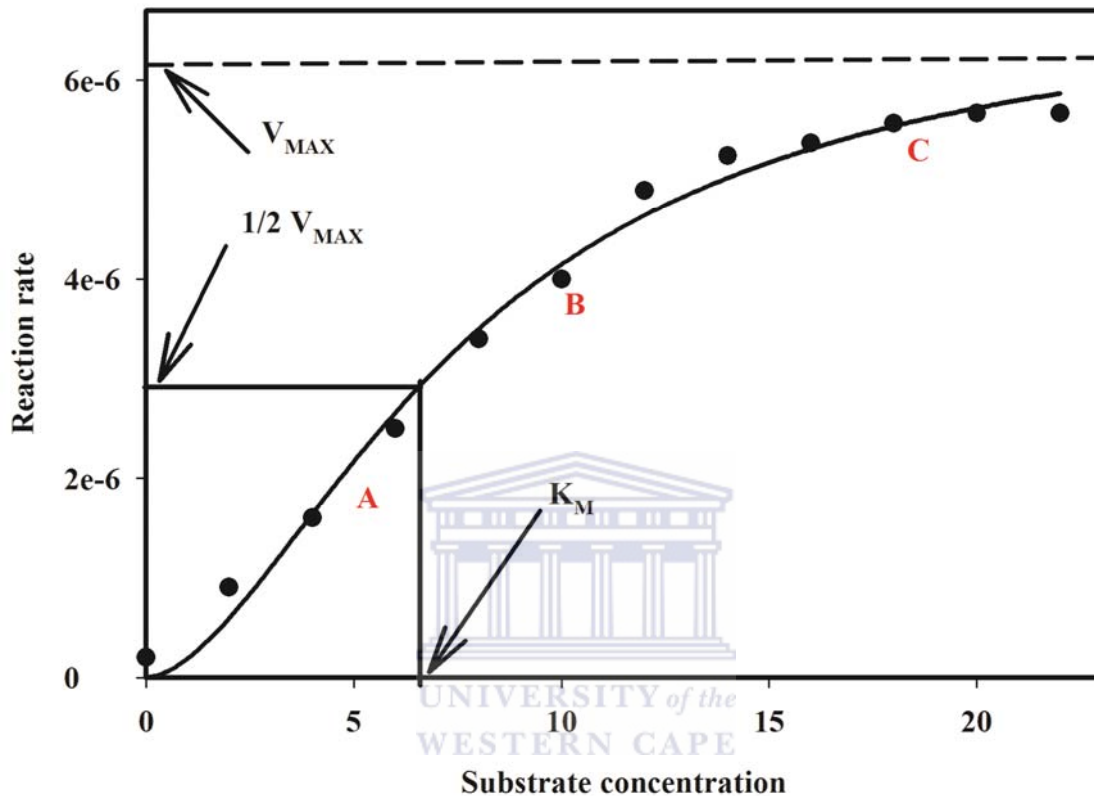


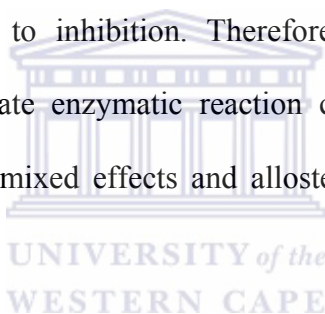
Figure 2.3: Illustration of Michaelis-Menten Kinetics

Point A and B are the lower substrate concentrations and here the velocities are lower which indicates that at any moment, a portion of the enzyme molecules are bound to the substrate. In fact, at the substrate concentration denoted by point B, exactly half of the enzyme molecules are in the enzyme-substrate complex at any instant and the rate is exactly one half of V_{MAX} . At substrate concentrations, near point A the rate appears to be directly proportional to substrate concentration, and the reaction rate is said to be first order (Fersht *et al.* 1984).

2.5.1 Enzyme Inhibition:

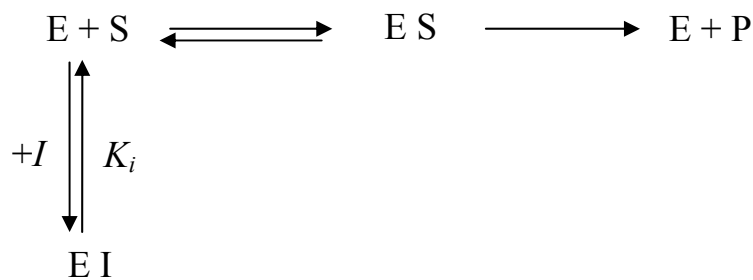
Enzyme inhibitors are compounds that have the ability to reduce the rate of enzyme-catalyzed reaction, by interacting with the enzyme, cofactor or the substrate. The enzyme-inhibitor reaction is often complex. Upon inhibition, the enzyme is unable to bind the substrate and the catalytic ability of the enzyme is reduced hence K_M and K_{CAT} are affected. There are two types of inhibitors namely; reversible and irreversible.

Irreversible inhibitors are unable to be physically separated from the enzyme and it had been observed that their degree of inhibition tends to increase with time. On the other hand, reversible inhibitors can be separated physically from the enzyme restoring the enzymatic activity it had prior to inhibition. Therefore a reversible inhibition process occurring for a single-intermediate enzymatic reaction can be described as competitive, uncompetitive, non-competitive, mixed effects and allosteric inhibition (Conn *et al.* 1987; Fersht *et al.* 1984).



2.5.1.1 Reversible Inhibition:

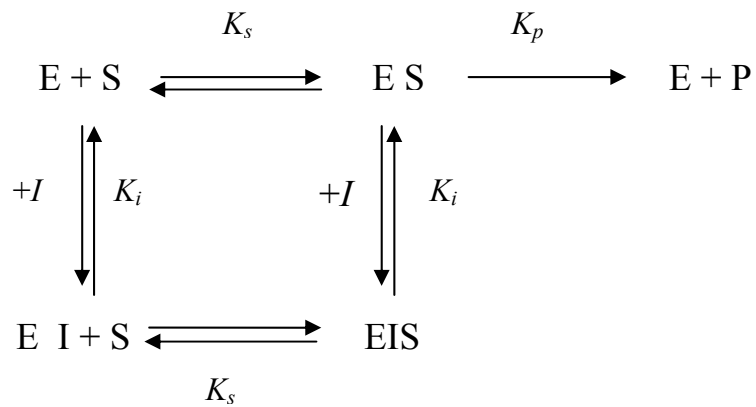
Competitive inhibitors slow reactions down as they have a similar structure to the normal substrate molecule K_s therefore compete K_p the substrate for the active site of the enzyme. The enzyme-bound inhibitor can either bind to an unfavourable position for the catalytic reaction to take place with potential substrate molecules or they can inactivate the enzyme's ability. During a catalytic reaction, at a particular enzyme and substrate concentration, if the inhibitor concentration is higher than that of the substrate, then the inhibitor will favourably compete with the substrate for the enzyme binding site and the degree of inhibition is high. When the substrate concentration is high, this effect is reversed (Paddle *et al.* 1996).



Scheme 2.1: Mechanism of Competitive Inhibition

On the other hand, non-competitive inhibitors are quite different in structure to the substrate molecule and therefore do not fit into the active site of enzymes. Usually, inhibition occurs at other parts of the enzyme thus changing the shape of the entire enzyme, including the active site in such a manner that the substrates can no longer bind. In this case the degree of inhibition is dependent on the concentration of the inhibitor as well as its affinity for the enzyme or the enzyme-substrate complex. This mechanism is clearly demonstrated by Songa *et al.* 2009 in which glyphosate inhibited the activity of the enzyme horseradish peroxidase.

Competitive and non-competitive inhibition affects enzyme kinetics differently. Competitive inhibitors increase K_M but do not change V_{MAX} ; while non-competitive inhibitors decrease V_{MAX} leaving K_M unchanged. These interactions are displayed in a Lineweaver-Burk Plots as illustrated in Figure 2.4 (Yung-chi *et al.* 1973).



Scheme 2.3: Mechanism of Non-competitive Inhibition

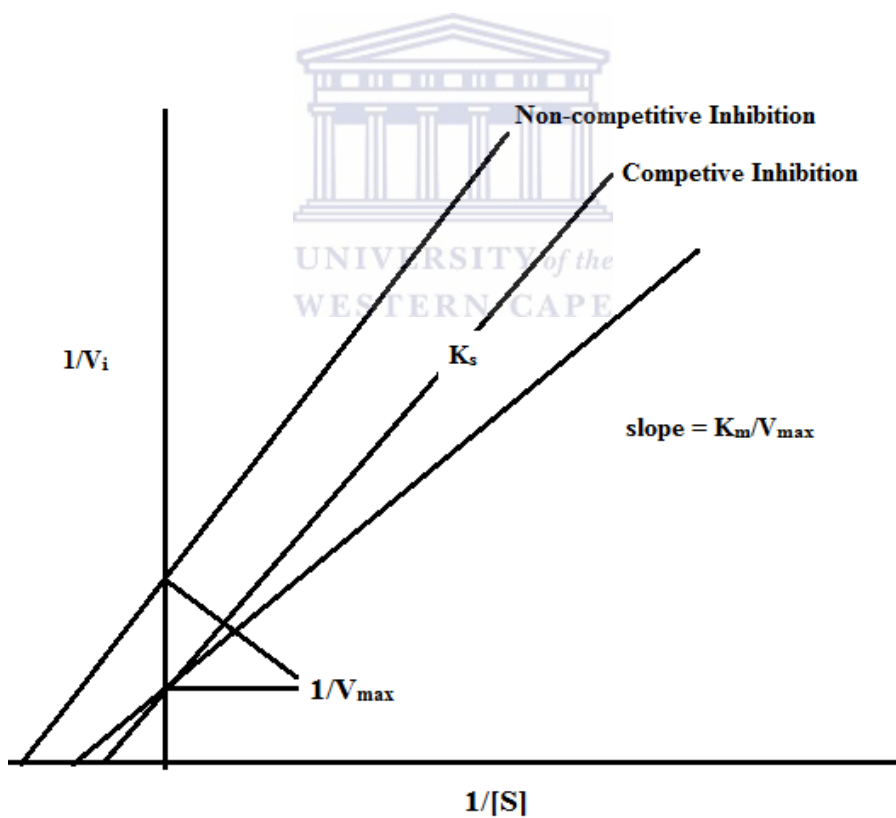
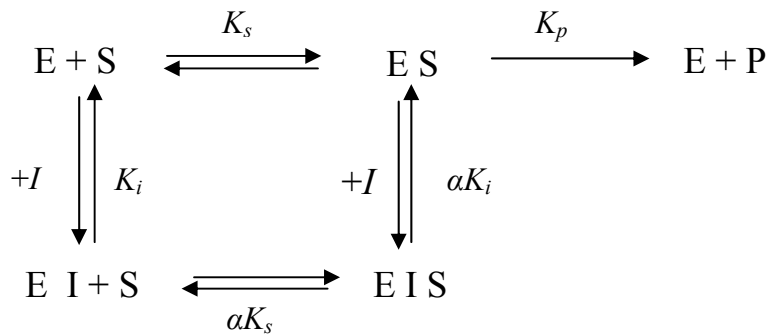


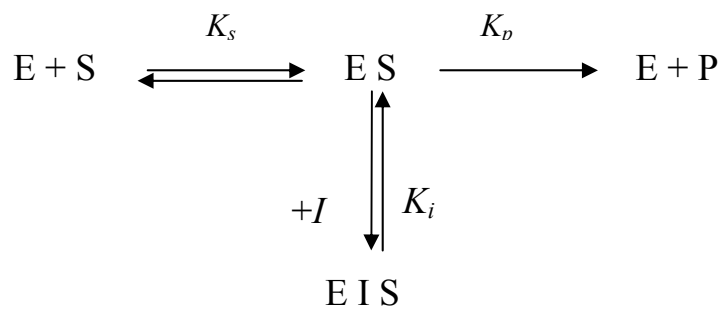
Figure 2.4: Illustration of Competitive and Non-competitive Inhibition

In the case of mixed-inhibition, the inhibitor binds the enzyme as well as the enzyme-substrate complex with a different affinity. These systems do not show any characteristics that are in any way similar to competitive and non-competitive inhibition. Both K_M and K_{CAT} are affected by such systems (Fersht *et al.* 1984).



Scheme 2.4: Mechanism of Mixed Inhibition

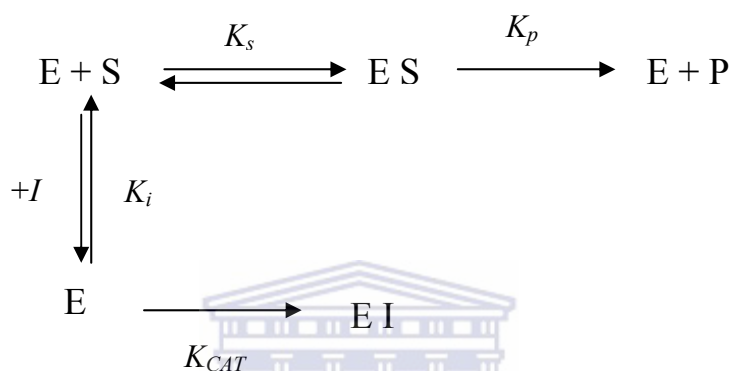
In uncompetitive inhibition, the inhibitor only binds upon the formation of the enzyme-substrate complex.



Scheme 2.5: Mechanism of Uncompetitive Inhibition

2.5.1.2 Irreversible Inhibition:

Irreversible inhibition is as a result of the formation of covalent bonds between the enzyme active centre and the inhibitor during enzyme-inhibitor interaction. The term irreversible means that the decomposition of the enzyme-inhibitor complex causes destruction of the enzyme (Yung-chi *et al.* 1973).



Scheme 2.6: Mechanism of Irreversible Inhibition

UNIVERSITY of the
WESTERN CAPE

2.6 Metal Nanoparticles and Conducting Polymers in Biosensors:

In recent years, nanostructured materials have received increasing attention due to their wide range of potential applications. Among these materials, composites of conducting polymers and inorganic nanoparticles in particular often exhibit improved physical and chemical properties over their single-component counterparts, and hence their use is highly recommended (Huang *et al.* 2009; Nabid *et al.* 2008). Metal nanoparticles, especially gold, silver and copper, have attracted much attention due to their interesting properties and potential applications in technical fields. On the other hand, chemical resistance and surface modification of these metal nanoparticles together with functional polymers are of significant importance, on which many research works have been developed (Sadik *et al.* 2009; Ahuja *et*

al. 2009). Furthermore, embedding these metal nanoparticles inside the core of conducting polymers such as polyaniline and polypyrrole has become a popular and interesting aspect of polymer/metal nanocomposites synthesis as a result of the possibilities of the development of materials for chemical sensors, microelectronic devices and electrocatalysts. This is due to their highly conductive nature of these polymers coupled with their ease of preparation and good stable environment which effectively accommodates the small dimensioned nanoparticles, thus improving specific electronic and catalytic properties. Various approaches have been employed to prepare polymer/metal composites (Alqudami *et al.* 2007; Li *et al.* 2005). The most popular method involves the electrodeposition of the monomer at electrode surfaces, followed by the electrodeposition of metal nanoparticles from a precursor salt using either a potential cyclic or a pulsed program. Another route of synthesis involves the polymerization of the monomer simultaneously with the formation of the metal nanoparticles using γ -irradiation or ultraviolet irradiation (Guascito *et al.* 2008).

A new challenge in this area has been the manipulation of polymer/metal composites together with biological molecules. This has led to the development of a novel class of modified electrodes in which both the charge transfer and the preservation of biological activity is obtained through experimental techniques designed to manipulate metal nanoparticles and polymers, tissues, DNA fragments, enzymes and other biological molecules. Two main problematic aspects with regards to the development of enzyme-based biosensors are the incorporation of sensing components in suitable matrices and the monitoring of the interaction of these components with analytes. Another aspect in enzymatic devices is the control of enzyme, which is dependent on the interface between the enzyme and polymers/metal composite. Such control has led to immobilization techniques suitable for anchoring the enzyme in close proximity to the electrode surface, thus preserving the biological activity. Therefore, in electrochemical devices where preservation of biological

activity at the polymer/metal-enzyme interface is priority towards efficient electrode design, the charge transfer between the enzyme and the electrode is usually fast and reversible (Liu *et al.* 2009; Mu *et al.* 2009; Cresphilho *et al.* 2009; Wang *et al.* 2006). The following section describes the most popular metal nanoparticles namely; silver, gold and copper nanoparticles, their characteristics, applications and use in biosensor devices.

2.6.1 Silver Nanoparticles

Nanomaterials, an emerging sub-discipline in Chemistry, have been extensively investigated in recent years due to their contribution towards the development in ultrasensitive electrochemical biosensors (Sadik *et al.* 2009; Zhang *et al.* 2000). Among the noble metal nanoparticles, silver are perhaps the most widely studied due to its unique optical and intrinsic shape-dependant properties (Sarkar *et al.* 2009; Hong *et al.* 2009). Silver nanoparticles have important application in sensors, in bio-labelling, as intercalation materials for electrical batteries, as antimicrobials, as catalysts in chemical reactions and filters. These nanoparticles also have the ability to purify drinking water, degrade pesticides and kill human pathogenic bacteria (Kathiresan *et al.* 2009; Mokhtari *et al.* 2009). A variety of methods have been employed to synthesize silver nanoparticles such as, molecular beam epitaxy, thermal deposition in organic solvents, laser ablation, chemical and photo-induced reduction (Zhang *et al.* 2000; Mokhtari *et al.* 2009; Sarkar *et al.* 2009; Hong *et al.* 2009). There has been considerable interest in the use of silver nanoparticles immobilized on polymeric films in nanobiosensor construction. This is due to their quantum size and surface effects, which result in novel physical, chemical magnetic and structural properties (Reddy *et al.* 2009) which enhances the conductivity of conducting polymers (Sadik *et al.* 2009).

This study reveals a novel method for the detection of TB drugs using an electroactive silver/polymer matrix on gold electrode surfaces.

2.6.2 Gold Nanoparticles:

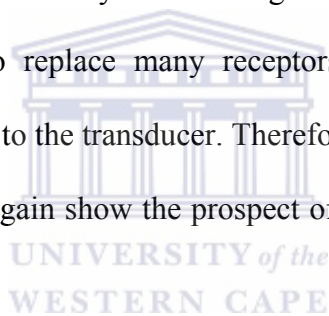
Much attention has been placed to gold nanoparticles as they have emerged as attractive nanomaterials for biological and biomedical applications. Their physical and chemical properties resulting from their inert core make them essentially non-toxic to cells. Upon excitation of their surface plasmon oscillation, these particles absorb and resonantly scatter visible and near-infrared light. The plasmon resonance band can be tuned over a wide spectral range by changing intrinsic parameters such as the size, shape or type of material.

Gold nanoparticles are advantageous in single molecule imaging due to their intense and brighter light-scattering signals which do not photobleach or blink. For particles below 30 nm, the absorption becomes dominant over scattering and can be used for detection by photothermal microscopy (Levy *et al.* 2010).

Gold salts in the presence of stabilizing agents used to prevent nanoparticle agglomeration and control growth, are used in the preparation of gold nanoparticles with varying core sizes. Furthermore, gold nanoparticles can be easily functionalized by anchoring thiol linkers in their monolayers. Besides these a wide variety of functional bionanoconjugates has been obtained, which include nanoparticles modified with peptides, proteins, antibodies, oligosaccharides, and nucleic acids. This has allowed gold nanomaterials to act as multifunctional platforms for both therapeutic and diagnostic purposes which include bio-imaging, single molecule tracking, drug delivery, transfection, and diagnostic (Levy *et al.* 2010). Because of their high effective surface area, catalysis and biocompatibility, gold nanoparticles are also used in biosensing due to their ability to adsorb redox enzymes without loss of their biological activities.

Norouzi *et al.* 2010; designed a new glucose electrochemical biosensor using a flow injection system. Glucose oxidase was used as the sensing material, immobilized on to the surfaces of gold nanoparticles and multiwall carbon nanotubes on glassy carbon electrode.

Fast Fourier transformation continuous cyclic voltammetry (FFTCCV) as the detection method showed acceptable reproducibility, good stability and low interferences for the biosensor developed in this study. Guo *et al.* 2007 reported an improved method for the detection of Concanavalin A (Con A) with a label-free optical biosensor. Success of the biosensor was based on self-assembling 1-Dodecanethiol (DDT) onto gold nanoparticles which were deposited on glass slides, with the insertion of glycolipid molecules into dodecanethiol by physical interactions. The recognition between Con A and carbohydrate was observed by Ultra-Visible spectrophotometry. The self-assembled bilayer on nanogold substrates had very high sensitivity for Con A, illustrating a low concentration detection limit. In addition to the ultra sensitivity for investigating interaction, the self-assembled bilayer structure, is expected to replace many receptors which require time-consuming organic syntheses for the fixation to the transducer. Therefore the simplicity and sensitivity of this biosensor architecture once again show the prospect of gold nanoparticles application in biosensor.



2.6.3 Copper Nanoparticles:

Over the years silver nanoparticles have been used in conductive inks which are mainly used in inkjet technology. However their high cost has limited their application in certain fields even though they are considered to possess high conductivity. Since copper is much cheaper, and also possesses very high conductivity (and which only 6% less than that of silver), copper nanoparticles can be considered as a replacement for silver nanoparticles in some fields of study (Magdassi *et al.* 2010). Many attempts have been made since the 1990's to synthesize copper nanoparticles by wet Chemistry as well as by gas or solid phase methods. These methods include, thermal reduction, polyol processes, and vacuum vapor deposition, radiation methods, and sonochemical methods, microemulsion techniques,

reducing flame synthesis, metal vapor synthesis and chemical reduction in solution (Magdassi *et al.* 2010). Recently, copper nanoparticles are used as an additive in lubricants, polymers/plastics, metallic coating and inks. Due to their excellent mending effect copper nanoparticles are added into lubricant oil as additives to effectively reduce friction and wearing, or to repair worn-out surfaces. When deposited on graphite surfaces, copper nanoparticles improve the charge discharge properties such as coulombic efficiency, cycle characteristics, and high rate performances and are commonly used as anode materials for lithium ion batteries. The unique chemical and physical properties of copper nanoparticles makes them extremely suitable for designing new and improved sensing devices, especially electrochemical sensors and biosensors. Important functions provided by copper nanoparticles include immobilization of biological components, labeling of biomolecules, catalysis of electrochemical reactions, enhancement of electron transfer between electrode surfaces and proteins and even acting as reactants (Luo *et al.* 2006).

A study by Heli *et al.* 2009; revealed the successful electrocatalytic oxidation of acetylcholine using copper microparticles modified carbon paste electrodes and copper nanoparticles modified carbon paste electrodes. Voltammograms recorded for the former electrode illustrated a single anodic peak related to the oxidation of acetylcholine while the latter showed two overlapped anodic peaks. The presence of copper nanoparticles facilitated the constructed of a nonenzymatic amperometric biosensor with a simple analysis procedure for the determination of acetylcholine. Another example of the importance of copper nanoparticles towards the construction of biosensor is seen in the work by Wang *et al.* 2008. An amperometric glucose biosensor was developed based on immobilization of glucose oxidase on a copper nanoparticles/chitosan/carbon nanotube modified glassy carbon electrode for the determination of hydrogen peroxidase. With the synergistic effect of both copper and carbon nanotubes towards the reduction of hydrogen peroxide in the chitosan matrix, an

amplified reduction current of hydrogen peroxide was observed. The developed biosensor exhibited excellent sensitivity, a lower detection limit, a fast response time, a wide linear range and perfect selectivity.

2.6.4 Polymers:

Traditional polymers take charge as conductors with a range of novel applications. Various experts are now in the process of combining expertise to study organic solids that exhibit remarkable conducting properties. A large proportion of organic compounds which effectively transport charge are divided into three groups such as; organometallic species, charge transfer complexes or ion radical salts and conjugated organic polymers. Recently a new class of intrinsically conducting polymers or electroactive conjugated polymers has just emerged. These materials exhibit interesting optical and electrical properties which were previously only found in inorganic systems. The key requirement for a polymer to become intrinsically electrically conductive is that there should be an overlap of molecular orbitals to allow the formation of delocalized molecular wave function. These molecular orbitals should be partially filled so that there is a free movement of electrons throughout the lattice (Gerard *et al.* 2002).

2.6.5.1 Conducting Polymers:

Conducting polymers contain π -electron backbones exerting charge mobility along the backbone which is responsible for their unusual electronic properties such as low energy optical transitions, electrical conductivity and high electron affinity (Gerard *et al.* 2002). The chemical bonding in conducting polymers is such that one unpaired electron is produced per carbon atom in the backbone of the polymer. The carbon atoms are π bonded in a sp^2p_z configuration where the orbital of successive carbon atoms overlap providing delocalization

of the electrons along the backbone of the polymer. The π bonds however are also highly susceptible to chemical, electrochemical oxidation or reduction processes. The formations of non-linear defects such as solitons, polarons and bipolarons produced during doping polymerization of a polymer, have made a contribution to the electrical conduction in these polymer materials. An increase in electrode modification as a result of these polymers has provided new and interesting properties, which have contributed to the wide application of conducting polymers. They have been applied in electrocatalysis, rechargeable batteries, membrane separation, optoelectronic, chromatography; solar cells (Ahuja *et al.* 2007; Malholtra *et al.* 2006) and most recently they have found great application in electrochemical biosensors. This is due to their mechanical flexibility, chemical specificities, tunable conductivities, high surface areas and easy processing (Zhu *et al.* 2006).



2.6.5.2 Synthesis of Conducting Polymers:

There are various available methods for the synthesis of conducting polymers, with oxidative coupling of the monomer being the most widely used technique. This technique involves the formation of a cation radical followed by another coupling to produce a di-cation and the repetition then leads to the polymer (Malholtra *et al.* 2006). With the advantage of simplicity and reproducibility, electrochemical synthesis has rapidly become the preferred method of synthesizing conducting polymers (Trivedi *et al.* 1996).

Electropolymerization is normally carried out in a single cell compartment where a three-electrode configuration is employed subjected to an electrochemical solution consisting of a monomer and a supporting electrolyte (in some case) all dissolved in an appropriate solvent which in most cases is an acidic. The polymerization can be carried out either potentiostatically where the potential is kept constant with a variation of the current with

time, or galvanostatically by keeping the current constant thereby monitoring the electrode potential. A three-electrode system employed during the polymerization comprises of a working electrode, a counter electrode and a reference electrode. Metals such as gold, platinum, carbon, nickel, titanium, palladium and most recently microelectrodes are used as working electrode and function as support systems for the polymer films. Counter electrodes on the other hand, supply the current required by the working electrode. A few commonly used counter electrodes include metallic foils of nickel, platinum and gold. Reference electrodes such as SCE, NCE, silver and mercurous sulfate establish stable potentials in electrochemical reactions and are used immersed in aqueous media (Ahuja *et al.* 2007).

Advantages associated with electrochemical polymerization reactions is that reactions can be carried out at room temperature by varying either the potential or the current with time, and the thickness of the film can be controlled. Free standing, homogenous and self doped films can be prepared through electrochemical synthesis. This method of polymer synthesis is an electro-organic process rather than an organic electrochemical one with great emphasis on the electrochemical process rather than organic synthesis. Electrochemical techniques employed in the polymerization of conducting polymers on the electrode surface are; pulse, galvanostatic, potentiostatic or sweeping techniques, with potentiodynamic techniques being more preferred because of their homogenous film production and strong adherence of the film to the electrode surface. Conductivity of the polymer is influenced by a number of factors including polaron length, the conjugation length, and the overall chain length and by the charge transfer to adjacent molecules (Gerard *et al.* 2002; Ahuja *et al.* 2007; Malholtra *et al.* 2006; Grennan *et al.* 2006; Trivedi *et al.* 1996).

2.6.5 Types of Conducting Polymers:

2.6.5.1 Polyaniline (PANI):

Polyaniline (PANI) is a conducting polymer of the semi-flexible rod polymer family that is electrically synthesized in the presence of an acidic medium by anionic oxidation of the aniline polymer onto an electrode surface. This attachment of PANI on the electrode surface can be done either by chemical or electrochemical means. Electrochemical polymerization is through galvanostatic, potentiostatic or potentiodynamic means, offering the potential to incorporate a wider range of dopant ions, since the reaction can be carried out in the presence of an appropriate electrolyte rather than a chemical oxidant. This procedure allows for film property control such as morphology and thickness allowing this polymer to be the most commonly used in biosensor preparation. For the polymer to retain its conductive property in the presence of non-acid media, it should be electrically neutral in the oxidized form of the polymer (Grennan *et al.* 2006; Naudin *et al.* 1998).

PANI is known for its very strong pH sensitivity existing between the half-oxidized emeraldine base (EB) and the emeraldine salt (ES) form of PANI, which is a reversible acid – base reaction. Therefore it is generally accepted that polyaniline has been observed to exist in three oxidation states namely: the half oxidized ES, the fully reduced leucoemeraldine (LEB) and the fully oxidized pernigraniline (PNB). In biosensor development, polyaniline serves as a point of attachment of bioactive compound such as enzymes, antibodies etc. as well as a means of electron transport between the electrode and the active site of the bioactive compound (Grennan *et al.* 2006; Lindfors *et al.* 2002; Slim *et al.* 2008).

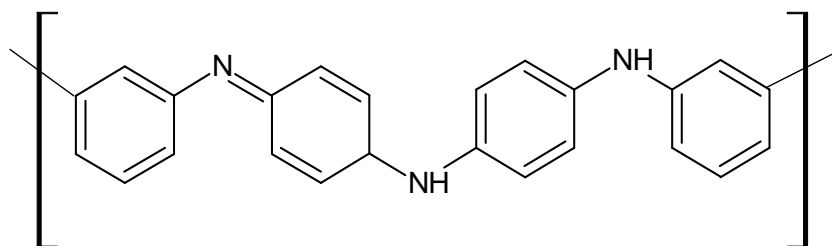


Figure 2.5: Structure of Polyaniline

2.6.6.2 Polypyrrole (PPY):

Polypyrrole is a conducting polymer which can be synthesized either chemically or electrochemically. Electrochemical synthesis of PPY is advantageous as the polymer produced is better conducting and the conductivity is stabilized for a long period of time (Lakard *et al.* 2007). Parameters such as the applied current or voltage can control the location, morphology, thickness and chemical composition of PPY. On the other hand, chemical synthesis involves the use of particular dopants during the synthesis. These dopants include heparin and heparin sulphate and their use is based on the fact that they have an ability to increase the conductivity of the polymer to a level of 10^3 S cm^{-1} . PPY polymerisation mainly occurs on platinum electrodes where a wide variety of enzymes are immobilized where the mechanism takes place at potentials above + 600 mV. There are a number of factors affecting the film including the crystallographic structure of the underlying electrode, the nature of the electrolyte, the speed of the potential of deposition of the polymer known as the scan rate, the concentration of the monomer, the presence of anions and polyanions or in some instances surfactants and finally the pH of the solution.

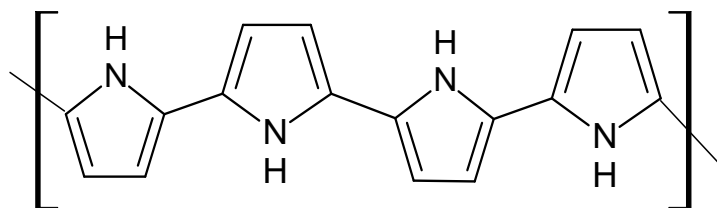


Figure 2.6: Structure of Polypyrrole

2.6.6.3 Polyindole (PND):

PND is another electroactive polymer, which is synthesized by anionic oxidation of indole in various electrolytes. Electrochemical oxidation of indole in LiClO_4 containing acetonitrile produces an electrochromic polymer film with good air stability (Pandey *et al.* 1998). PND is green in colour in its doped state and possesses an electrical conductivity in the range of 10^{-2} to $10^{-1} \text{ S cm}^{-1}$ depending on the nature of counter anion. The polymer is closely structured to polypyrrole and polyaniline however its conductivity is much lower although it has a better thermal stability than them. Derivatives of indole are found abundantly in natural plants and possess various physiological properties which are potential bioactive components.

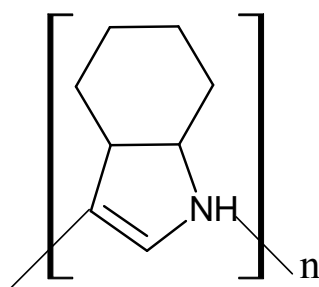


Figure 2.7: Structure of Polyindole

2.6.6.4 Polycarbozole (PCZ):

As opposed to the former discussed polymers, polycarbazoles are less studied. Their ability to exhibit some photoconductivity and electrochromic properties somehow makes them to be of particular interest. These polymers are synthesized by two main procedures. The first route is the most commonly used and involves the electrochemical or chemical oxidation of carbazole derivatives in solution (Fernandes *et al.* 1999). The second method employs the activation of the carbon-halogen bond of 3, 6-dihalogenated of the carbazole monomer in the presence of a zero valent nickel complex. The dehalogenative polycondensation can be carried either chemically or electrochemically and leads to well defined polymers with 3, 6-linkages. The electrochemical stability of this polymer has been observed to be less when compared to those of other conducting polymers however, this property can be enhanced by decreasing the poly disparity of the material (Tran-Van *et al.* 2002).

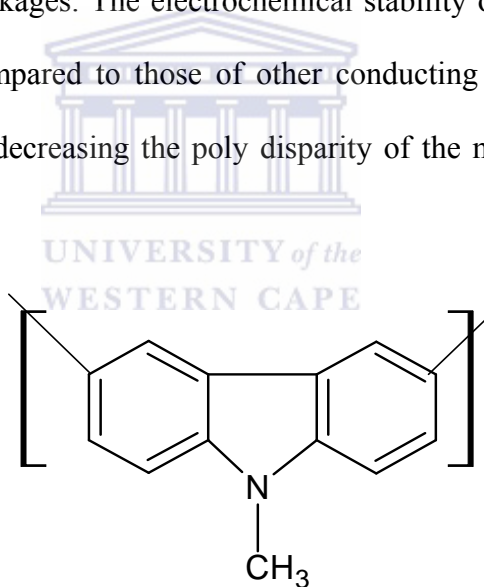


Figure 2.8: Structure of Polycarbozole

2.6.6.5 Poly(8-anilino-1-naphthalene sulphonic acid) (PANSA):

In this study 8-anilino-1-naphthalene sulfonic acid (ANSA) was polymerized in the presence of sulfuric acid to produce poly (8-anilino-1-naphthalene sulfonic acid) (PANSA) incorporating the enzyme cytochrome P450-2E1 (CYP2E1) for the detection of TB treatment drugs. ANSA belongs to a family of substituted naphthalene's which are normally used as fluorescent probes in the study of biologically active molecule structures. These compounds are moderately soluble in water but in most cases they prefer a more hydrophobic environment (Catena *et al.* 1989). Since ANSA is viewed as aniline substituted naphthalene we have successfully polymerised the aniline substituent with the assistance of the sulphuric acid substituent attached on gold electrode. Even though conducting polymers show admirable qualities towards the construction of nanobiosensors, we have also observed the role of silver nanoparticles coupled with PANSA towards the nanobiosensor construction.

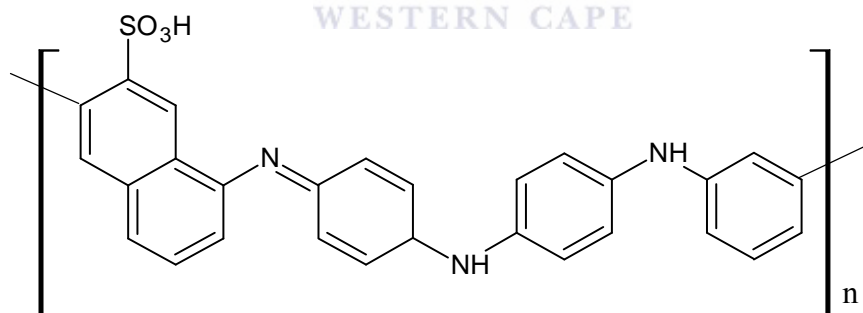


Figure 2.9: Structure of Poly(8-anilino-1-naphthalene sulphonic acid)

2.7 Tuberculosis:

Tuberculosis (TB) is a common and infectious disease caused by mycobacterium, mainly *Mycobacterium tuberculosis* (Wang et al. 2009). The infection is spread as exhaled drops in coughs, spits or sneezes from infected individuals, where the contagion may be caused by even a single bacterium ingested (Schweon *et al.* 2009). Primarily TB attacks the lungs as pulmonary TB but it can also affect the lymphatic system, central nervous system, the genitourinary system, the circulatory system, the gastrointestinal system, joints, bones and even the skin. This disease is said to be a slow-growing pathogen which has the unusual propensity to shut down its metabolism during adverse conditions such as, starvation or immune stress (Wang *et al.* 2009; Hernandez *et al.* 2008).

Treatment for TB uses antibiotics to kill the bacteria. These drugs are administered as part of the directly observed treatment short course (DOTS) therapy which is a multiple drug regimen given over a long duration of time. This regime employs an initial phase which is usually 2 months, with at least three drugs (Isoniazid (INH), Rifampin (RIF), and Pyrazinamide (PZA)) to reduce the bacterial load as rapidly as possible. This is followed by a continuation phase employing only two drugs (INH and RIF) given for 4 months (Eoh *et al.* 2009).

2.7.1 The Bacterial Cell:

The effectiveness and success antibacterial agents; which in this case are antituberculous drugs, owes much to the fact that these agents can act selectively against bacterial cells as opposed to animal cells. This is attributed to the fact that bacterial cells and animal cells differ both in structure as well as in their biosynthetic pathways. The following are some of the differences between bacterial and animal, also illustrated in Figure 2.10.

-
- ✓ Animal cells have defined nuclei while bacterial cells have none.
 - ✓ Bacterial cells are quite simple while animal cells contain a variety of structures such as mitochondria, endoplasmic reticulum; called organelles.
 - ✓ The biochemistry between these two cells is also very different. For instance bacterial cells are required to synthesize essential vitamins which animal cells are able to acquire intact from food. Bacterial cells therefore should have enzymes to catalyse these reactions but animal cells should not since the reactions are not required.
 - ✓ The bacterial cell has a cell membrane and a cell wall while an animal cell only has a cell membrane. The cell wall is crucial to the survival of bacterial cells as they have to survive a wide range of environments and osmotic pressures, whereas animal cells do not (Patrick *et al.* 2005).



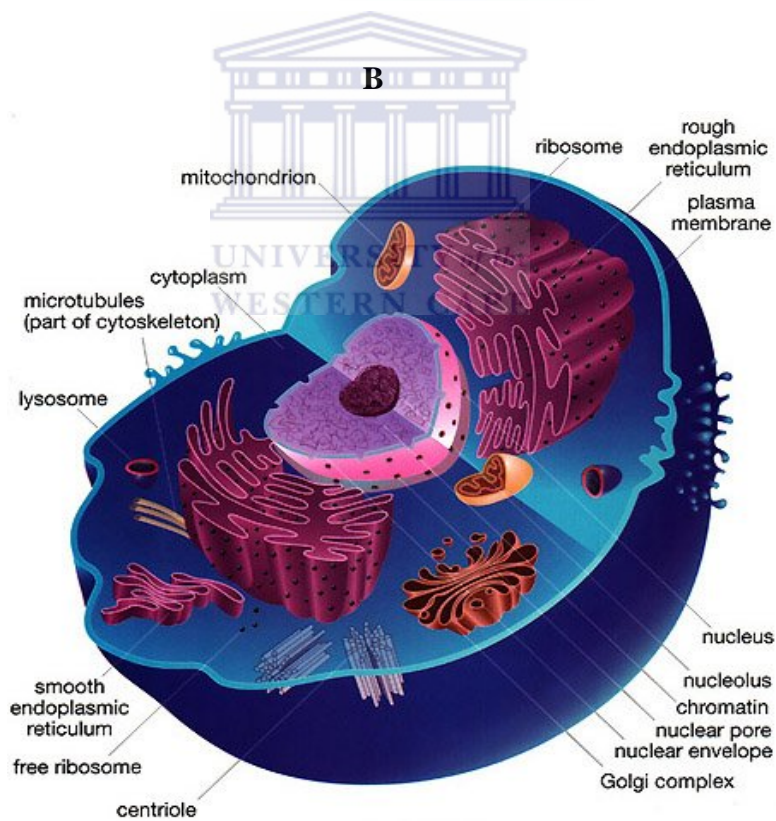
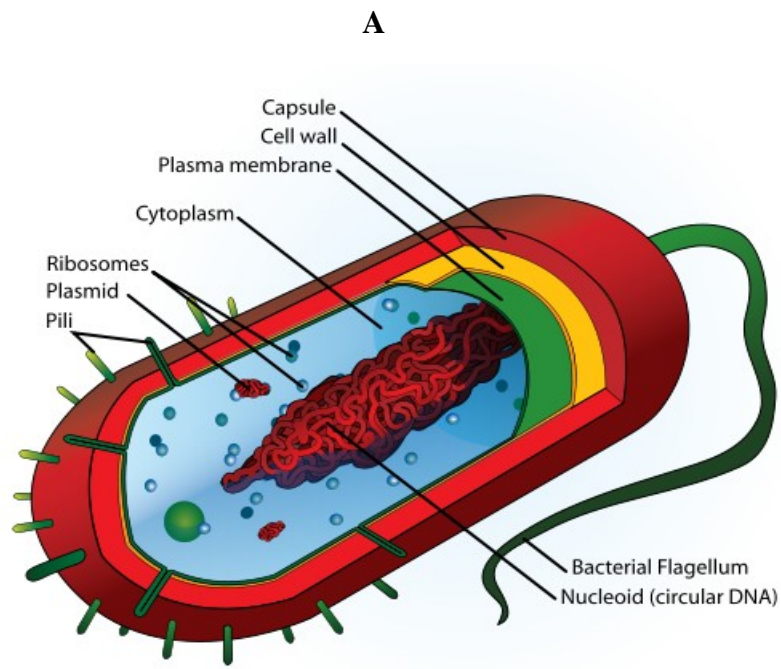


Figure 2.10: Structures of (A) bacterial cell
 (<http://rpscportal2010.blogspot.com/2010/09/component-of-bacterial-cell.html>) (B)
 animal cell (<http://www.animalport.com/animal-cells.html>)

2.7.2 Principles of Anti-tuberculous Therapy:

- To kill a large number of actively multiplying bacilli. Isoniazid achieves this successfully.
- They treat persisters; which are semi-dormant bacilli that metabolize slowly or intermittently. Rifampicin and pyrazinamide are the most efficacious.
- To prevent the emergence of drug resistance by multiple therapies to suppress single-drug-resistant mutants that may exist de nova or emerge during therapy. Isoniazid and rifampicin are the best in these cases.
- Combined formulations are used to ensure that poor compliance does not result in monotherapy with consequent drug resistance.

After extensive clinical trials, the following 3 facts have been found satisfactory:

- An unsupervised regime of daily dosage which comprise of isoniazid and rifampicin for 6 months including pyrazinamide for the first 2 months.
- A supervised (DOTS) regime for patients who cannot be relied on to complete treatment. This comprises of three weekly doses of isoniazid and rifampicin for 6 months, and pyrazinamide for the first two months. As opposed to the unsupervised regime, isoniazid and pyrazinamide are given in high dosages. However, with both regimes, ethambutol or streptomycin is also added for the first 2 months to prevent the likelihood of drug resistance or if the patient is severely ill with extensive active lesions.
- A low cost and even free (in developing countries), yet effective, regime favoured by most if not all affected countries comprises the supervised regime; daily administration of isoniazid, rifampicin, pyrazinamide and either ethambutol or streptomycin.

Although the DOTS regime has contributed significantly towards the falling incidences of TB, incomplete implementation of the campaign has also been a major cause of the high occurrences of the drug resistant strains of *Mycobacterium tuberculosis* coupled with the spread of HIV/Aids in tuberculosis-endemic regions (Wallis *et al.* 2009; Zvavamwe *et al.* 2009). This stems from the fact that patients with fully susceptible TB develop secondary resistance during the TB therapy as a result of inappropriate dosing of treatment, inadequate treatment, not taking the prescribed regimen appropriately or using low quality medication. Multidrug-resistant TB (MDR-TB) defined as an isolate showing resistance to the two most effective first-line TB drugs INH and RIF and the extensively drug resistant (XRD-TB) defined as an isolate showing resistance to INH, RIF and three or more of the six classes of second line drugs, are phenomena threatening to destabilize TB control (Eoh *et al.* 2009, Castagnolo *et al.* 2009, Balganes *et al.* 2008). MDR-TB and XRD-TB are more difficult to treat than sensitive TB since they require the administration of expensive and less effective second-line TB drugs for longer treatment duration than first line drugs (Eoh *et al.* 2009). A few second-line TB drugs are listed in Table 2.7. It is therefore acknowledged that new approaches are required in order to promptly address the issue of patients falling ill as a result of inappropriate dosing of treatment and inadequate treatment administration.

Table 2.7: List of first and second-line antimicrobials used in the treatment of tuberculosis

Drug	Typical Adult-Daily Dosage
First-line Drugs (In appropriate order of preference)	
Isoniazid	300 mg/d
Rifampicin	600 mg/d
Pyrazinamide	25 mg/kg/d
Ethambutol	15-25 mg/kg/d
Streptomycin	15 mg/kg/d
Second-line Drugs (In appropriate order of preference)	
Amikacin	15 mg/kg/d
Aminosalicylic acid	8-12 g/d
Capreomycin	15 mg/kg/d
Ciprofloxacin	1500 mg/d, divided
Clofazimine	200 mg/d
Cycloserine	500-1000 mg/d, divided
Ethionamide	500-750 mg/d
Ofloxacin	600-800 mg/d
Rifabutin	300 mg/d

2.7.3 Isoniazid (INH):

Isoniazid (Figure 2.11) was introduced in 1952, and is the most active tuberculostatic drug against susceptible strains. INH is a hydrazide of isonicotinic acid and is a small simple molecule (molecular weight 137 g/mol), a white crystalline powder that is freely soluble in water. Commercially this drug is known as Laniazid or Nydrazid depending on the country of purchase. The structure of isoniazid is shown below.

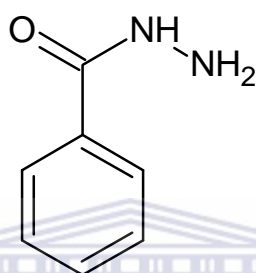


Figure 2.11: Structure of Isoniazid.

2.7.3.1 Mechanism of Action and Basis of Resistance:

Research has shown that INH inhibits most tubercle bacilli in a concentration of $\mu\text{g/mL}$ or less and is bactericidal for effective in actively growing tubercle bacilli. INH inhibits the synthesis of mycolic acids, which are essential components of mycobacterial cell walls. The mechanism of action of INH is not yet known. INH apparently combines with an enzyme that is peculiar to INH-susceptible strains of *Mycobacterium Tuberculosis*, displaying a pigment precursor molecule and leading to a variety of disorders in cellular metabolism.

Resistance is associated with overproduction of the *inhA* gene and with mutation of *katG*, which encodes mycobacterial catalase. The loss of catalase activity which is the result of INH resistance is not yet completely understood, but is assumed that catalase maybe important for an activation step permitting INH to interact with its target protein. On the other

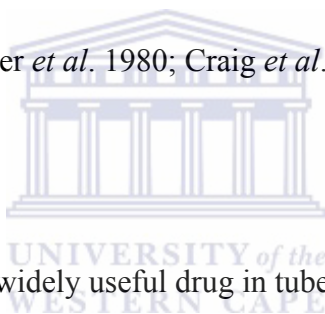
hand, *inhA* overproducers express low level resistance and cross-resistance to other antituberculous drugs such as rifampicin and ethambutol, while KatG mutants express high-levels INH resistance and are not cross-resistant to other antituberculous drugs. The simultaneous use of any 2 of these drugs markedly delays the emergence of resistance to one of them (Meyer *et al.* 1980; Craig *et al.* 1990). Resistant mutants tend to occur in susceptible mycobacterial populations and tend to be selected out both in vitro and in vivo in the presence of INH with a frequency of 1 bacillus in 10^6 . Since tuberculous lesions often contain more than 10^8 tubercle bacilli, with resistant mutants readily selected out if INH is administered solely. However, administration of a second independently acting drug, to which resistance also merges at a frequency of 1 in 10^6 to 10^8 , is effective. The odds that a bacillus is resistant to both drugs approximately 1 in $10^6 \times 10^6$, or 1 in 10^{12} , which is several orders of magnitude more than the number of infecting organism. Singular drug therapy with INH and failure to use INH in combination with other drugs to which the strains are susceptible has led to the 20-30 % prevalence of INH resistance in South Africa (Meyer *et al.* 1980; Craig *et al.* 1990).

2.7.3.2 Pharmacokinetics:

INH is readily absorbed from the gastrointestinal tract. The administration of a 300 mg oral dose; with 5 mg/kg in children; results in peak concentrations of 3 - 5 $\mu\text{g/mL}$ within 1 - 2 hours. INH diffuses readily into all body fluids and tissues, including the central nervous system and cerebrospinal fluid with ranging between 20 % and 100 % of simultaneous serum concentration.

Metabolism of INH, particularly the acetylation by the liver is under genetic control. Two groups of people are recognized through acetylation; the 'slow' and the 'rapid' acetylators of the drug. The 'slow' acetylators appear to possess autosomal homozygous

recessive hereditary traits, while 'rapid' acetylators show intermediate dominance. Therefore, the average concentration of INH in the plasma of 'rapid' acetylators is about one-third to one half of that in 'slow' acetylators with average half-lives of less than 1 hour and 3 hours, respectively. More rapid clearance of INH by rapid acetylators is of no therapeutic consequence when the drug is administered daily, but sub-therapeutic concentrations may occur if the drug is administered as a once-daily dose. INH is excreted mainly in the urine, partly as unchanged drug and partly as the acetylated form and partly as other conjugates. The percentage of unchanged INH in urine of 'slow' acetylators is higher; while the percentage of the acetylated form is higher in the 'rapid' acetylators. The dose need not be adjusted in cases of renal failure, but a third to a half of the normal dose is recommended in severe hepatic insufficiency (Meyer *et al.* 1980; Craig *et al.* 1990).



2.7.3.3 Clinical Uses:

INH is probably the most widely useful drug in tuberculosis. The usual dosage of INH is 5- 10 mg/kg/d, with a typical adult dose being 300 mg given once daily. In cases of serious infections up to 10 mg/kg/d may be used. However, where cases of malabsorption develop, or in children, a 15 mg/kg dose, or 900 mg may be used in a twice weekly regime in combination with a second anti-tuberculous drug. INH is usually given by mouth but can be given parentally in the same dosage (Meyer *et al.* 1980; Craig *et al.* 1990).

2.7.3.4 Adverse Reactions

Severity and incidences of untoward reactions to INH are related to dosage and the duration of administration (Meyer *et al.* 1980; Craig *et al.* 1990).

2.7.3.5 Allergic Reactions

Fever and skin rashes are seen occasionally but drug-induced systematic lupus erythematosus have also been reported (Meyer *et al.* 1980; Craig *et al.* 1990).

2.7.3.6 Direct Toxicity

The most common toxic effects attributed to INH are on the peripheral and central nervous system; also known as peripheral neuropathy. These toxic reactions include insomnia, peripheral neuritis, muscle twitching, restlessness, convulsions, urinary retention and psychotic episodes. Peripheral neuropathy is observed in 10 – 20% of patients administered 5 mg/kg/d but is infrequently seen with the standard 300 mg adult dose. This condition is more likely to occur in ‘slow’ acetylators and patients with predisposing conditions such as malnutrition, alcoholism, AIDS, uraemia and diabetes (Meyer *et al.* 1980; Craig *et al.* 1990). INH-induced hepatitis has however been found to be the most frequent major toxic effect. Clinical hepatitis with loss of appetite, vomiting, nausea, jaundice occurs in 1 % of INH recipients and can be fatal, especially if the drug is not discontinued. The risk of hepatitis depends on age. It occurs rarely under age 20, in 0.3 % of those from aged 21 – 35, 1.2 % of those aged 36 – 50, and 2.3 % for those aged 50 and above. The risk of hepatitis has been seen to be much higher among alcoholic, post partum period and possibly during pregnancy (Meyer *et al.* 1980; Craig *et al.* 1990).

2.7.4 Rifampicin (RIF):

Rifampicin (Figure 2.12) commercially known as either Rifadin, Rimactane or Riadin; is a large complex (with Molecular weight 823 g/mol) semisynthetic derivative of rifamycin, which is an antibiotic produced by *Streptomyces mediterranei*. In vitro this drug is active against gamma-positive and gamma-negative cocci, some enteric bacteria, mycobacteria and *Clamydia*. Susceptible organisms are inhibited by less than 1 µg/mL but resistant mutants are present in all microbial populations at a frequency of approximately 1: 10⁶. The administration of rifampicin as a single drug is responsible for the selection for these highly resistant organisms. There is no documented evidence to suggest any cross-resistance to RNA other to other classes of antimicrobial drugs, but there is cross-resistance to other rifamycin derivatives such as rifabutin (Bennet *et al.* 2007; Meyer *et al.* 1980; Craig *et al.* 1990).

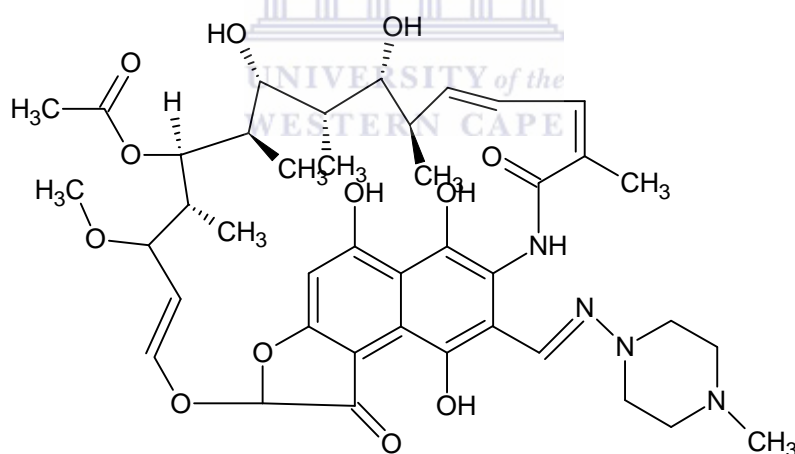


Figure 2.12: Structure of Rifampicin

2.7.4.1 Mechanism of Action, Resistance and Pharmacokinetics:

RIF forms strong bonds with the β subunits of bacterial DNA-dependant polymerase and thereby inhibits RNA synthesis. Resistance results from one of several possible point mutations that prevent binding of RIF to RNA polymerase. Human RNA polymerase does

not bind rifampicin and is not inhibited by it. Therefore since RIF is bactericidal for mycobacteria, it readily penetrates most tissues and into phagocytic cells. This drug is capable of killing organisms that are poorly accessible to many other drugs, such as intracellular organisms and those sequestered in abscesses and lung cavities.

RIF is well absorbed in the body after oral administration and excreted mainly through the liver into bile. It then undergoes enterohepatic recirculation, with the bulk excreted as a deacylated metabolite in faeces and a small amount in the urine. With oral doses of 600 mg daily serum levels exceed 5 µg/mL for 4 – 6 hours and urine levels may be 10 – 100 times higher. In tuberculosis, a single oral dose of RIF, usually 600 mg daily (10 – 20 mg/kg), is administered together with INH, ethambutol and another antituberculous in order to delay the emergence of rifampicin-resistant mycobacteria (Bennet *et al.* 2007; Meyer *et al.* 1980; Craig *et al.* 1990).



2.7.4.2: Mycobacterial Infections:

In some short-course therapies, 600 mg of RIF is given twice weekly. RIF is also effective in some atypical mycobacterial infections as well as in leprosy when used together with sulfone. This drug is sometimes used as an alternative to INH prophylaxis for patients who are unable to take INH or who have been in close contact with a case of active tuberculosis caused by an INH-resistant, rifampicin susceptible strain (Bennet *et al.* 2007; Meyer *et al.* 1980; Craig *et al.* 1990).

2.7.4.3 Other Indications:

RIF is used in a number of other clinical situations. RIF, 20 mg/kg/d for 4 days is used as prophylaxis in contacts of children with *Haemophilus influenzae* type b disease. Also, an oral dosage of 600 mg twice daily for 2 days can eliminate meningococcal carriers. RIF

together with a second-line drug is used to eradicate staphylococcal carriers. This combination therapy is also used in the treatment of serious staphylococcal infections such as osteomyelitis and prosthetic valve endocarditis (Bennet *et al.* 2007; Meyer *et al.* 1980; Craig *et al.* 1990).

2.7.4.4 Adverse Reactions:

RIF manifests as a harmless orange colour in urine, tears and contact lenses. Occasional adverse effects also include rashes, nephritis and thrombocytopenia. This drug commonly causes light chain proteinuria. If RIF is administered less often than twice weekly, RIF causes flu-like symptoms characterized by chills, fever, anaemia, and thrombocytopenia and sometimes associated with acute tubular necrosis. RIF induces microsomal enzymes (cytochrome P450), which increases the elimination of numerous other drugs including methadone, anticoagulants, contraceptives and some anticonvulsants (Bennet *et al.* 2007; Meyer *et al.* 1980; Craig *et al.* 1990).

2.7.5 Ethambutol (ETH):

This is a synthetic, water-soluble, heat-stable compound, the dextro isomer of the structure shown below (Figure 2.13), is dispensed as the dihydrochloric salt (Bennet *et al.* 2007; Meyer *et al.* 1980; Craig *et al.* 1990). Commercially, ethambutol is referred to as Myambutol.

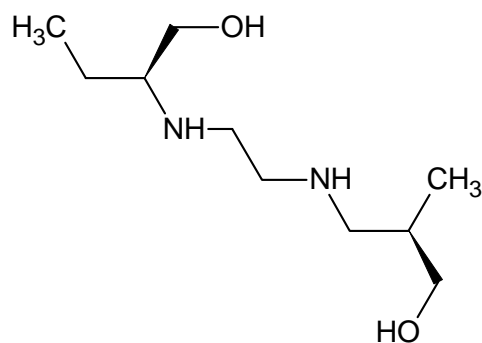


Figure 2.13: Structure of Ethambutol

2.7.5.1 Mechanism of Action, Resistance and Pharmacokinetics:

Susceptible strains of mycobacterium tuberculosis and other mycobacteria are inhibited in vitro by ETH with concentration 1 - 5 µg/mL. ETH functions by inhibiting the synthesis of arabinogalactan, an essential component of the mycobacterial cell wall. It enhances the activity of lipophilic drugs such as RIF that cross the cell wall primarily in lipid domain of this structure.

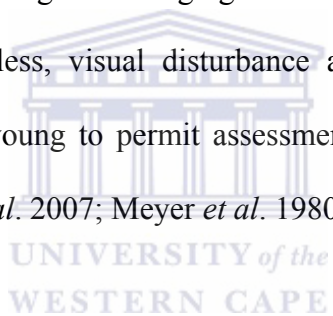
ETH is well absorbed the gut following ingestion of 25 mg/kg. A blood level peak of 2 – 5 µg/mL is reached in 2 – 4 hours with about 20 % of the drug excreted in faeces and 50 % in urine in unchanged form. In cases of renal failure, ETH accumulates and therefore drug dose should be reduced in half if creatine clearance is less than 10 mL/min. ETH is able to cross the blood-brain barrier only if the meninges are inflamed. Cerebrospinal fluid is highly variable, ranging from 4 – 64 % of serum levels in the setting of meningeal inflammation. Similarly to all antituberculous drugs, resistance to ETH emerges at a very rapid rate when the drug is administered alone. Therefore, ETH is always administered in combination with other antituberculous drugs. As of date, there is no known documentation about the mechanism of resistance (Bennet *et al.* 2007; Meyer *et al.* 1980; Craig *et al.* 1990; Clayton *et al.* 2001).

2.7.5.2 Clinical Uses:

ETH hydrochloride, 15 – 25 mg/kg, is usually given as a single daily dose in combination with rifampicin and INH. Higher doses are however required for the treatment of tuberculosis meningitis. The dose of ETH is 50 mg/kg when a twice-weekly dose schedule is used (Bennet *et al.* 2007; Meyer *et al.* 1980; Craig *et al.* 1990).

2.7.5.3 Adverse Reactions:

The most common serious adverse event associated with ETH is retro-bulbar neuritis resulting in loss of visual acuity and red-green blindness. This is a dosage-related side effect and is more likely to occur at a dosage of 25 mg/kg/d which is continued for several months. With doses of 15 mg/kg/d or less, visual disturbance are very rare. ETH is relatively contraindicated in children too young to permit assessment of visual acuity and red-green colour discrimination (Bennet *et al.* 2007; Meyer *et al.* 1980; Craig *et al.* 1990).



2.7.6 Pyrazinamide (PYR):

This compound is a relative of nicotinamide (Figure 2.14), stable, slightly soluble in water and quite inexpensive and whose brand name is Rifter. At neutral pH, PYR is inactive *in vitro*, but at pH 5.5 it strongly inhibits the growth of tubercle bacilli within cells in concentrations of 20 µg/mL. The drug is taken up by macrophages and kills bacilli residing within this acid environment (Bennet *et al.* 2007, Craig *et al.* 1990; Clayton *et al.* 2001).

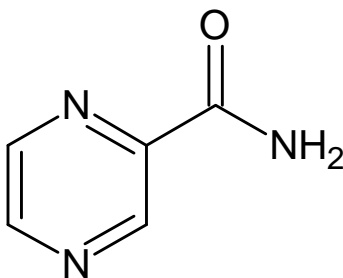


Figure 2.14: Structure of Pyrazinamide

2.7.6.1 Clinical Uses:

PYR is well absorbed from the gastrointestinal tract and widely distributed in body fluids as well as inflamed meninges with serum concentrations of 30 – 50 µg/mL achieved with dosages of 25 mg/kg/d. The half-life of 12 - 24 hours permits once-daily dosing, while a 50 -70 mg/kg dose is used for twice or thrice-weekly treatment regimes. Tubercle bacilli develop resistance to PYR readily, but there is no evidence of cross-resistance with INH or other antituberculous drugs. As a result of this, PYR is used in combination with other drugs such as ciprofloxacin or ofloxacin for the treatment of active disease and exposure to multidrug- resistant bacilli (Bennet *et al.* 2007, Craig *et al.* 1990).

2.7.6.2 Adverse Reactions:

Major adverse effects of PYR include hepatotoxicity (1 – 5 % of patients), drug fever, vomiting, hyperuricemia and nausea. PYR should always be considered only as part of a combined drug regimen in patients harbouring tubercle bacilli resistant to first choice drugs (Bennet *et al.* 2007, Craig *et al.* 1990).

2.8 Detection of Tuberculosis Treatment Drugs:

Owing to the widespread and therapeutic importance of tuberculosis treatment drugs, considerable attention has been paid to construct rapid and sensitive analytical techniques for their determination either in pharmaceutical preparation, biological fluids or in their respective pure forms. Among these techniques, the most cited are those involving titrimetry, fluorimetry, chemiluminescence, high performance liquid chromatography, capillary electrophoresis and electroanalytical methods (Jena *et al.* 2010; Bergamini *et al.* 2010).

Electroanalytical techniques are of particular advantage because of their simplicity, low-cost, good sensitivity, precision and rapidity of real time detection. Literature suggests

that there are a few biosensors available for the analytical detection of the TB drugs pyrazinamide, ethambutol and rifampicin. An example is a crayfish walking leg neuronal biosensor which was constructed by Leech and Rechnitz, 1993 for the selective determination of pyrazinamide and selected anesthetics.

In a study by Lomillo *et al.* 2003, a rifampicin biosensor was developed on platinum electrode using pyrrole and horseradish peroxidase (HRP) in the presence of LiO_4 at constant H_2O_2 concentration. This biosensor was applied to the determination of rifampicin in pharmaceutical preparations and biological samples. A study by Girousi *et al.* 2004 also reports a rifampicin biosensor. A DNA modified carbon paste electrode was applied in the study of the interaction of rifampicin and DNA in solution and at the electrode surface. A β -cyclodextrin (β -CD)-based sensor was also developed for a simple and sensitive determination of rifampicin. β -CD was immobilized onto a Pt electrode by means of pyrrole electropolymerization. RIF was also deposited on the surface of the modified electrode through complex formations and quantified amperometrically (Lomillo *et al.* 2005).

Interestingly enough, particular interest has been placed on isoniazid allowing it to be the most, extensively studied drug among all the other TB drugs. This is due to the fact that in most cases isoniazid can be quantified without the use of any special reagents (Jena *et al.*, 2010). Ghomeim *et al.* 2003 explored this phenomenon where he studied the polarographic reduction of isoniazid using square wave adsorptive cathodic stripping method where two irreversible cathodic waves were observed at two different solutions. This interaction suggested the possibility of applying this method for the determination of isoniazid in pharmaceutical formulations and human body fluids. In a study carried out by Hamman *et al.* 2004, the electrochemical oxidation of isoniazid by cyclic and square wave voltammetry was investigated at a carbon paste electrode. One irreversible anodic peak was observed which was attributed to the oxidation of the amide group of isoniazid. Co-workers M.S.M. Quintino

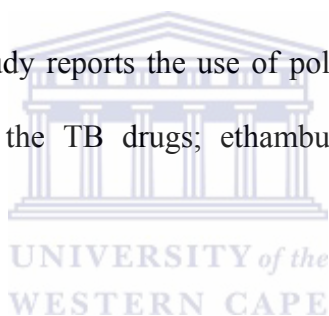
and L. Agnes, 2006, presented a direct determination of isoniazid based on the electrochemical oxidation of the substrate at a glassy carbon electrode in an alkaline medium using a batch injection analysis procedure.

A major concern with electrochemical techniques is the high overpotential required for the oxidation of isoniazid associated with unmodified electrodes. Traditionally, mediator and polymer based electrodes have been used to decrease the over-potential; however the lack of long-term stability is one of the disadvantages associated with mediator modified electrodes. The use of metal nanoparticles on electrode surfaces for the oxidation of isoniazid have also been explored however, they require high over-potentials as large as 1 V and voltammetric responses are not well-defined (Jena *et al.* 2010). To curb this problem, scientists have developed techniques capable of manipulating nanomaterials and biopolymers to allow for better oxidation processes and the attachment of biological components (Crespilho *et al.* 2009).

A nafion-ordered mesoporous carbon modified electrode with a low over-potential for the electrochemical oxidation of isoniazid was successfully developed by Yan *et al.* 2011. The method suggested the modified electrode to be a potential candidate for a stable and efficient electrochemical sensor for the determination of isoniazid in tablets. A high sensitivity of 3.1 A/ μ M, a low detection limit of 8.4×10^{-8} μ M and a wide linear range was provided by the biosensor. Yang *et al.* 2008 successfully demonstrated a poly (amidosulfonic acid) modified glassy carbon electrode for the determination of isoniazid in pharmaceuticals. The modified electrode showed excellent electrocatalytic effect of injection and tablet isoniazid. The proposed procedure showed that the good properties associated with modified electrodes such as easy of fabrication, reproducibility, stability and high sensitivity are promising for the measurement of isoniazid in vivo and in vitro.

Composites of conducting polymers and inorganic nanoparticles in particular often exhibit improved physical and chemical properties over their single-component counterparts, and hence their use is highly recommended (Huang *et al.* 2009; Nabid *et al.* 2008). In electrochemical devices where preservation of biological activity at these polymer/metal interfaces is priority towards the efficient electrode design, the charge transfer between the electrode and enzyme is usually fast and reversible (Liu *et al.* 2009; Mu *et al.* 2009; Cresphilho *et al.* 2009; Wang *et al.* 2006). This makes the concept of modified electrodes very popular in the electroanalytical area as there has been a gradual improvement in sensitivity, selectivity and reactivity of electrode reactions in many applications (Yan *et al.* 2011).

For the first time, this study reports the use of polymer/metal enzyme biosensor for the analytical determination of the TB drugs; ethambutol, isoniazid, pyrazinamide and rifampicin.



2.8 Electrochemical Techniques:

Electrochemistry is the study of chemical and physical events as a result of electrons through oxidation and reduction reactions. Not only is electrochemistry a cheap and efficient way of dealing with some of the most common extant pollutants, it is also showing itself to be a greener alternative to several other forms of cleanup now available. Advantages associated with using electrochemistry include versatility, energy efficiency, safety, selectivity, environmental compatibility, cost effectiveness and amenability to automation. Although there is a tremendous interest in using electrochemistry to develop novel and healthier ways of manufacturing and using chemical products, there is a broader need to address pollution, waste and deteriorating health issues produced by non-green processes of the past. Because electrochemistry can generate charged species; whether through oxidation

or reduction at will, and can deal with solid, liquid, or gaseous pollutants, it only takes a scientist's imagination to develop new methods of use (Lesney *et al.* 2002).

Electrochemical techniques are among the most widely used current applications in waste treatment, environmental protection and medical diagnostics devices. The following section describes a few commonly used electrochemical techniques.

2.9.1 Sweep Techniques:

Potential sweep techniques such as cyclic voltammetry (CV) have been applied to an increasing range of systems over the past couple of decades. The mathematical descriptions of these techniques have been sufficiently developed to enable kinetic parameters to be determined for a variety of reaction and mechanisms. This technique indicates the potentials at which processes occur while from the sweep rate dependence, the involvements of coupled homogeneous reactions are identified and complications of absorption are detected. Because of these capabilities, CV is nearly always the technique of choice when studying a system for the first time (Greef *et al.* 1990; Monk *et al.* 2002).

Voltammetry is a microanalysis technique analyzing only small proportions of a given solution at solid working electrodes. In Linear Sweep Voltammetry (LSV); which is the simplest of these techniques, the potential is swept from an initial potential E_1 , to a final potential E_2 at a known scan rate before halting the potential. Figure 2.15 (<http://www.cartage.org.lb/en/themes/sciences/Chemistry/Electrochemis/Electrochemical/CyclicVoltammetry/CyclicVoltammetry.htm>) shows a linear sweep voltammogram for the reduction of a solution phase analyte illustrated as a function of scan rate (Greef *et al.* 1990; Monk *et al.* 2002).

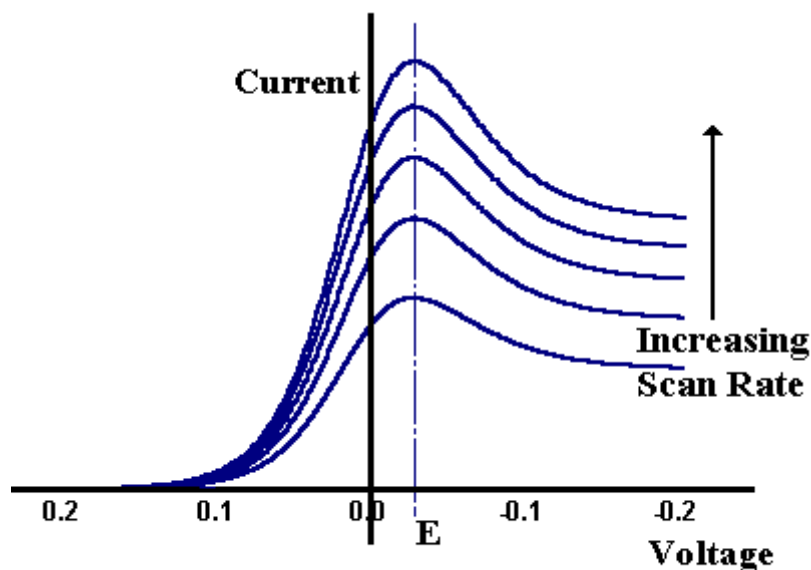


Figure 2.15: Linear sweep voltammogram for the reduction $O + ne^- \rightarrow R$, at a solid electrode, shown as a function of the scan rate
 (<http://www.cartage.org.lb/en/themes/sciences/Chemistry/Electrochemis/Electrochemical/CyclicVoltammetry/CyclicVoltammetry.htm>)

A more useful technique is CV where the potential is similarly swept from initial potential E_1 , however at the end of the linear sweep, the potential scan is reversed rather than terminated. The potential sweep may be reversed again, halted or continued further to another value, E_3 . In an experiment where a reverse in the potential occur, then the potential at which the reverse occurs is known as the switch potential (E_2). The scan rate between E_1 and E_2 is the same as that between E_2 and E_1 while the values of the scan rate v_{forward} and v_{reverse} are always written as positive values.

When studying a system for the first time using CV, it is common to start by carrying out quantitative experiments so as to get a feel for the system before proceeding semi-quantitative and finally quantitative ones. In a study voltammograms are recorded over a wide range of sweep rates and various values of potential; as seen in Figure 2.16 (http://www.thefullwiki.org/Cyclic_voltammetry). Commonly there are several peaks of

similar shape on either sides of the voltammogram, however if fully reversible, their magnitudes can be identified. These peaks indicate either oxidation or reduction taking place at the forward or reverse scan. Just as other forms of voltammetry, the magnitude of the current (I) is proportional to the concentration and this parameter is usually the most commonly observed.

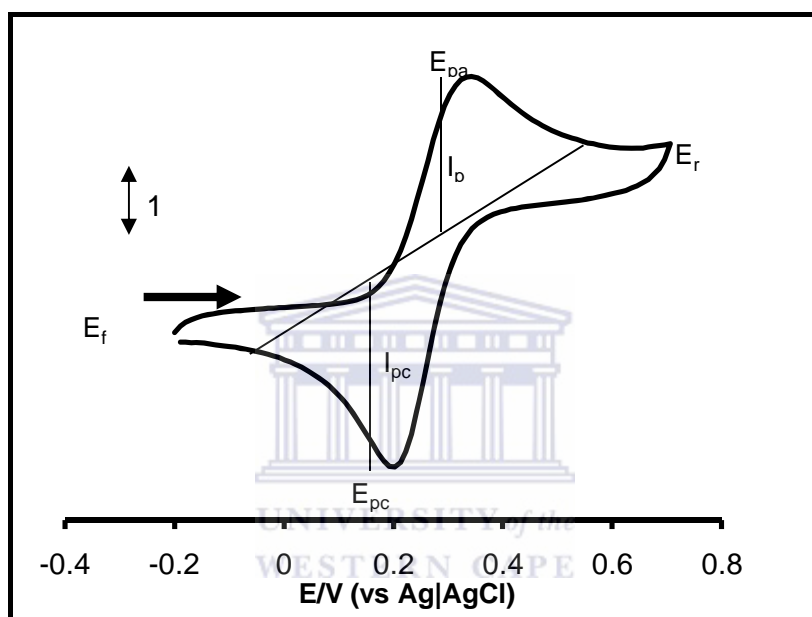


Figure 2.16: Schematic cyclic voltammogram for the reduction of an analyte at a solid electrode (http://www.thefullwiki.org/Cyclic_voltammetry).

2.9.2 Pulse Voltammetry:

Pulse voltammetric techniques have been developed largely to provide enhanced sensitivity in analytical application. Pulse methods were developed in the 1950s to improve the sensitivity of polarographic measurements made by pharmaceutical companies. Presently two techniques dominate the analytical field; Differential and Normal Pulse Voltammetry. Pulse techniques are based on rate decay differences of the charging and the faradaic currents following a potential step (or "pulse"). The rate of decay of the charging current is considerably faster than the decay of the faradaic current (Greef *et al.* 1990; Monk *et al.*

2002). What happens is that the charging current decays exponentially, while the faradaic current (usually for a diffusion-controlled current) decays as a function of $1/(\text{time})^{1/2}$. At a time of $5R_uC_{dl}$ after the potential step, the charging current is negligible. R_uC_{dl} is known as the time constant for the electrochemical cell, and it ranges from μs to ms . After this time, the measured current consists solely of the faradaic current; that is, measuring the current at the end of a potential pulse allows discrimination between the faradaic and charging currents (Greef *et al.* 1990; Monk *et al.* 2002).

The important parameters for pulse techniques are as follows:

- The height of the potential pulse is known as the pulse amplitude which may or may not be constant depending upon the technique in question.
- The duration of the potential pulse is also known as the pulse width.
- The sample period is the time at the end of the pulse during which the current is measured.
- The pulse period or drop time must also be specified depending on the pulse technique used. This parameter defines the time required for one potential cycle, and is particularly significant for pulse voltammetry.

Differential Pulse Voltammetry (DPV); Figure 2.17

(http://www.basinc.com/mans/EC_epsilon/Techniques/Pulse/pulse.html) can be considered as a derivative of linear sweep LSV with a series of regular potential pulses superimposed on the potential sweep or stair steps. The current is measured immediately before every change in the potential, while the current difference is plotted as a function of potential (Greef *et al.* 1990; Monk *et al.* 2002).

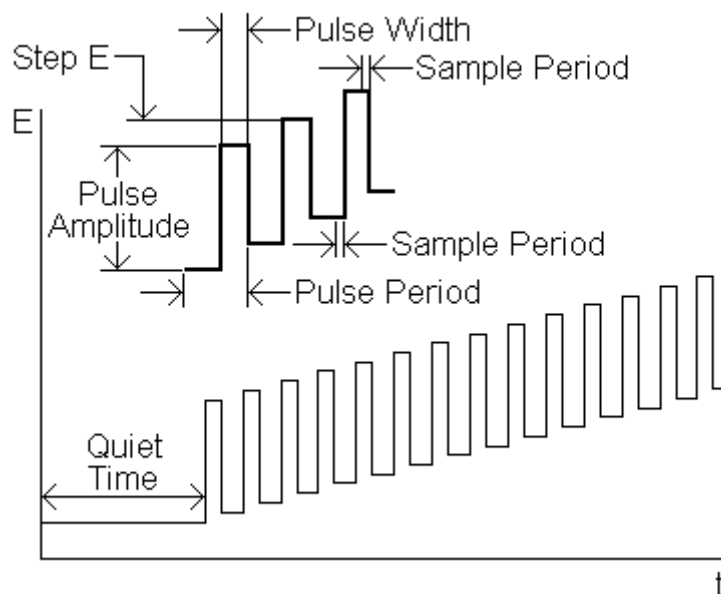


Figure 2.17: Potential wave form for Normal and Differential Pulse Voltammetry (http://www.basinc.com/mans/EC_epsilon/Techniques/Pulse/pulse.html)

On the other hand, in Normal Pulse Voltammetry (NPV) the current resulting from a series of ever larger potential pulses is compared with the current at a constant baseline potential and is chosen to be sufficiently anodic for currents to be zero (Greef *et al.* 1990; Monk *et al.* 2002).

2.9.3 Square wave voltammetry (SWV):

Just like DPV, Square Wave voltammetry (SWV) is a derivative of linear sweep voltammetry. As mentioned before LSV involves the measurement of the current at a working electrode while the potential between the working electrode and a reference electrode is swept linearly with time. In SWV, a potential waveform is applied to the working electrode while pairs of current are measured for each wave cycle. The oxidation or reduction of involved species is observed as peaks in these current signals at potentials where the species began to be oxidized or reduced (Chang *et al.* 2010; Shumyantseva *et al.* 2005). A

SWV votammogram illustrates the difference between these two currents as a function of the applied potential as illustrated in Figure 2.18 (http://www.basinc.com/mans/EC_epsilon/Techniques/Pulse/pulse.html)

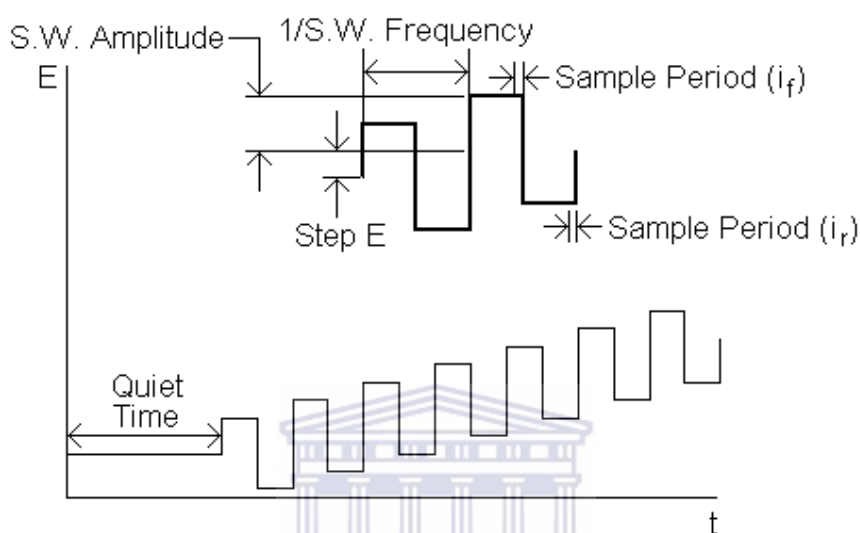


Figure 2.18: Potential wave form for Square Wave Voltammetry (http://www.basinc.com/mans/EC_epsilon/Techniques/Pulse/pulse.html)

2.9.4 Electrochemical Impedance Spectroscopy (EIS):

Electrochemical impedance spectroscopy (EIS) has been part of the electrochemistry community for more than a century and is one of the most effective techniques for studying the properties at the electrode/electrolyte interface. In an electrochemical system the electrode/electrolyte interface is fully characterized when impedance measurements have been made in a whole range of frequencies. Unfortunately, to make such measurements takes relatively long, somewhere between about 30 min and a few hours, depending on the frequency range and the stability of the electrochemical system because the frequency needs to be scanned for the measurements. Often by the time the impedance measurements are

made the electrochemical system has been changed completely in the full frequency range, particularly at a given potential. Therefore in EIS, the system under study is exposed to a sinusoidal voltage of small amplitudes (5 - 10 mV) with variable frequency (0.1 Hz - 100 kHz), and the resulting change in impedance (Z) is measured. The imaginary impedance (Z_{Im}) and the real impedance (Z_{Re}) are recorded as a function of the applied frequency with the result that the Nyquist plots (Z_{Im} vs Z_{Re}) is fitted to simple electrical equivalent circuits (EECs). By fitting EECs, important information of the interface such as solution resistance (R_s), electron transfer resistance (R_{ct}), Warburg element (R_w) and double layer capacitance (C_{dl}), are measured (Chang *et al.* 2010; Shumyantseva *et al.* 2005).

No matter how well the measurement is made, the current flowing at an electrode/electrolyte interface always contains nonfaradaic components. Electrons are transferred across the interface as illustrated in Figure 2.19 (Chang *et al.* 2010) with the charge transfer resulting in both faradaic and nonfaradaic components. The faradaic component arises from the electron transfer through a reaction across the interface by overcoming an appropriate activation barrier, also known as the polarization resistance (R_p), along with (R_{ct}) while the nonfaradaic currents results from charging the double layer capacitor (C_d) (Siddiqui *et al.* 2010).

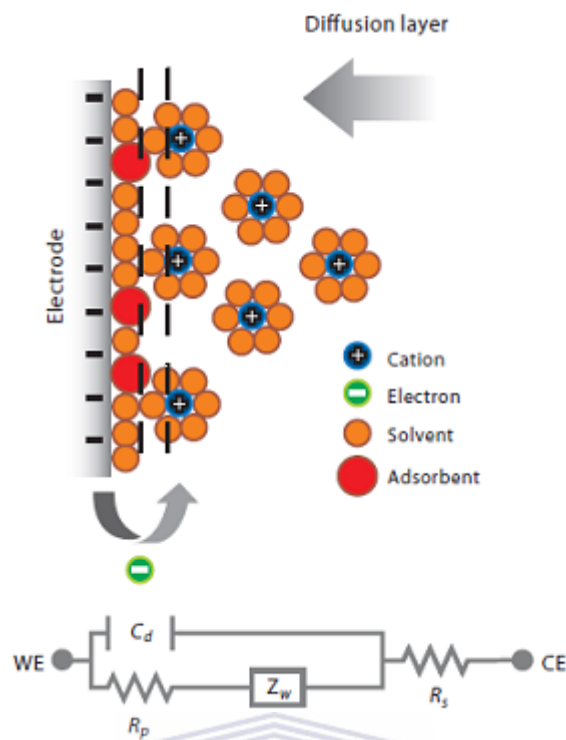


Figure 2.19: An electrified interface in which the electrode is negatively charged and where counter anions are aligned along the surface. Below that are the electrical circuit corresponding to each interface component (Siddiqui *et al.* 2010)

UNIVERSITY of the
WESTERN CAPE

Typically, in electrochemical systems three types of Nyquist plots are observed:

- (1) A straight line, which illustrates a diffusion-limited process with facile electron transfer;
 - (2) A semicircle that is accompanied by a straight line at low frequencies of the spectrum;
- and
- (3) A semicircle, which represents an electron transfer-limited process with its diameter (x -axis) corresponding to the R_{ct} at the electrode (Yoo *et al.* 2003).

For biosensor applications, a semicircle spectrum with negligible noise from an unmodified electrode is preferable as it provides higher sensitivity. This was clearly demonstrated by the work of Sun *et al.* 1998 where a single-stranded deoxyribonucleic acid was immobilized on gold electrode with self-assembled aminoethanethiol monolayer for

DNA electrochemical sensor applications. The success of the DNA electrochemical sensor was based on hybridization with a complementary DNA and the intercalation of daunomycin as a hybridization indicator to form a dsDNA: daunomycin system on the gold electrode surface. The DNA sensor was shown to be highly stable and sensitive.

2.10 Other Characterization Techniques:

For this study techniques such Ultraviolet Visible Spectroscopy (UV-vis), Transmission Electron Microscopy (TEM), Atomic Force Microscopy (AFM) and Scanning Electron Microscopy (SEM) were used to study the morphology of PVP-AgNP, PANSA/PVP-AgNPs nanocomposite, PANSA film and PANSA/PVP-AgNP/CYP2E1 nanobiosensor. This section describes the principles behind some of these techniques as well their applications.

2.10.1 Ultraviolet Visible Spectroscopy (UV-vis):

Ultraviolet-visible spectroscopy sometimes known as ultraviolet-visible spectrophotometry refers to absorption spectroscopy or reflectance spectroscopy in the ultraviolet-visible region of the spectrum. This ultimately means that light in the visible and adjacent (near-UV and near-infrared) ranges is used resulting in absorption or reflectance of any chemical involved. Molecules undergo electronic transitions in this region of the spectrum. UV-vis is a complementary technique to fluorescence spectroscopy, since fluorescence deals with transitions from the excited state to the ground state, while absorption measures transitions from the ground state to the excited state. UV/Vis spectroscopy is applied in analytical chemistry for the quantitative determination of different analytes, such as highly conjugated organic compounds, transition metal ions and biological macromolecules with analyses usually carried out in solutions (Skoog *et al.* 1992; Jenkel *et al.* 1994).

-
- ✓ The solutions of transition metal ions may be coloured so as to absorb visible light because d electrons within the metal atoms can be excited from one electronic state to another. The presence of other species such as ligands or certain anion, are capable of affecting the colour of metal ion solutions.
 - ✓ Highly conjugated organic compounds absorb light in the UV or visible regions of the electromagnetic spectrum. The solvents for these determinations are often water for water soluble compounds, or ethanol for organic-soluble compounds. The absorption spectrum of organic compounds may be highly affected by solvent polarity and pH.
 - ✓ While charge transfer complexes also give rise to colours, the colours are often too intense to be used for quantitative measurement (Skoog *et al.* 1992; Kenkel *et al.* 1994). Figure 2.20 illustrates how a UV-vis spectrometer functions. (http://pulse.yahoo.com/_6HVLWLKIRHDJDG2Q2QSUFAH7RU/blog/articles/321131)

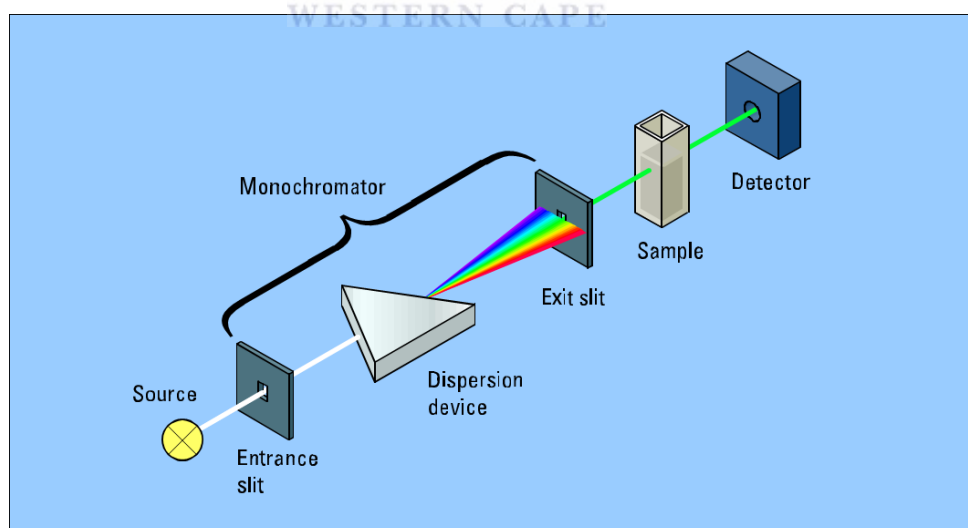


Figure 2.20: Illustration of how a UV-vis spectrometer functions
(http://pulse.yahoo.com/_6HVLWLKIRHDJDG2Q2QSUFAH7RU/blog/articles/321131)

Our study successfully utilized UV-vis to characterize PVP-AgNPs, PANSA/PVP-AgNPs nanocomposite, PANSA and PANSA/PVP-AgNP/CYP2E1 dissolved respectively in phosphate buffer. The resultant spectra illustrated absorbance peaks for each compound with a strong soret band for CYP2E1 suggesting successful attachment of the enzyme on the /PVP-AgNPs nanocomposite.

In a study by Arshi *et al.* 2011; silver/polyvinylpyrrolidone synthesized respectively in water and ethylene glycol were compared using UV-vis resulting in plasmon absorption peaks at 435 and 445 nm respectively. Similar results were observed in our study for PVP-AgNPs synthesized in the presence of methanol. In another study by Hagedoorn *et al.* 2002 ferrous enzymes studied using UV-vis showed strong soret bands at approximately 409 nm. This value is characteristic of most heme enzymes such as CYP2E1. Our study revealed a strong soret band at 410 nm indicating the oxidation of CYP2E1.



2.10.2 Transmission Electron Microscopy (TEM):

Transmission electron microscopy (TEM) is a microscopic technique operational when a beam of electrons is transmitted through an ultra thin sample material, interacting with the sample as it passes through. The electrons behave as a light source with much lower wavelengths making it possible to obtain resolutions a thousand times better than using light microscopes. Depending on the density of the material present, some of the electrons are scattered and disappear from the beam, while at the bottom of the microscope the unscattered electrons hit a fluorescent screen, which gives rise to a "shadow image" of the sample in question with its different parts displayed in varied darkness according to their respective densities. The interaction of the electrons with the sample create an image which is magnified and focused onto an imaging device, such as a layer of photographic film, a fluorescent screen or to be detected by a sensor such as a CCD camera (is a device for the

movement of electrical charge, usually from within the device to an area where the charge can be manipulated (Skoog *et al.* 1992; Jenkel *et al.* 1994).

As a result of this, instrument users are able to exam fine details, even as small as a single column of atoms, which is tens of thousands times smaller than the smallest resolvable object in a light microscope. TEM is one of the important major analysis methods in physical and biological sciences finding application in virology, material science, and pollution, cancer and semiconductor research (Skoog *et al.* 1992; Jenkel *et al.* 1994). The orientation of the instrument and its way of function is depicted below, in Figure 2.21 (A) (http://edu.glogster.com/glog.php?glog_id=17548229&scale=54&isprofile=true) (B) (<http://www.ifn.upr.edu/people/8-carlos-cabrera-martinez>).

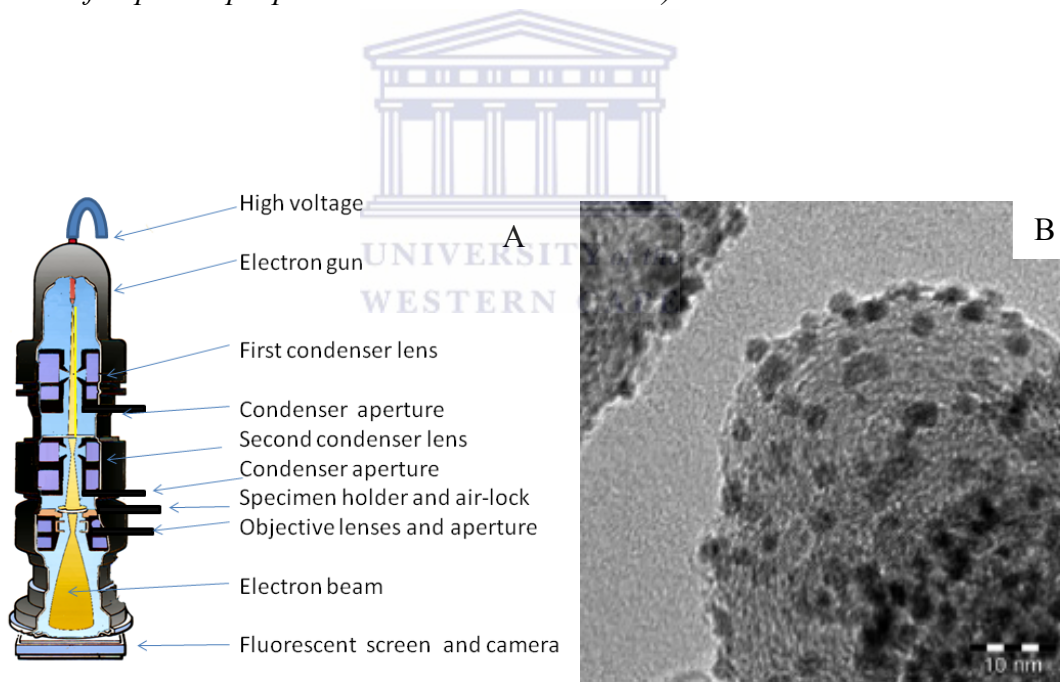


Figure 2.21: (A) Schematic presentation of transmission electron microscope (TEM) (http://edu.glogster.com/glog.php?glog_id=17548229&scale=54&isprofile=true) and (B) An example of a TEM image (<http://www.ifn.upr.edu/people/8-carlos-cabrera-martinez>)

In this study TEM was used to study the morphology, shape, distribution and size of PVP-AgNP, PANSA/PVP-AgNPs nanocomposite, PANSA film and PANSA/PVP-AgNP/CYP2E1 nanosensor. In a similar study carried out by Reddy *et al.* 2008; TEM was used to characterize poly (*o*-toluidine) - silver nanocomposite synthesized by chemically oxidizing *o*-toluidine in the presence of negatively charged silver nanocolloids. Just like our study, the TEM images in this study revealed that silver nanoparticles of approximately 20 nm sizes were dispersed in the poly (*o*-toluidine) matrix. Most importantly, this nanocomposite exhibited a higher electrical conductivity than that of the poly (*o*-toluidine).

2.10.4 Atomic Force Microscopy (AFM):

The Atomic Force Microscope is an instrument that can analyze and characterize samples at the microscope level. Surface characteristics can be studied with very accurate resolution ranging from 100 μm to less than 1 μm . Operating AFM involves an extremely fine sharp tip coming in contact or in very close proximity to the sample of interest. Usually this tip is a couple of microns long and often less than 100 \AA in diameter and is located at the free end of a cantilever (which one may think of as a spring) that is 100 to 200 μm long. Different forces either attract or repel the tip allowing the sample to be scanned beneath the tip. Imaging softwares record and process these deflections producing a topographical representation of the sample that was imaged as illustrated in Figure 2.22 (http://asdlib.org/onlineArticles/ecourseware/Bullen/SPMModule_BasicTheoryAFM.pdf).

One may also be able to know other features about the sample rather than just a view of its surface using different imaging modes for different types of analysis (Binnig *et al.* 1986).

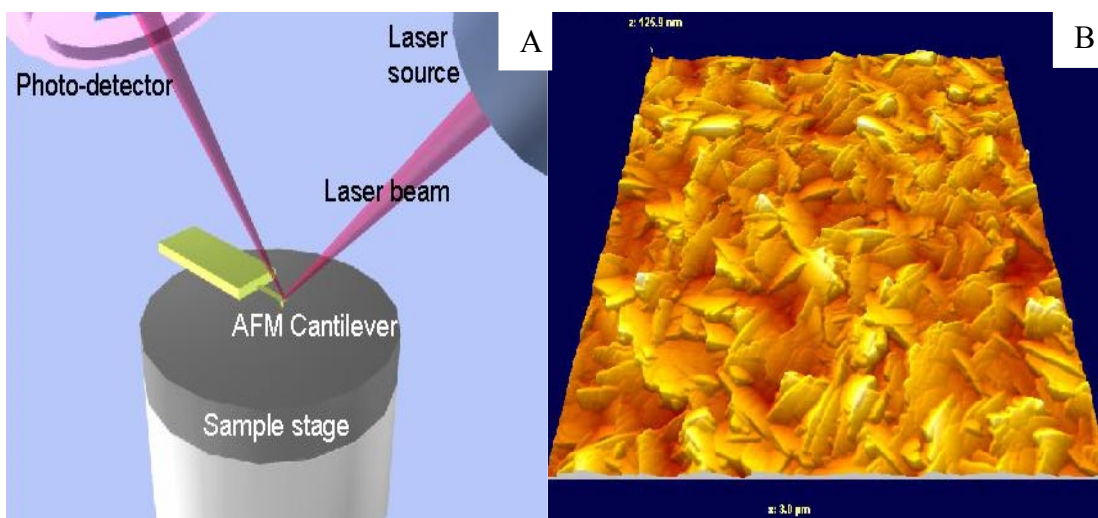


Figure 2.22: (A) An illustration of AFM probing a sample surface with a sharp tip
(B) An example of an AFM image showing sharp, randomly-oriented peaks
(http://asdlab.org/onlineArticles/ecourseware/Bullen/SPMModule_BasicTheoryAFM.pdf)

AFM provides a number of advantages over conventional microscopy techniques. AFMs make measurements in three dimensions, x , y , and z , producing three-dimensional images of a sample surface. With good samples resolution in the x - y plane ranges from 0.1 to 1.0 nm and in the z direction is 0.01 nm. Neither a vacuum environment nor any special preparations are required for AFM since an ambient or liquid environment is always suitable. With these advantages AFM has significantly impacted the fields of chemistry, materials science, physics and biology (Blanchard *et al.* 1996; Binnig *et al.* 1986).

Work by Crespilho *et al.* 2009 give an account of using AFM towards the construction of a urea biosensor. The surface of the biosensor displayed a globular morphology and large roughness than the electrode without enzyme. A similar profile of events was also observed for the study in question.

The following chapter gives detailed experimental methods involved in this study.

2.11 References:

Adhikari B.; Majumdar S., 'Polymers in sensor application' (2004) *Progress in Polymer* **29** pg 700-701.

Ahuja T.; Mir I. A.; Kumar D., 'Biomolecular immobilization on conducting polymers for biosensing application' (2007) *Biomaterials* **28** pg 791-794.

Ahuja T.; Kumar D., 'Recent progress in the development of nano-structured conducting polymers/nanocomposites for sensor applications' (2009) *Sensors and Actuators B* **136** pg 275-276.

Alqudami A.; Annapoorni S.; Sen P.; Rawat R.S., 'The incorporation of silver nanoparticles into polypyrrole: Conductivity changes' (2007) *Synthetic Metals* **157** pg 53-54.

Arshi N.; Ahmed F.; Koo B. H.; Lee C. G., 'Comparative study of the Ag/PVP nanocomposites synthesized in water' (2011) *Current Applied Physics* **11** pg 347-348.

Bistolos N.; Wollenberger U.; Jung C.; Scheller F.W., 'Cytochrome P450 biosensors a review' (2005) *Biosensors and Bioelectronics* **20** pg 2409-2411.

Bennett P. N.; Brown M. J., '*Clinical Pharmacology*' Tenth Edition, (2007) Churchill Livingstone Elsevier Ltd: Spain pg 219-222.

Brennan S., 'Comparative Studies of the organic and aqueous phase reactivities of a Pthathalic anhydride-modified hydrogen peroxide biosensor, (1996) *Phd Thesis*, Dublin City University

Bergamini M. F.; Santos D. P.; Zanoni M.V. B., 'Determination of isoniazid in human urine using screen-printed carbon electrode modified with poly-L-histine' (2010) *Bioelectrochemistry* **77** pg 133-134.

Binning G.; Quate C. F., 'Atomic Force Microscope' (1986) *Physical Review Letters* **56** pg 930-933.

Blanchard C.R.; 'Atomic Force Microscopy' (1996) *The Chemical Educator* **1** pg 1431-1432.

Catena G.C.; Bright F. V., 'Thermodynamic study of the effects of B-Cyclodextrin Inclusion with Anilino-naphthalenesulphonates' (1989) *Analytical Chemistry* **61** pg 905-906

Chang B.; Park S., 'Electrochemical Impedance Spectroscopy' (2010) *Annual Review of Analytical Chemistry* **3** pg 208-209.

Chaubey A.; Malhotra B.D., 'Mediated Biosensors' (2002) *Biosensors and Bioelectronics* **17** pg 441-446.

Conn E.E.; Stumff P.K.; Bruening G., 'Outline of Biochemistry' Fifth Edition, (1987) John Wiley and Sons, pg 115-163.

Clayton B. D.; Stock Y. N., 'Basic Pharmacology for Nurses' Twelfth Edition, (2001) Mosby Inc: Missouri, pg 574-576.

Craig C. R.; Stitzel R. E., 'Modern Pharmacology' Third Edition, (1990) Little, Brown and Company: Boston, pg 700-708.

Cresphilho F.; Travains S. A.; Oliveira Jr O.N., 'Enzyme immobilization on Ag nanoparticles/polyaniline nanocomposite' (2009) *Biosensors and Bioelectronics* **24** pg 3073-3074.

D'Orazio P., 'Biosensors in clinical chemistry' (2003) *Clinica Chimica Acta* **334** pg 41-42.

De Groot M. J.; Ekins S., 'Pharmacophore modelling of cytochrome P450' (2002) *Advanced Drug Delivery Reviews* **54** pg 375-376.

Duggleby R.G., 'Product inhibition of reversible enzyme-catalysed reactions' (1994) *Biochimica et Biophysica Acta (BBA) - Protein Structure and Molecular Enzymology* **1209** Pg 238-240.

Eoh H.; Brennan P.J., 'The *Mycobacterium tuberculosis* MEP (2C-methyl-D-erythritol 4-phosphate) pathway as a new drug target' (2009) *Tuberculosis* **89** pg 1-2.

Fernandes J.B.; Kubota L.T., 'Potentiometric biosensor for L-ascorbic acid based on ascorbate oxidase of natural source immobilized on ethylene-vinylacetate membrane' (1999) *Analytica Chimica Acta* **385** pg 3-1

Fersht A., '*Enzyme structure and mechanism*' Second Edition, (1984) W. H. Freeman and Company, pg 98-107.

Gerard M.; Chaubey A., 'Application of conducting polymers to biosensor' (2002) *Biosensors and Bioelectronics* **17** pg 346-347.

Ghoneim M. M.; El-Baradie K.Y., 'Electrochemical behavior of the antituberculosis drug isoniazid and its square-wave adsorptive stripping voltammetric estimation in bulk form, tablets and biological fluids at a mercury electrode' (2003) *Journal of Pharmaceutical and Biomedical Analysis* **33** pg 680-681.

Ghosal A.; Ramanathan R.; Narendra S.; Chowdhury S. K.; Alton K. B., 'Chapter 12 Cytochrome p450 (cyp) and udp-glucuronosyltransferase (ugt) enzymes: role in drug metabolism, polymorphism, and identification of their involvement in drug metabolism' (2005) *Progress in Pharmaceutical and Biomedical Analysis* **6** pg 295-305.

Girousi S. Th.; Gherghit I. Ch.; Karava M. K., 'DNA-modified carbon paste electrode applied to the study of interaction between Rifampicin (RIF) and DNA in solution and at the electrode surface' (2004) *Journal of Pharmaceutical and Biological Analysis* **36** pg 851-852.

Grennan K.; Killard A. J.; Hanson C. J., 'Optimisation and characterisation of biosensors based on polyaniline' (2006) *Talanta* **68** pg 1591-1600.

Guascito M. R.; Malitesta C.; Manno D.; Serra A.; Turco A., 'A new amperometric nanostructured sensor for the analytical determination of hydrogen peroxide' (2008) *Biosensors and Bioelectronics* **24** pg 1057-1058.

Guo C.; Boullanger P.; Jiang L.; Liu T., 'Highly sensitive gold nanoparticles biosensor chips modified with a self-assembled bilayer for detection of Con A' (2007) *Biosensors and Bioelectronics* **22** Pages 1830-1831

Hagedoorn P. L.; de Geus D.C.; Hagen W.R., 'Spectroscopic characterization and ligand-binding properties of chlorite dismutase from the chlorate respiring bacterial strain GR-1' (2002) *European Journal of Biochemistry* **269** pg 4906-4907.

Hammon E.; Beltagi A. M.; Ghoneim M.M., 'Voltammetric assay of rifampicin and isoniazid drugs, separately and combined in bulk, pharmaceutical formulations and human serum at a carbon paste electrode' (2004) *Microchemical Journal* **77** pg 55-56.

Harris D.; Loew G.; Waskell L., 'Calculation of the electronic structure and spectra of model cytochrome P450 compound I' (2001) *Journal of Inorganic Biochemistry* **83** pg 309-311.

Huang L.; Liao W.; Ling H.; Wen T., 'Simultaneous synthesis of polyaniline nanofibers and metal (Ag and Pt) nanoparticles' (2009) *Materials Chemistry and Physics* **116** pg 474-475.

Hermeryck A.; Belpaire F.M., 'Selective Serotonin Reuptake Inhibitors and Cytochrome P-450 Mediated Drug-Drug Interactions: An Update' (2003) *Current Drug Metabolism* **3** pg 13-17.

Hong L.; Li Q., 'Synthesis of flower-like silver nanoarchitectures at room temperature' (2009) *Materials research Bulletin* **44** pg 1201-1202.

Iwuoha E.I.; Smyth M.R., 'Reactivities of organic phase: 6.Square-wave and differential pulse studies of genetically engineered cytochrome P450_{cam} (CYP101) bioelectrodes in selected solvents' (2003) *Biosensors and Bioelectronics* **18** pg 237-238.

Heli H.; Jabbari A.; Hajjizadeh M.; Moosavi-Movahedi A. A., 'A nonenzymatic biosensor based on copper nanoparticles modified electrode for detection of acetylcholine' (2009) *Biosensors and Bioelectronics* **24** pg 2328-2329.

Hernandez C.; Cetner A., 'Tuberculosis in the age of biologic therapy' (2008) *Journal of American Academy of Dermatology* **59** No 3 pg 363-364.

Jena B. K.; Raj C. R., 'Au nanoparticle decorated silicate network for the amperometric sensing of isoniazid' (2010) *Talanta* **80** pg 1653-1654.

Joseph S.; Rusling J. F., 'An amperometric biosensor with human CYP3A4 as a novel drug screening tool' (2003) *Biochemical Pharmacology* **65** pg 1817-1818.

Kathiresan K.; Manivannan S., 'Studies of silver nanoparticles synthesised by a marine fungus, *Penicillium fellutanum* isolated from coastal mangrove sediment' (2009) *Colloids and Surfaces B: Biointerfaces* **71** pg 133-134.

Key E.R.M.; Biochemistry (1966) Collier-Macmillan Limited, London pg 290-291.

Jenkel J.; 'Analytical Chemistry for Technicians' (1994) Lewis Publishers, Boca Raton, United States of America.

Lakard B.; Lakard S., 'Potentiometric miniaturized pH sensor based on polypyrrole films' (2007) *Sensors and Actuators B* **122** pg 101-102

Leech D.; Rechnitz G. A., 'Crayfish walking leg neuronal biosensor for the detection of pyrazinamide and selected local anesthetics' (1993) *Analytica Chimica Acta* **274** pg 25-26.

Lesney M. S., 'Today's Chemistry at Work' (2002) *American Chemical Society* **1** pg 33-34.

Levy R.I.; Shaheen U.; Cesbron Y.; See V., 'Gold nanoparticles delivery in mammalian live cells: a critical review' (2010) *Nano Reviews* **1** pg 1-2.

Li M.; Gao Y.; Wang G.; Fang B., 'Preparation of novel mercury-doped silver nanoparticles film glassy carbon electrode and its application for electrochemical biosensor' (2005) *Analytical Biochemistry* **341** pg 52-53.

Lindfors T.; Ivaska A., 'Potentiometric and UV-vis characterisation of N-substituted Polyanilines' (2002) *Journal of Electroanalytical Chemistry* **535** pg 65-66

Liu C.; Hu J., 'Hydrogen peroxide biosensor based on the direct electrochemistry of myoglobin immobilized on silver nanoparticles doped carbon nanotubes film' (2009) *Biosensors and Bioelectronics* **24** pg 2149-2150.

Lomillo M. A. A.; Kauffmann J.M.; Martinez M. J. A., 'HRP-based biosensor for monitoring rifampicin' (2003) *Biosensors and Bioelectronics* **18** pg 1165-1166.

Lomillo M. A. A.; Renedo O. D.; Martinez M. J. A., 'Optimization of a cyclodextrin-based sensor for rifampicin monitoring' (2005) *Electrochimica Acta* **50** pg 1807-180.

Luo X.; Morrin A.; Killard A.J.; Smyth M.R. 'Application of Nanoparticles in Electrochemical Sensors and Biosensors' (2006) *Electroanalysis* **18** pages 319-320.

Magdassi S.; Grouchko M.; Kamyshny A., 'Copper Nanoparticles for Printed Electronics: Routes towards Achieving Oxidation Stability' (2010) *Materials* **3** pg 4626-4627.

Malhotra B.D.; Chaubey A., 'Prospects of conducting polymers in biosensors' (2006) *Analytica Chimica Acta* **578** pg 60-61.

Meyers F. H.; Jawetz E.; Goldfien A., '*Review of Medical Pharmacology*' (1980) Seventh Edition, Lange Medical Publication Ltd: California, pg 565-567.

Mokhtari N.; Daneshpajouh S., 'Biological synthesis of very small silver nanoparticles by culture supernatant of *Klebsiella pneumoniae*: The effects of visible-light irradiation and the liquid mixing process' (2009) *Materials Research Bulletin* **44** pg 1415-1415.

Mu S.; Qu Y.; Jiang L., 'Effect of refluxed silver nanoparticles on inhibition and enhancement of enzymatic activity of glucose oxidase' (2009) *Colloids and Surfaces A: Physicochemical Engineering Aspects* **345** pg 101-102.

Nabid M. R.; Dinarvand R.; Sedghi R., 'Polyaniline/TiO₂ Nanocomposite: Enzymatic Synthesis and Electrochemical Properties' (2008) *International Journal of Electrochemical Science* **3** pg 1117-1118.

Naudin E.; Gouerec P.; Belanger D., 'Electrochemical preparation and characterization in non-aqueous electrolyte of polyaniline electrochemically prepared from an anilinium salt' (1998) *Journal of Electroanalytical Chemistry* **1** pg 459

Norouzi P.; Faridbod F.; Larijani B.; Ganjali M.R., 'Glucose Biosensor Based on MWCNTs-Gold Nanoparticles in a Nafion Film on the Glassy Carbon Electrode Using Flow Injection FFT Continuous Cyclic Voltammetry' (2010) *International Journal of Electrochemical Science* **5** pg 1213 – 1214.

Paddle B. M., 'Biosensors for chemical and biological agents of defense interest' (1996) *Biosensors and Bioelectronics* **11** pg 1079-1083.

Pandey P.C.; Prakash R., 'Polyindole modified potassium ion-sensor using dibenzo-18-crown-6 mediated PVC matrix membrane' (1998) *Sensors and Actuators B* **46** pg 61-62

Patrick G. L., '*Medical Chemistry*' (2005) Third Edition, Oxford University Press Ltd: New York pg 381-282.

Porubsky P.R.; Meneely K. M., 'Structures of Human Cytochrome P-450-2E1' (2008) *Journal of Biological Chemistry* **48** pg 33698-33701.

Quintino M.S.M.; Angus L., 'Fast BIA-amperometric determination of isoniazid in tablets' (2006) *Journal of Pharmaceutical and Biomedical Analysis* **42** pg 402-403.

Reddy A. S.; Chen C., 'Synthesis of silver nanoparticles using surfactin A biosurfactant as stabilizing agent' (2009) *Materials Letters* **63** pg 1227-1228.

Reddy K. R.; Lee K.; Lee Y.; Gopalan A. I., 'Facile synthesis of conducting polymer-metal hybrid nanocomposite by in situ chemical oxidative polymerization with negatively charged metal nanoparticles' (2008) *Materials Letters* **62** pg 1815-1816.

Ryne-Byrne S., 'Development of and Amperometric anti-biotin Immunosensor' (1997) *Thesis*, Dublin City University.

Sadik O.A.; Mwilu S. K.; Aluoch A., 'Smart Electrochemical Biosensors: From advanced materials to ultrasensitive devices' (2009) *Electrochimica Acta* **55** pg 4290-4291.

Sarkar P.; Bhui D. K., 'Synthesis and photophysical study of silver nanoparticles stabilized by unsaturated dicarboxylates' (2009) *Journal of Luminescence* **129** pg 704-705.

Schweon S.J., 'Tuberculosis Update' (2009) *Journal of Radiology and Nursing* **28** pg 12-14.

Shin J. H., 'Potentiometric biosensors using immobilized enzyme layers mixed with hydrophilic polyurethane' (1998) *Sensors and Actuators B* **50** pg 20-21.

Skoog D. A.; West D. M.; Holler F. J., 'Fundamentals of Analytical Chemistry' (1992) Saunders College Publishing, Fort Worth, United States of America pg 100-200.

Shumyantseva V.V.; Bulko T.V.; Archakov A.I., 'Electrochemical reduction of Cytochrome P450 as an approach to the construction of biosensors and bioreactors' (2005) *Journal of Inorganic Biochemistry* **99** pg 1057-1058.

Shumyantseva V.V.; Bulko T.V.; Archakov A.I., 'electrochemical properties of cytochromes P450 using nanostructured electrodes: Direct electron transfer and electro catalysis' (2007) *Journal of Inorganic Biochemistry* **101** pg 859-860.

Siddiqui S.; Chen H.; Li J.; Meyyappan M., 'Characterization of Carbon Nanofiber Electrode Arrays Using Electrochemical Impedance Spectroscopy: effect of Scaling down Electrode Size' (2010) *American Chemical Society* **4** pg 955-956.

Songa E.A.; Arotiba O.A.; Jahed N., 'Electrochemical detection of glyphosate herbicide using horseradish peroxidase immobilized on sulfonated polymer matrix' (2009) *Bioelectrochemistry* **75** pg 121-122.

Spracklin D.K.; Hankins D. C., 'Cytochrome P450 2E1 is the Principal Catalyst of Human Oxidative Halothane Metabolism *in Vitro*' (1997) *The Journal of Pharmacology and Experimental Therapeutics* **1** pg 401-402.

Sun X.; He P.; Liu P.; Fang Y., 'Immobilization of single-stranded deoxyribonucleic acid on gold electrode with self-assembled aminoethanethiol monolayer for DNA electrochemical sensor applications' (1998) *Talanta* **47** pg 487-488.

Tran-Van F.; Henri T.; Cverot C., 'Synthesis and electrochemical properties of mixed ionic and electronic modified polycarbazole' (2002) *Electrochimica acta* **47** pg 2927-2928

Trivedi D. C., '*Handbook of Organic Conductive Molecules and Polymers: Volume 2 Conductive Polymers: Synthesis and Electrical Properties*' (1996) John Wiley and Sons Ltd: New York, p 506-572.

Wallis R.S.; Doherty T. M., 'Biomarkers for tuberculosis disease activity, cure and relapse' (2009) *Lancet Infectious Disease* **9** pg 162-163.

Wang J., 'Electrochemical biosensors: Towards point-of-care cancer diagnostics' (2006) *Biosensors and Bioelectronics* **21** pg 1889-1891.

Wang Y.; Wei W.; Zeng J.; Liu X.; Zeng X., 'Fabrication of a copper nanoparticle/chitosan/carbon nanotube-modified glassy carbon electrode for electrochemical sensing of hydrogen peroxide and glucose' (2008) *Microchimica Acta* **140** pg 253-254.

Wang W.; Chen J., 'Tuberculosis of the head and neck: a review of 20 cases' (2009) *Oral Surgery, Oral Medicine, Oral Pathology, Oral Radiology, and Endodontology* **107** pg 381-382.

Worsfold P.J., 'Classification of immobilized enzymes' (1995) *Pure and Applied Chemistry* **67** pg 597-600.

Yan X.; Bo X.; Guo L., 'Electrochemical behaviour and determination of isoniazid at ordered mesoporous carbon modified electrode' (2011) *Sensors and Actuators B* **155** pg 837-842

Yang Y., 'An amperometric horshradish peroxidise inhibition biosensor based on a cysteamine self-assembled monolayer for the determination of sulfides' (2004) *Sensors and Actuators B* **102** pg 164-166.

Yang G.; Wang C.; Hu X., 'Poly (amidosulfonic acid) modified glassy carbon electrode for the determination of isoniazid in pharmaceuticals' (2008) *Bioelectrochemistry* **73** pg 37-38.

Yoo J.; Song I.; Park S., 'Real-Time Impedance Measurements during Electrochemical Experiments and Their Application to Aniline Oxidation' (2003) *Analytical Chemistry* **75** pg 3294-3295.

Yung-Chi C.; Prusoff W. H., 'Relationship between the inhibition constant (K_I) and the concentration of inhibitor which causes 50 per cent inhibition (I_{50}) of an enzymatic reaction' (1973) *Biochemical Pharmacology* **12** Pages pg 3099-3108.

Zhang S.; Wright G., 'Materials and techniques for electrochemical biosensor design and construction' (2000) *Biosensors & Bioelectronics* **15** pg 274-276.

Zhu N.; Chang Z., 'Electrochemically fabricated polyaniline nanowire-modified electrode for voltammetric detection of DNA hybridization' (2006) *Electrochimica Acta* **51** pg 3759-3760.

Zvavamwe Z.; Ehlers V., 'Experiences of a community-based tuberculosis treatment programme in Namibia: A comparative cohort study' (2009) *International Journal of nursing Studies* **46** pg 303-304.

CHAPTER 3

Experimental Method

Summary

This section provides detailed experimental methods involved in this study. Outlined here are the procedures involved in the synthesis of poly (8-anilino-1-naphthalene sulphonic acid) and silver nanoparticles, their characterization and their application in this study. Also included in this section is the enzyme immobilization technique used towards the development of the nanobiosensors as well as the description of the characterization methods employed for the success of the nanobiosensors. Finally, the methods used towards the detection of Tuberculosis treatment drugs by the nanobiosensors are also described. Techniques employed in this study were steady state amperometry, CV, DPV, SWV, EIS, TEM, AFM and SEM.

3.1 Reagents:

Analytical grade methanol, silver nitrate (AgNO_3) and polyvinylpyrrolidone (PVP) were purchased from Sigma-Aldrich and used for the synthesis of the silver nanoparticles. Electropolymerization was achieved by the use of 8-anilino-1-naphthalene sulfonic acid, ammonium hydrate salt 97% (ANSA) (Sigma-Aldrich) in the polymerization medium, sulphuric acid (Fluka). The nanobiosensors were prepared using, Cytochrome P450-2E1 Isozyme (CYP 2E1) or 4-nitrophenol 2-hydroxylase; EC 1.14.14.1 (Sigma-Aldrich). One unit of CYP2E1 is said to be the required amount to convert 1 picomole of p-nitrophenol to 4-nitrocatechol per minute at a pH of 7.4 and at temperature of 37 °C. The enzyme modification reagents, such as; disuccinimidyl octanedioate [suberic acid bis (*N*-hydroxysuccinimide ester) (SA-NHS)] and ethylene glycol bis(succinimidyl succinate) [ethylene glycol bis(succinic acid *N*-hydroxysuccinimide ester) (EG-NHS)] were products of Sigma-Aldrich South Africa and stored at -4 °C under anhydrous conditions when not in use. The reaction medium, pH 7.4, 0.1 M phosphate buffer was prepared from dihydrogenorthophosphate dehydrate, anhydrous and disodium hydrogenorthophosphate all purchased from Sigma-Aldrich. The nanobiosensor substrates, ethambutol [(2*S*, 2'*S*)-2, 2'-(ethane-1, 2-diyldiimino) dibutan-1-ol] - $\text{C}_{10}\text{H}_{20}\text{N}_2\text{O}_2$], isoniazid [4-pyridinecarboxylic acid - $\text{C}_6\text{H}_7\text{N}_3\text{O}$], rifampicin [3 - [[(4-methyl-1 -piperaziny) imino] -methyl] -rifamycin; or 5,6,9,17,19,21 -hexahydroxy-23methoxy-2,4,12,16,18,20,22 heptamethyl-8-[*N*-(4-methyl-1-piperaziny)formimidoyl]-2,7-(epoxypentadeca [1,1 1,13] trienimino)naphtha [2,1-b] furan-1, 1 l (2H)-dione 21-acetate - $\text{C}_{43}\text{H}_{58}\text{N}_4\text{O}_{12}$] and pyrazinamide [pyrazinecarboxamide - $\text{C}_5\text{H}_5\text{N}_3\text{O}$] capsules were supplied by the University of Western Cape Health Centre courtesy of Kaaselsvlei Clinic in Bellville South, Cape Town. All these drugs were used without further purification dissolved in pH 7.4, 0.1 M phosphate buffer solution. De-ionized ultra-purified water used throughout these experiments was prepared with a Milli-Q water purification

system. Analytical grade argon obtained from Afrox, SA was used for degassing the cell solutions and all the solutions were kept refrigerated at -4 °C when not in used.

3.2 Apparatus and Measurement:

All electrochemical experiments were carried out using a BAS 100W integrated automated electrochemical workstation BioAnalytical Systems (BAS, West Lafayette, IN) controlled by a computer and a conventional three-electrode system with a 0.0201 cm² gold (Au) disk or screen printed gold electrode (SPAuE) as the working electrode, a platinum (Pt) wire auxiliary electrode and Ag/AgCl reference electrode with a 3 M NaCl salt bridge solution, all purchased from (BAS, West Lafayette, IN). All the results obtained for the PANSA, PANSA/PVP-AgNPs and [PANSA/PVP-AgNPs/CYP2E1; PANSA/PVP-AgNPs/SA-CYP2E1 or PANSA/PVP-AgNPs/EG-CYP2E1] modified electrodes using cyclic (CV), differential pulse (DPV) square wave (SWV) voltammograms and steady state amperometry (constant potential amperometry) were recorded with a computer interfaced to the electrochemical workstation. Alumina micropolish (1.0, 0.3 and 0.05 mm alumina slurries) and polishing pads (Buehler, IL, USA) were used for polishing the electrode.

Electrochemical impedance spectroscopy (EIS) of the PANSA, PANSA/PVP-AgNPs and [PANSA/PVP-AgNPS/CYP2E1; PANSA/PVP-AgNPs/SA-CYP2E1 or PANSA/PVP-AgNPs/EG-CYP2E1] modified electrodes was measured with a Voltalab instrument (Radiometer Analytical, France). Impedance measurements were performed in the frequency range from 10⁵ to 50⁻¹ Hz at 0 V, which was found to have the least impedance after potential step from 0 to 800 mV with AC amplitude of 5 mV. Cyclic voltammetry (CV) characterization of the PANSA, PANSA/PVP-AgNP and [PANSA/PVP-AgNPS/CYP2E1; PANSA/PVP-AgNPS/SA-CYP2E1 or PANSA/PVP-AgNPS/EG-CYP2E1] modified electrodes were carried out at a potential window of -300 mV (initial potential, E_i) to +1100

mV (switch potential, E_{λ}), sensitivity of 10 $\mu\text{A/V}$ and at different scan rates (10 – 200 mV/s). The modified electrodes were also investigated using Differential Pulse Voltammetry (DPV). The DPV experimental conditions were: potential window of +1000 mV to -300 mV, sensitivity of 10 $\mu\text{A/V}$, pulse amplitude of 50 mV, current sampling width of 17 msec, pulse width of 50 msec and at different scan rates (10 – 200 mV/s). Characterization of the modified electrodes was also carried out using Square Wave voltammetry (SWV). SWV experimental conditions were: potential window of +1100 mV to -300 mV, sensitivity of 10 $\mu\text{A/V}$, SWV amplitude of 25 mV, Step potential of 4 mV and at different SWV frequencies (10 – 200 Hz). Ultraviolet-Visible (UV-Vis) spectra of PANSA, PANSA/PVP-AgNP and [PANSA/PVP-AgNP/CYP2E1; PANSA/PVP-AgNP/SA-CYP2E1 or PANSA/PVP-AgNP/EG-CYP2E1] were recorded on a Nicolet Evolution 100 (Thermo Electron Cooperation, UK). After electrodeposition of PANSA, PANSA/PVP-AgNPs and immobilization of CYP2E1, SA-CYP2E1 and EG-CYP2E1 onto the PANSA/PVP-AgNP electrode, the samples were immobilized on ITO and their UV-Vis spectra recorded. Free CYP2E1 and SA-CYP2E1 and EG-CYP2E1 samples were dissolved in buffer and their spectra recorded.

The modified SPAuE were used for scanning electron microscopy (SEM) studies while the modified Au electrodes were used for the detection of TB drugs, using the same reference electrode and counter electrode. SEM images were taken with a Hitachi S3000N scanning electron microscope at an acceleration voltage of 20 kV at various magnifications. Gold sputtering of the SEM samples was done using a SC7640 Auto/ Manual high resolution super coater (Quorum Technology Ltd., England) at a voltage of 2 kV and plasma current of 25 mA for one minute. Morphological studies of PANSA, PANSA/PVP-AgNPs and [PANSA/PVP-AgNPs/CYP2E1; PANSA/PVP-AgNPs/SA-CYP2E1 or PANSA/PVP-AgNPs/EG-CYP2E1] were carried out using transmission electron microscopy (TEM). After

electrodeposition of PANSA, PANSA/PVP-AgNPs and immobilization of CYP2E1, SA-CYP2E1 and EG-CYP2E1 onto the PANSA/PVP-AgNPs electrode, the samples were all dissolved in ethanol. A drop of each sample was placed over carbon copper grids and allowed to dry prior to measurements. TEM images were acquired on Philips Technai-FE 12 TEM instrument operated at an accelerating voltage of 120 kV. The instrument was equipped with an Energy dispersive X-ray (EDAX) detector (Oxford LINK-ISIS 300) for elemental composition analysis and the EDAX spectra were measured at an accelerating voltage of 10 kV. Further confirmation studies to study the film morphology and thickness were investigated with Multimode atomic force microscope controlled by a Digital Instruments Nanoscope III controller (Vee Instruments, USA).

3.3 Synthesis of Silver Nanoparticles (PVP-AgNPs):

Silver nanoparticles were prepared by a soft solution technique starting with a solution of AgNO_3 and an aqueous solution of PVP. In a typical synthesis; 30 mg AgNO_3 was dissolved in 140 mL of methanol and brought to a boil. A second solution was prepared by dissolving 200 mg PVP in hot deionized water and 10 mL of this second solution was then added dropwise to the AgNO_3 solution under vigorous stirring. The colour of the mixture became pale red several minutes after methanol began to boil. Addition of the PVP solution caused the mixture to become increasingly darker until a red-orange colour was reached signifying completion of the silver nanoparticles synthesis. 20 μL of AgNP were drop casted onto Au electrode and allowed to dry for 3hrs after which the Au/PVP-Ag electrode was characterized at various scan rates using CV, DPV and SWV at +1100 mV to -300 mV at various scan rates in pH 7.4, 0.1 M phosphate buffer.

3.4 Synthesis of Poly (8-anilino-1-naphthalene sulphonic acid) PANSA:

The electropolymerization of ANSA was performed in a cell solution containing 0.01 M of the ANSA monomer in 20 mL 0.5 M H₂SO₄ solution degassed with argon for 15 min. The potential was cycled from -300 mV to +1100 mV, at a potential scan rate of 50 mV/s. An argon blanket was maintained on top of the cell solution during the polymerization process which was stopped after 5 voltammetric cycle. Poly (8-anilino-1-naphthalene sulfonic acid) PANSA was conditioned for biosensor application by rinsing out superficial acid and unreacted monomer and then incubated in buffer. This electrode will be referred to as Au/PANSA electrode. To develop the Au/PANSA/PVP-AgNP electrode, 20 μL of PVP-AgNP were drop casted onto the Au/PANSA and allowed to dry at room temperature for 1 h after which it was characterized using CV, DPV and SWV at +1100 to -300 mV at various scan rates in pH 7.4, 0.1 M phosphate buffer.

3.5 Preparation of TB Drugs Nanobiosensors:

3.5.1 Modification of CYP2E1:

SA-NHS and EG-NHS were used in the modification of CYP2E1. 15 mg of SA-NHS or 18 mg of EG-NHS was dissolved in 250 μL of 5% DMSO. A 10 μL sample of the solution was reacted with 4 μL of CYP2E1 dissolved in 100 μL of, pH 7.4, 0.1 M phosphate buffer. The reaction was allowed to proceed for 60 min in room temperature and terminated by adding 100 μL of 0.1 M cold Tris-HCl buffer pH 7.0. The modified CYP2E1 solutions were stored in the refrigerator at 4 °C and used within 3 days of preparation.

3.5.2 Preparation of Au/PANSA/PVP-AgNP/CYP2E1 Nanobiosensors:

To develop the Au/PANSA/PVP-AgNP electrode, 20 μL of PVP-AgNP were drop casted onto the Au/PANSA and allowed to dry at room temperature for 1 h. A freshly

prepared PANSA/PVP-AgNPs electrode was reduced at a constant potential of -600 mV under an argon blanket in a 5 mL solution of buffer until a steady state current was attained which took 5 min to attain. 20 μ L of CYP2E1, SA-CYP2E1 or EG-CYP2E1 were added respectively to a 5 mL solution of buffer, and the Au/ PANSA/PVP-AgNPs nanocomposite was oxidized at a potential of +700 mV for 10 min during which the PANSA/PVP-AgNPs nanocomposite was electrostatically attached with CYP2E1, A-CYP2E1 or EG-CYP2E1. The resultant PANSA/PVP-AgNPs/CYP2E1; PANSA/PVP-AgNPs/SA-CYP2E1 or PANSA/PVP-AgNPs/EG-CYP 2E1/nanobiosensors were rinsed in buffer and stored refrigerated at -4 °C when not in use.

3.5.3 Application of PANSA/PVP-AgNP/CYP2E1 Modified Gold Electrodes as Amperometric TB Drug Nanobiosensors:

All experiments were carried out at room temperature. All modified electrodes; Au/PANSA, Au/PANSA/PVP-AgNPs and [Au/PANSA/PVP-AgNPs/CYP2E1; Au/PANSA/PVP-AgNPs/SA-CYP 2E1 or Au/PANSA/PVP-AgNPs/EG-CYP 2E1] were tested for the amperometric sensing of the TB drugs namely; Isonaizid (INH), ethambutol (ETH), rifampicin (RIF) and pyrazinamide (PYR). Standard solutions were prepared daily by dissolving a capsule of each drug type in 50 mL phosphate buffer resulting in final concentrations of INH = 0.015 M ; ETH = 0.08 M ETH; RIF = 0.015 M and PYR = 0.08 M. Different concentrations of each drug were varied independently in 20 mL of phosphate buffer solutions. INH and ETH were monitored using the Au/PANSA/PVP-AgNPs/CYP2E1 nanobiosensor; RIF was monitored using Au/PANSA/PVP-AgNPs/EG-CYP2E1 nanobiosensor and PYR was monitored using Au/PANSA/PVP-AgNPs/SA-CYP2E1 nanobiosensor. The volumetric determination of these drugs was carried out in 20 mL phosphate buffer under the following parameters.

CV experiments were carried out at a potential window of +300 mV to -800 mV, sensitivity of 10 $\mu\text{A/V}$ and at 20 mV/s at different concentrations of each drug; and the DPV experimental conditions were: potential window of +300 mV to -800 mV, sensitivity of 10 $\mu\text{A/V}$, pulse amplitude of 50 mV, current sampling width of 17 msec, pulse width of 50 msec and at 50 mV/s at different concentrations of each drug; while the SWV experimental conditions were: potential window of +300 mV to -800 mV, sensitivity of 10 $\mu\text{A/V}$, SWV amplitude of 25 mV, Step potential of 4 mV and at 15 Hz and at different concentrations of each drug. Data obtained from these detection experiments were not included as the data was not consistent even after several trials of changing the working parameters. Steady state amperometric determination of the drugs was carried out at an applied potential of -250 mV with stirring maintained at 500rpm in buffer solution as the supporting electrolyte. The background current was allowed to reach a steady value before aliquots of standard drug solutions were successively added into the supporting electrolyte while steady-state current values were recorded as the response.

3.6 Stability, Reproducibility and Interference Studies:

The stability and reproducibility of the Au/PANSA/PVP-AgNPs/CYP2E1, Au/PANSA/PVP-AgNPs/SA-CYP2E1 and Au/PANSA/PVP-AgNPs/EG-CYP2E1 nanobiosensor was investigated in pH 7.4, 0.1 M phosphate buffer solution for two weeks and the modified bioelectrodes were stored at 4 $^{\circ}\text{C}$ when not in use. Ten successive measurements of either 2 μM ETH, 2 μM INH, 2 μM RIF or 2 μM RIF was carried out independently for two weeks. For the interference studies, K^+ , Mg^{2+} , Na^+ , NH_4^+ , Cl^- , SO_4^{2-} and NO_3^- ions were dissolved in distilled water and each was added independently to 2 μM of each TB drug solution. The resultant solutions were then analysed without any further pre-treatment by amperometry at 20 mV.

CHAPTER 4

Results and Discussion: Part 1

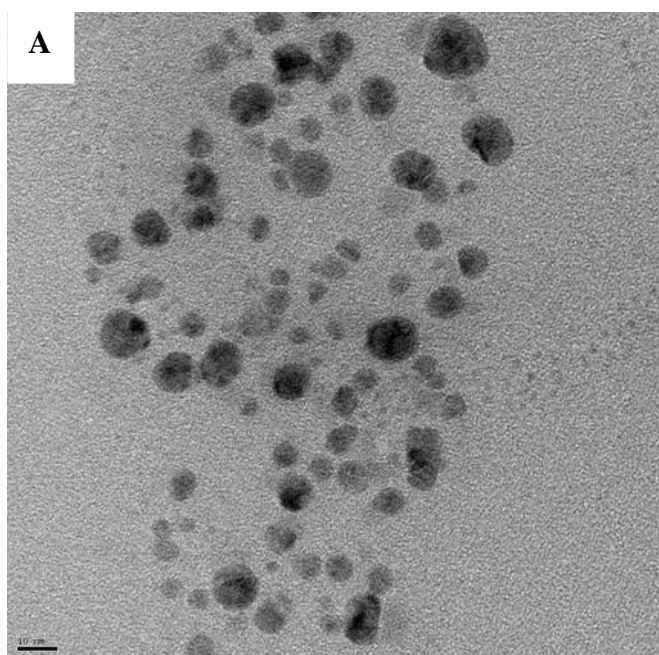
Summary

This is the first of three chapters outlining and discussing the results obtained from this study. This chapter deals specifically with the characterization of poly(8-anilino-1-naphthalene sulphonic acid), silver nanoparticles as well as the PANSA/Silver nanoparticulate composite used for the development of the nanobiosensor. Physical and electrochemical properties of these materials were interrogated using techniques such as CV, DPV, SWV, TEM, SEM and AFM. Therefore, this chapter clearly illustrates the success of using these techniques to study these nanomaterials and illustrates their potential towards the development of nanobiosensors for the detection of tuberculosis treatment drugs.

4.1 Morphology Characterization of PANSA, PVP-AgNPs and PANSA/PVP-AgNPs:

4.1.1 PVP-AgNPs:

In this study TEM was utilized to study the fine details of PANSA, PVP-AgNPs and PVP-AgNPs/PANSA nanocomposite. Figure 4.1 shows the TEM images of PVP-AgNPs dispersed in ethanol. The nanoparticles formed were predominately spherical and polydispersed with average diameter of 20 – 50 nm as indicated in Figure 4.1 A. The particle size was calculated by using approximately 100 randomly selected individual nanoparticles from the TEM micrograph giving a range of values (Arshi *et al.* 2011). Besides the above mentioned characteristics, some of the nanoparticles are seen to lay one above the other. Dark nanoparticles in Figure 4.1 B illustrate these under laying nanoparticles and in some areas on the image; these silver nanoparticles are clearly visible from beneath.



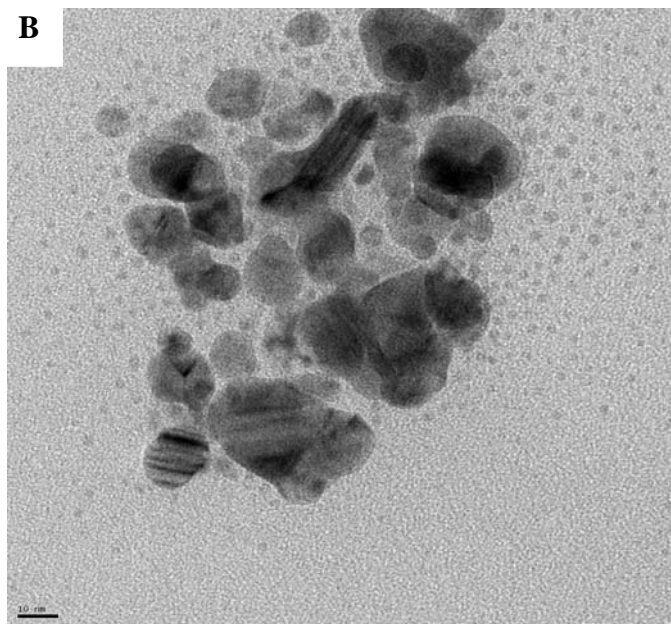


Figure 4.1: TEM images (A) indicating spherical and polydispersed PVP-AgNPs (B) Layer by layer orientation of some nanoparticles

The EDAX analysis (Figure 4.2) revealed the elemental composition of the synthesized nanoparticles suggesting silver as the predominant element. An optical absorption peak near 3 keV indicates the presence of metallic nano-sized silver. Other elemental signals were also recorded namely; carbon and oxygen and copper. Carbon and oxygen are due to presence of PVP in the nanoparticles while copper is a result of the copper grid onto which the nanoparticles were immobilization for TEM analysis (Kumar *et al.* 2011).

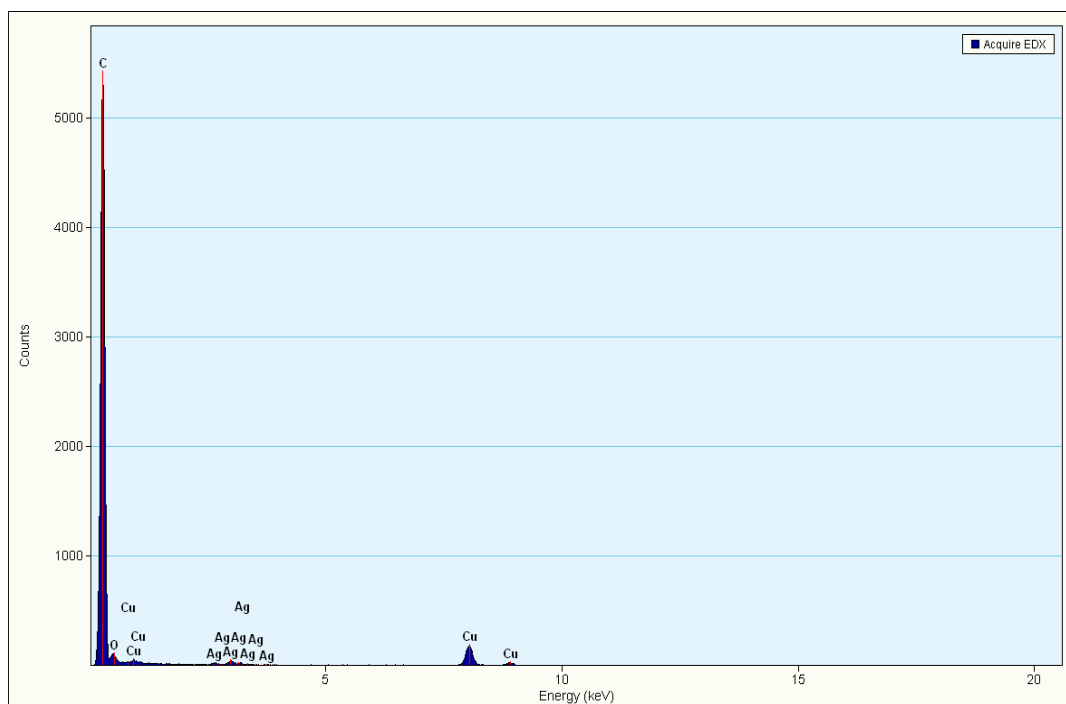


Figure 4.2: Energy dispersive X-ray spectrum of PVP-AgNPs

These silver nanoparticles are credited with producing the absorbance band at 450 nm, as observed in the UV-vis spectrum, Figure 4.3. The broadness of the peak is a further indication of the spheroid nature of the nanoparticles. Looking closely at the spectrum, one might notice that there is an undeveloped peak at around 410 nm which is due to transverse plasmon vibrations in the PVP-AgNPs, whereas the former is due to the excitation of longitudinal plasmon vibrations (Sathishkumar *et al.* 2009). Literature suggests that absorption spectra of spherical silver nanoparticles show maximum between 420 nm and 450 nm with a blue or red shift when silver nanoparticles either diminish or increase. As a result of this, the PVP-AgNPs synthesized in this study indicate a plasmon which is red shifted (Arshi *et al.* 2011).

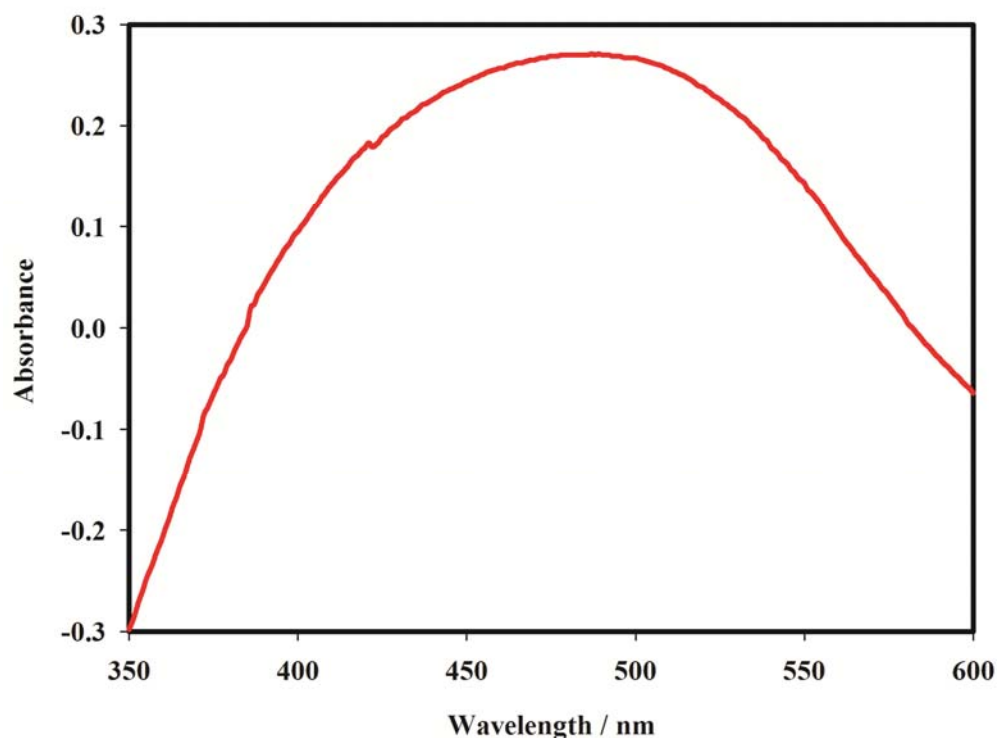


Figure 4.3: UV-vis spectrum of silver nanoparticles

The PVP-AgNPs synthesized in this study were almost identical to those produced from sun dried leaf powder of *Cinnamomum camphora* resulted from a reducing agent present in the plant (Huang *et al.* 2007). In a study by Basavaraja *et al.* 2008, spherical and polydispersed silver nanoparticles were also synthesized by an extracellular biosynthesis method using the fungus *Fusarium semitectum*. The results obtained in this study were also in agreement with those reported by Mukherjee *et al.* 2008; where silver nanoparticles were synthesized via a green synthesis process involving a non-pathogenic and agriculturally important fungus, *T. asperellum*.

4.1.2 PANSA:

The morphology of PANSA was also studied using TEM, however the structure was not clearly observed as seen in Figure 4.4. The polymeric material was observed from the image with no information on the orientation of PANSA. SEM was found to be the best technique to study PANSA because the distinct structure of the polymeric material was observed as seen in Figure 4.7. Therefore, the surface morphology of PANSA nanocomposites was observed with SEM.

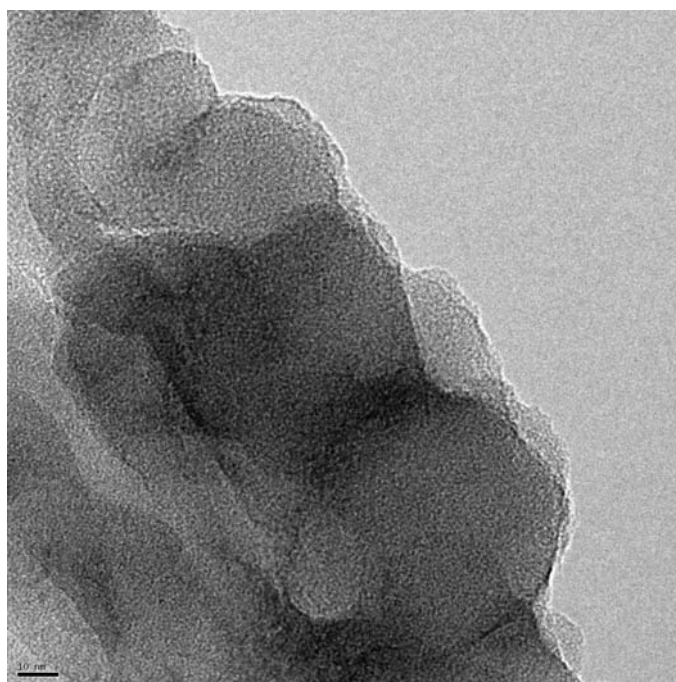


Figure 4.4: TEM image of PANSA

EDX analyses (Figure 4.5) gave the components of PANSA which are C-O-N-S from low to high energy respectively with energy scale of maximum approximately 3 keV. The O atom is due to the ITO glass substrate components while the observed S atom is contributed by the sulfonic substituent on PANSA. The N atom is as a result of the aniline substituent which forms part of the repetitive backbone of the polymer.

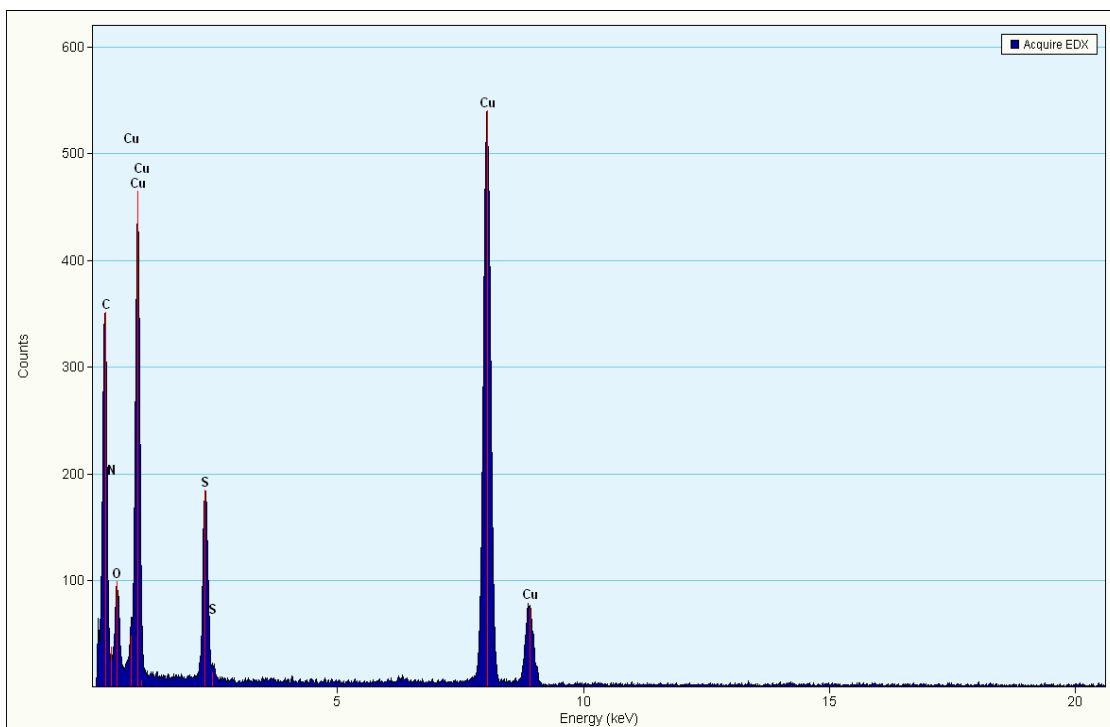


Figure 4.5: Energy dispersive X-ray spectrum of PANSA

Figure 4.6 shows the SEM morphology of PANSA film obtained in a solution containing 0.01 M ANSA and 0.50 M H₂SO₄ where regular and uniform PANSA nanotubes are observed. Their network structure increased the effective surface area of the electrode. The layer-by-layer nanotubes observed for the morphology of PANSA was seen to cover the electrode surface allowing the adsorption of both silver nanoparticles and enzymes as discussed in the next chapter. PANSA was also evaluated using UV-vis spectroscopy (Figure 4.7) where two distinct peaks were observed at 265 nm and 370 nm. These peaks are attributed to $\pi - \pi^*$ transition of benzoid rings and are indicative that nanostructured PANSA showed the formation or the presence of the stable pernigraniline salt. Because of the self-limiting nature of PANSA, there are no peaks observed between 600 nm and 800 nm which are normally observed in PANI. Depending on their specific location, the presence of these peaks is either associated with charge transfer excitons of the quinoid structure or are due to the doping level (Iwuoha *et al.* 2006).

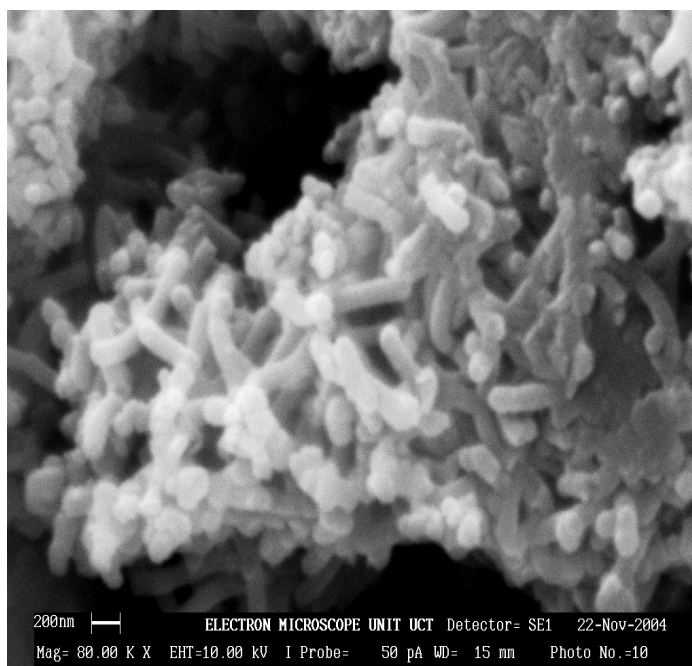


Figure 4.6: SEM image of electropolymerized PANSA

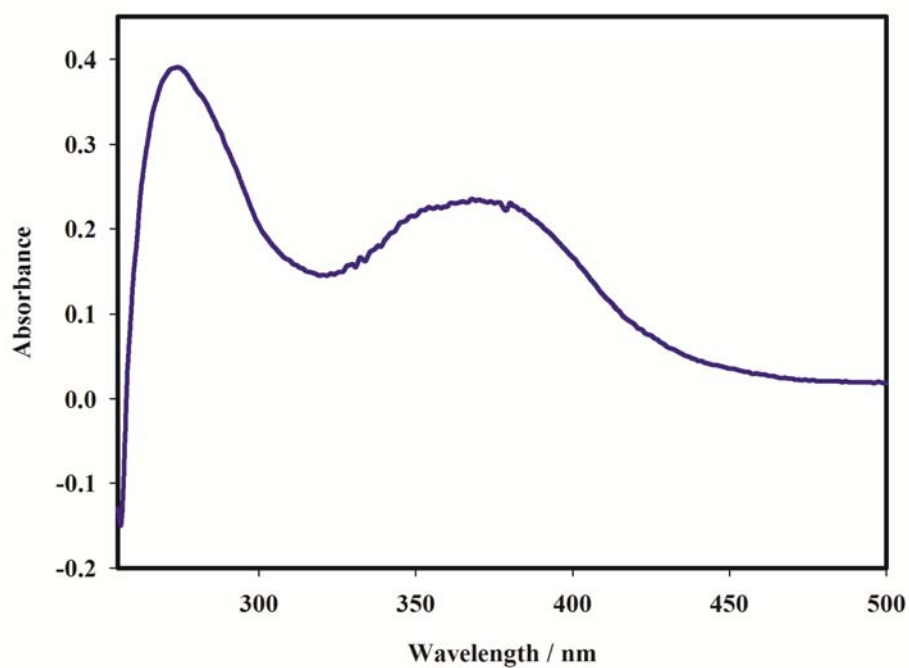


Figure 4.7: UV-vis spectrum of PANSA

4.1.3 PANSА/PVP-AgNPs:

After drop coating PVP-AgNPs onto PANSА, the resultant nanocomposite was evaluated using TEM. Figure 4.8 gives the TEM image of the PANSА/PVP-AgNPs nanocomposite. One can find that the PVP-AgNPs with a mean diameter of 20 nm – 50 nm are the core of the nanocomposite and the PANSА (as seen by the blob like structure) as the shell wrap of the PVP-AgNPs while some PVP-AgNPs are dispersed on the surface of PANSА. Agglomerated particles as large as 100 nm were also observed since the nanoparticles were deposited after the polymerization of PANSА.

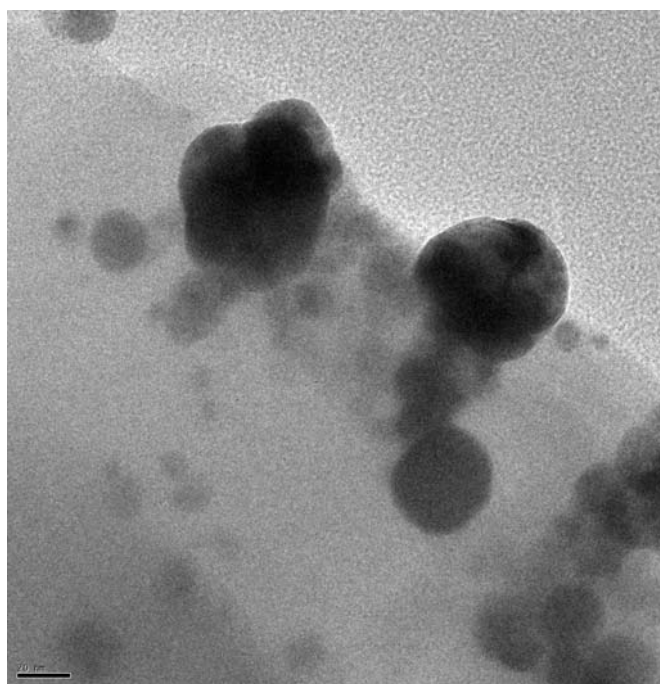


Figure 4.8: TEM image of PANSА/PVP-AgNPs nanocomposite

EDX analyses (Figure 4.9) gave the components of PANSА which are C-O-Si-S from low to high energy respectively with energy scale of maximum approximately 2.5keV. O-Si is due to the ITO glass substrate components while S is contributed by the sulphonic substituent of PANSА. On the other hand, the presences of PVP-AgNPs are indicated by an optical

absorption peak near 3keV which was also observed for the individual PVP-AgNPs reported previously.

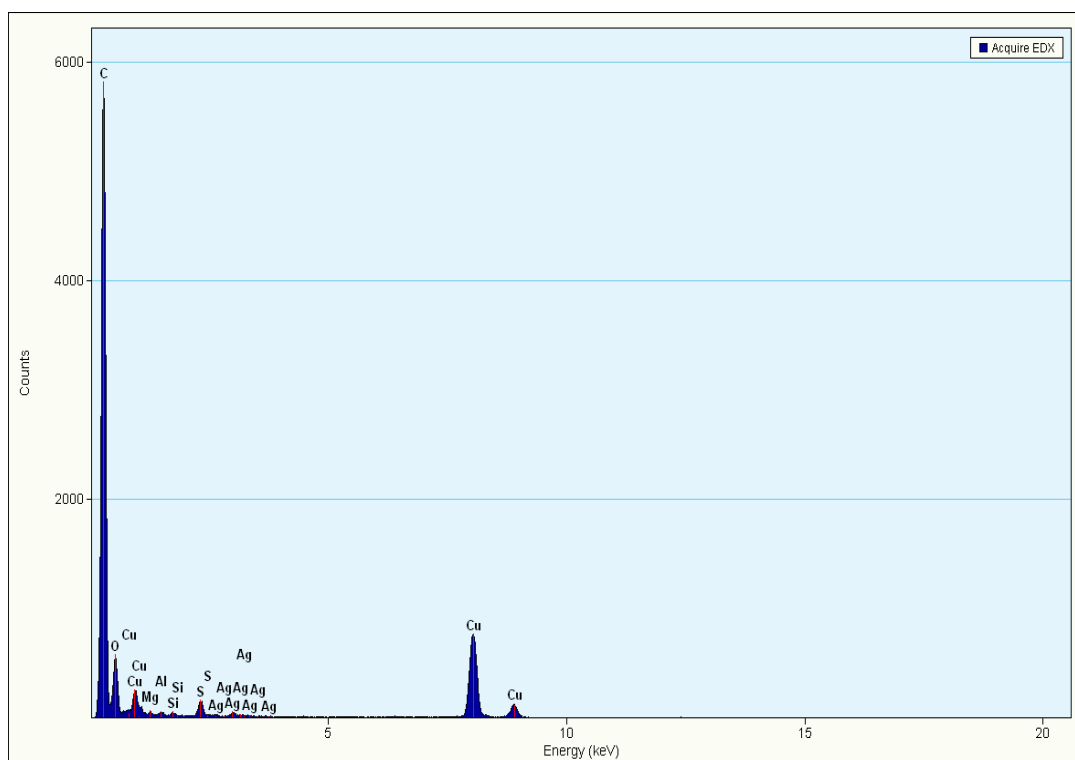


Figure 4.9: Energy dispersive X-ray spectrum of PANSAs/PVP-AgNPs

The PANSAs/PVP-AgNP nanocomposite was also studied using UV-vis. The resultant spectrum (Figure 4.10), illustrated two absorbance broad peaks at 425 nm and 535 nm and an undeveloped peak at approximately 410 nm. As indicated previously, the peak at 425 nm is due to excitation of longitudinal plasmon vibrations of PVP-AgNPs while that at around 410 nm is due to transverse plasmon vibrations in the PVP-AgNPs (Sathishkumar *et al.* 2009). The peak at 535 nm is as a result of $\pi - \pi^*$ transition of benzoid rings and that nanostructured PANSAs indicated the presence of the stable pernigraniline salt. A study by Jing *et al.* 2007 involving the synthesis and characterization of Ag/polyaniline core-shell nanocomposites also showed a similar behaviour for the nanocomposite.

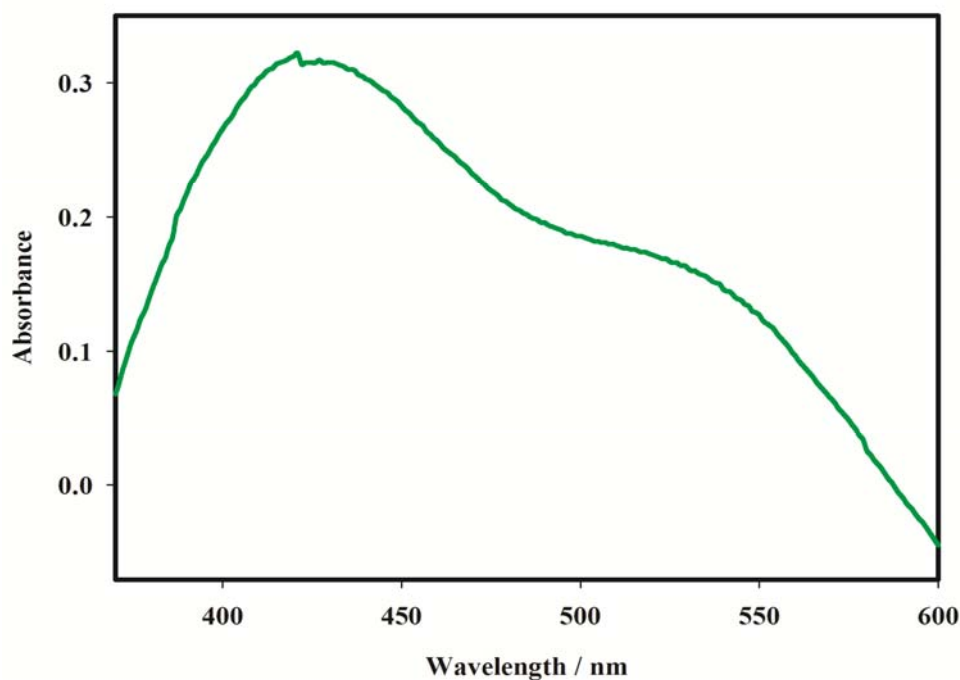


Figure 4.10: UV-vis spectrum of PANSA/PVP-AgNPs

4.1.4 EIS analysis:

4.1.4.1 Nyquist plot characterization:

Scheme 4.2 gives the stepwise fabrication procedure of the enzyme electrode. To monitor the self assembly process and in some cases, the electrochemical attachments, EIS was used to get information between each step. EIS is an effective method that is often used for probing the changes of surface-modified electrodes. Figure 4.11 shows curves of each modified step presented as Nyquist plot (Z_{im}^{∞} versus Z_{re}^0) where significant differences in EIS were observed during the assembly process. The total impedance was determined by several parameters such as solution resistance R_s ; double layer capacitance C_{dl} ; charge transfer resistance R_{ct} ; and Warburg impedance W ; among which C_{dl} and R_{ct} depend on the dielectric and insulating features at the electrode/electrolyte interface. On the other hand the

electron transfer kinetics of the redox-probe at the electrode interfaces being greatly affected by R_{ct} .

In this study, EIS measurements were carried out in pH 7.4, 0.1 M phosphate buffer at the potential window +1100 mV to -300 mV where bare Au, Au/PVP-AgNPs, Au/PANSA and Au/PVP-AgNP/PANSA were investigated. The change in electron transfer resistance arising after each surface modification step was investigated and represented as Nyquist diagrams as indicated in Figure 4.11. After the electrodeposition of PANSA on Au electrode, the semi-circle increased dramatically (curve a) compared to that of the bare Au electrode (curve c) indicating that the layer of PANSA functioned as a barrier making interfacial charge transfer more difficult. This semi-circle was found to be much larger than that observed for (curve d) Au/PVP-AgNPs indicating that PVP-AgNPs have a much higher conductivity than PANSA.

Drop-coating PVP-AgNPs on the PANSA film resulted in a further decrease in the semi-circle (curve b). Since PVP-AgNPs have a much higher conductivity than PANSA, this interaction allowed a much easier electron transfer process to occur between the electrode surface and the nanocomposite. The nanocomposite indicated to possess increased conductivity as opposed to PVP-AgNPs and PANSA individually. Therefore, the smaller the impedance as illustrated by the reduced semi-circles, the higher the conductivity. The PVP-AgNPs nanocomposite was then ready for the immobilization of the CYP2E1 to form the nanobiosensor whose impedance was also studied (Yin *et al.*2010; Arotiba *et al.*2010; Ding *et al.*2003).

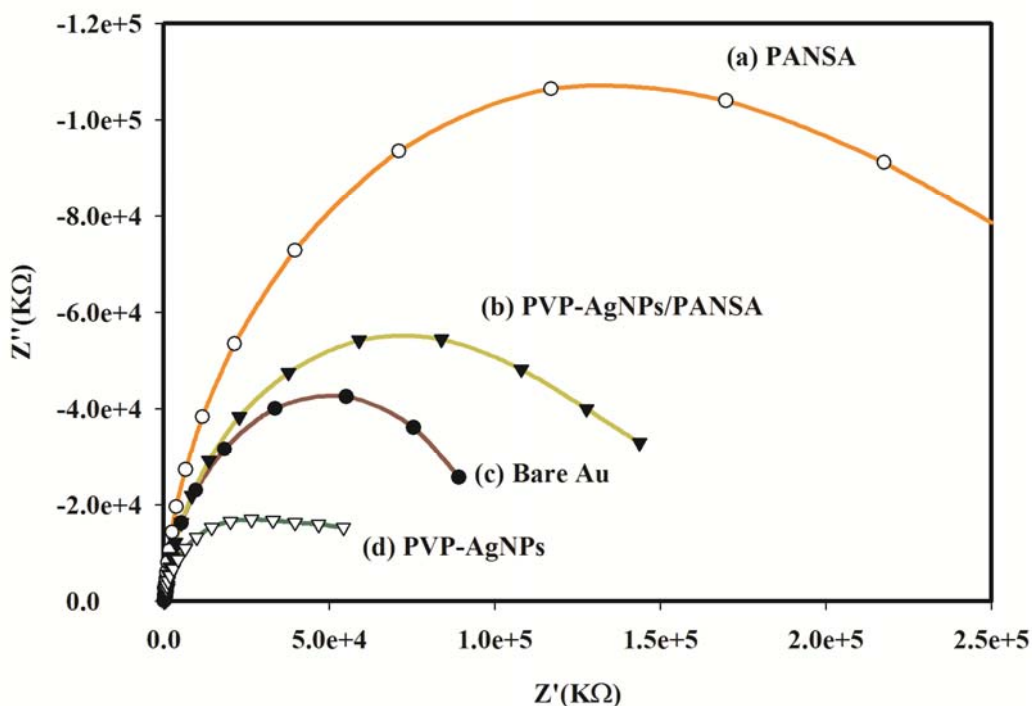


Figure 4.11: EIS Nyquist plot of PANSAs, PVP-AgNPs and PANSAs/PVP-AgNPs modified electrodes

4.2.4.2 Bode plot characterization:

Bode plot analysis (Figure 4.12) for the Au/PANSAs/PVP-AgNP nanocomposite showed a higher conductivity than bare Au electrode with a lower charge transfer resistance when compared to the Au/PVP-AgNP and Au/PANSAs electrodes. This is indicative of a fast electron transfer between the Au electrode and the nanocomposite. The direct interaction of the electrons with the bare Au electrode resulted in a high R_{ct} value of 89.27 KOhm while values for Au/PVP-AgNP (118 KOhm), Au/PANSAs (217.6 KOhm) and Au/PANSAs/PVP-AgNP (35.51 KOhm) were observed. These values revealed the hindering ability of PANSAs and PVP-AgNP on the electrode thus impeding electron transfer. The exchange current value obtained for the bare electrode further confirmed its ability to transfer electron fast when compared to modified electrodes. The bode plot in Figure 4.12 confirmed this behaviour by a

huge increase in impedance after the electrode was modified with either PANSA, PVP-AgNPs or PVP-AgNPs with observable shifts in phase angles for the bare, PANSA, PVP-AgNPs and PANSA/PVP-AgNPs modified electrodes (Yin *et al.*2010; Arotiba *et al.*2010; Ding *et al.*2003).

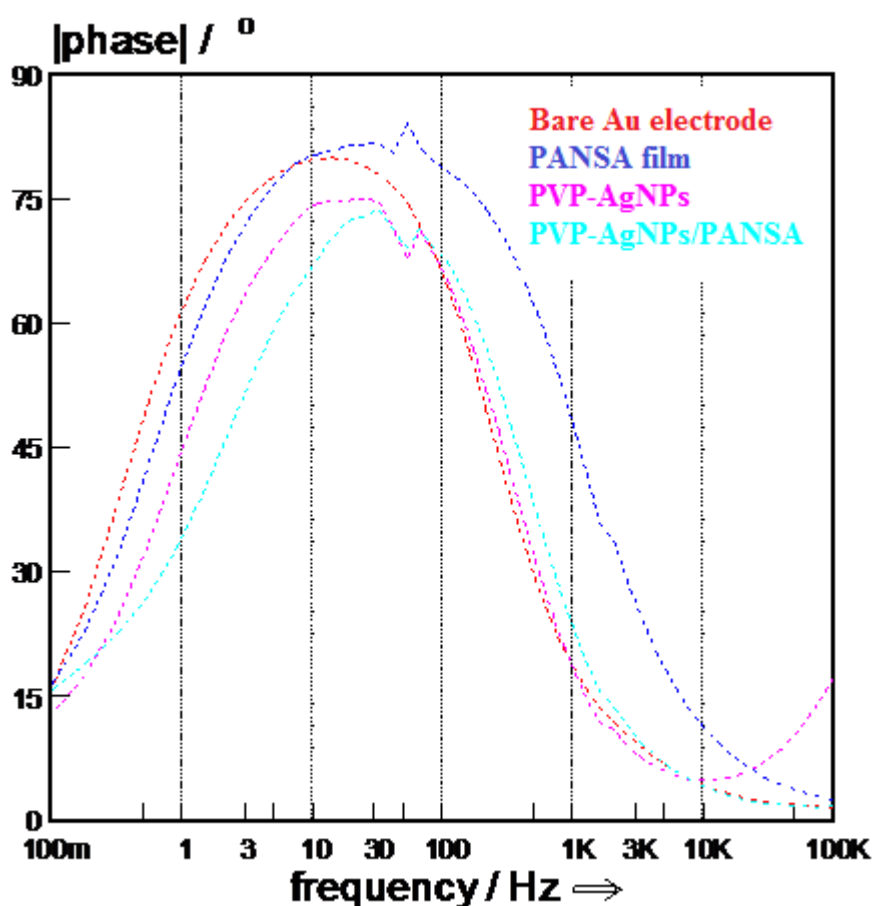


Figure 4.12: Bode plot of PANSA, PVP-AgNPs and PANSA/PVP-AgNPs modified electrodes

Table 4.1 gives a list of all the parameters; R_s , C_{dl} , R_{ct} and Warburg element, Z_w , resulting from the EIS study. The parameters were used to calculate the time constant using equation 4.1 a and 4.1 b (where Time constant = τ) and the exchange current (i_o) by using equation 4.2. Where C_{dl} = double layer capacitance; τ = time constant; R_{ct} = charge transfer

resistance. K_{et} , the homogeneous rate constant was determined by using equation 4.3. The resulted parameters are clearly illustrated in Table 4.2.

Table 4.1: EIS parameters attained from the circuit fitting of plots in Figure 4.15 for bare Au, PANSA, PVP-AgNPs and PANSA/PVP-AgNP modified Au electrode

Parameter	Bare Au	Au/PANSA	Au/PVP-AgNP	Au/PANSA/PVP-AgNP
Electrolyte resistance (R_s) (Ohms)	159.1	134.4	461.4	222
Charge transfer resistance (R_{ct}) (KOhms)	89.27	217.6	118	35.51
Warburg impedance (W) (kDW)	2.905	26.63	16.83	13.82
Double layer capacity (C_{dl}) (uF)	2.888	845.7	880.1	1.417

$$\omega_{\max} = \frac{1}{R_{ct} C_{dl}} \quad \text{Equ. 4.1(a)}$$

$$\tau = R_{ct} C_{dl} \quad \text{Equ. 4.1(b)}$$

$$i_o = \frac{RT}{nFR_{ct}} \quad \text{Equ.4.2}$$

$$i_o = nFAK_{et} C^* \quad \text{Equ. 4.3}$$

Table 4.2: Results for time constant, exchange current and homogeneous rate constant for bare Au, PANSA, PVP-AgNPs and PANSA/PVP-AgNPs modified Au electrode

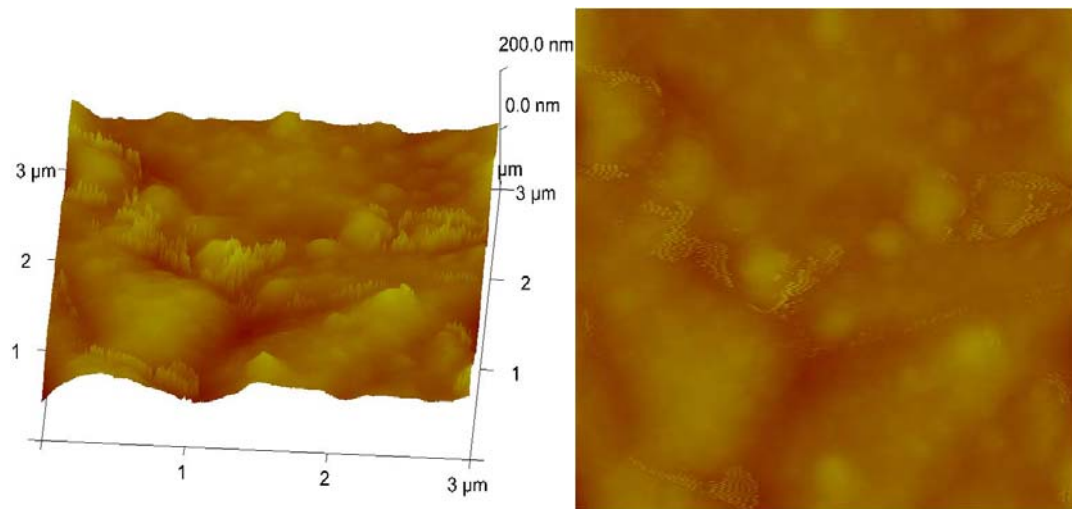
Element	Bare AuE	PANSA	PVP-AgNPs	PANSA/PVP-AgNPs
Time Constant τ (s rad ⁻¹)	8.54×10^{-3}	4.70×10^{-2}	1.59×10^{-3}	1.49×10^{-3}
Exchange current i_0 (A)	1.43×10^{-4}	5.00×10^{-5}	1.09×10^{-4}	3.61×10^{-4}
K_{et} (cm s ⁻¹)	3.68×10^{-4}	1.52×10^{-4}	2.80×10^{-4}	9.31×10^{-4}

4.2.4.3 AFM Analysis:

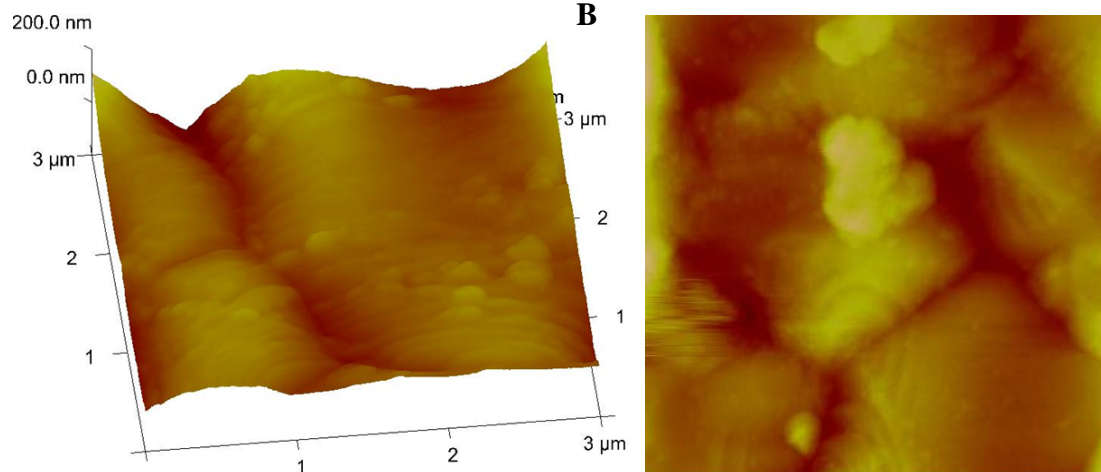
AFM analyses were carried out for PANSA, PVP-AgNPs and PANSA/PVP-AgNP to investigate the differences in their surface morphology. Figure 4.13 exhibits the AFM images of the bare screen printed gold electrode (SPAuE) (Figure 4.13 A) and the substrate modified with different nanomaterials; PANSA film, PVP-AgNPs and PANSA/PVP-AgNP nanocomposite, respectively. As can be seen from Figure 4.13 B, silver nanoparticles are obviously assembled on the gold substrate. The size of the formed silver nanoparticles is about 20 nm - 50 nm, and the roughness of the formed silver nanoparticles layer is about 10 nm. Similar to SEM, the electrodeposited PANSA film (Figure 4.13 C) shows a porous structure, indicating the tubular nature of PANSA with a roughness of 10 nm. It can be seen that for the PANSA/PVP-AgNPs nanocomposite in Figure 4.13 D, the produced silver nanoparticles are almost homogeneously distributed within the electrodeposited PANSA film. Of interest is the fact that the surface of the nanocomposite is rougher than both of the PANSA and silver nanoparticles film independently. The reason for the difference can be attributed to the highly hydrophilic nature of the polymer which is able to adsorb metal particles and forms rigid nanocomposites. In the presence of PANSA, the assembled silver

nanoparticles are covered by PANSA evenly and thus prevent it from growing bigger. Moreover, PANSA adsorbed onto silver nanoparticles can also stabilize the formed silver nanoparticles, and with the electrodeposition of PANSA, silver nanoparticles can be entrapped into the PANSA film.

A



B



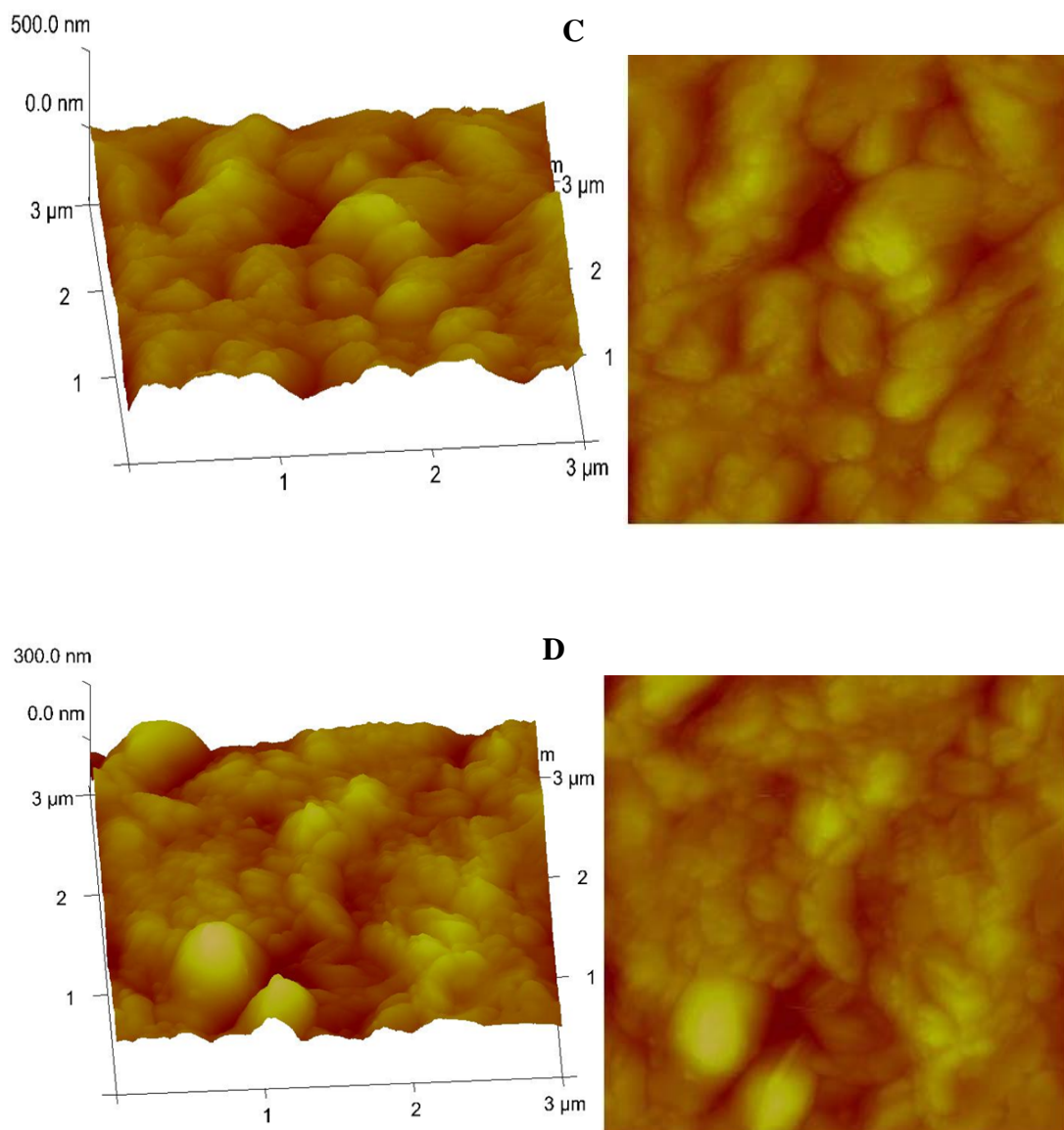
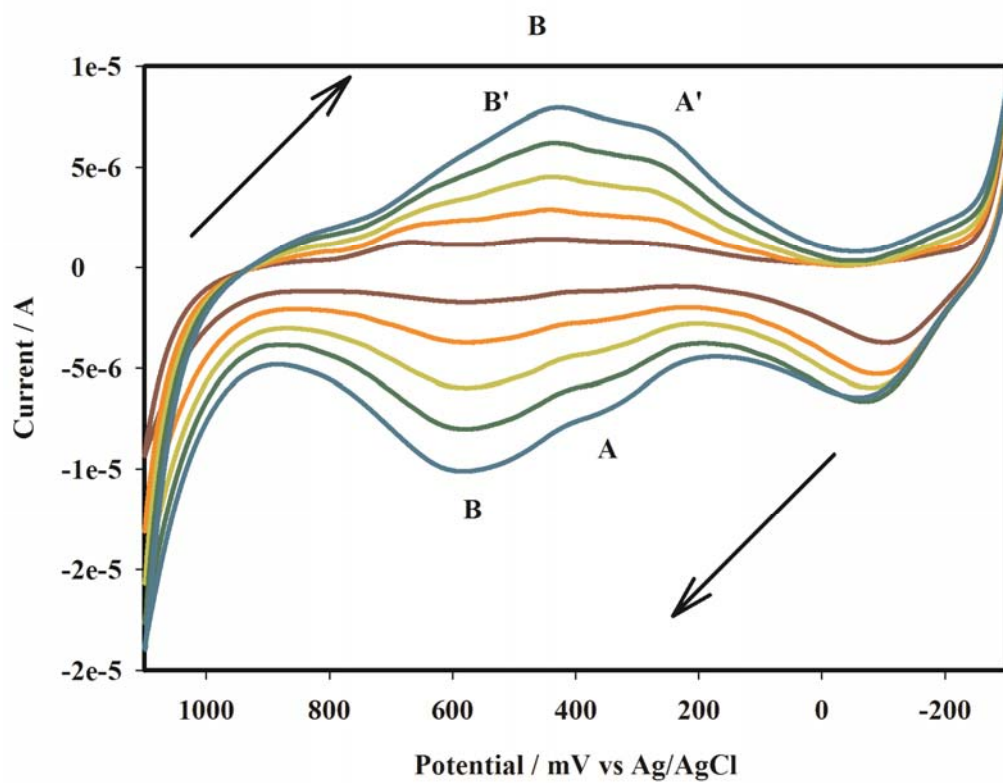
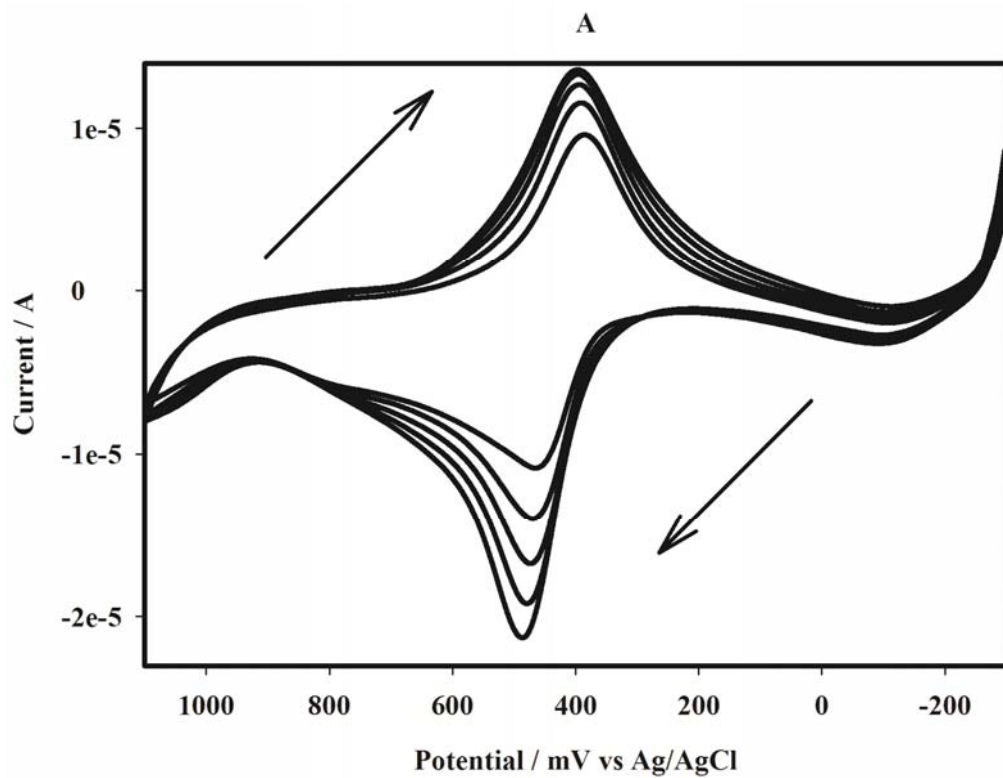


Figure 4.13: AFM images of (A) bare SP AuE (B) SP AuE/PVP-AgNPs (C) SP AuE/PANSA and (D) SP AuE/PANSA/PVP-AgNPs

4.2. CV Characterization of PANSA:

PANSA was prepared from 0.01 M ANSA in 0.5 M H₂SO₄ by electropolymerization on a 0.0201 cm² diameter Au disk working electrode using CV at 50 mV/s from -300 to +1100 mV. Figure 4.14 A shows a typical cyclic voltammogram of the nanotubular polymeric film on Au produced after 5 voltammetric cycles with Scheme 4.1 clearly illustrating the polymerization process. It can be seen that, PANSA possesses one redox couple illustrating an anodic shift in the polymerisation peak potential with the result that the formal potential; $E^{0'}$ values increased from +425 mV for the first polymerisation cycle to +440 mV with an average of 433 mV and error of 8.89. This indicates that the oxidation of ANSA on already deposited polymer involves charge transportation across the polymer film and is therefore energetically more demanding, whereas the reduction of the accumulated polymer film becomes easier. The observed increased anodic peak currents and decreased cathodic peak currents are attributed to the influence of the naphthalene sulphonic acid moiety which makes the aniline substitute self-limiting upon polymerization. This differs from the electropolymerization of aniline alone which is well known to be of a self-accelerating character. This behaviour of PANSA was found to be closely related to that observed in a study carried out by Mazeikiene *et al.* 2006 in which one redox couple was also observed when aminonaphthalene sulphonates were polymerized in the presence of 0.1 M sulphuric acid where a $E^{0'} = +415$ mV was obtained. One redox couple was also observed in another study in which PANI was polymerized in the presence and absence of sodium dodecyl sulphate where an $E^{0'}$ value was estimated to be +410 mV (Mazeikiene *et al.* 2006).



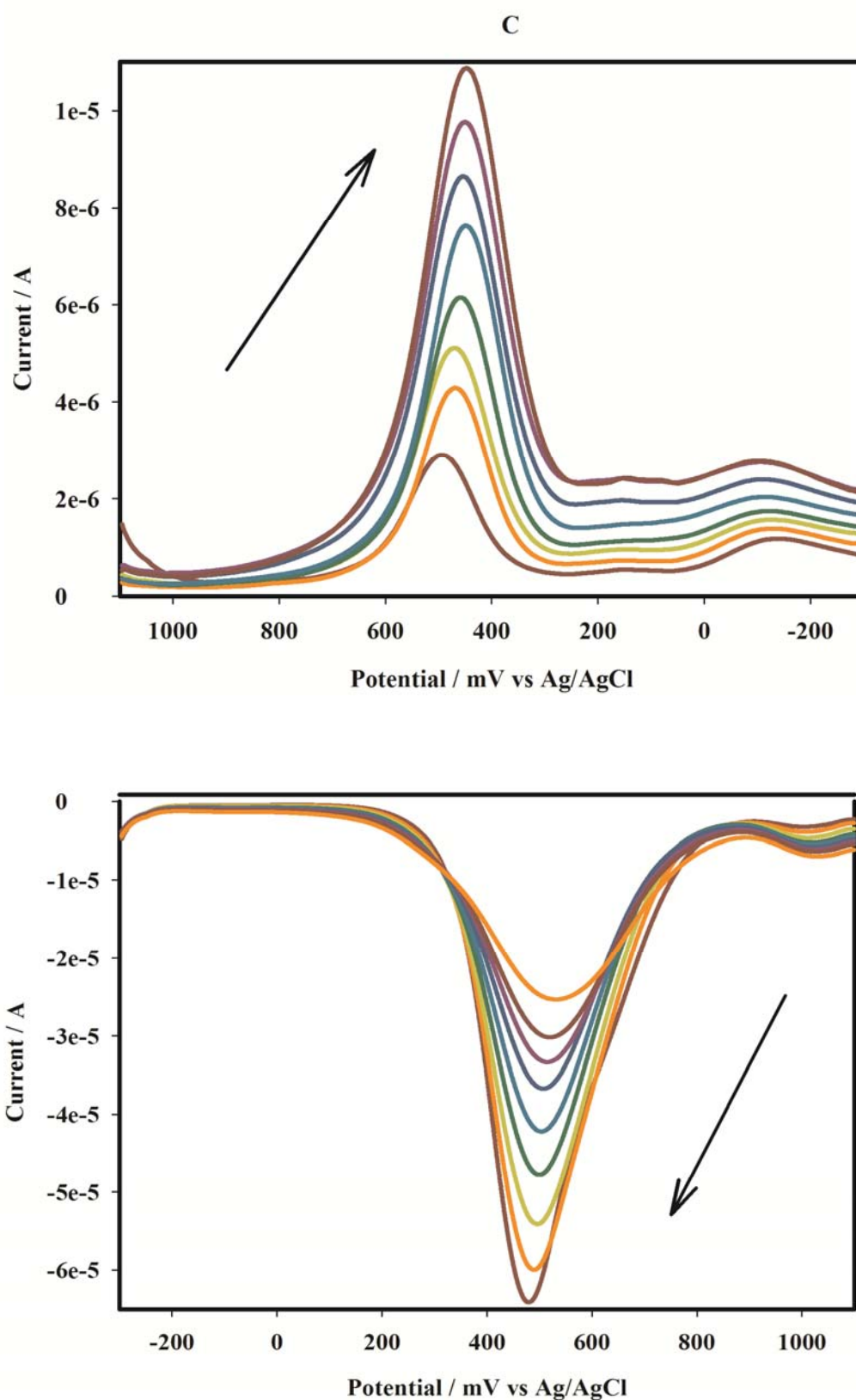
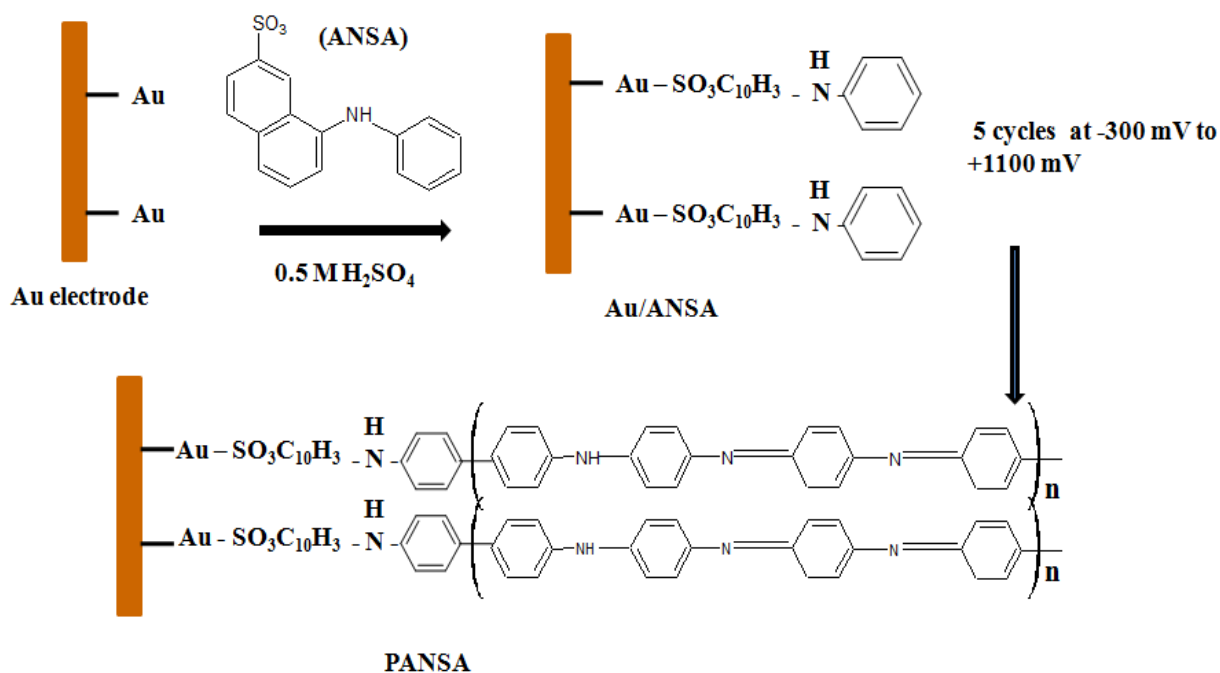


Figure 4.14: Cyclic voltammograms of (A) electrochemical synthesis of PANSAs at 50 mV/s and electrochemical characterization of PANSAs using (B) CV and (C) SWV of Au/PANSAs electrode in 0.5 M H_2SO_4 at different scan rates



Scheme 4.1: Schematic representation of ANSA polymerization on Au electrode to produce PANSA

Using the CV of polyaniline (PANI) as a reference point, the redox couple observed in the synthesis of PANSA is indicative of the most stable form of PANI, the emeraldine radical cation/emeraldine transition. CV characterizations at different scan rates (10, 20, 30, 40, 50, 50, 70, 80, 90 and 100 mV/s) of both PANSA and PANI in the presence of their respective polymerization acidic media show similar electrochemistry as denoted by the configuration of their peaks. Evidence of this can be seen in Figure 4.14 B where the characterization of PANSA shows a similar electrochemistry to that of PANI in the work done by Lindofors *et al.* 2002. This interaction is also reflected in the accompanying square wave (Figure 4.14 C). The redox couples A'/A and B'/B are attributed to intrinsic redox processes of the polymer. Similar voltammograms have been reported for polyaniline confirming that aniline in anilinonaphthalene sulfonic acid can be polymerized. The redox couple; A'/A is as a result of the transformation of aniline in ANSA from the reduced polyleucoemeraldine state to the partly oxidized polyemeraldine state. The second redox

peak; B/B is due to the transition of polyleucoemeraldine state to the pernigraniline state, which is accompanied by oxidation of ANSA monomer (Lindofors *et al.* 2002; Iwuoha *et al.* 2006; Mathebe *et al.* 2004; Pu *et al.* 2007). At low scan rates, there is an observed third anodic peak attributed to the electrochemistry of p-benzoquinone formed in the polymerization process (Iwuoha *et al.* 2007). Of interest is the fact that at high scan rates, two anodic peaks which appeared at the initial stage of polymerization were seen to merge into one peak. This explains the broadness of the outer anodic peak confirming the self-limiting character of PANSAs.

The multiscan voltammograms of the PANSAs film modified Au electrode in 0.50 M H₂SO₄ solution shown in Figure 4.14 B indicates that the peak potentials as well as the peak currents were seen to vary with scan rate. Slopes of plots of log scan rate versus log current are commonly used to identify diffusion controlled or adsorption controlled peaks or even a mixture of the two. In such plots, a slope of 1 is indicative of an adsorption controlled peak while 0.5 indicates a diffusion controlled peak with intermediate values indicating mixed diffusion/adsorption controlled peaks. In this study, all plots of log scan rate versus log current gave values in the range of approximately 1 as indicated in Figure 4.15. This indicates an adsorbed electroactive polymer with electron diffusion taking place along the polymer chain (Kanungo *et al.* 2002; Mu *et al.* 1997; Bistolas *et al.* 2005). Therefore, the role of the PANSAs film in the nanobiosensor construction was to shuttle electrons between the Au disk electrode and the active site of the immobilized enzyme and served as a point of attachment for the enzyme CYP2E1 and silver nanoparticles. This interaction is clearly illustrated in Scheme 4.2.

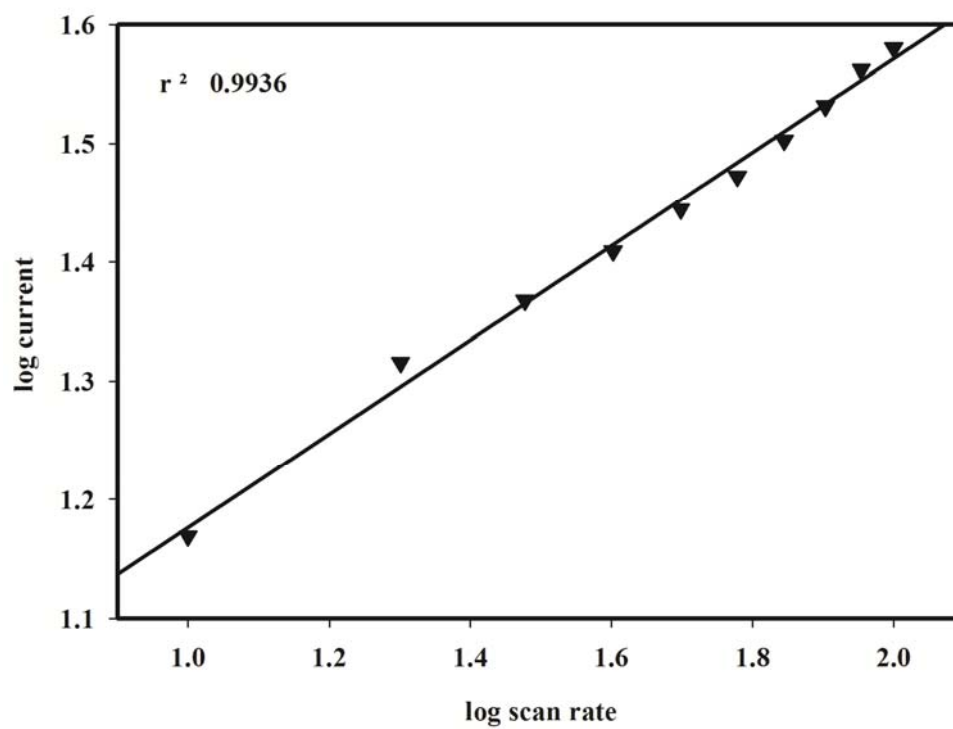
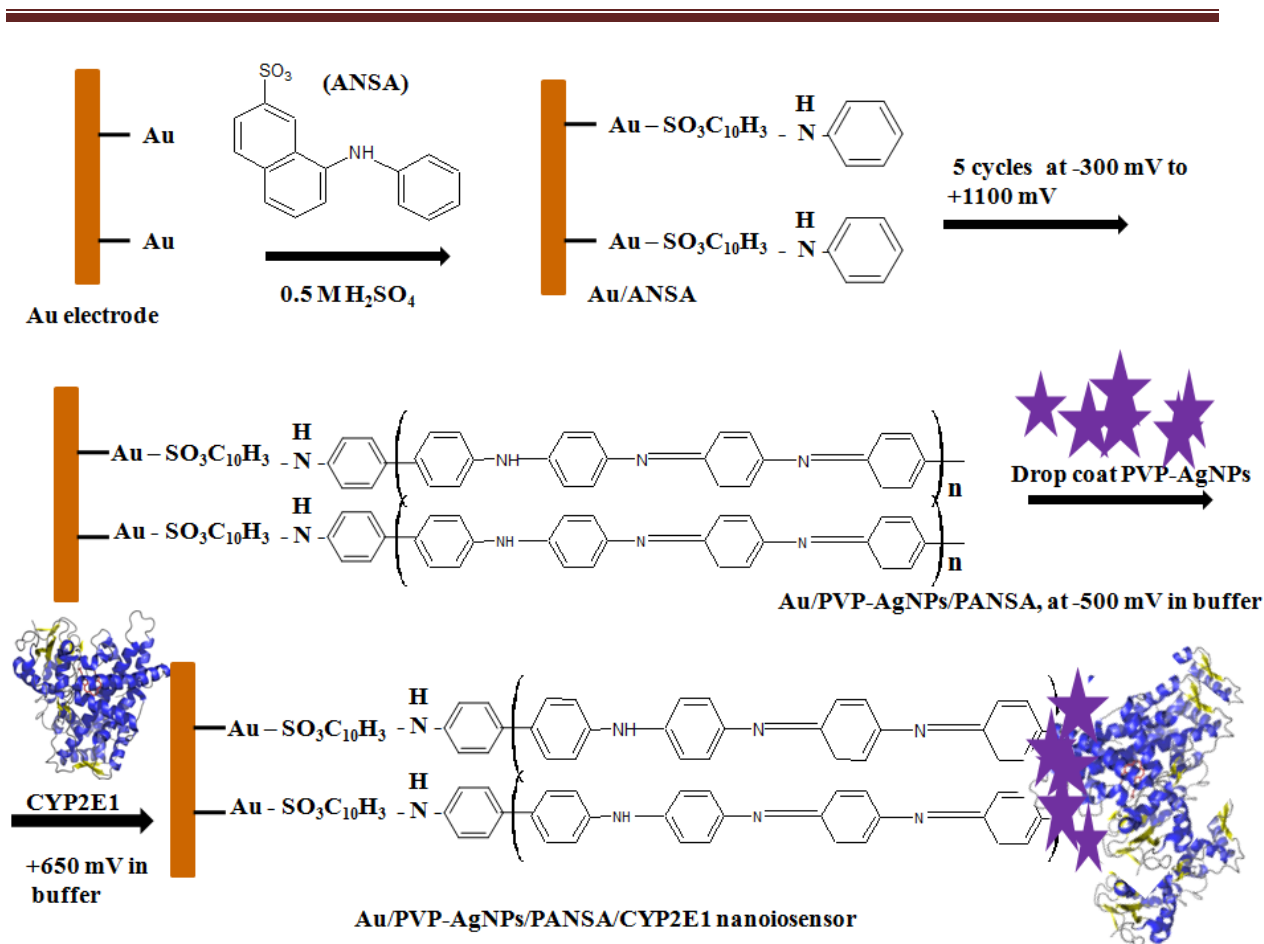


Figure 4.15: Plots of log scan rate versus log current



Scheme 4.2: Schematic representation of PANSA on Au electrode and the illustration of the immobilization of PVP-AgNPs and CYP2E1

Also illustrated in Figure 4.14 B, is the linear dependency of the current on the scan rate for the main redox couple B/B. This is indicative of a thin surface bound conducting electro-active polymer film undergoing a rapid reversible electron transfer reaction along the polymer backbone possibly through the conjugated benzene ring units making up the chain. $I_{p,c}$ (peak B') / $I_{p,a}$ (Peak B) which was obtained to be ~ 1.1 confirming that the polymer behaved as a stable redox species adsorbed on the electrode surface undergoing reversible electrochemistry. A similar behaviour was also observed in the work carried out by Brahim *et al.* 2003 and Mu *et al.* 1997. $\Delta E_p [E_{p,a} (\text{Peak B}') - E_{p,c} (\text{Peak B})]$ was calculated for the polymer film grown at different scan rates but the film grown at 50 mV/s resulted in a value

of ΔE_p lower than 65 mV, which was also seen from the work of Bistolos *et al.* 2005. This suggested that the polymer grown at this scan rate exhibited a reversible and a fast electrochemistry as compared to polymer grown at other scan rates which are suggestive of slow electron transfer rates. Using the Brown-Anson method (Equation 4.4), the surface concentration of the polymer was estimated to be $1.0257 \times 10^{-6} \text{ mol cm}^{-2}$ (0.6 ± 0.1).

$$\frac{I_p}{4RT} = \frac{n^2 F^2 \Gamma^*_{PANSa} A \nu}{4RT} \quad \text{Equ. (4.4)}$$

Where n represents the number of electrons involved in the reaction, F the Faraday constant, 96,584 C/mol, Γ^*_{PANSa} is the surface concentration of the PANSa film in mol cm^{-2} , ν the scan rate in mV/s, A is the electrode area of the electrode (0.0201 cm^2), R the universal gas constant, $8.314 \text{ J mol K}^{-1}$ and T is the temperature of the system, 298 K. The magnitude of the peak currents was seen to increase upon increment of the scan rate suggesting that the peak currents are diffusion controlled. D_e , the electron charge transport coefficient, also known as the rate of electron charge propagation along the polymer chain and is determined using the Randel-Sevcik method (Equation 4.5). For this study, this coefficient was estimated to be $3.8225 \times 10^{-2} \text{ cm s}^{-1}$. Accuracy of this calculation is based on non-variation of the potential with scan rate, with variation in scan rate being the essential parameter. An increased value was obtained in this study as compared to that of $8.68 \times 10^{-9} \text{ cm s}^{-1}$ observed in PANI studies reported by Iwuoha *et al.* 2004 and a value of $6.46 \times 10^{-8} \text{ cm s}^{-1}$ (0.6 ± 0.1) reported by Iwuoha *et al.* 1997.

$$\frac{I_p}{\nu^{1/2}} = \frac{0.4463 (nF)^{3/2} D_e \Gamma_{PANSAs}^* A}{L(RT)^{1/2}} \quad \text{Equ. (4.5)}$$

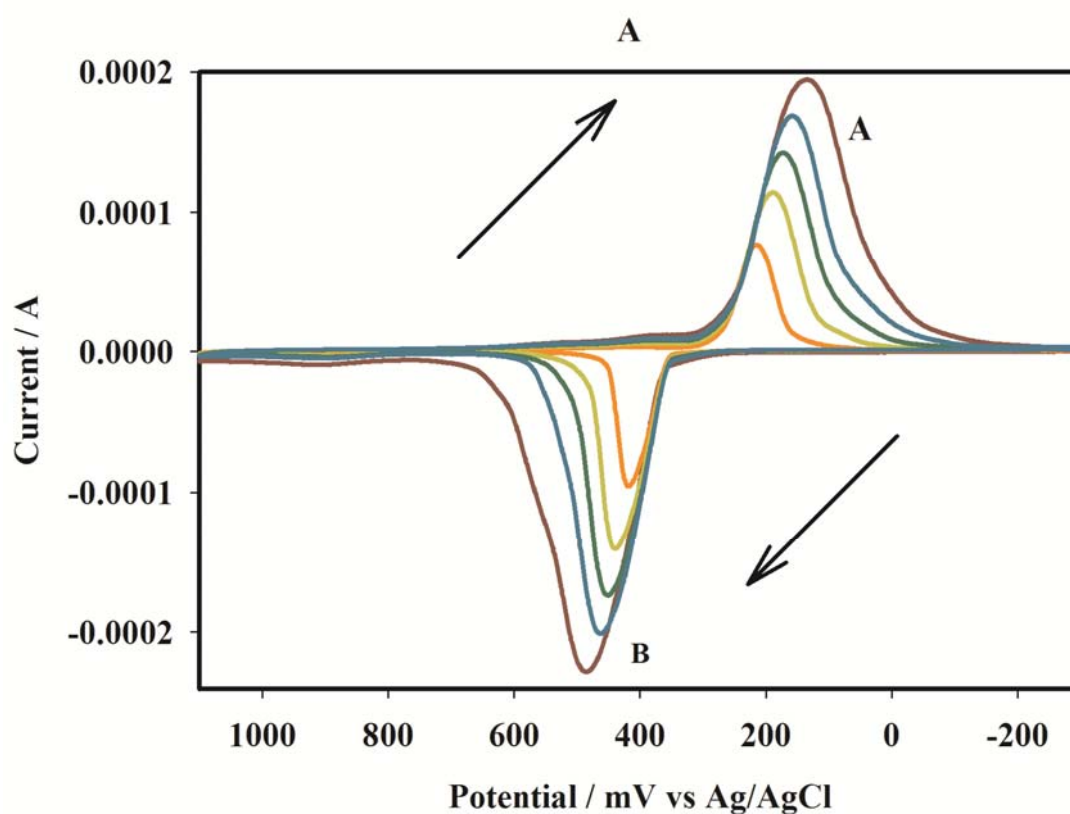
Where L represents the polymer thickness.

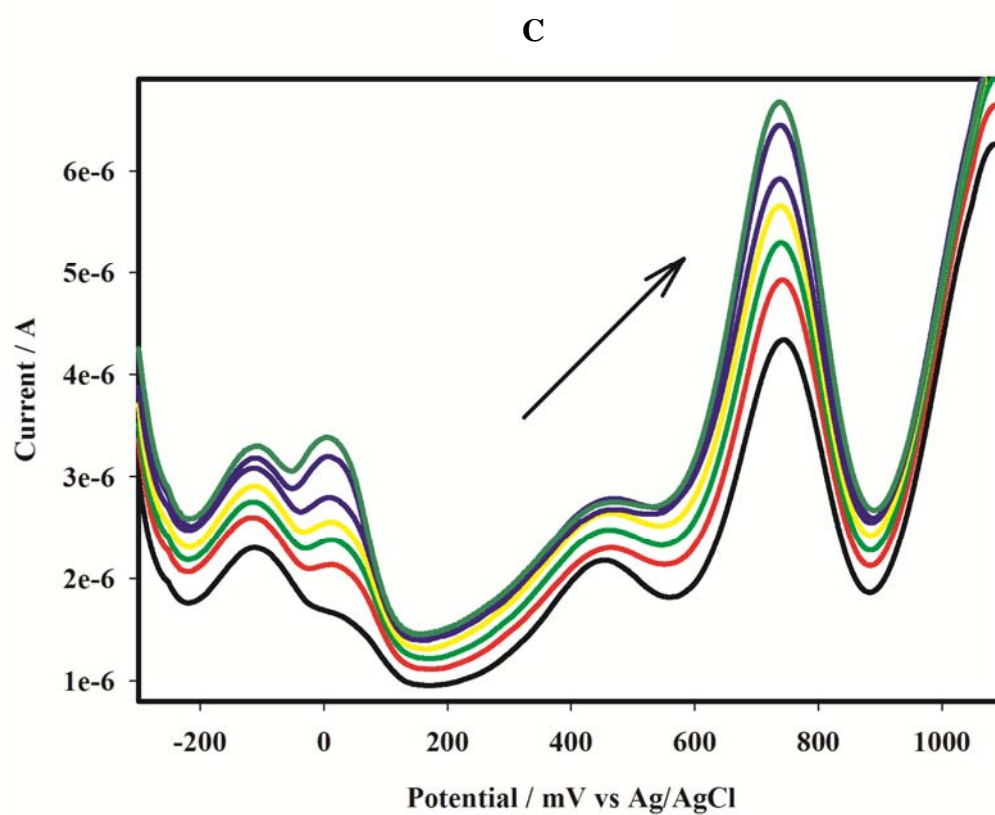
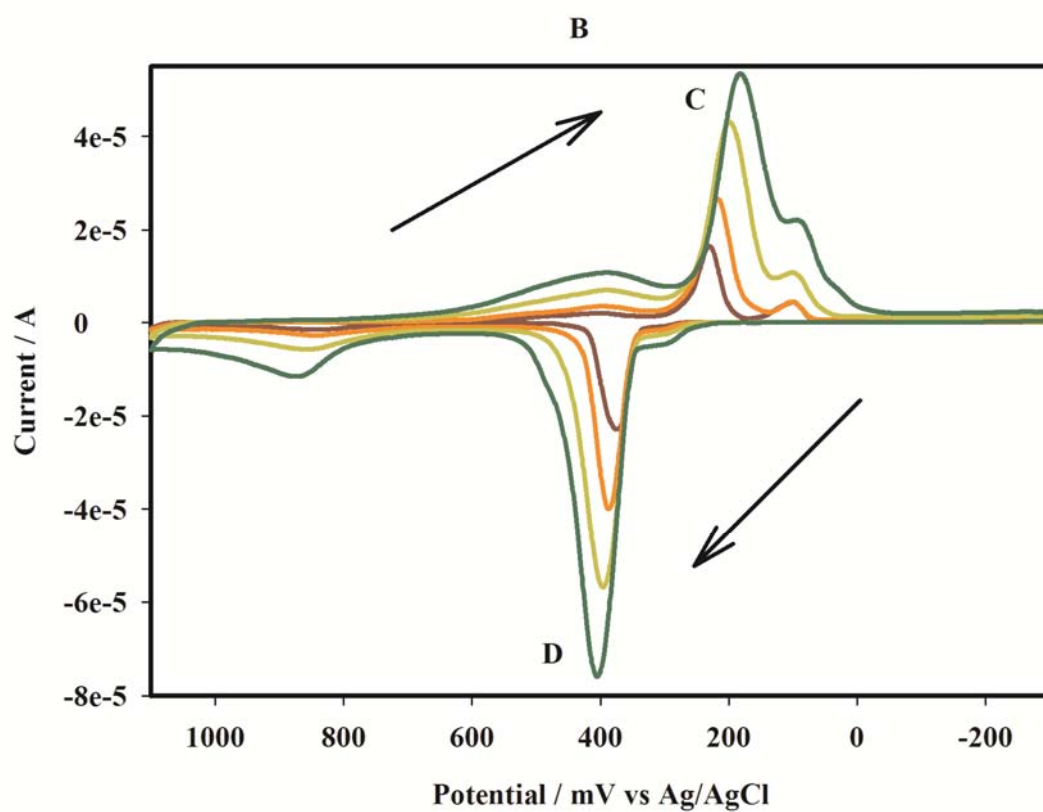
4.3 CV Characterization of PVP-AgNPs and PANSAs/PVP-AgNPs:

A layer of the PVP-AgNPs was deposited by drop-coating on the Au/PANSAs electrode after polymerization of PANSAs. The effect of the PVP-AgNPs on the electroactivity of PANSAs was evaluated by comparing the profile of the three electrodes namely; Au/PANSAs (Figure 4.14 B), Au/PVP-AgNPs (Figure 4.16 A) and Au/PANSAs/PVP-AgNPs (Figure 4.16 B). For the Au/PVP-AgNPs electrode, a pair of quasi-reversible redox peaks was obtained at +490 mV and +180 mV resulting from the Ag(0) to Ag(I) transition. With increasing scan rate, the PVP-AgNPs oxidation peak was seen to be shifted oxidatively, from +180 mV (peak A in Figure 4.16 A) to +195 mV (peak C in Figure 4.16 B) and the reduction peak cathodically from +490 mV (peak B in Figure 4.16 A) to +395 mV (peak D in Figure 4.16 B).

The shift in potential is accompanied by a large background current, indicating that the electroactive area of Au electrode has been increased due to the high special surface area of PVP-AgNPs. Of great interest is the fact that for the Au/PANSAs/PVP-AgNPs electrode, both PANSAs (as observed from the Au/PANSAs electrode) and the PVP-AgNPs redox peaks are clearly evident in the voltammograms illustrated in (Figure 4.16 B) and further illustrated by SWV as indicated in Figure 4.16 C indicating a strong interaction between PANSAs and PVP-AgNPs. Li and co-workers also reported a similar pattern illustrating more negative peaks on glassy carbon electrode. In another study where glassy carbon electrode was used (Li *et al.* 2005), the oxidation peak was observed at +700 mV and the reduction peak at +330 mV. A decrease in peak current was observed for the Au/PANSAs/PVP-AgNPs electrode

compared to the Au/PVP-AgNPs electrode. This is attributed to further modification of PANSAs by PVP-AgNPs on the electrode surface, with the resultant nanocomposite blocking mass transfer of electroactive probe. The reduced current did not affect the electroactivity of PANSAs since there was no significant shift or change in the PANSAs peaks as demonstrated by the peak at around +120 mV resulting from the transformation of aniline in ANSA from the reduced polyleucoemeraldine state to the partly oxidized polyemeraldine state (Guasquito *et al.* 2008; Wang *et al.* 2006; Owino *et al.* 2008; Lin *et al.* 2008).





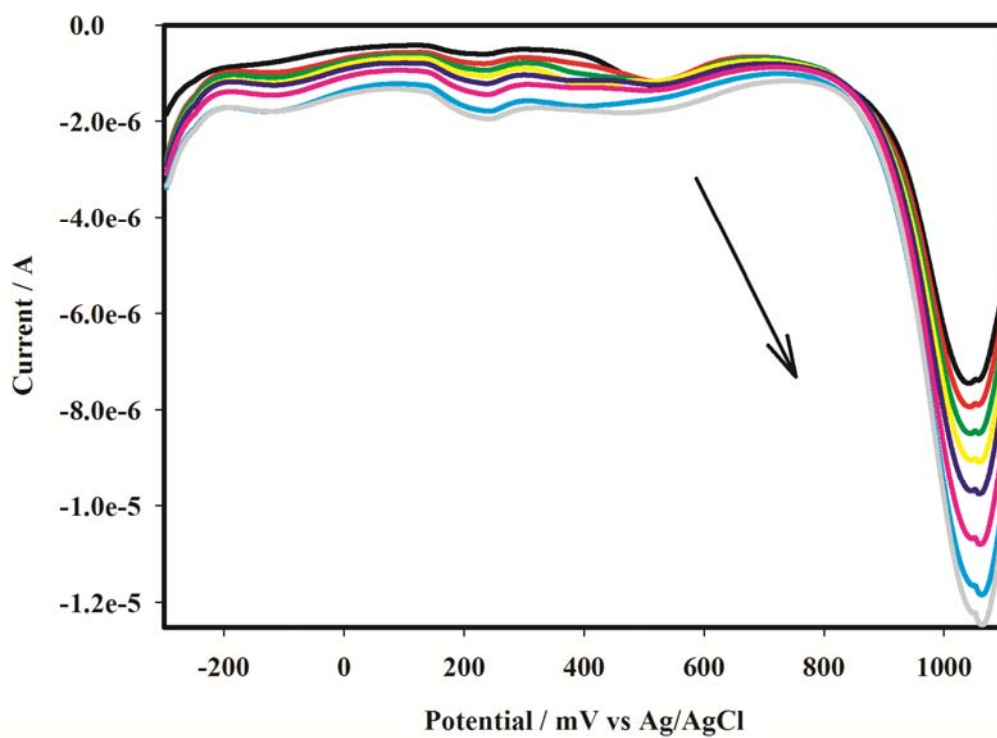


Figure 4.16: (A) CVs of Au/PVP-AgNPs electrodes, (B) CVs of Au/PANSA/PVP-AgNPs and (C) SWV of Au/PANSA/PVP-AgNPs at different scan rates in pH 7.4, 0.1 M phosphate buffer

4.4 References:

Arshi N.; Ahmed F.; Koo B. H.; Lee C. G., 'Comparative study of the Ag/PVP nanocomposites synthesized in water' (2011) *Current Applied Physics* **11** pg 347-348.

Bistolos N.; Wollenberger U.; Jung C.; Scheller F.W., 'Cytochrome P450 biosensors a review' (2005) *Biosensors and Bioelectronics* **20** pg 2409-2410.

Brahim S.; Guiseppi-Elie A., 'Chemical and Biological Sensors Based on Electrochemical Detection Using Conducting Electroactive Polymers' (2003) *Michim Acta* **143** pg 133-134.

Guascito M. R.; Malitesta C.; Manno D.; Serra A.; Turco A., 'A new amperometric nanostructured sensor for the analytical determination of hydrogen peroxide' (2008) *Biosensors and Bioelectronics* **24** pg 1057-1058.

Huang L.-M.; Chen C-H.; Wen T-C., 'Development and characterization of flexible electrochromic devices based on polyaniline and poly(3,4-ethylenedioxythiophene)-poly(styrene sulfonic acid)' (2006) *Electrochimica Acta* **51** pg 5858-5863.

Iwuoha E. I.; Howel M.; Wilson A., 'Cytochrome P450_{2D6} (CYP2D6) Bioelectrode for Fluoxetine' (2004) *Analytical Letters* **37** pg 933-939.

Iwuoha E. I.; Mavundla S. E.; Somerset V.S., 'Electrochemical and Spectroscopic Properties of Fly Ash-Polyaniline Matrix Nanorod Composites' (2006) *Microchim Acta* **155** pg 456-457.

Iwuoha E.I.; de Villaverde D.S.; Smyth M.R., 'Reactivities of organic phase biosensors. 2. The amperometric behaviour of horseradish peroxidase immobilised on a platinum electrode modified with an electrosynthetic polyaniline film' (1997) *Biosensors and Bioelectronics* **12** 753-754.

Iwuoha E.; Ngece R.; Baker P., 'Amperometric responses of CYP2D6 drug metabolism nanobiosensor for sertraline: a selective serotonin reuptake inhibitor' (2007) *IET Nanobiotechnology* **1** pg 62-64.

Jing S.; Xing S.; Yu L.; Zhao C., 'Synthesis and characterization of Ag/polyaniline core-shell nanocomposites based on silver nanoparticles colloid' (2007) *Materials Letters* **61** pg 2796-2797.

Kanungo M.; Kumar A.; Contractor A.Q., 'Studies on electropolymerization of aniline in the presence of sodium dodecyl sulphate and its application in sensing urea' (2002) *Journal of Electroanalytical Chemistry* **528** pg 51-52.

Kumar C. G.; Mamidyala S. K., 'Extracellular synthesis of silver nanoparticles using culture supernatant of *Pseudomonas aeruginosa*' (2011) *Colloids and Surfaces B: Biointerfaces* **84** pg 463-464.

Li M.; Gao Y.; Wang G.; Fang B.; 'Preparation of novel mercury-doped silver nanoparticles film glassy carbon electrode and its application for electrochemical biosensor'(2005) *Analytical Biochemistry* **341** pg 52-53.

Lindfors T.; Ivaska A.; 'Potentiometric and UV-vis characterisation of N-substituted polyanilines' (2002) *Journal of Electroanalytical Chemistry* **535** pg 69-71.

Mathebe N.G.R.; Morrin A.; Iwuoha E.I., 'Electrochemistry and scanning electron microscopy of polyaniline/proroxide-based biosensor' (2004) *Talanta* **64** pg 116-119.

Mazeikiene R.; Niaura G.; Malinauskas A., 'Raman spectroelectrochemical study of self-doped copolymers of aniline and selected aminonaphthalenesulfonates' (2006) *Electrochimica Acta* **51** pg 1919-1920.

Mu S.; Cheng C.; Wang J., 'The kinetic behaviour for the electrochemical polymerization of aniline in aqueous solution' (1997) *Synthetic Metals* **88** pg 249-254.

Owino J. H. O.; Arotiba O. A.; Baker P. G. L.; Guiseppi – Elie A.; Iwuoha, E. I., 'Synthesis and characterization of poly (2-hydroxyethyl methacrylate)-polyaniline based hydrogel composites' (2008) *Reactive and Functional Polymers* **68** pg 1239-1244.

Sathishkumar M.; Won S.W.; Cho C-W.; Yun Y-S., 'Cinnamon zeyanicum bark extract and powder mediated green synthesis of nano-crystalline silver particles and its bactericidal activity' (2009) *Colloids and Surfaces B: Biointerfaces* **73** pg pg 336-337.

Wang J., 'Electrochemical biosensors: Towards point-of-care cancer diagnostics' (2006) *Biosensors and Bioelectronics* **21** pg 18-19.

CHAPTER 5

Results and Discussion: Part 2

Summary

This chapter provides a detailed account of the development of nanobiosensors used for the detection of tuberculosis treatment drugs. Herein the morphological studies of the developed PANSA/PVP-AgNPs/CYP2E1 bioelectrode using TEM, AFM and EIS will be discussed. Furthermore an in-depth discussion of the electrochemical properties of the developed nanocomposite is also given from results obtained from amperometric studies. The most important aspect of this section of the study was to see whether the fundamental properties of CYP2E1 were retained after chemical modification and after being immobilization onto PANSA/PVP-AgNPs nanocomposites.

5.1 Morphology Characterization of PANSA/PVP-AgNPs/CYP2E1 Nanobioelectrode:

5.1.1 TEM Analysis:

As mentioned in Chapter 3, CYP2E1 was chemically modified using suberic acid bis (N-hydroxysuccinimide ester) (SA-NHS) and ethylene glycol bis(succinic acid N-hydroxysuccinimide ester) (EG-NHS). SA-NHS and EG-NHS reacted with the primary amino acids such as the ϵ -amino functions of lysine residues or even available N-termini to form stable amide bonds (Iwuoha *et al.*1997). Part of this study was to study CYP2E1 and the modified forms of CYP2E1; SA-CYP2E1 and EG-CYP2E1 after being electrochemically immobilized onto PANSA/PVP-AgNPs using TEM.

Figure 5.1 indicates TEM images of PANSA/PVP-AgNPs/CYP2E1, PANSA/PVP-AgNPs/SA-CYP2E1 and PANSA/PVP-AgNPs/EG-CYP2E1 all dispersed in ethanol with no observable morphological differences. Spherical and polydispersed silver nanoparticles with average diameter of 20 nm – 50 nm are seen attached onto the polymeric film seen as colourless while CYP2E1, SA-CYP2E1 and EG-CYP2E1 the white crystalline layers in the images are seen to be attached onto both the polymeric film and silver nanoparticles. EDX analyses (Figure 5.2) gave the components of PANSA/PVP-AgNPs/CYP2E1 which are C-O-Fe-S-Ag from low to high energy respectively with energy scale of maximum approximately 7.5 keV. O is due to the ITO glass substrate components while S is contributed by the sulphonic substituent of PANSA. The presence of PVP-AgNPs is indicated by an optical absorption peak near 3keV which was also observed for the individual PVP-AgNPs reported previously. The active site of CYP2E1 is indicated by the presence of Fe as seen by optical peaks near 7.5 keV. Very similar if not the same EDX patterns were observed for the PANSA/AgNPs/NHS-CYP2E1 and PANSA/PVP-AgNPs/SA-CYP2E1 nanobioelectrodes therefore, their patterns were excluded.

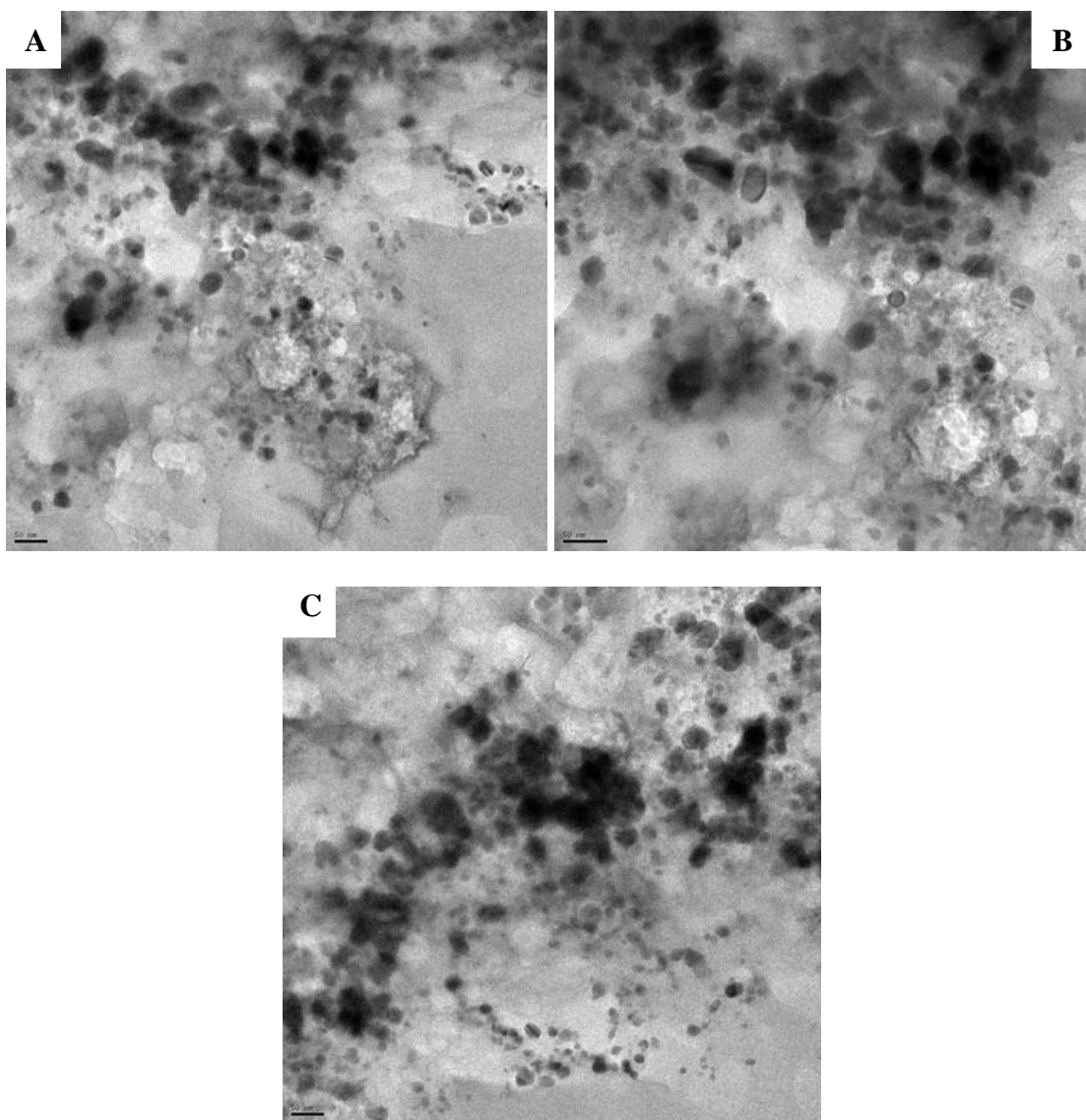


Figure 5.1: TEM images of (A) PANSAs/PVP-AgNPs/CYP2E1 (B) PANSAs/PVP-AgNPs/EG-CYP2E1 and (C) PANSAs/PVP-AgNPs/SA-CYP2E1

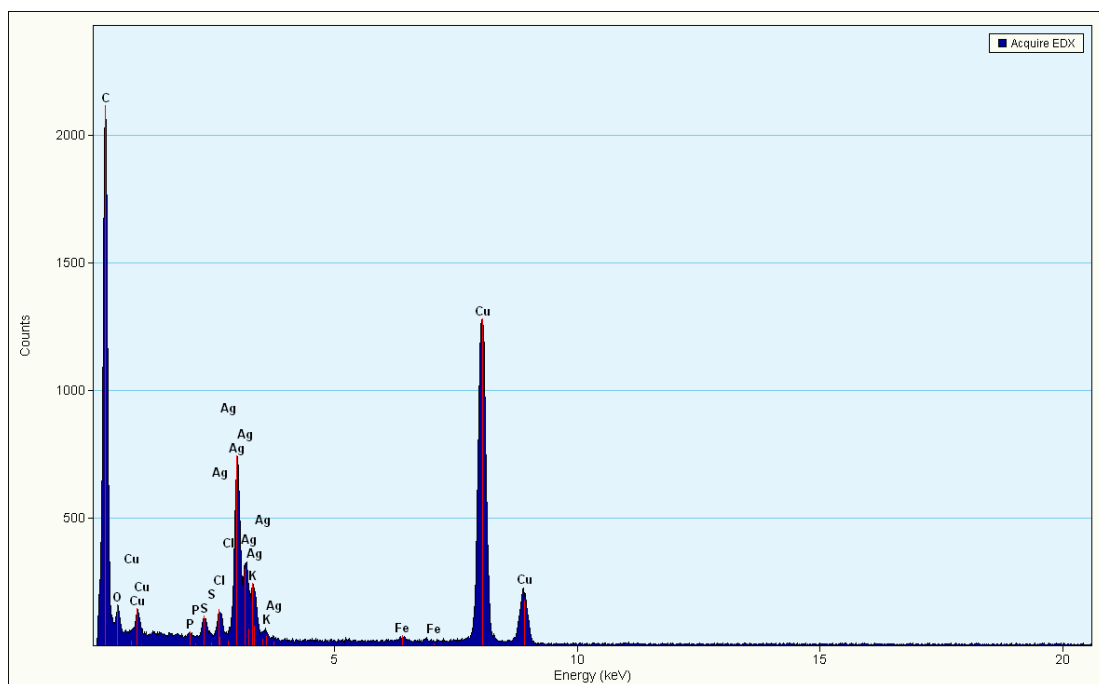


Figure 5.2: Energy dispersive X-ray spectrum of PANSA/PVP-AgNPs/CYP2E1

5.1.2 UV-Visible Spectroscopic Analysis:

UV-visible spectroscopy is a useful tool for monitoring the possible changes in the Soret absorption band which exists in heme group regions. Band shifts provide information of possible denaturation of heme proteins particularly that of conformational changes. Therefore, in this study this technique was employed to investigate the interaction between CYP2E1 and PANSA/PVP-AgNPs (Salimi *et al.* 2009; Lui *et al.* 2007). Figure 5.3 shows the spectra of CYP2E1 in buffer and CYP2E1 immobilized onto PANSA/PVP-AgNP electrodeposited on ITO electrode. As seen from Figure 5.3, a strong soret was observed at 449 nm for pure CYP2E1, while lower peaks at 451 nm for PVP-AgNP/CYP2E1 and 353 nm for Au/PANSA/PVP-AgNP/CYP2E1. The slight shift of 4 nm in the Soret band is due to the interaction between CYP2E1 and the PANSA/PVP-AgNP nanocomposite. Such an interaction neither destroyed the protein structure nor changed the fundamental microenvironment of the protein and its conformation. This result indicates no observable

denaturation of CYP2E1 occurred on the PANSA/PVP-AgNP film. A similar interaction has also been observed by the work carried out by Yu and co-worker.2010 where haemoglobin was immobilized on colloid silver nanoparticles-chitosan film.

The spectrum observed for PANSA/PVP-AgNP illustrates two absorbance peaks at around 425 nm and 535 nm and an undeveloped peak at approximately 410 nm. As indicated previously, the peak at 535 nm is as a result of $\pi - \pi^*$ transition of benzoid rings with the nanostructured PANSA indicating the presence of the stable pernigraniline salt. The peak at 425 nm is due to excitation of longitudinal plasmon vibrations of PVP-AgNPs while that at around 410 nm is due to transverse plasmon vibrations in the PVP-AgNPs (Sathishkumar *et al.* 2009). The same behaviour was observed in a study by Jing *et al.* 2007 involving the synthesis and characterization of Ag/polyaniline core-shell nanocomposites.

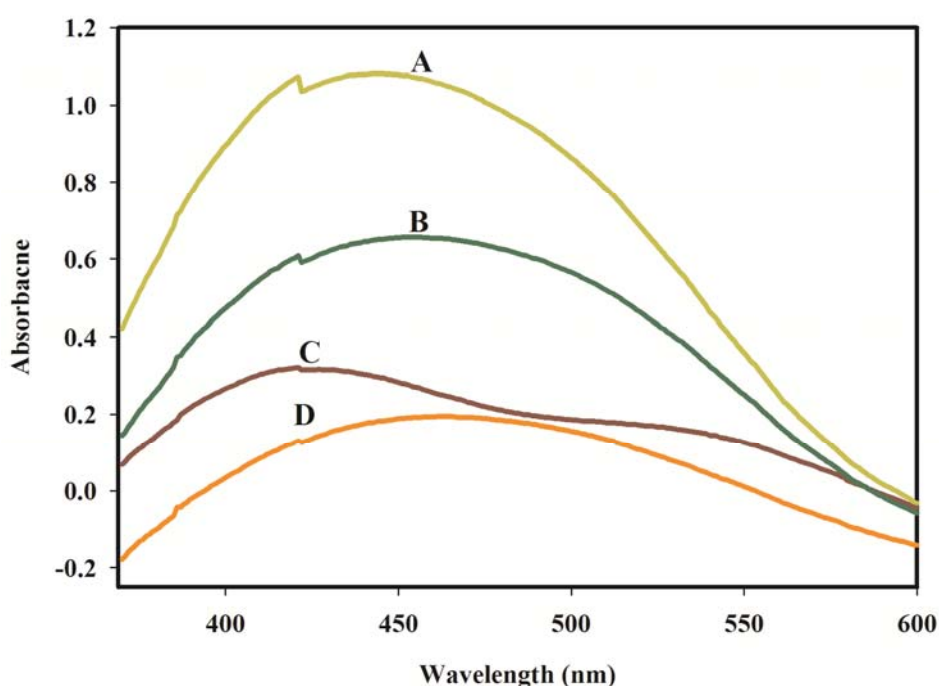


Figure 5.3: UV - visible spectra of (A) CYP2E1 (B) PVP-AgNPs/ CYP2E1 (C) PANSA/PVP-AgNPs composite and (D) PANSA/PVP-AgNPs/CYP2E1

5.1.3 EIS Analysis:

5.1.3.1 Nyquist Plot Characterization:

EIS measurements were carried out in pH 7.4, 0.1 M phosphate buffer at the potential window; -300 mV to +1100 mV where bare Au electrode, Au/PVP-AgNPs, Au/PANSA, Au/PVP-AgNP/PANSA and PANSA/PVP-AgNPs/CYP2E1 nanobioelectrode were investigated. The change in electron transfer resistance arising after each surface modification step was investigated and represented as Nyquist diagrams as indicated in Figure 5.4. As discussed in the previous chapter, EIS studies indicated that PVP-AgNPs is more conductive than PANSA as seen by the different sizes of the semi-circles. Immobilization of PVP-AgNPs onto the PANSA film resulted in a further decrease in the semi-circle (curve a). The nanocomposite was found to be more conductive than PVP-AgNPs and PANSA individually thus allowing a much faster electron movement between Au electrode and the nanocomposite. Immobilization of and (b) SA-CY2E1, (c) EG-CYP2E1 and (d) CYP2E1 onto PANSA/PVP-AgNPs resulted in increased semi-circles. This illustrated a slight restriction in electron transfer between the Au electrode (curve e) and the PANSA/PVP-AgNPs/CYP2E1 nanobioelectrode. The same impedance profile was observed for EG-CYP2E1 and SA-CY2E1 nanobiosensors (Yin *et al.*2010; Arotiba *et al.*2010; Ding *et al.*2003).

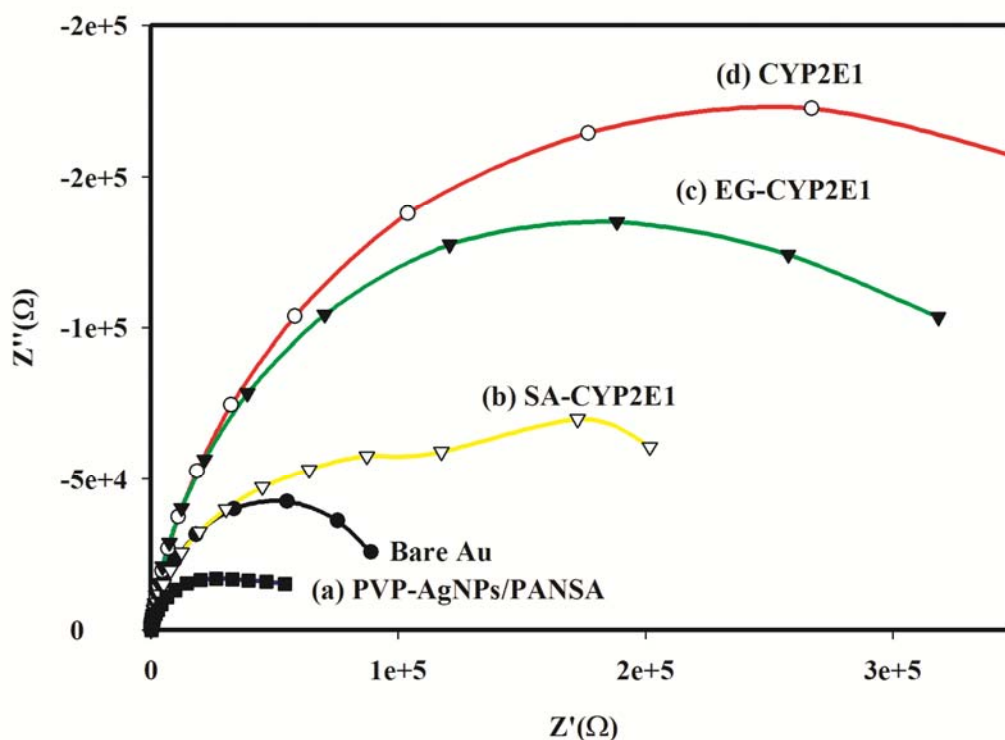


Figure 5.4: EIS Nyquist plot of Au/PVP-AgNPs, Au/PANSA and Au/PVP-AgNPs/PANSA and PANSA/PVP-AgNPs/CYP2E1 nanobioelectrode

5.1.4.2 Bode Plot Characterization:

Bode plot analysis (Figure 5.5) for the Au/PANSA/PVP-AgNPs/CYP2E1 nanobioelectrodes showed a lower conductivities than bare Au electrode with a slightly higher charge transfer resistance when compared to the Au/PANSA/PVP-AgNPs electrode indicating a slower electron transfer between the Au electrode and the nanocomposite. As indicated in the previous chapter, R_{ct} values for PVP-AgNP, PANSA and PANSA/PVP-AgNP modified gold electrodes were obtained as 118 KOhm, 217.6 KOhm and 35.51 KOhm respectively. For the Au/PANSA/PVP-AgNP/CYP2E1 nanobioelectrode a R_{ct} value of 335 KOhm was found and for (Au/PANSA/PVP-AgNP/SA-CYP2E1 = 119.6 KOhm) and (Au/PANSA/PVP-AgNP/EG-CYP2E1 = 275 KOhm) which reveal the hindering ability of PANSA/PVP-AgNPs and CYP2E1 on the electrode surface thus, impeding electron transfer.

An increase in impedance was observed from the Bode plot (Figure 5.5) for the PANSA/PVP-AgNP/CYP2E1 nanobioelectrode as compared to the PANSA, PVP-AgNP and PANSA/PVP-AgNPs modified gold electrodes with corresponding shifts in phase angles respectively (Yin *et al.*2010; Arotiba *et al.*2010; Ding *et al.*2003). As seen from the diagram the angle shift of the Au/PANSA/PVP-AgNP/CYP2E1 nanobioelectrode was found to be similar to that of Au/PANSA/PVP-AgNP/SA-CYP2E1 and Au/PANSA/PVP-AgNP/EG-CYP2E1 nanobioelectrodes (not shown since bode plots are the same as the Au/PANSA/PVP-AgNP/CYP2E1 nanobioelectrode).

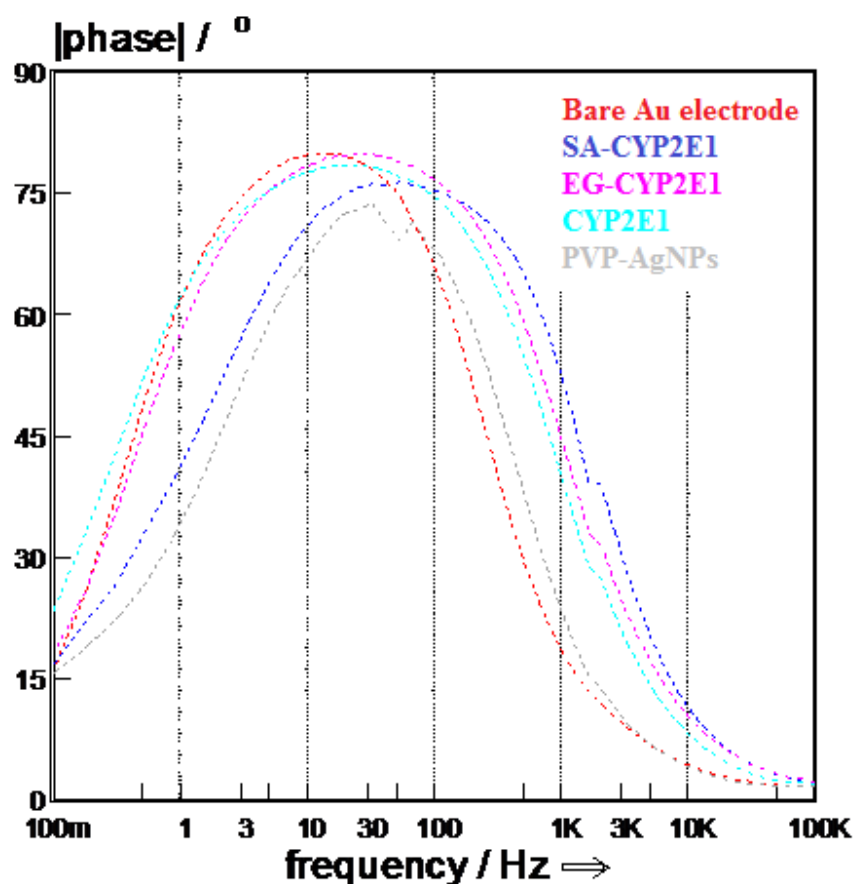


Figure 5.5: Bode plot of Au/PVP-AgNPs, Au/PANSA and Au/PVP-AgNPs/PANSA and PANSA/PVP-AgNPs/CYP2E1 nanobioelectrode

Table 5.1 gives a list of all calculated EIS parameters; R_s , C_{dl} , R_{ct} and Warburg element, Z_w , resulting from the EIS study. The parameters were used to calculate the time constant using equation 4.1 a and 4.1 b (where Time constant = τ) and the exchange current (i_o) by using equation 4.2 (Yin *et al.*2010; Arotiba *et al.*2010; Ding *et al.*2003). Where C_{dl} = double layer capacitance; τ = time constant; R_{ct} = charge transfer resistance. K_{et} , the homogeneous rate constant was determined by using equation 4.3. The resulted parameters are clearly illustrated in Table 5.2

Table 5.1: EIS parameters attained from the circuit fitting of plots in Figure 4.15 for PANSA, PVP-AgNPs and PANSA/PVP-AgNPs and PANSA/PVP-AgNPs/CY2E1 modified Au electrode

Parameter	Au/PANSA	Au/PVP-AgNPs	Au/PANSA/PVP-AgNP	Au/PANSA/PVP-AgNP/CYP2E1
Electrolyte resistance (R_s) (Ohms)	159.1	461.4	222	176.7
Charge transfer resistance (R_{ct}) (KOhms)	89.27	118	35.51	275
Warburg impedance (W) (kDW)	2.905	16.83	13.82	33.53
Double layer capacity (C_{dl}) (uF)	2.888	880.1	1.417	706.5

Table 5.2: Results for time constant, exchange current and homogeneous rate constant for bare PANSA, PVP-AgNPs and PANSA/PVP-AgNPs and PANSA/PVP-AgNPs/CYP2E1 modified Au electrode

Element	PANSA	PVP-AgNPs	PANSA/PVP/AgNPs/CYP2E1
Time Constant τ (s rad ⁻¹)	4.70x10 ⁻²	1.59x10 ⁻³	8.90 x10 ⁻¹
Exchange current i_0 (A)	5.00x10 ⁻⁵	1.09x10 ⁻⁴	4.67x10 ⁻⁵
K_{et} (cm s ⁻¹)	1.52x10 ⁻⁴	2.80x10 ⁻⁴	2.29 x10 ⁻⁴

5.1.5 AFM Analysis:

1D and 3D AFM images are shown in Figure 5.6. The surface of SPAuE/PANSA/PVP-AgNPs/CYP2E1 (Figure 5.6 B) nanobioelectrode displayed a globular morphology and larger roughness than the electrode without enzyme (Figure 5.6 A). The latter is consistent with the close packing of enzymes onto solid surfaces as reported by Crespilho *et al.* 2009 and Wang *et al.* 2009. Globular and increased roughness was also observed for the SPAuE/PANSA/AgNPs/EG-CYP2E1 and SPAuE/PANSA/PVP-AgNPs/SA-CYP2E1 nanobioelectrodes (not shown since images are the same as SPAuE/PANSA/PVP-AgNPs/CYP2E1). This is indicative of the fact that the chemical modification of CYP2E1 did not drastically alter the morphology of the enzyme.

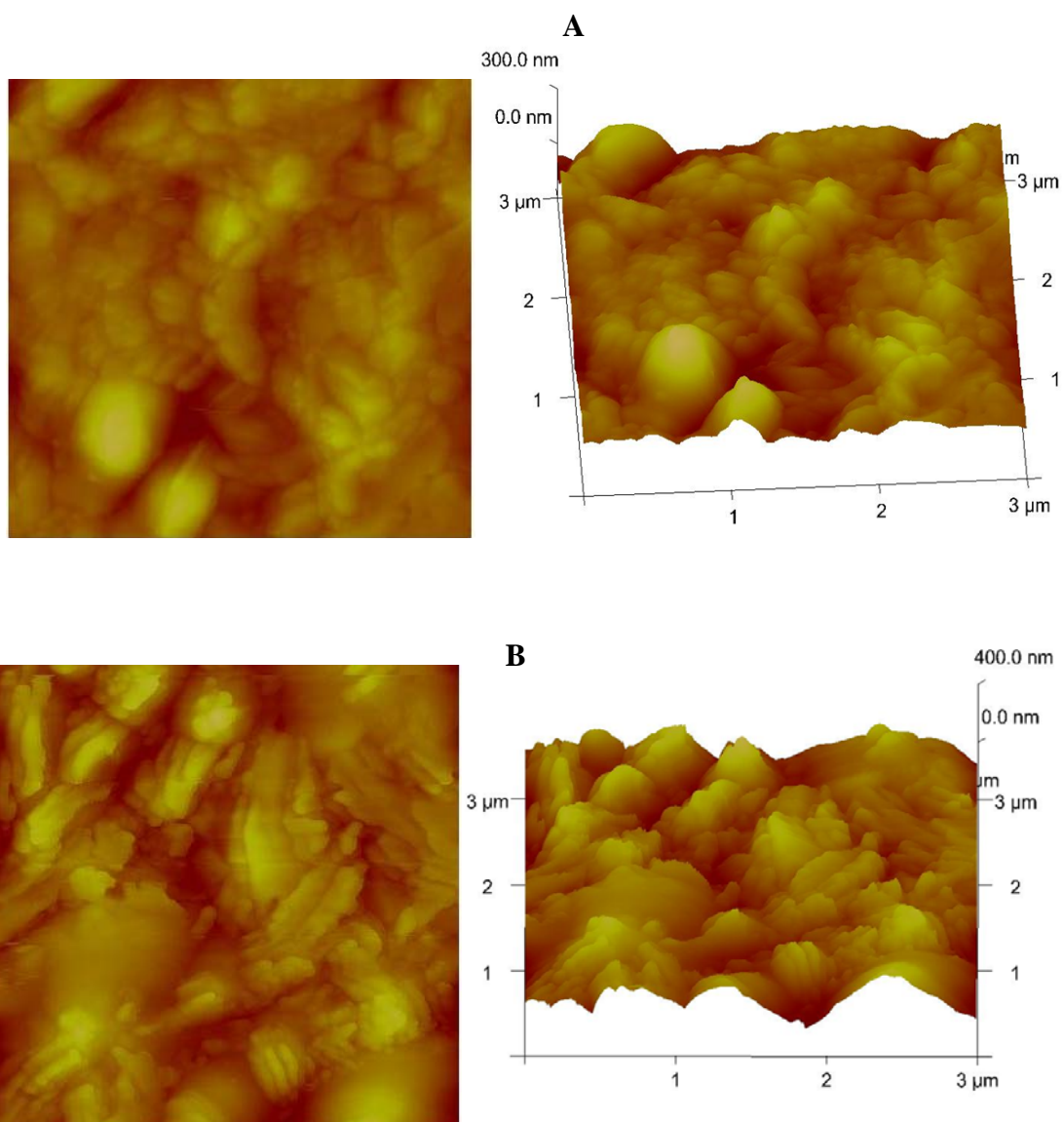
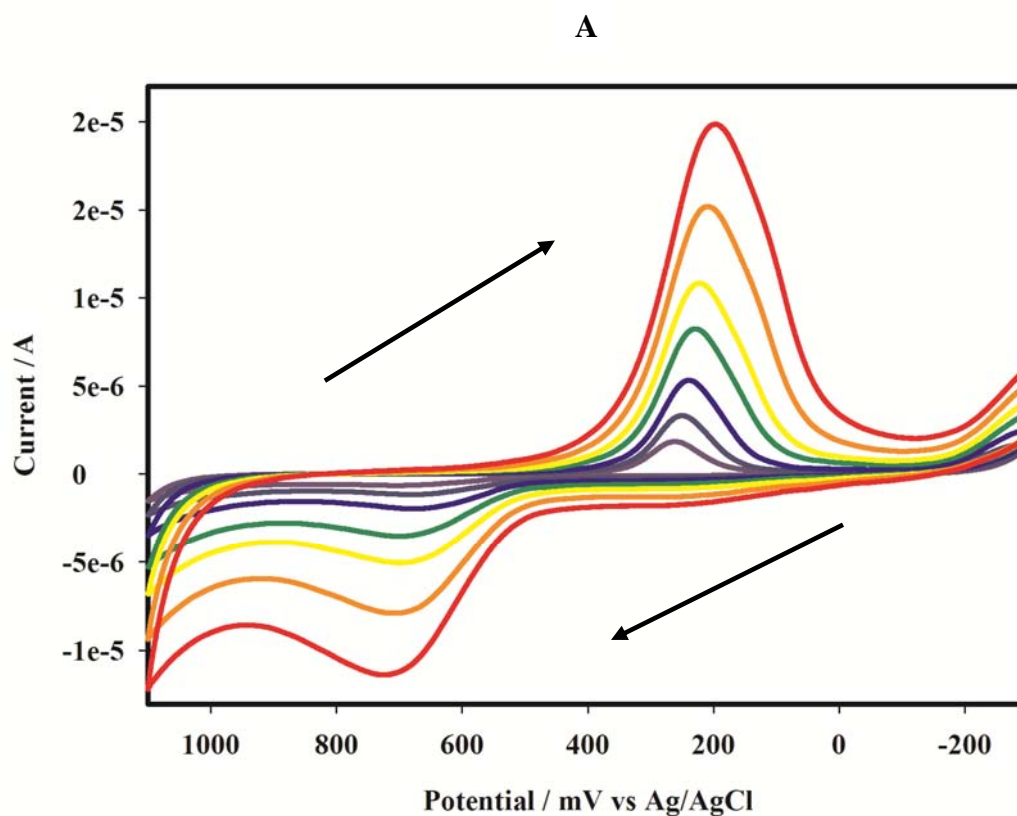


Figure 5.6: 1D and 3D AFM images of (A) SPAuE/PANSA/PVP-AgNPs and (B) SPAuE/PANSA/PVP-AgNPs/CYP2E1

5.1.4 Amperometric characterization of PANSa/PVP-AgNPs/CYP2E1 nanobioelectrode:

CYP2E1, EG-CYP2E1 and SA-CYP2E1 were individually electrostatically attached onto PANSa/PVP-AgNPs nanocomposites by applying a potential of +700 mV in anaerobic pH 7.4, 0.1 M Phosphate buffer solution. After immobilization it was crucial to access whether the enzymes were attached onto the nanocomposites. CV was used for this study at a potential window of -300 mV to +1100 mV at varying scan rates. Figure 5.7 shows the CV voltammogram of the characterization at 10, 20, 30, 40, 60, 80 and 100 mV/s where one redox couple was observed for CYP2E1's heme ($\text{Fe}^{3+}/\text{Fe}^{2+}$) electron transition (Figure 5.7 A) while for the EG-CYP2E1 (Figure 5.7 B) and SA-CYP2E1 bioelectrodes, (Figure 5.7 C) two redox peaks were observed. The redox peak towards the more positive potentials is attributed to the enzymes ($\text{Fe}^{3+}/\text{Fe}^{2+}$) transition while the other is due to the PVP-AgNPs ($\text{Ag}(0)/\text{Ag}(1)$) transition.



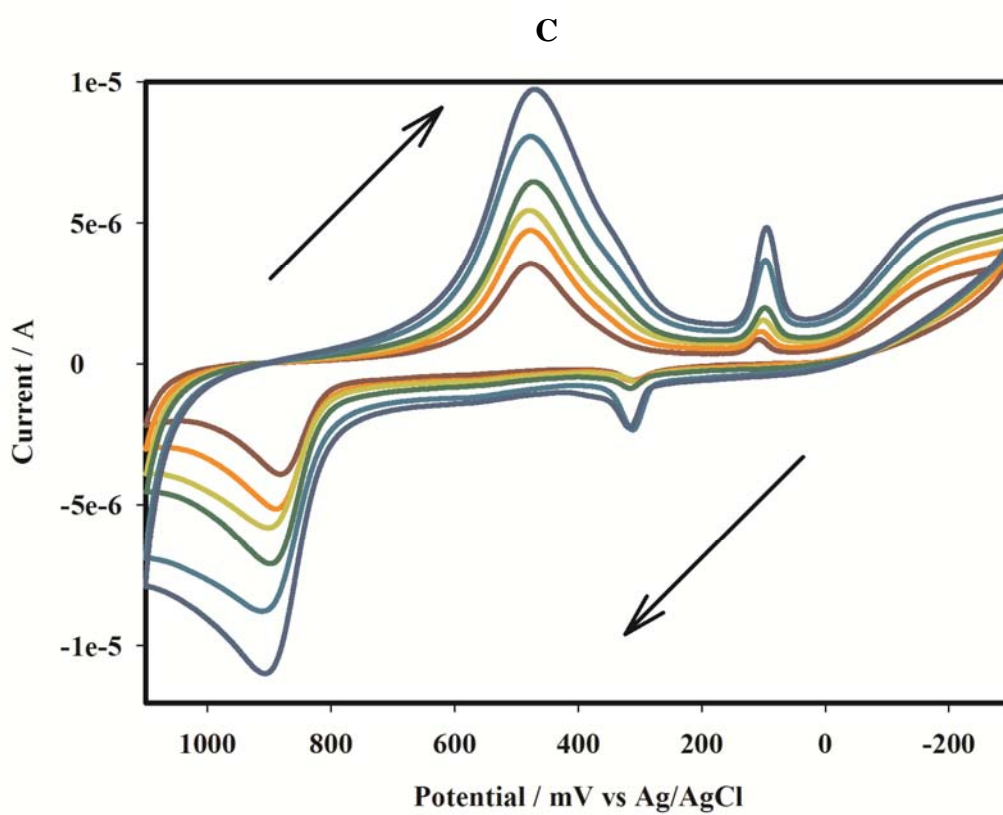
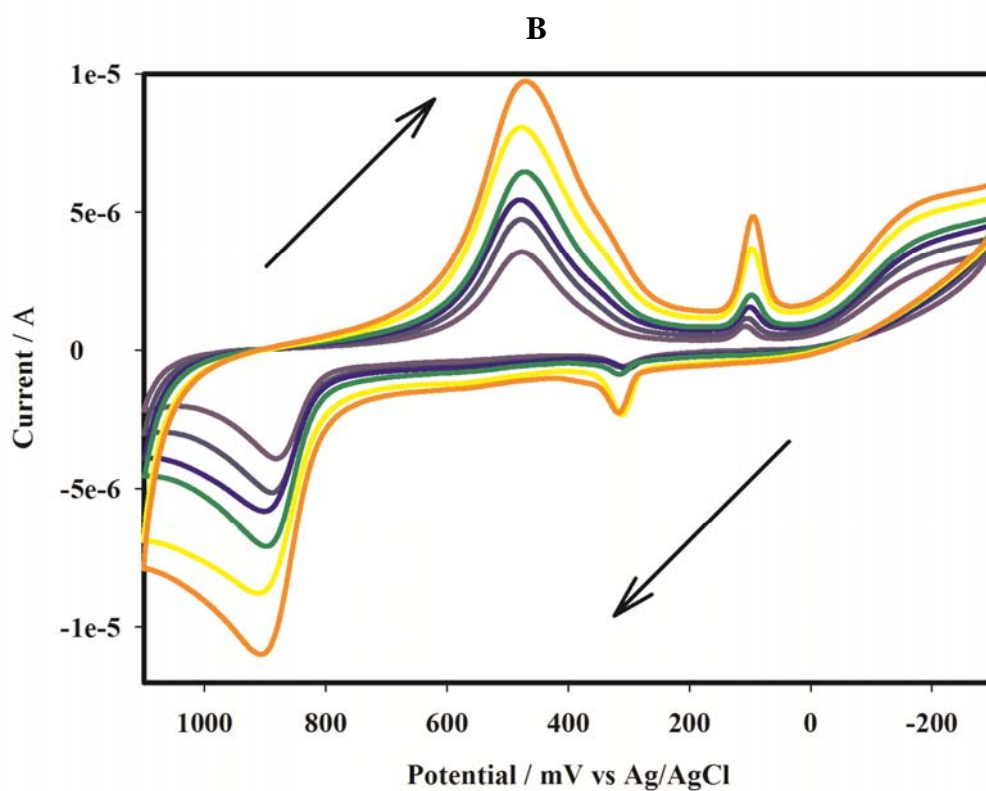
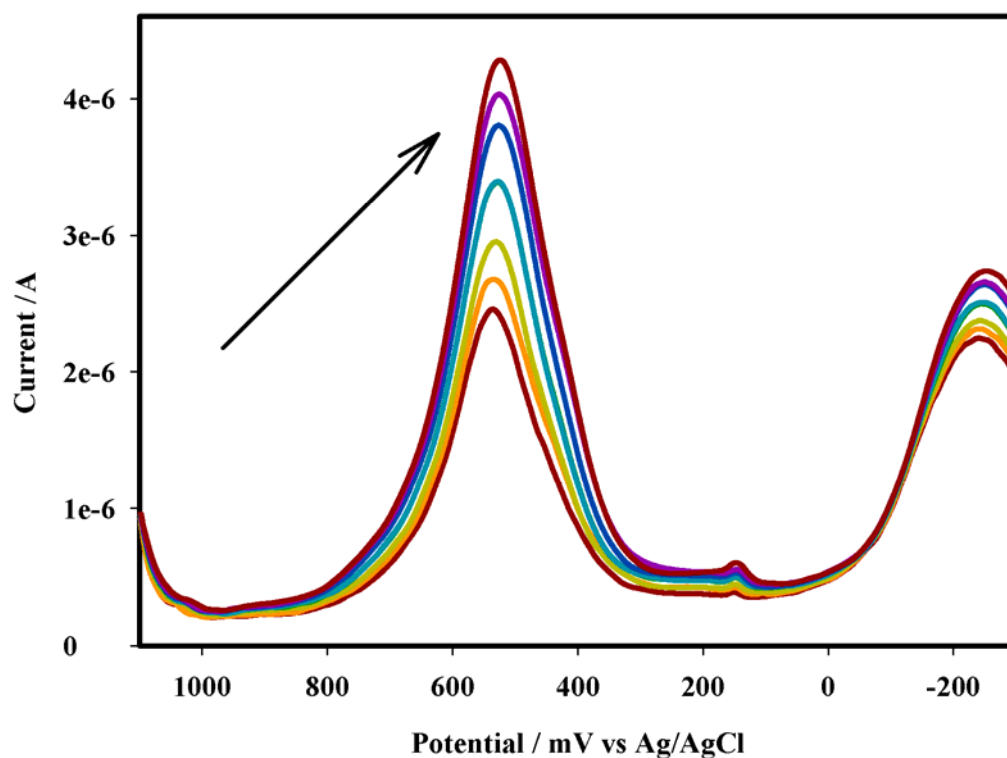


Figure 5.7: CV characterization of (A) PANSA/PVP-AgNPs/CYP2E1, PANSA/PVP-AgNPs/EG-CYP2E1 and (C) PANSA/PVP-AgNPs/SA-CYP2E1 in pH 7.4, 0.1 M, phosphate buffer at 10, 20, 30, 40, 60, 80 and 100 mV/s

As seen from the voltammograms in Figure 5.7, as the scan rates increased the peak amplitudes also increased confirming immobilization of the enzymes. On the other hand, a slight shift in both the current and the potential was observed illustrating that the PANSA/PVP-AgNPs nanocomposite had not lost its conductivity and electro-activity upon enzyme immobilization (Iwuoha *et al.* 1998; Iwuoha *et al.* 1997; Qu *et al.* 2005). This is clearly indicated by the second redox peak illustrated for the PANSA/PVP-AgNPs/EG-CYP2E1 and PANSA/PVP-AgNPs/SA-CYP2E1 nanobioelectrode. The same interaction observed in CV for the bioelectrode was also observed in DPV (Figure 5.8) and SWV (Figure 5.9) analyses. DPV and SWV reveal another redox peak at approximately -200 mV which is confirmation of immobilization of PANSA. The DPV and SWV profiles of the PANSA/PVP-AgNPs/EG-CYP2E1 and PANSA/PVP-AgNPs/SA-CYP2E1 bioelectrodes are not shown since they resemble that of PANSA/PVP-AgNPs/CYP2E1.



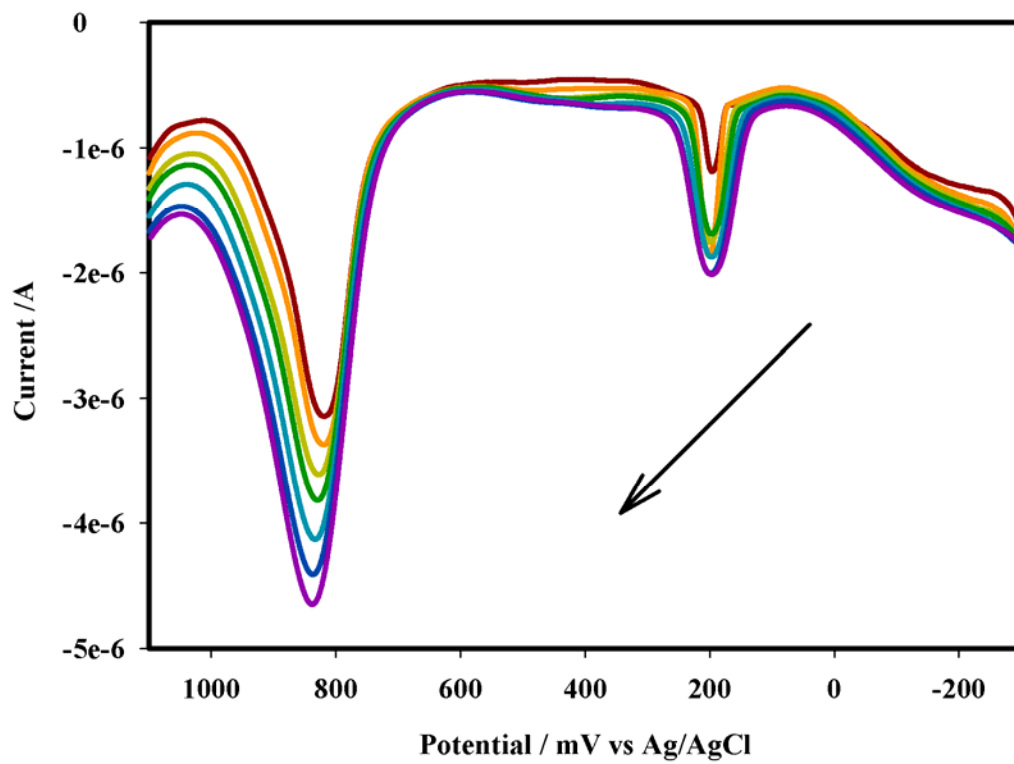


Figure 5.8: DPV characterization of PANSa/PVP-AgNPs/CYP2E1 pH 7.4, 0.1 M, phosphate buffer at 10, 20, 30, 40, 60, 80 and 100 mV/s.

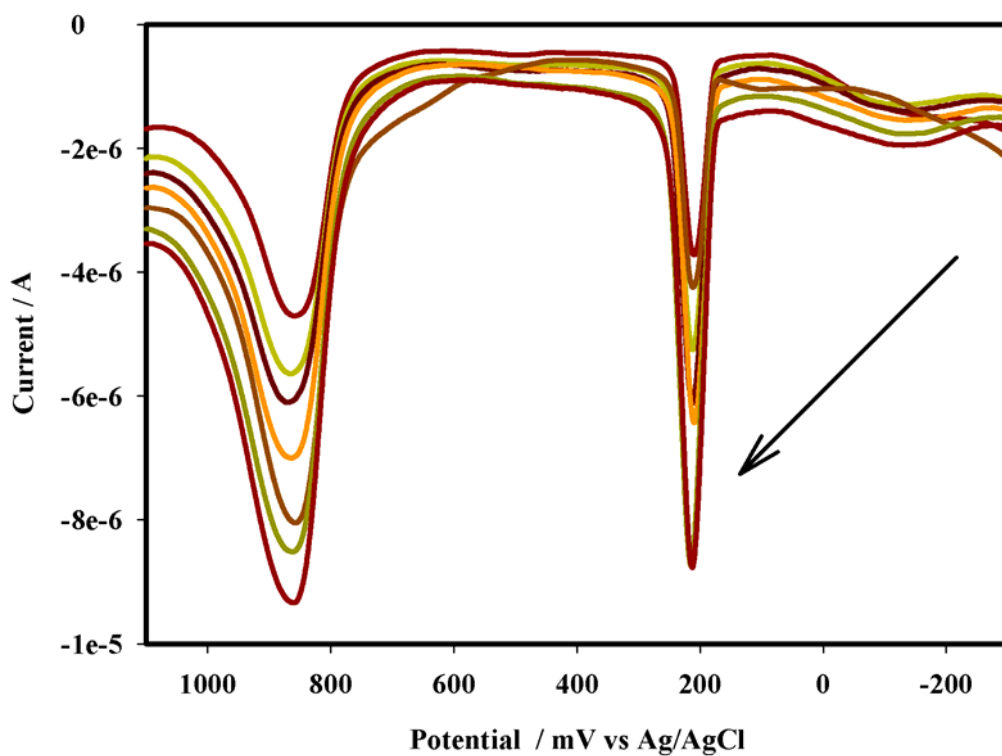
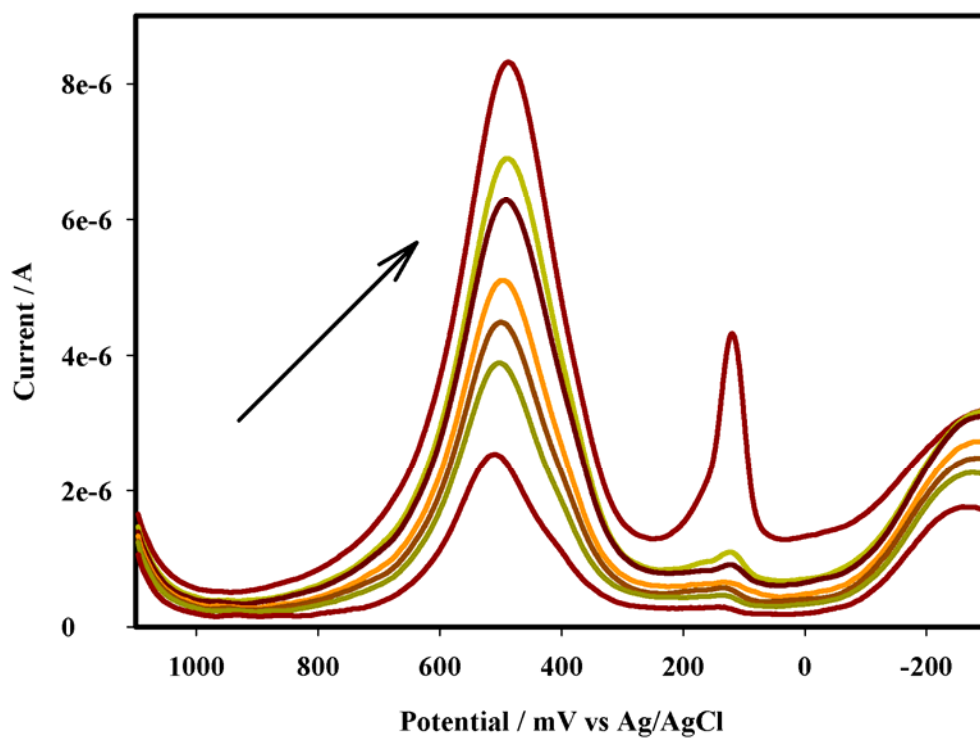


Figure 5.9: SWV characterization of PANSAs/PVP-AgNPs/CYP2E1 in pH 7.4, 0.1 M, phosphate buffer at 10, 20, 30, 40, 60, 80 and 100 mV/s

In order to effectively investigate the electrochemical properties of the Au/ PANSAs PVP-AgNPs/CYP2E1 nanobioelectrode, CV of different electrodes in buffer were recorded, as shown in Figure 5.10. No peaks were observed at bare gold electrode (green curve A,) while peaks were observed for the PANSAsPVP-AgNPs modified electrode (black curve B), with the (red curve C) obtained after injection of 20 μL CYP2E1 in pH7.4, 0.1 M phosphate buffer under anaerobic conditions and PANSAs (blue curve A) modified electrode.

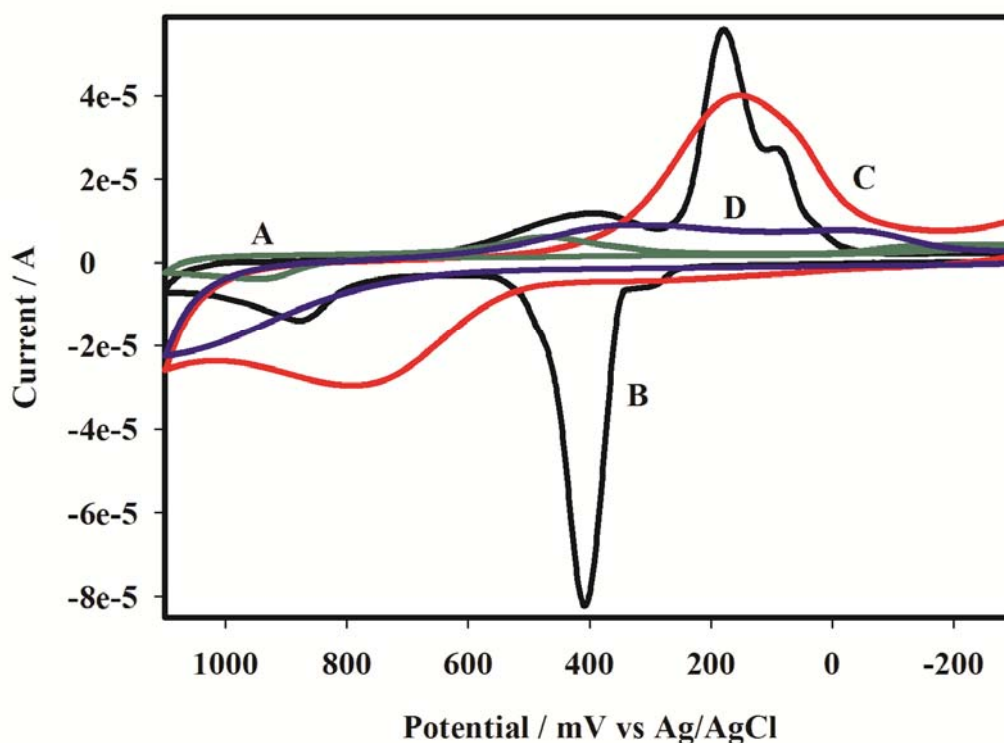


Figure 5.10 CVs of (A) bare Au electrode (green line) (B) of Au/PANSAsPVP-AgNPs (black line) and (C) Au/PANSAsPVP-AgNPs after CYP2E1 immobilization (red line) and (D) of PANSAs at 50 mV/s in pH 7.4, 0.1 M phosphate buffer

The pair of redox peaks arose from the redox of the heme Fe centre of CYP2E1 embedded in the PANSAsPVP-AgNPs nanocomposite attributed to the ($\text{Fe}^{2+}/\text{Fe}^{3+}$) transition (Ashe *et al.* 2007; Cerqueira *et al.* 2000). Thus, PANSAsPVP-AgNPs must have a great effect on the kinetics of electrode reaction providing a suitable environment for CYP2E1 to transfer

electrons with the underlying electrode. It was found that the peak currents of the CYP2E1 enzyme at the PANSA/PVP-AgNPs modified electrode were larger than those of at the bare gold electrode with a clear defined redox pair at +790 (oxidation peak) and +150 mV (reduction peak) with the separation of peak potential (ΔE_p) of +640 mV and formal potential (defined as the average of the anodic and cathodic peak potential) or $E^{0'} = E_{p,a} + E_{p,c} / 2 = +450$ mV (Iwuoha *et al.* 2003). A similar profile was also seen for the Au/ PANSA PVP-AgNPs/EG-CYP2E1 and Au/ PANSA PVP-AgNPs/SA-CYP2E1 hence, all discussions will be referred in terms of Au/ PANSA PVP-AgNPs/CYP2E1.

Heme proteins exhibit different formal potentials which are attributed to the effect of different system configurations and different microenvironments on the direct electron transfer (Guascito *et al.* 2008). Zong *et al.* 2005 obtained a formal potential of -36 mV for the direct electron transfer hemoglobin immobilized in multi-walled carbon nanotubes enhanced grafted collagen. On the other hand, Yang *et al.* 2006 immobilized myoglobin and gold nanoparticles on a glassy carbon electrode by a nafion film, where a pair of reversible redox peaks appeared with a formal potential of -373 mV. Varying the scan rates for the Au/ PANSA PVP-AgNPs/CYP2E1 electrode illustrated an increase in the peaks current with increasing scan rates, indicating that the electrochemical behaviour of CYP2E1 immobilized on Au/PANSA/PVP-AgNPs nanocomposite was a surface controlled process. It was also found that the peak potentials varied with an increase in scan rate, while the formal potential was kept almost unchanged, showing that CYP2E1 does not hinder charge transport across the PANSA/PVP-AgNPs film but enhances electron transportation between the CYP2E1 active site and the electrode surface (Zhang *et al.* 2007).

According to Laviron equation (Equ. 5.1);

$$I_p = n^2 F^2 A \Gamma^* \nu / 4 RT = n F Q \nu / 4 RT \quad \text{Equ. (5.1)}$$

Where Γ^* is the electroactive CYP2E1 amount (mol cm^{-2}) and Q is the quantity of charge (C) with the symbols n , I_p , R , F and T bearing their usual meaning. From the slope of $I_{p,c}$ versus v plot (Figure 5.11), n was calculated to be 2.21 indicating a two electron reaction of CYP2E1 on PANSA/PVP-AgNPs. The average coverage of CYP2E1 on the surface of the modified electrode was estimated to be $8.25 \times 10^{-5} \text{ mol cm}^{-2}$ and $4.56 \times 10^{-5} \text{ mol cm}^{-2}$ for the Au/PANSA/AgNP electrode. Since $\Delta E_p \geq 200 \text{ mV}/n$, the heterogeneous rate constant (ks) was estimated using the revised Laviron equation; Equation 5.2.

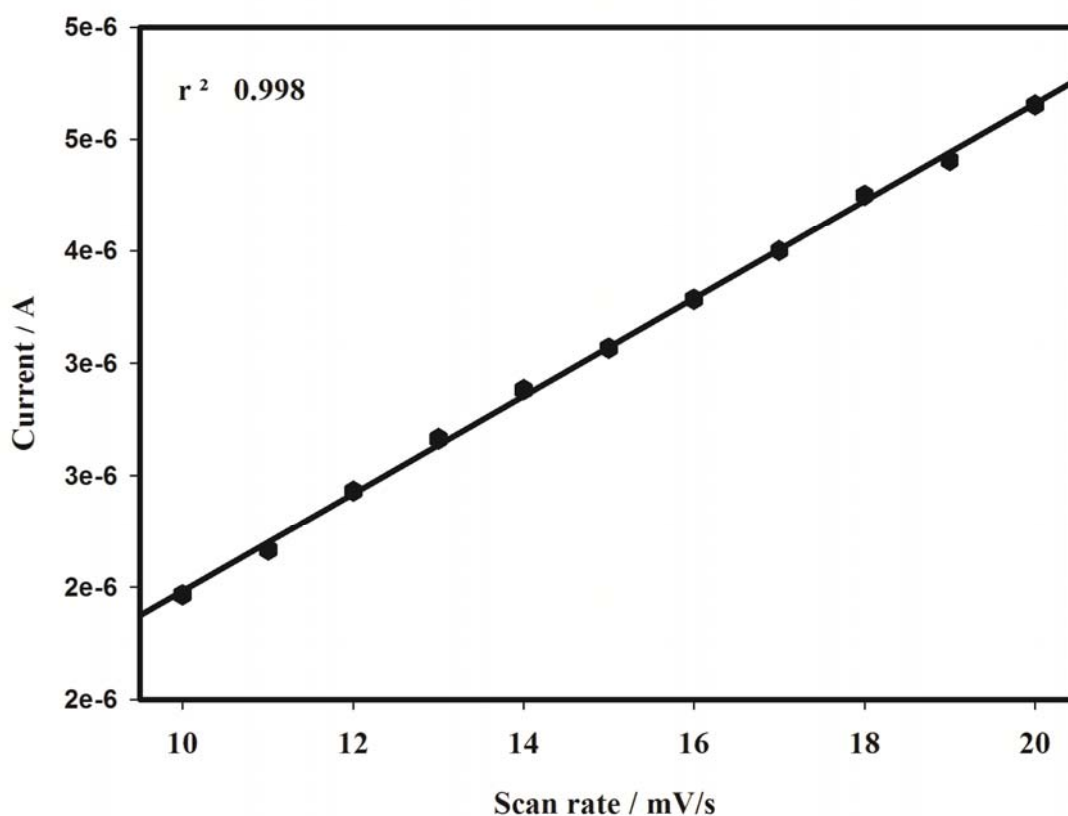


Figure 5.11: Plot of $I_{p,c}$ versus v plot used to calculate n , the number of electrons transferred in the reaction

$$\log ks = \alpha \log(1 - \alpha) + (1 - \alpha) \log \alpha - \log(RT / nF v) - \alpha(1 - \alpha)nF \Delta E_p / 2.3 RT \quad (5.2)$$

Taking the electron transfer coefficient α of 0.52, calculated from a plot of E_p versus $\log v$ (Figure 5.12), a scan rate of 100 mV/s and ΔE_p of +640 mV, the heterogenous rate constant was estimated to be 1.75 s^{-1} . The estimated value is in the controlled range of the surface-controlled quasi-reversible process, and is in agreement with the values (0.41 s^{-1} , 0.71 s^{-1} and 0.62 s^{-1} respectively) reported by Laviron and co for heme proteins suggesting that the active centre ($\text{Fe}^{3+}/\text{Fe}^{2+}$) of CYP2E1 underwent a quasi reversible process (Zhang *et al.* 2005; Laviron *et al.* 1979a; Laviron *et al.* 1979b).

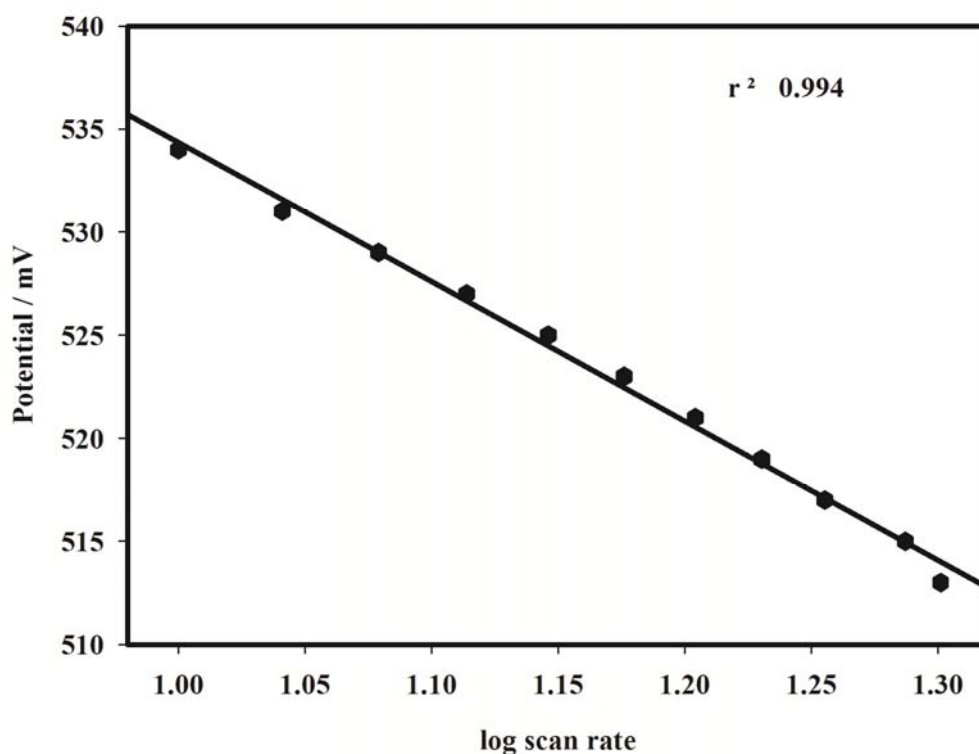


Figure 5.12: Plot of E_p versus $\log v$ used to calculate α , electron transfer coefficient

5.2 References:

Arotiba O.A.; Owino J.O.; Baker P.G.; Iwuoha E.I., 'Electrochemical impedimetry of electrodeposited poly (propylene imine) dendrimer monolayer' (2010) *Journal of Electroanalytical Chemistry* **638** pg 287–292.

Ashe D.; Alleyne T.; Iwuoha E., 'Serum cytochrome c detection using a cytochrome c oxidase biosensor' (2007) *Biotechnology and Applied Biochemistry* **46** pg 188-189.

Cerqueira P.M.; Cesarino E.J.; Bonato P.S.; Lanchote V.L., 'Enantioselectivity of debrisoquine 4-hydroxylation in Brazilian Caucasian hypertensive patients phenotyped as extensive metabolizers' (2000) *Journal of Chromatography B* **749** pg 153-154.

Cresphilho F.; Travains S.A.; Oliveira Jr O.N., 'Enzyme immobilization on Ag nanoparticles/polyaniline nanocomposite' (2009) *Biosensors and Bioelectronics* **24** pg 3073-3074.

Hongbo Ding H.; Park S-M., 'Electrochemistry of Conductive Polymers XXVII. Effects of Polystyrene Sulfonate on Electrochemical Behavior of Polyaniline' (2003) *Journal of the Electrochemical Society*, **150** pg E34-E38.

Guascito M. R.; Malitesta C.; Manno D.; Turco A., 'A new amperometric nanostructured sensor for the analytical determination of hydrogen peroxide' (2008) *Biosensors and Bioelectronics* **24** pg 1057-1058.

Iwuoha E. I.; Miland E.; Smyth M. R.; Fagain C. O., 'Reactivities of Organic-Phase Biosensors. 1. Enhancement of the Sensitivity and Stability of Amperometric Peroxidase Biosensors Using Chemically Modified Enzymes' (1997) *Analytical Chemistry* **69** pg 1674-1675.

Iwuoha E. I.; Joseph S., 'Drug metabolism biosensors: electrochemical reactivities of cytochrome P459_{cam} immobilized in synthetic vesicular systems' (1997) *Journal of Pharmaceutical and Biomedical Analysis* **17** pg 1101-1110.

Iwuoha E.I.; de Villaverde D.S.; Smyth M.R., 'Reactivities of organic phase biosensors 2. The amperometric behaviour of horseradish peroxidase immobilised on a platinum electrode modified with an electrosynthetic polyaniline film' (1997) *Biosensors and Bioelectronics* **12** 753-754.

Iwuoha E.I; Smyth M.R., 'Reactivities of organic phase biosensors: 6. Square-wave and differential pulse studies of genetically engineered cytochrome P450cam (CYP101) bioelectrodes in selected solvents' (2003) *Biosensors and Bioelectronics* **18** 240-241.

Jing S.; Xing S.; Yu L.; Zhao C., 'Synthesis and characterization of Ag/polyaniline core-shell nanocomposites based on silver nanoparticles colloid' (2007) *Materials Letters* **61** pg 2796-2797.

Laviron E., 'The use of linear potential sweep voltammetry and of a.c. voltammetry for the study of the surface electrochemical reaction of strongly adsorbed systems and of redox modified electrodes' (1979b) *Journal of Electrochemical Chemistry and Interfacial Electrochemistry* **100** 263-270.

Laviron E., 'General expression of the linear potential sweep voltammogram in the case of diffusionless electrochemical systems' (1979a) *Journal of Electrochemical Chemistry and Interfacial Electrochemistry* **101** pg 19-28.

Liu C.; Hu J., 'Hydrogen peroxide biosensor based on the direct electrochemistry of myoglobin immobilized on silver nanoparticles doped carbon nanotubes film'(2009) *Biosensors and Bioelectronics* **24** pg 2151-2152.

Qu F.; Yang M.; Jiang J.; Yu R., 'Amperometric biosensor for choline based on layer-by-layer assembled functionalized carbon nanotube and polyaniline multilayer film' (2005) *Analytical Biochemistry* **344** pg 110-111.

Salimi A.; Solranian S., 'Immobilization of haemoglobin on electrodeposited cobalt-oxide nanoparticles: Direct voltammetry and electrocatalytic activity' (2007) *Biophysical Chemistry* **130** pg 124-125.

Sathishkumar M.; Won S.W.; Cho C.-W.; Yun Y.-S., 'Cinnamon zeyanicum bark extract and powder mediated green synthesis of nano-crystalline silver particles and its bactericidal activity' (2009) *Colloids and Surfaces B: Biointerfaces* **73** pg pg 336-337.

Wang S.; Xie F.; Liub G., 'Direct electrochemistry and electrocatalysis of heme proteins on SWCNTs-CTAB modified electrodes' (2009) *Talanta* **77** pg 1345-1346.

Yang W.W.; Li Y.; Sun C.Q., 'Hydrogen peroxide biosensor based on myoglobin/colloidal gold nanoparticles immobilized on glassy carbon electrode by a Nafion film' (2006) *Sensors and Actuators B: Chemistry* **115** pg 42-48.

Yin.; Zhou Y.; Ai S.; Zhu L.; 'Electrochemical behavior of bisphenol A at glassy carbon electrode modified with gold nanoparticles, silk fibroin, and PAMAM dendrimers' (2010) *Microchim Acta* **170** pg 100–105.

Yu C.; Zhou X.; Gu H., 'Immobilization, direct electrochemistry and electrocatalysis of haemoglobin on colloidal silver nanoparticles-chitosan film' (2010) *Electrochimica Acta* **55** pg 8743-8744.

Zhang Z.; Jiang X.; Wang E.; Dong S., 'Attachment of gold nanoparticles to glassy carbon electrode and its application for the direct electrochemistry and electrocatalytic behavior of hemoglobin' (2005) *Biosensors and Bioelectronics* **213** pg 342-343.

Zhang H.; Hu N., 'Conductive Effect of Gold Nanoparticles Encapsulated Inside Polyamidoamine (PAMAM) Dendrimers on Electrochemistry of Myoglobin (Mb) in {PAMAM–Au/Mb}_n Layer-by-Layer Films' (2007) *Journal of Physical Chemistry B* **111** pg 10583-10590.

CHAPTER 6

Results and Discussion: Part 3

Summary

This chapter gives details on the detection of the tuberculosis drugs namely; Isoniazid (INH), Ethambutol (ETH), Rifampicin (RIF) and Pyrazinamide (PYR) using PANSA/PVP-AgNPs/PANSA/CYP2E1, PANSA/PVP-AgNPs/PANSA/SA-CYP2E1 and PANSA/PVP-AgNPs/PANSA/EG-CYP2E1 nanobiosensors on gold electrodes. Detection of these drugs was achieved by using techniques such as CV, DPV, SWV and steady state amperometry. Thorough discussions based on the interaction of CYP2E1 and the individual drugs are provided in sections below.

6.1 PANSA/PVP-AgNPs -mediated Electrocatalytic Reduction of TB Drugs:

Amongst the TB drugs INH is a known substrate inhibitor of CYP2E1 whose metabolism is via a hydroxylation process. RIF and ETH are also metabolism by CYP2E1 but too a much lesser extent than INH while PYR is known to be metabolised to 5-hydroxypyrazinamide by the molybdenum iron-sulphur flavin hydroxylase enzyme, xanthine oxidase/xanthine dehydrogenase (Yamamoto *et al.* 2001; Rasoulzadeh *et al.* 2009). For the first time, this study introduces a new biotransformation method by studying the metabolism of these drugs using the enzyme CYP2E1 coupled to a nanocomposite of silver nanoparticles/poly (8-anilino-1-naphthalene sulphonic acid). The initial stage of this study involved the detection of all four drugs using PANSA/PVP-AgNPs/CYP2E1 nanobiosensors however; these nanobiosensors were found to be more selective for only INH and ETH. Therefore, modifying CYP2E1 with [suberic acid bis (*N*-hydroxysuccimide ester) (SA-NHS)] and [ethylene glycol bis (succinic acid *N*-hydroxysuccinimide ester) (EG-NHS)] allowed for the successful detection of PYR and RIF. Thus, the next step of the study was the detection of these drugs using PANSA/PVP-AgNPs/SA-CYP2E1 nanobiosensors which were found to be more selective for PYR and finally, these drugs were detected using PANSA/PVP-AgNPs/EG-CYP2E1 nanobiosensors which were found to be more selective for RIF.

In the sections below the CV, DPV or SWV and steady state amperometric results of the compounds namely; INH, ETH, PYR and RIF obtained from their respective nanobiosensors are discussed. By plotting calibration curves; which are plots of current against analyte concentrations (above mentioned TB drugs), parameters such as K_M , K_M^{app} and I_{MAX} were determined from the linear ranges of the nanobiosensor systems. From the calibration curves the sensitivity (determined as the slope of the plot) and the detection limits of the individual nanobiosensors were also determined. Detection limits are dependent on the background current exhibited by the nanocomposite and the importance of their estimation is

to know the least amount a particular nanobiosensor can detect (Grennan *et al.* 2006). The nanobiosensors showed increased sensitivities resulting from the presence of CYP2E1 embedded in the electron transfer mediator PANSA/PVP-AgNPs (Svobodova *et al.* 2002). The sensitivity and detection limit values are stipulated in Table 6.1 were a clear comparison among the nanobiosensor systems is made.

6.1.1 Electrocatalytic Reduction of Isoniazid and Ethambutol using PANSA/PVP-AgNPs/CYP2E1 Nanobiosensors:

Of all the TB drugs studied, the Au/PANSA/PVP-AgNPs/CYP2E1 nanobiosensor was found to be greatly selective for INH and ETH. Interestingly enough, the electrochemistry of ETH (Figure 6.2 A) and INH (Figure 6.5 A) was seen to be very similar. Illustrated in the following sections are the voltammetric responses of the Au/PANSA/PVP-AgNPs/CYP2E1 nanobiosensors under aerobic and anaerobic conditions in the presence of pH 7.4, 0.1 M phosphate buffer solution.

6.1.1.1. Electrocatalytic Reduction of Ethambutol:

The electrocatalytic activity of CYP2E1 in the PANSA/PVP-AgNPs nanocomposite was evaluated by SWV, DPV, CV and chronoamperometric methods. Au/PANSA/PVP-AgNPs/CYP2E1 was employed as the working electrode and its electrochemical response towards ethambutol was investigated in pH 7.4, 0.1 M phosphate buffer under aerobic conditions at 20 mV/s. Figure 6.1 illustrates the chronoamperometric analysis at different ETH concentrations (2 μ M - 22 μ M), where the current as a function of time was monitored. The steady state amperometry experiments were performed at -250 mV in an air saturated cell solution with stirring maintained at 500 rpm. The first addition of ETH caused an increase in the current and the amperometric response of the nanobiosensor was allowed to

attain steady state value which took about 20 s to acquire, showing that the nanobiosensor can achieve real time responses. Using SWV, DPV and CV with only CV and DPV shown in (Figure 6.2 A and B), a well-defined reduction peak was observed for the Au/PANSA/PVP-AgNP/CYP2E1 nanobiosensor in deoxygenated buffer. However, when ETH was injected into the buffer reaction medium, the reduction peak increased with no corresponding oxidation peak observable. In anaerobic conditions we only have the electrochemistry of Au/PVP-PANSA/CYP2E1 which is essential for the oxidation and reduction of PANSA and PVP-AgNPs respectively.

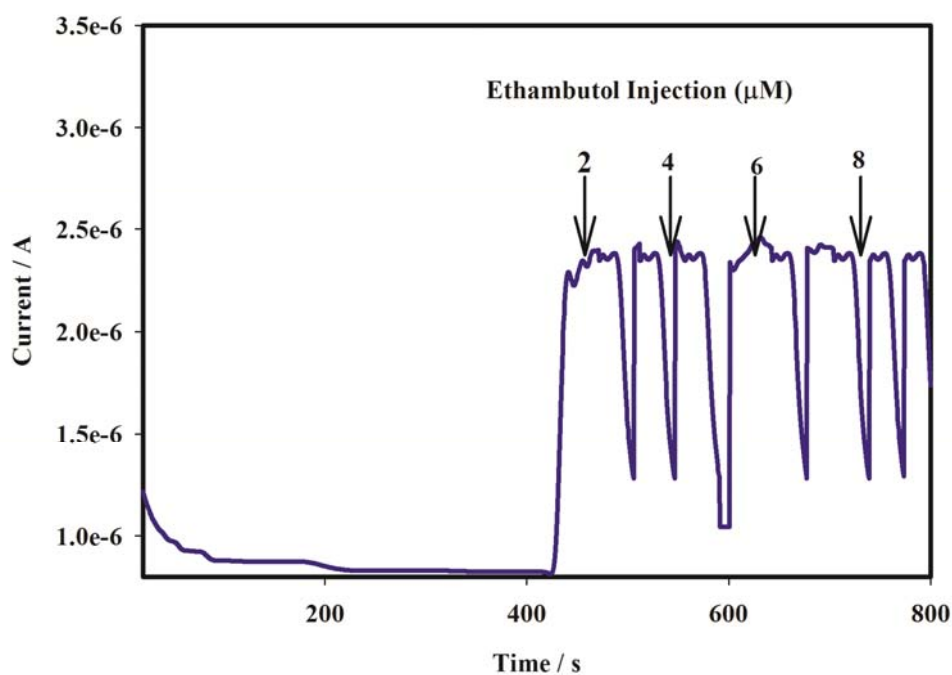
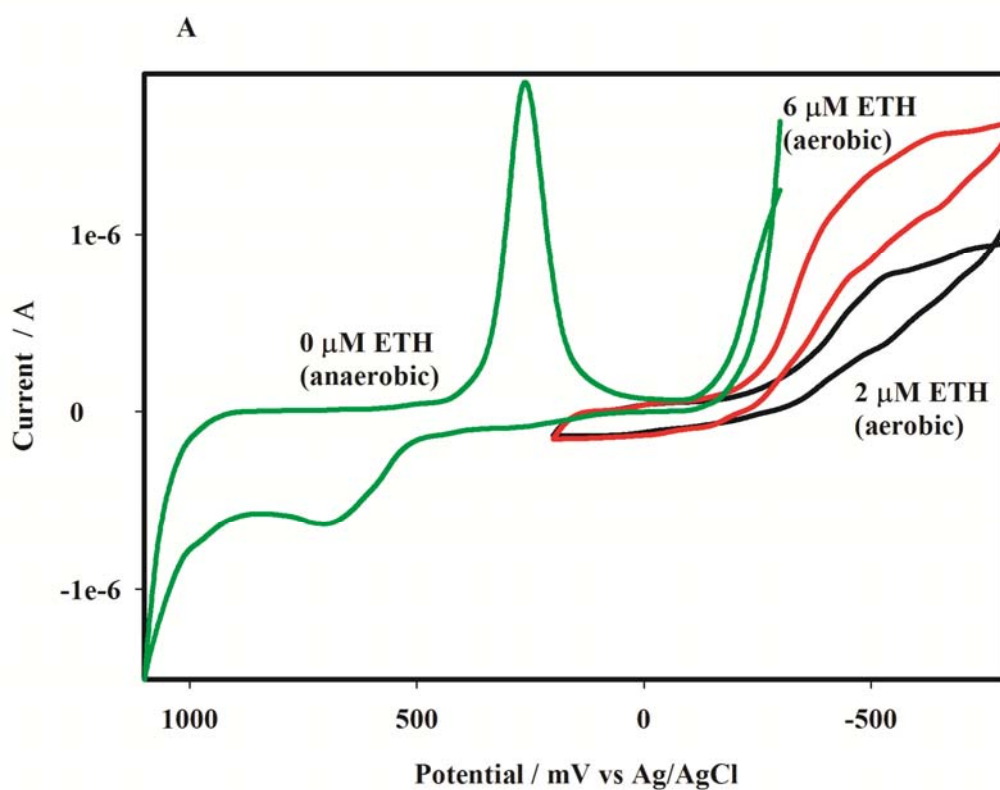


Figure 6.1: Steady state responses at applied potential of -250 mV with response time of 20 s

With reference to Scheme 6.1, the reduction peak observed in aerobic conditions suggests the one electron electrochemical reduction of the hexa-coordinated low-spin ferric enzyme (Fe^{3+}) to the high spin ferrous enzyme (Fe^{2+}). This form of the enzyme has a high affinity for oxygen and thus binds molecular oxygen present in the solution forming the

CYP2E1 (Fe^{2+}) O_2 complex. This interaction results in the development of an aldehyde intermediate followed by the release of a water molecule. The result is a highly active iron-oxoferryl intermediate CYP2E1 (Fe^{4+}) during which a dicarboxylic acid form of ETH is produced upon reduction (Spracklin *et al.*1997; von Moltke *et al.*1997).



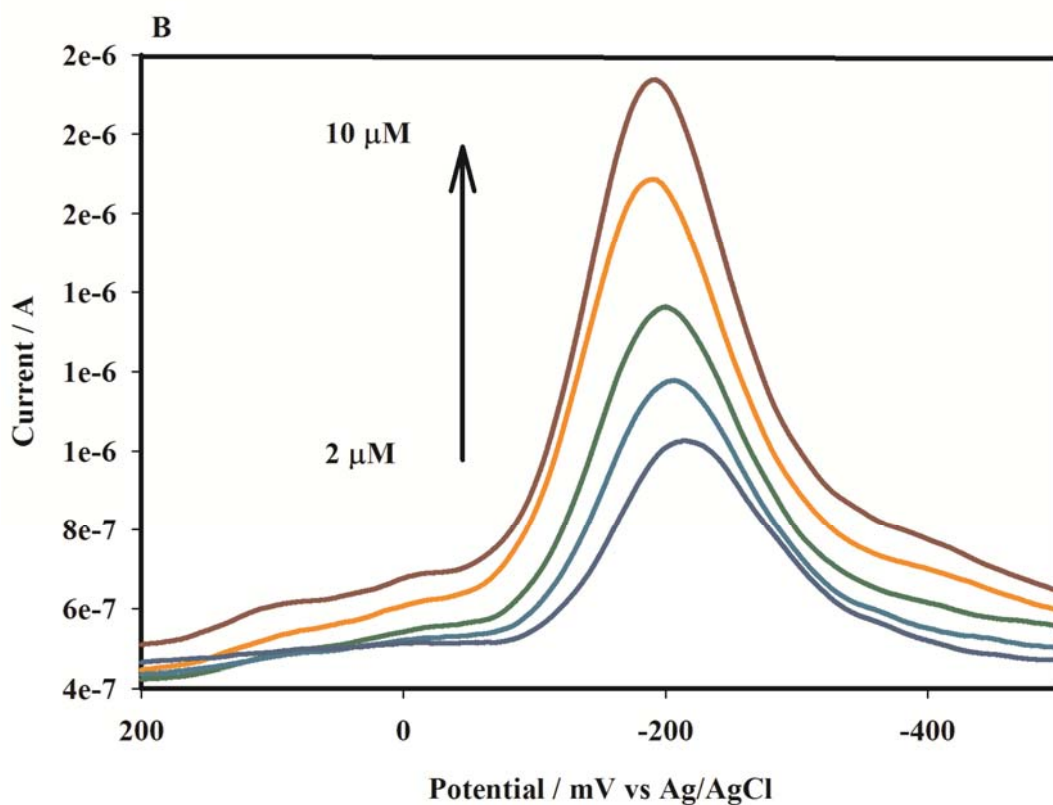
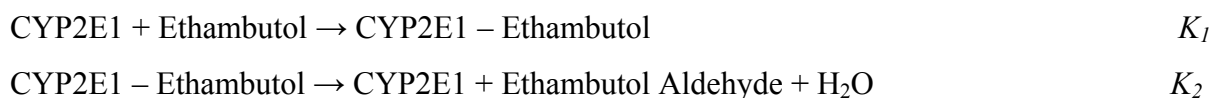


Figure 6.2: (A) CV and (B) DPV responses at different ethambutol concentrations for the Au/PVP-AgNPs/PANSA/CYP2E1 nanobiosensor

As expected for enzymatic processes, the response upon ETH addition led to a Michaelis-Menten profile, with a linear response up to 16 μM , a sensitivity of 1.13 $\mu\text{A}/\mu\text{M}$ and a detection limit of 0.7 μM (Figure 6.3). Compared to a study by Wu *et al.* 2011 where ETH was determined using a sensitive fluorescent probe; this nanobiosensor system showed to be more sensitive and effective. Thus, the Au/PANSA/PVP-AgNPs/CYP2E1 electrode provided a comfortable and friendly environment for the biocatalytic reaction to take place, which was more evident by the determination of the Michaelis-Menten constant (K_M). The enzymatic reaction at the PANSA/ PVP-AgNPs electrode surface can be considered as follows:



Therefore, based on the Michaelis-Menten reaction, the enzymatic kinetics of CYP2E1 as shown in Equation 6.1 is written as follows:

$$V = K_2 [\text{CYP 2E1}] [\text{ETHAMBUTOL}] / K_M + [\text{ETHAMBUTOL}] \quad \text{Equ. (6.1)}$$

Where V is the rate, K_2 the equilibrium constant, K_M the Michaelis-Menten constant, [CYP2E1] the concentration of CYP2E1 and [ETHAMBUTOL] is the concentration of ethambutol. Naturally, lower K_M and higher V values are preferred since they indicate a high enzyme biocatalytic activity. These parameters were studied from Figure 6.3, where the entire enzymatic reaction is represented by the hyperbolic graph. At lower ETH concentrations, the rate of reaction is directly proportional to the ETH concentration illustrated in the linear range of Figure 6.3. Therefore, when $V = V_{MAX}$ (the maximum rate, represented as I_{MAX} in our calculations), then K_M is numerically equal to half the ETH concentration. The value of K_M was therefore determined and found to be 6.30 μM (Bai *et al.* 2007; Cornish-Bowden *et al.* 1974; AL-Thabaiti *et al.* 2008). The electrochemical Lineweaver-Burk equation (Equation 6.2) was used to evaluate K_M^{app} of the biosensor. In this case, the x-intercept of the graph represents $-1/K_M$ and the y-intercept is equivalent to the inverse of V_{MAX} .

$$\frac{1}{I_{SS}} = \frac{1}{I_{MAX}} + \frac{K_M^{app}}{I_{MAX}} [S] \quad \text{Equ. (6.2)}$$

Here I_{SS} is the measured steady state current, I_{MAX} the maximum current under saturated substrate concentration, K_M^{app} the apparent Michaelis-Menten constant and $[S]$ is the concentration of ethambutol. According to the intercept and slope of the above equation, the value for K_M^{app} was estimated to be 1,01 μM , whereas the value for the maximum I_{MAX} was calculated to be $2.1 \times 10^{-6} \mu\text{A}$. The K_M^{app} is lower than previously reported for HRP immobilized in sol-gel-derived ceramic-carbon nanotubes composite film (Bai *et al.* 2007; Cornish-Bowden *et al.* 1974; AL-Thabaiti *et al.* 2008). The smaller value of K_M^{app} indicated for the present nanobiosensor indicates that CYP2E1 embedded in the PANSA/ PVP-Ag nanocomposite has better affinity towards ETH and that this new electrode configuration is promising for building enzymatic devices with improved biocatalytic properties.

Of great interest is the fact that the blood peak level of ethambutol (1 – 5 $\mu\text{g/mL}$) or 6 – 18 μM occurring between 4 - 8 hr post a daily dosage of 200 mg, is within the dynamic linear response range (2 – 16 μM). With an upper dynamic linear range of 16 μM it means that the nanobiosensors are effective and can be applied to systems where concentrations are 0.7 μM - 16 μM .

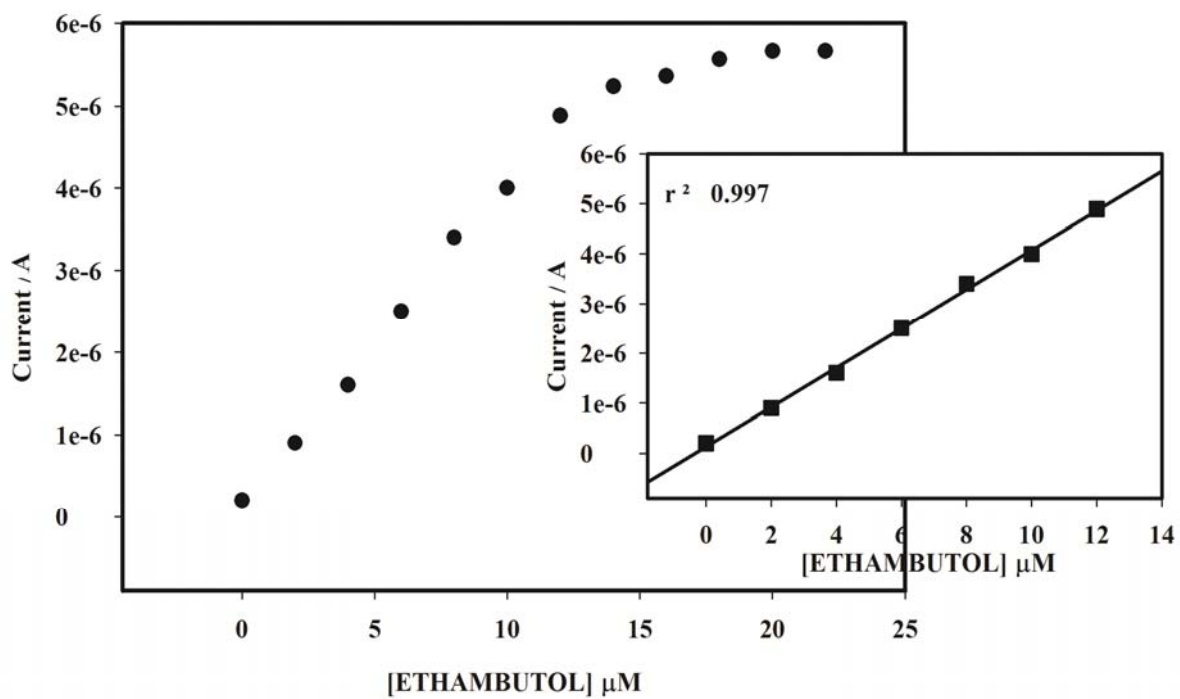
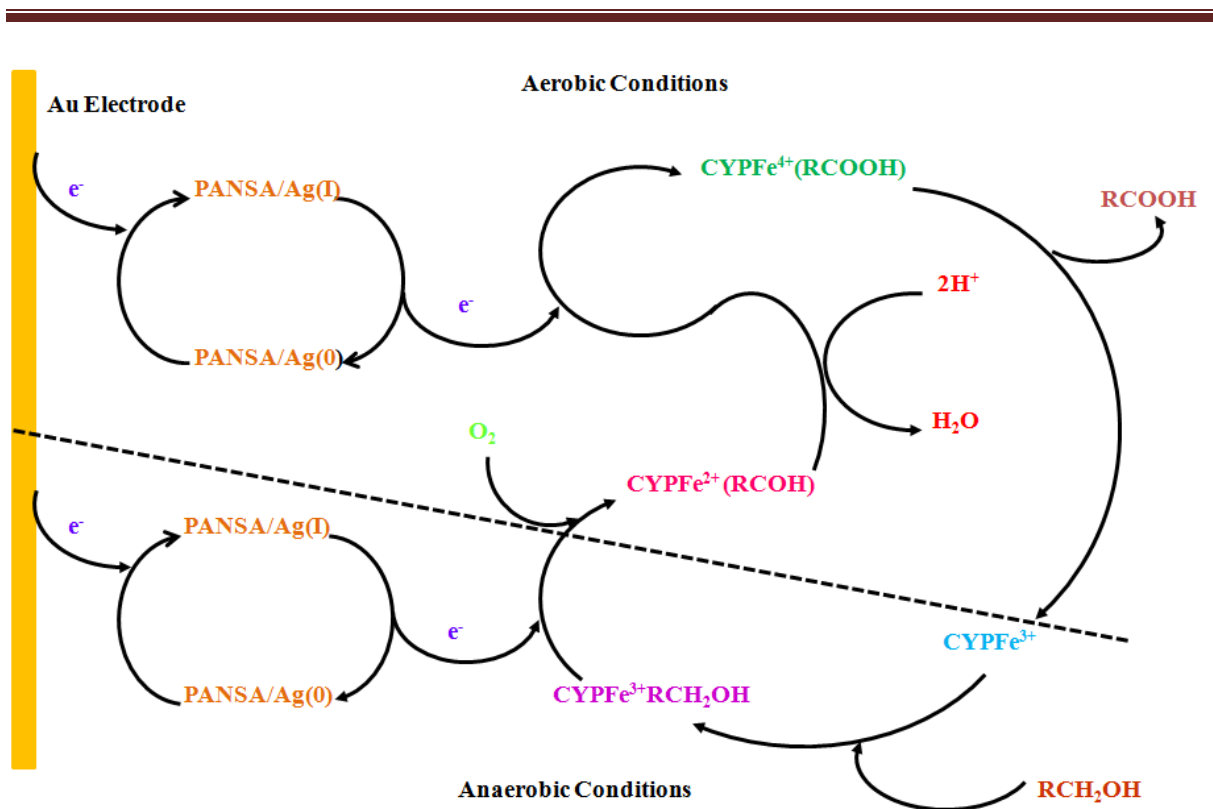


Figure 6.3: Calibration curve of ethambutol showing the linear range (inset) for the Au/PVP-AgNPs/PANSA/CYP2E1 nanobiosensor

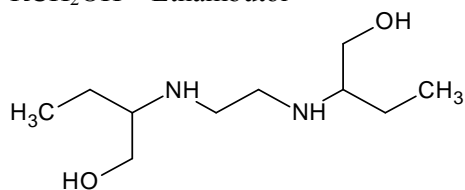


KEY

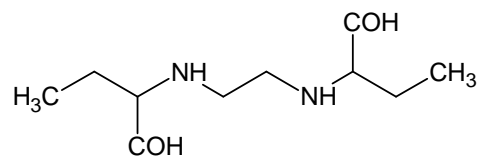
CYP^{4+, 3+, 2+} - Different oxidation states of Cytochrome P450-2E1

PANSA/Ag - poly (8-anilino-1-naphthalene sulphonic acid)/ silver nanoparticle nanocomposite

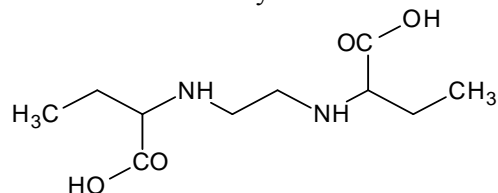
RCH₂OH – Ethambutol



RCOH – Ethambutol aldehyde intermediate



RCOOH – Dicarboxylic acid ethambutol



Scheme 6.1: Reaction scheme showing the metabolism of ethambutol using the Au/PANSA/PVP-AgNPs/CYP2E1 nanobiosensor

6.1.1.2. Electrocatalytic Reduction of Isoniazid:

The Au/ PANSAs/PVP-AgNPs/CYP2E1 nanobiosensor responses towards INH were investigated using SWV, DPV, CV and chronoamperometric methods in pH 7.4, 0.1 M phosphate buffer solution under aerobic conditions at 20 mV/s. Comparing results from this study, DPV and CV conditions were chosen for the analytical application with steady state amperometry used as further confirmation of the results obtained. The current as a function of time was monitored at different INH concentrations (2 μ M – 30 μ M), as illustrated by the steady state amperometry responses in Figure 6.4. The first addition of INH caused an increase in the current and the amperometric response of the nanobiosensor was allowed to attain steady state value which took about 20 s to acquire. However, as can be readily seen from Figure 6.5 A and B, a well-defined reduction peak was observed for the reduction of INH by the Au/PANSAs/PVP-AgNP/CYP2E1 nanobiosensor in deoxygenated buffer while a different electrochemistry was observed in anaerobic conditions. It should be noted that the electrochemistry of Au/PANSAs/PVP-AgNP/CYP2E1 was studied at the potential window of +1100 mV to -300 mV. Increasing the concentration of INH increased the reduction peak however, for the CV responses which were observed at +300 mV to -800 mV, no corresponding oxidation peak was observed.

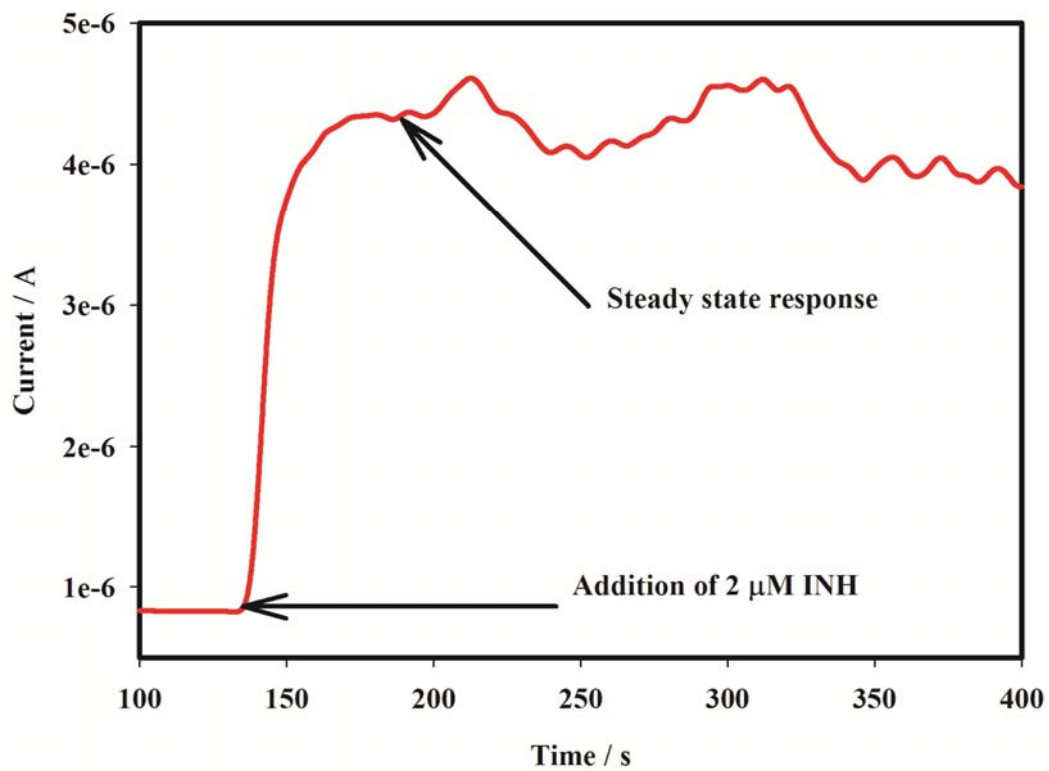
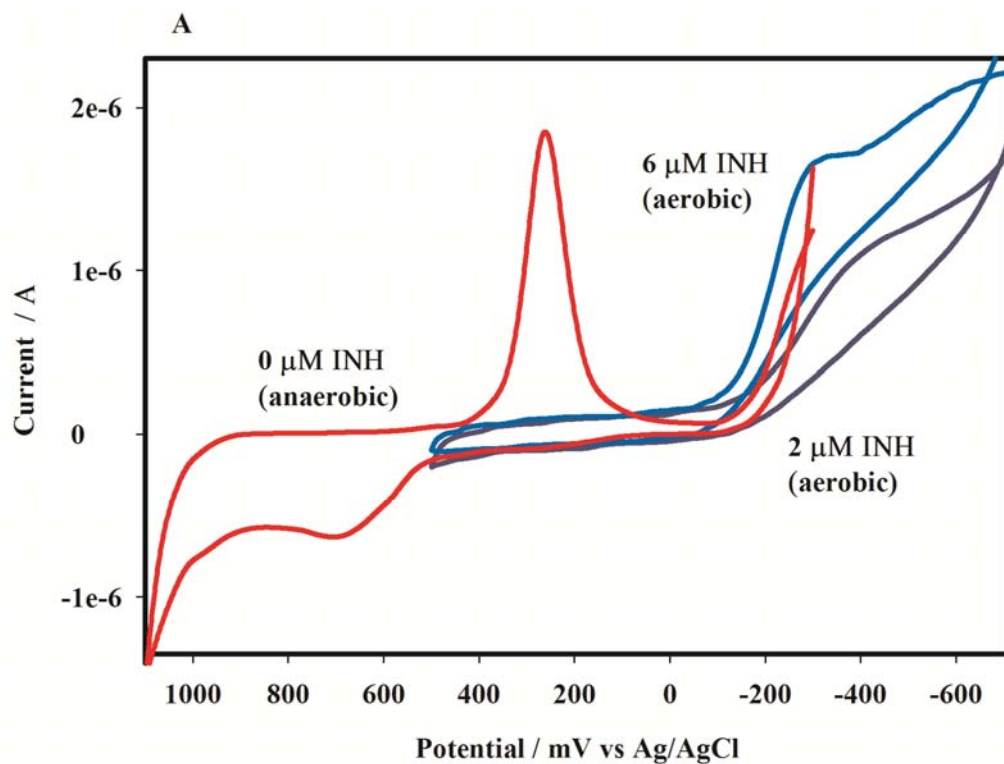


Figure 6.4: Steady state responses of isoniazid at applied potential of -250 mV with response time of 20 s



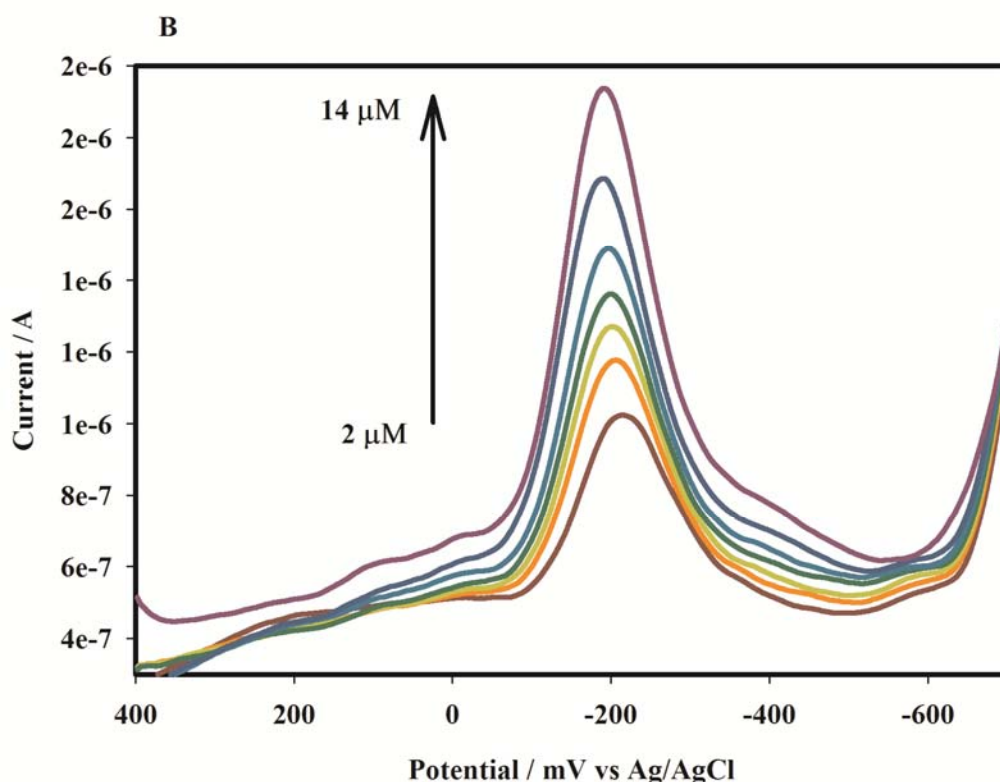
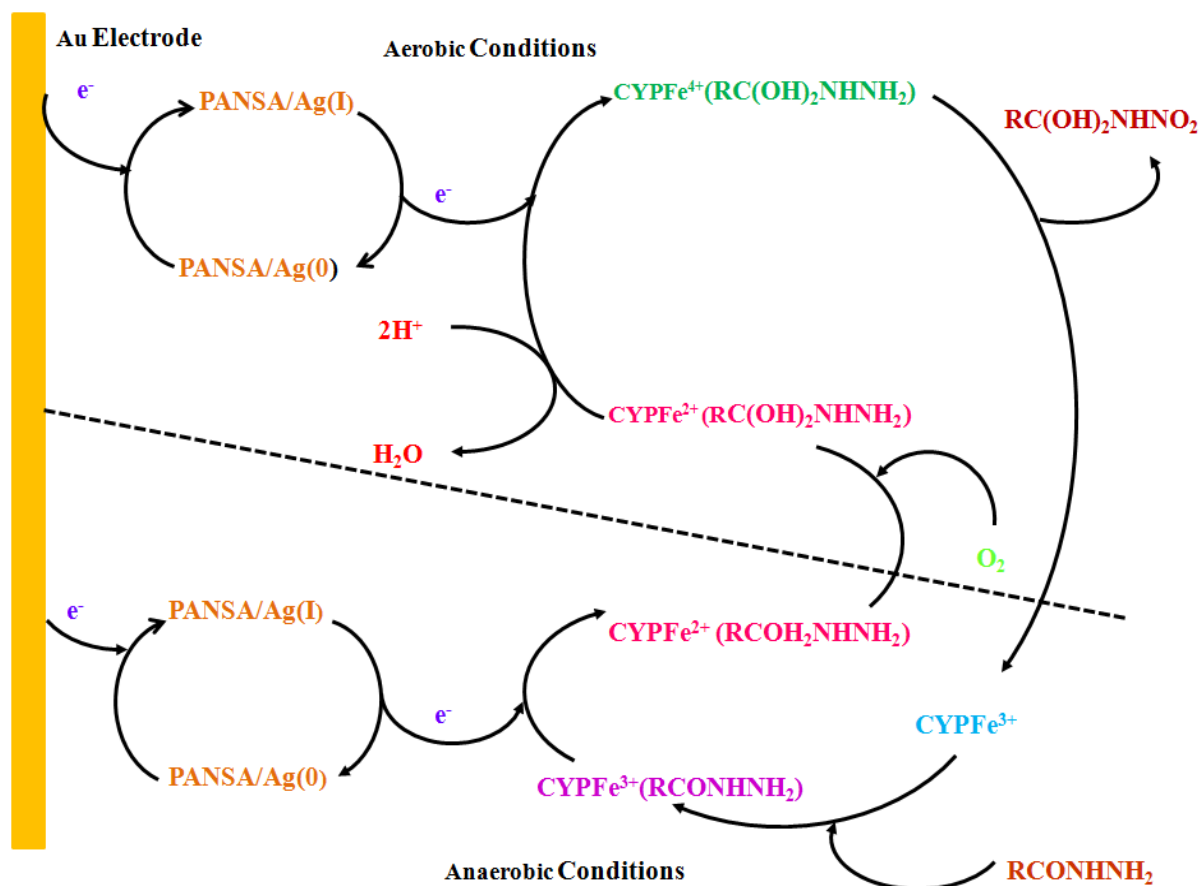


Figure 6.5: (A) CV and (B) DPV responses at different isoniazid concentrations for the Au/PVP-Ag-PANSA/CYP2E1 nanobiosensor

As illustrated in Scheme 6.2, these responses are resultant from a reaction initiated by the one electron reduction of the hexa-coordinated low-spin ferric enzyme (Fe^{3+}) to the high spin ferrous enzyme (Fe^{2+}) during which INH is reduced to an alcohol form. This form of CYP2E1 attracts molecular oxygen subjected to the solution forming the CYP2E1 (Fe^{2+}) O_2 complex introducing coupled an $-\text{OH}$ group to the INH alcohol via a hydroxylation process followed by the release of a water molecule. A highly active iron-oxoferryl intermediate CYP2E1 (Fe^{4+}) was the result with a nitro form of INH produced upon reduction which was then released (Spracklin *et al.*1997; von Moltke *et al.*1997).

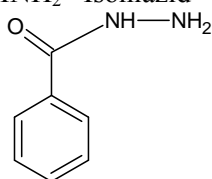


KEY:

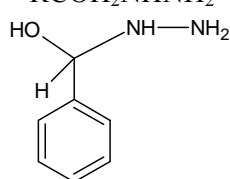
CYP^{4+, 3+, 2+} - Different oxidation states of Cytochrome P450-2E1

PANSA/Ag - poly (8-anilino-1-naphthalene sulphonic acid)/ silver nanoparticle nanocomposite

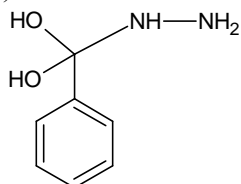
RCONHNH₂ - Isoniazid



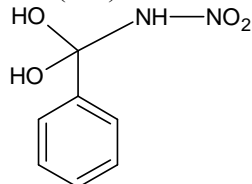
RCOH₂NHNH₂ - alcohol form of Isoniazid



RC(OH)₂NHNH₂ - Intermediate isoniazid complex



RC(OH)₂NHNO₂ - Nitro Isoniazid



Scheme 6.2: Reaction scheme showing the metabolism of isoniazid using the Au/PVP-AgNPs/PANSA CYP2E1 nanobiosensor

The response upon INH addition led to a Michaelis-Menten profile, with a linear response up to 14 μM , a sensitivity of 1.25 $\mu\text{A}/\mu\text{M}$ and a detection limit of 0.65 μM (Figure 6.7). This shows that a friendly and comfortable environment was created by the Au/PANSA/PVP-AgNP/CYP2E1 nanobiosensor for the successful biocatalytic reaction to take place. This resulted in the determination of K_M , K_M^{app} and I_{MAX} . The enzymatic reaction at the PANSA/ PVP-AgNPs electrode surface can be considered as follows:



Therefore, based on the Michaelis-Menten reaction, the enzymatic kinetics of CYP2E1 as shown in Equation 6.3 is written as follows:

$$V = K_2 [\text{CYP 2E1}] [\text{ISONIAZID}] / K_M + [\text{ISONIAZID}] \quad \text{Equ. (6.3)}$$

With V , K_1 , K_2 , K_M and $[\text{CYP2E1}]$ have their usual definitions and $[\text{ISONIAZID}]$ being the concentration of isoniazid. As indicated in Figure 6.6, the rate of reaction at lower concentrations of INH is directly proportional to the INH concentrations. The values of I_{MAX} , K_M^{app} and K_M were determined from the hyperbolic region of the plot with the aid of Equation 6.3 and estimated to be $1.9 \times 10^{-6} \mu\text{A}$, 1,34 μM and 5.8 μM , respectively. The reduced K_M and higher I_{MAX} values are indicative of high enzyme biocatalytic activity taking place at the electrode surface (Bai *et al.* 2007; Cornish-Bowden *et al.* 1974; AL-Thabaiti *et al.* 2008). A more sensitive and efficient sensor system is reported here compared to previously reported sensor systems such as that developed by Haghghi *et al.* 2010; where a flow injection chemiluminescence sensor was developed for the determination of INH. The efficiency of the nanobiosensor is based on the fact that the blood peak concentration of INH,

3 $\mu\text{g/mL}$ or (22 μM) which occurs 4 – 8 hr after administration of a 200 mg INH dose, is within the dynamic linear response range of the nanobiosensor (2 μM – 20 μM). Finally, with an upper dynamic linear range of 30 μM , it means that the nanobiosensor can be applied to systems where the concentration range is 0.65 μM – 30 μM .

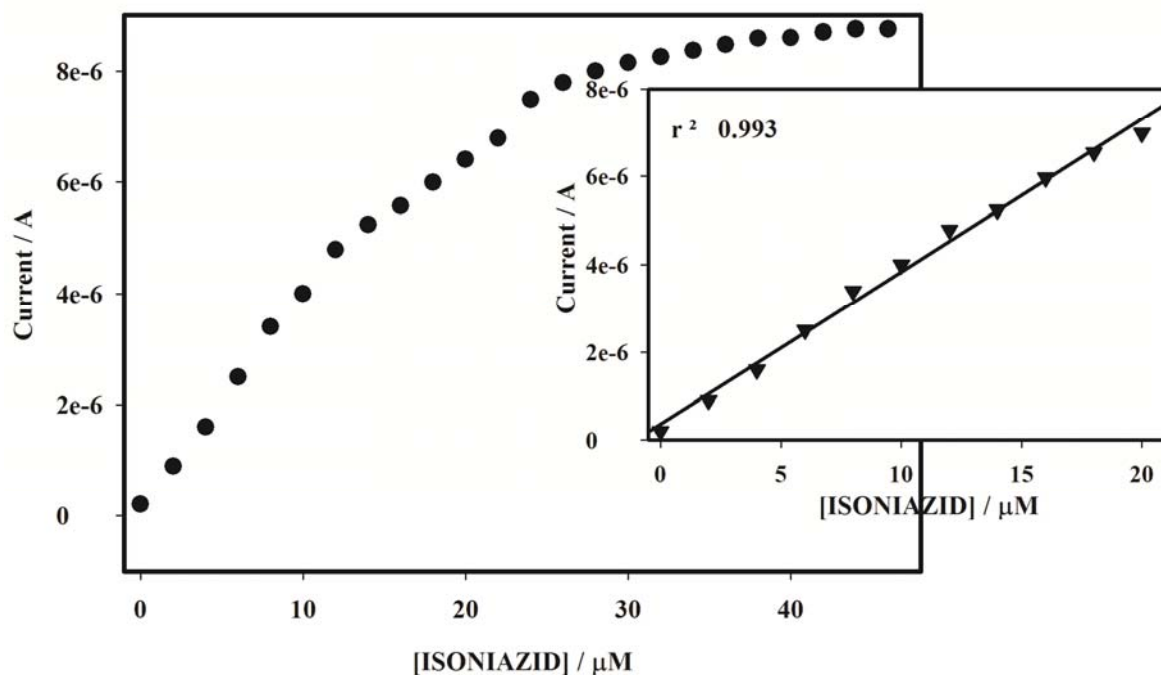
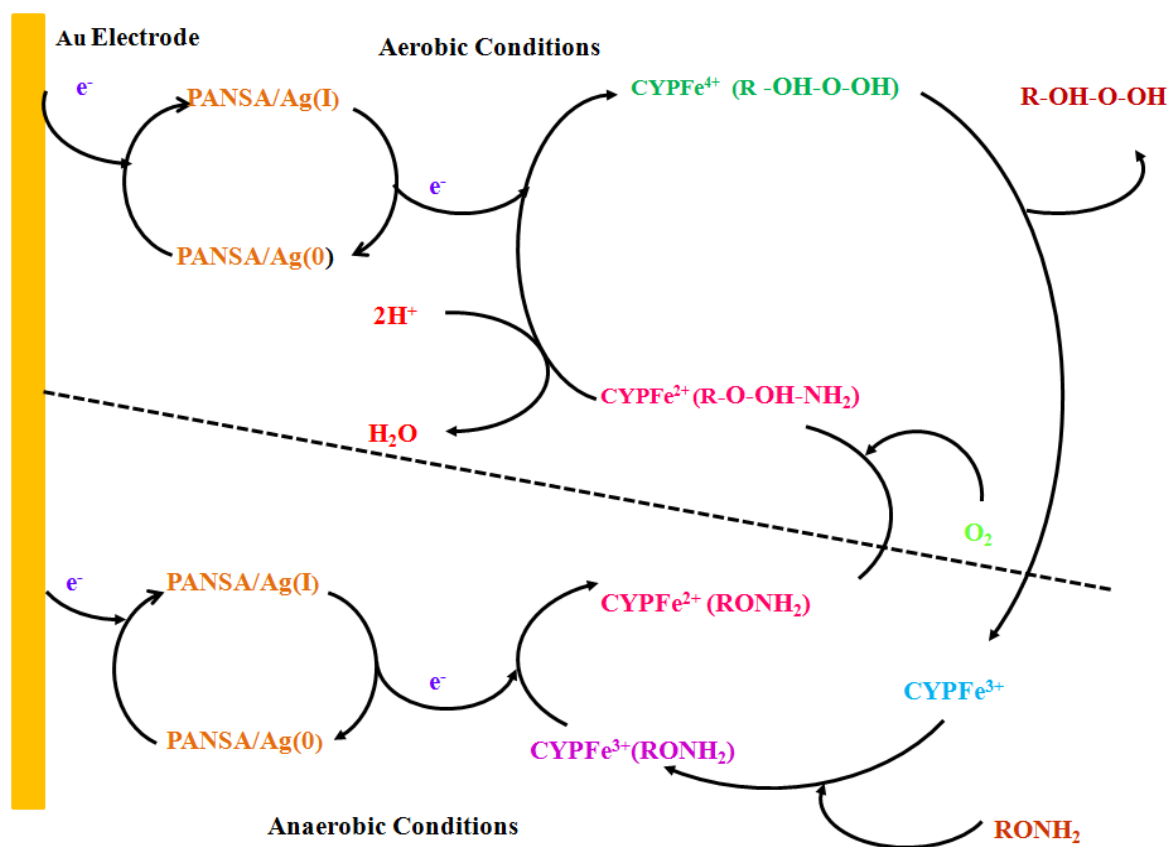


Figure 6.6: Calibration curve of isoniazid showing the linear range (inset) for the Au/PVP-AgNPs/PANSA/CYP2E1 nanobiosensor

6.1.1.3 Electrocatalytic Reduction of Pyrazinamide (PYR):

Figure 6.7 A illustrates the cyclic voltammetric responses of the Au/PVP-AgNPs/PANSA/SA-CYP2E1 nanobiosensor in the absence and presence of PYR at low potential scan rate of 20 mV/s. Voltammograms obtained in the absence of PYR were performed in anaerobic and aerobic solutions. In anaerobic solutions, only the electrochemistry of Au/PVP-AgNPs/PANSA essential for the oxidation and reduction of PVP-AgNPs and PANSA is observed. Under anaerobic conditions the CV of Au/PVP-AgNPs/PANSA/SA-CYP2E1 electrode is at the potential window of +1100 mV to -300 mV.

However, upon immobilization of SA-CYP2E1 under aerobic conditions, the CV gave a catalytic voltammetric wave at the potential window of +300 mV to -800 mV. This response is due to the binding of PYR to SA-CYP2E1 catalysing the low to high spin transition of iron increasing the rate of reduction of the ferric haem to ferro haem. As indicated in Scheme 6.3 the ferro haem state of the enzyme binds molecular oxygen during which PYR is hydroxylated to 5-hydroxypyrazinamide. This is followed by the cleaving of the O-O bond resultant by the introduction of the second electron producing a highly active iron-oxoferryl intermediate CYP2E1 (Fe^{4+}) with 5-hydroxypyrazinoic acid as the product which is released (Mehmedagic *et al.* 1997; Yamamoto *et al.* 1986). Indicated in Figure 6.7 B the responses of the Au/PVP-AgNPs/PANSA/SA-CYP2E1 nanobiosensor to PYR are also recorded. The figure shows that the DPV peak current increases as the concentration of PYR increases from 2 μM to 24 μM . A calibration curve was derived from this data from which a sensitivity of 1.38 $\mu\text{A}/\mu\text{M}$ was determined.

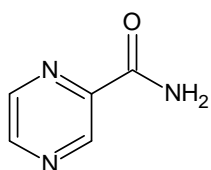


KEY:

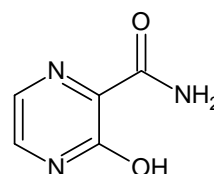
CYP^{4+, 3+, 2+} - Different oxidation states of Cytochrome P450-2E1

PANSA/Ag - poly (8-anilino-1-naphthalene sulphonic acid)/ silver nanoparticle nanocomposite

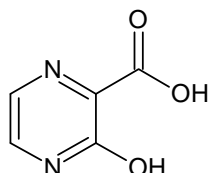
RONH₂ - Pyrazinamide



R-O-OH-NH₂ - 5-hydroxypyrazinamide



R-OH-O-OH - 5-hydroxypyrazinoic acid



Scheme 6.3: Reaction scheme showing the metabolism of pyrazinamide using the Au/PVP-AgNPs/PANSA/SA-CYP2E1 nanobiosensor

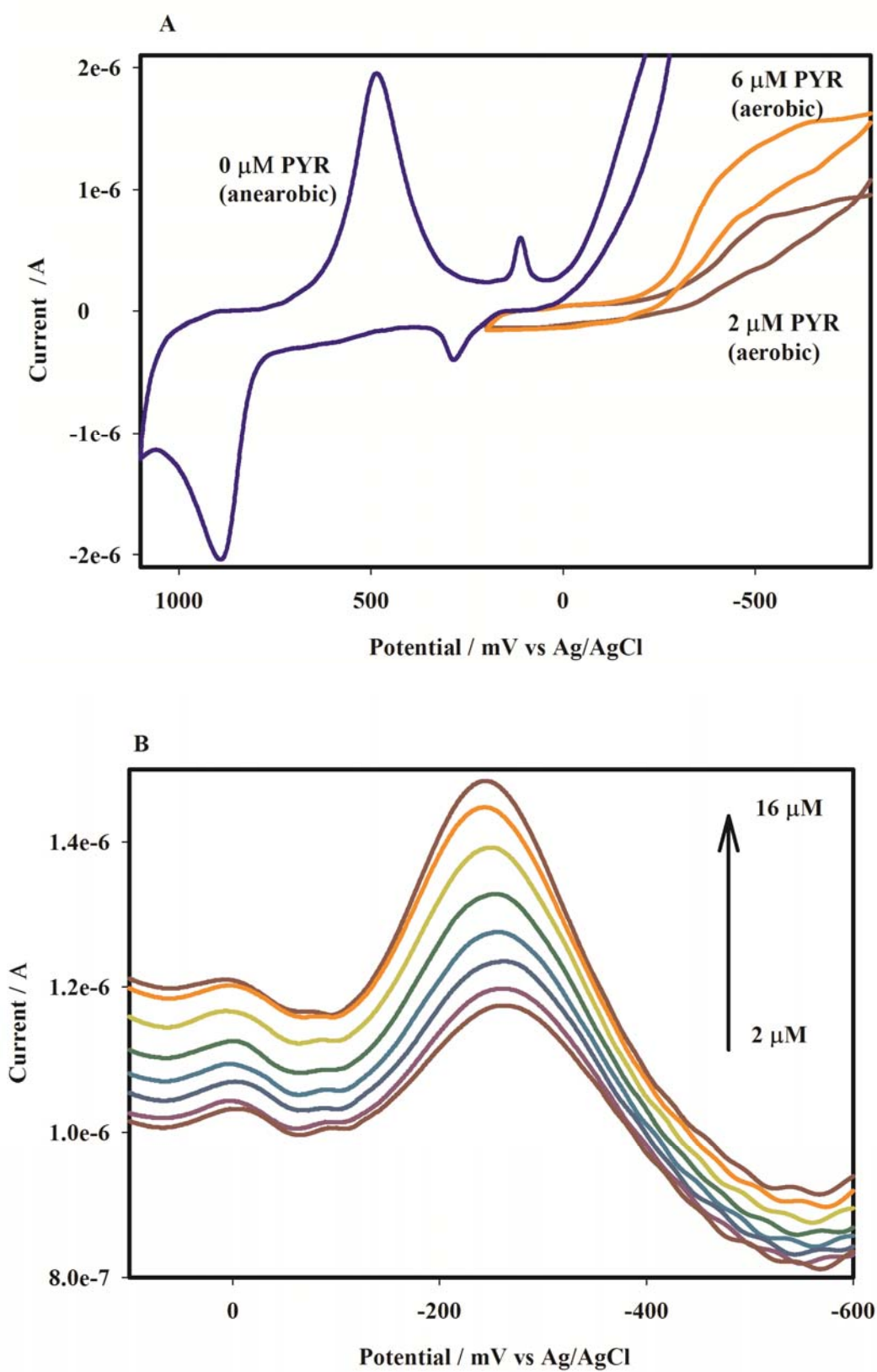


Figure 6.7: (A) CV and (B) DPV responses at different pyrazinamide concentrations for the Au/PVP-AgNPs/PANSA/SA-CYP2E1 nanobiosensor

The nanobiosensor response time was evaluated from steady state amperometry experiments performed at -250 mV (Figure 6.8). The Au/PVP-AgNPs/PANSA/SA-CYP2E1 nanobiosensor was used as the working electrode in an air-saturated buffer cell solution which was stirred at 500 rpm. The nanobiosensor was polarized at -250 mV and the background current was allowed to decay to a constant value which occurred after about 430 s. Upon addition of 2 μM PYR into the cell solution, the amperometric response of the nanobiosensor was allowed to attain steady state value which took about 25 s indicating that the response of the nanobiosensor can be achieved in real time. The detection limit was calculated to be 0.054 μM which implies that the nanobiosensor can be applied to systems where the concentration range is 0.054 μM to 24 μM as indicated by the calibration curve in Figure 6.9. The Michaelis-Menten parameters; K_M , K_M^{app} and I_{MAX} were also determined and found to be 6.0 μM , 1.41 μM and 1.51×10^{-6} μA respectively.

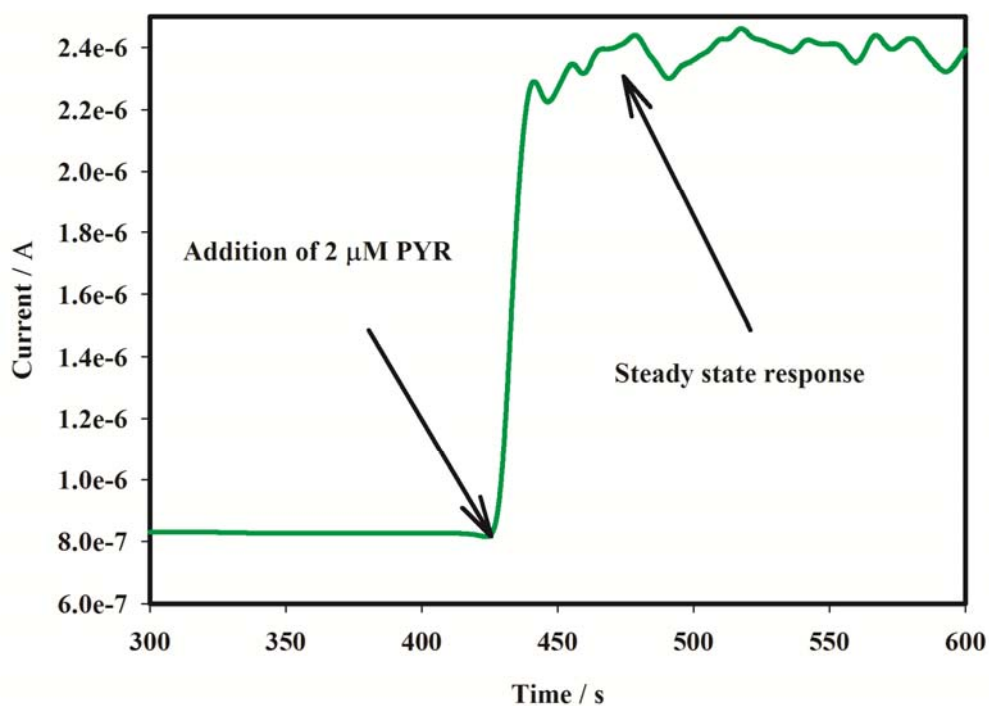


Figure 6.8: Steady state responses of pyrazinamide at applied potential of -250 mV with response time of 25 s

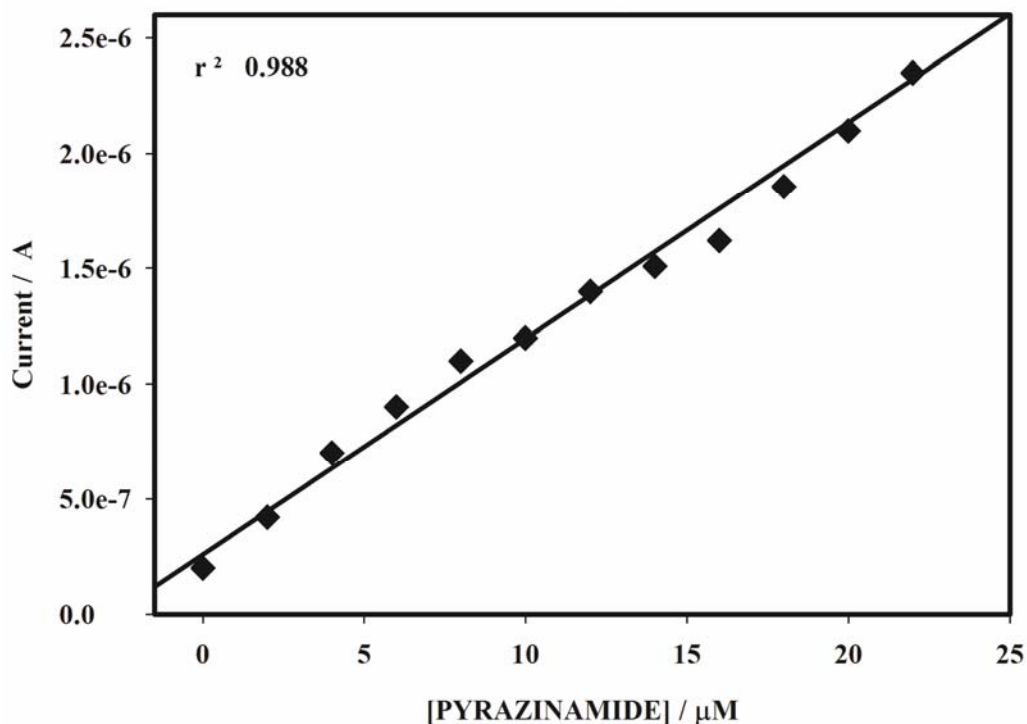
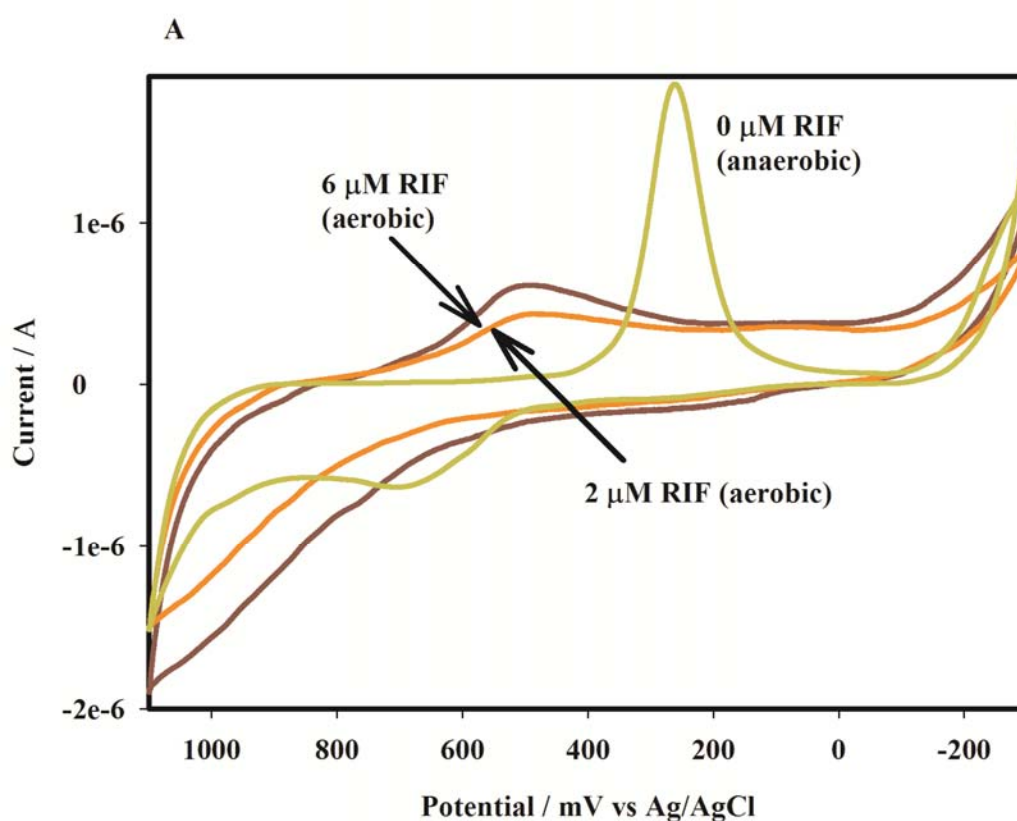


Figure 6.9: Calibration curve of pyrazinamide for the Au/PVP-AgNPs/PANSA/SA-CYP2E1 nanobiosensor

6.1.1.4 Electrocatalytic Reduction of Rifampicin (RIF):

Figure 6.10 A illustrates the cyclic voltammetric responses of the Au/PVP-AgNPs/PANSA/EG-CYP2E1 nanobiosensors in the absence and presence of RIF under aerobic and anaerobic conditions in the presence of buffer solution. The voltammogram show that as the potential was scanned reductively from +800 mV to -300 mV, the cathodic current steadily increased to a maximum value after which the current decreased until the switch potential was reached. However, scanning anodically no peak was observed. DPV (Figure 6.10 B) was used to further confirm data observed in CV. One prominent peak was observed in the cathodic scan when the RIF's concentration was increased steadily from 2 μM to 14 μM . As indicated in Scheme 6.4 this defined cathodic peak depicts the coupling of a fast

electron transfer reaction taking place at the electrode surface to a fast chemical process in which the reduced electro-active species have been used up. During the cathodic scan CYP (Fe^{3+}) was reduced to CYP (Fe^{2+}) as a result of the binding of RIF to the active sites of EG-CYP2E1 which was then used up in a fast follow-up chemical reaction, making it unavailable for re-oxidation during the anodic scan. This is why there is no corresponding anodic peak.



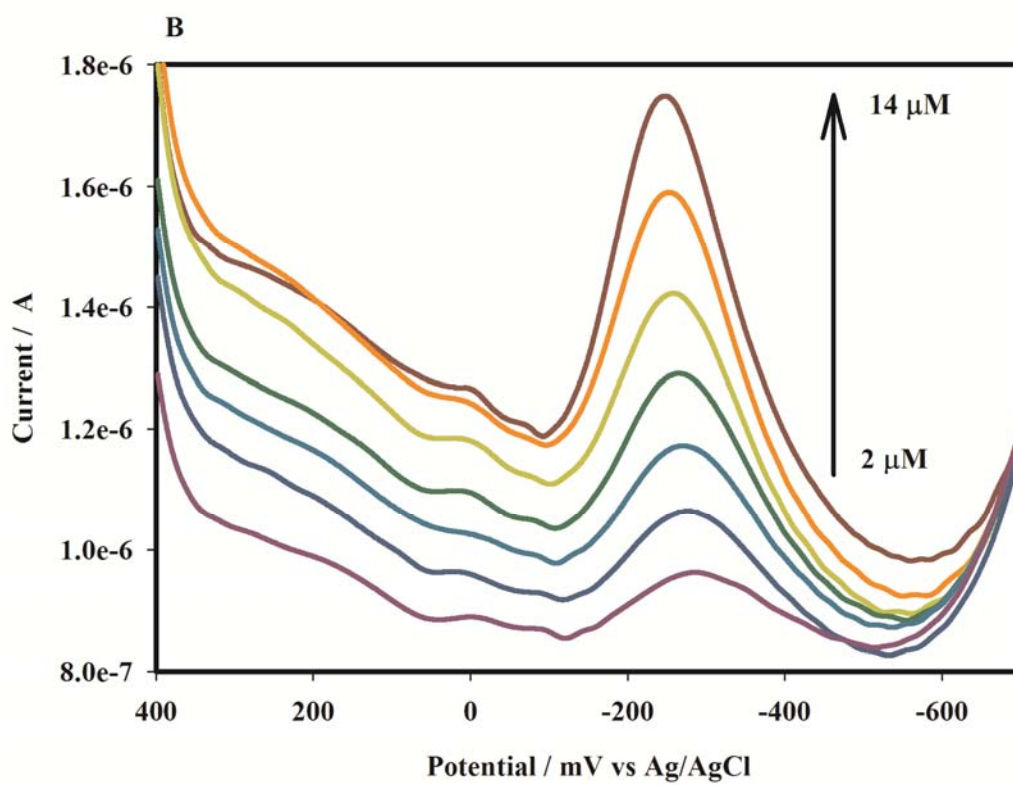
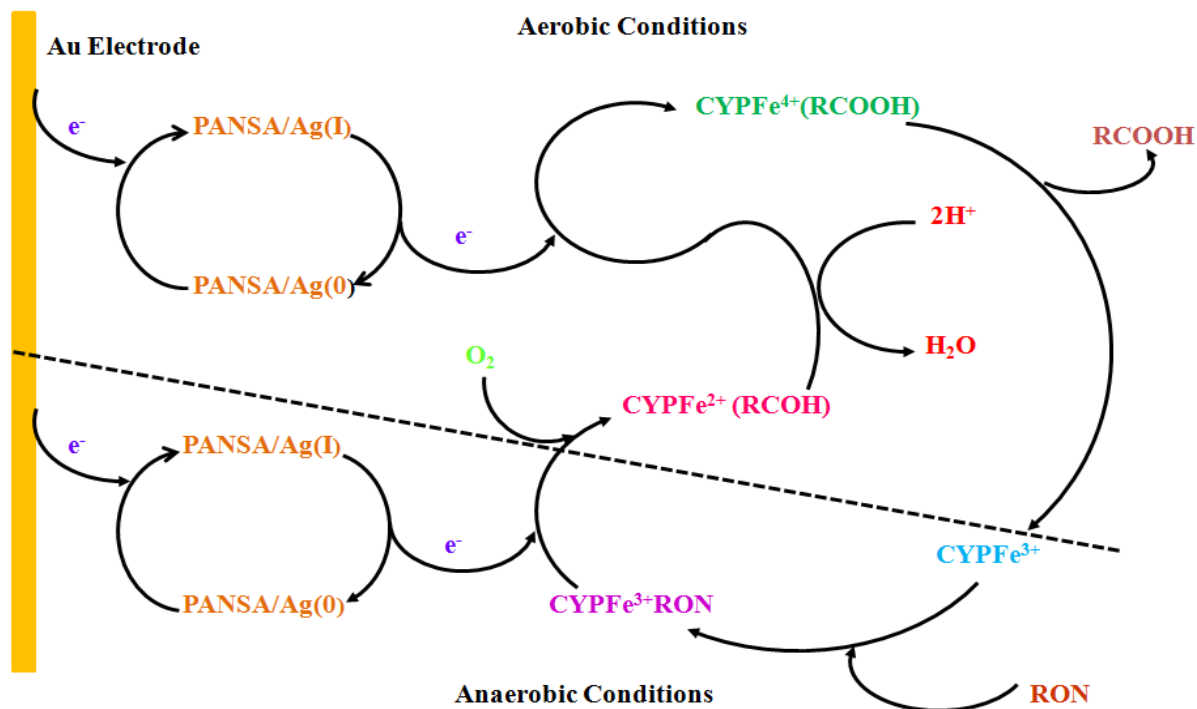


Figure 6.10: (A) CV and (B) DPV responses at different rifampicin concentrations for the Au/PVP-AgNPs/PANSA/EG-CYP2E1 nanobiosensor

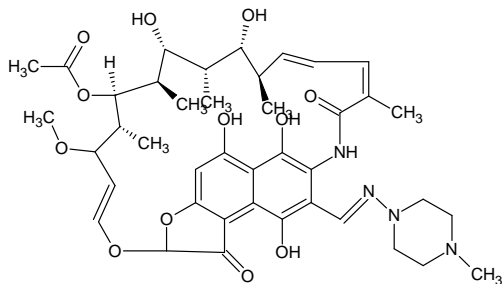


KEY:

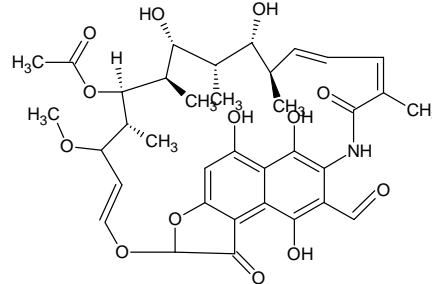
CYP^{4+, 3+, 2+} - Different oxidation states of Cytochrome P450-2E1

PANSA/Ag - poly (8-anilino-1-naphthalene sulphonate) / silver nanoparticle Nanocomposite

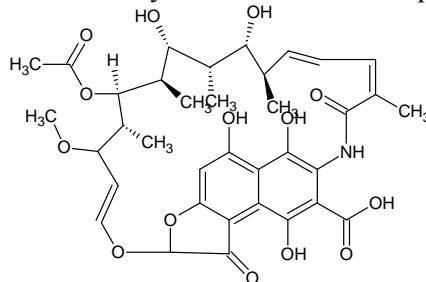
RON – Rifampicin



RCOH - Formylrifampicin



RCOOH – Carboxylic acid form of rifampicin



Scheme 6.4: Reaction scheme showing the metabolism of rifampicin using the Au /PVP-AgNPs/PANSA/EG-CYP2E1 nanobiosensor

The irreversible cyclic voltammograms recorded in aerobic conditions suggests that there is a binding of molecular oxygen to the CYP (Fe^{2+}) heme redox centre of the enzyme (Iwuoha *et al.* 2004). As indicated in Scheme 6.4, this process involves a second electron which is responsible for the cleavage of the di-oxygen bond leading towards the generation of products (Shumyanteva *et al.* 2005). In the case of the biotransformation of RIF by the Au/PVP-AgNPs/PANSA/EG-CYP2E1 nanobiosensor, the product generated is a carboxylic acid form of RIF. The initial step in the biotransformation is the formation of formylrifampicin after the first reduction process. Following that this product is further reduced to the carboxylic acid form of RIF which is later released. In human traces of formylrifampicin are detected in urine but at very low concentrations. These products were also obtained in a study by Loos *et al.* 1986 involving the pharmacokinetics of oral and intravenous RIF's administration to chronically ill TB patients. HPLC studies by Koicha *et al.* 1983 also revealed the presence of these metabolites in a study involving the biochemical and microbiological bioavailability of RIF in pulmonary tuberculosis patients.

The nanobiosensor response time was evaluated from steady state amperometry experiments (Figure 6.11) performed at -250 mV. In the experiment, the Au/PVP-AgNPs/PANSA/EG-CYP2E1 nanobiosensor was used as the working electrode in an air saturated buffer cell solution which was stirred at 500 rpm. The response time was estimated to 25 s and the detection limit was estimated to be 0.05 μM while a sensitivity of 1.40 $\mu\text{A}/\mu\text{M}$ from the calibration curve stipulated in Figure 6.12 was determined. Even though RIF is not a substrate inhibitor of CYP2E1, the parameters K_M , K_M^{app} and I_{MAX} were estimated to be 5.0 μM , 1.25 μM and 1.78×10^{-6} μA respectively. The peak serum concentration of RIF of 5 $\mu\text{g}/\text{mL}$ (6 μM) obtained 4 -8 hr after administration of 600 mg RIF, was found to be within the linear range of the nanobiosensor suggesting that the nanobiosensor can be applied to systems with concentrations from 0.05 μM and above. The

Michaelis-Menten parameters confirm the highly electroactive nature of the nanobiosensor and its affinity for the biotransformation of RIF.

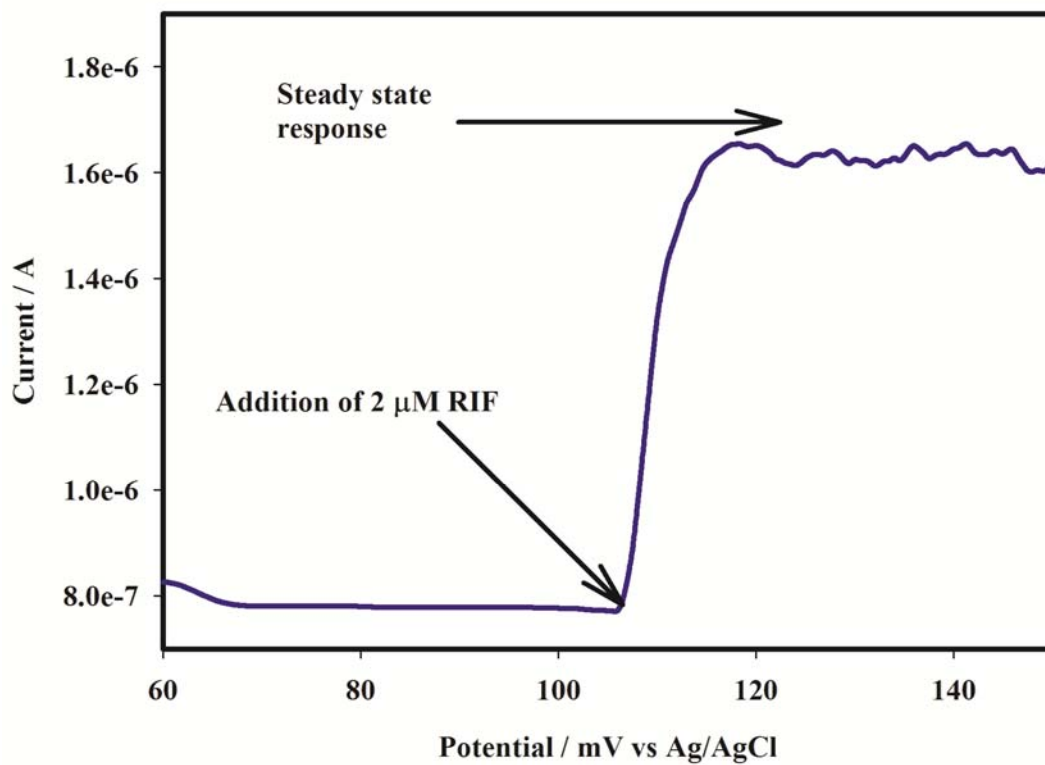


Figure 6.11: Steady state responses of rifampicin at applied potential of -250 mV with response time of 25 s

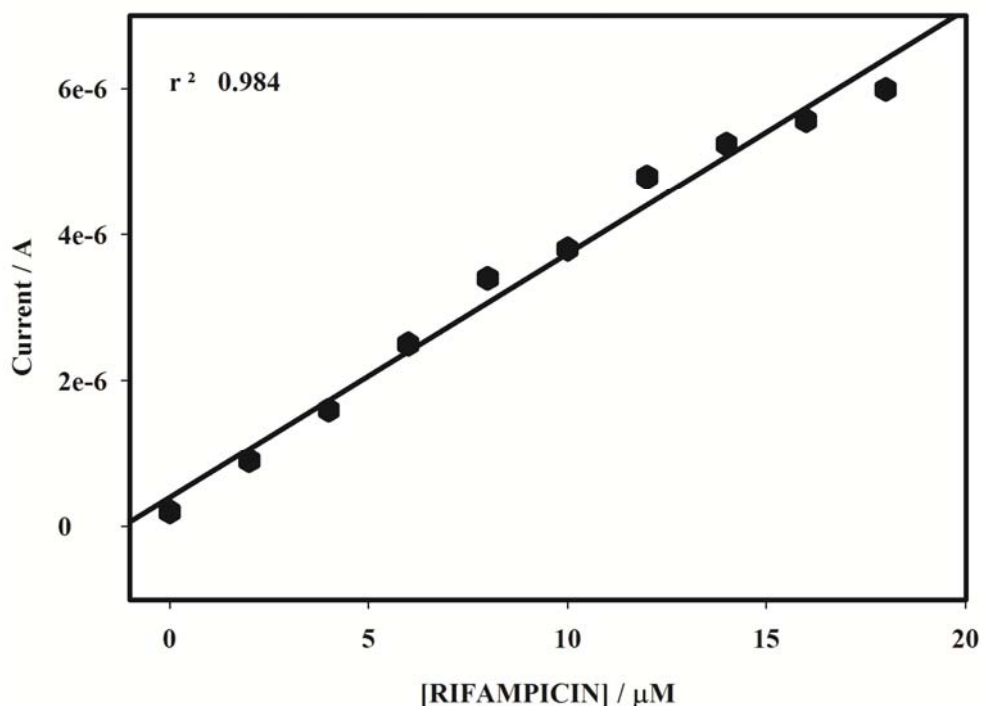


Figure 6.12: Calibration curve for rifampicin for the Au/PVP-AgNPs/PANSA/EG-CYP2E1 nanobiosensor

6.2 Stability and Reproducibility of the Modified Electrodes:

The stability and reproducibility of the Au/PANSA/PVP-AgNP/CYP2E1, Au/PANSA/PVP-AgNP/SA-CYP2E1 and Au/PANSA/PVP-AgNP/EG-CYP2E1 bioelectrodes was also investigated. When the modified bioelectrodes were stored at 4 °C in pH 7.4, 0.1 M phosphate buffer solution for two weeks, the current response retained more than 90 % of its original response for the Au/PANSA/PVP-AgNP/CYP2E1 nanobiosensor, more than 85 % for the Au/PANSA/PVP-AgNP/SA-CYP2E1 nanobiosensor and more than 80 % for the Au/PANSA/PVP-AgNP/EG-CYP2E1 nanobiosensor. Determination of the relative standard deviation (R.S.D) for ten successive measurements of either 2 μM ETH, 2 μM INH, 2 μM RIF and 2 μM RIF were 3.2 %, 3 %, 2.9 % and 3 % respectively, indicating excellent precision for each measurement. The nanobiosensors were used daily and stored in

pH 7.4, 0.1 M phosphate buffer solution at 4 °C when not in use. The data received from these experiments indicated that the current responses only decreased by an average of less than 15 % suggesting that the nanobiosensors reported for this work have long-term stability.

6.3 Interference Studies of the Modified Electrodes:

In the reduction of the TB drugs; INH, ETH, PYR and RIF, several interference substances have been reported. These substances include inorganic species such K^+ , Mg^{2+} , Na^+ , NH_4^+ , Cl^- , SO_4^{2-} and NO_3^- ions dissolved individually in distilled water and each was added individually to 2 μM of each of the TB drugs. Using DPV measurements, the TB drugs illustrated increased currents when measured independently while a mixture of each TB drug and interferences generated reduced currents upon addition of 1:1 ratio of the interferences when the TB drug concentrations were 2 μM individually. It was found that addition of the interferences caused a slight decrease of the anodic peak current and hence negligible interferences in the range of 2.1% to 2.4 % were observed.

The following table represents all the parameters determined from the nanobiosensors.

Table 6.1: Compounds and their respective nanobiosensor analyses

Drug	Detection Limit (μM)	Sensitivity ($\mu A/\mu M$)	K_M	$K_M^{app}(\mu M)$	$I_{MAX}(\mu A)$	Response Time (s)
ETH	0.7	1.13	6.3	1.01	2.1×10^{-6}	20
INH	0.65	1.25	5.8	1.34	1.9×10^{-6}	20
PYR	0.054	1.38	6.0	1.41	1.51×10^{-6}	25
RIF	0.05	1.40	5.5	1.25	1.78×10^{-6}	25

6.4 References:

AL-Thabaiti.; Al-Nowaiser F.M.; Al-Youbi A.O.; Khan Z., ‘ Formation and characterization of surfactant stabilized silver nanoparticles: A kinetic study’ (2008) *Colloids and Surfaces B: Biointerfaces* **67** pg 230-237

Bai Y.; yang H.; Li Y.; Sun C., ‘Gold nanoparticles-mesoporous silica composite used as an enzyme immobilization matrix for the amperometric glucose biosensor construction’ (2007) *Sensors and Actuators B* **124** pg 179-186

Cornish-Bowden A., ‘A Simple Graphical Method for the Determining the Inhibition Constants of Mixed, Uncompetitive and Non-competitive Inhibitors’ (1974) *Biochemistry Journal* **137** pg 143-144

Grennan K.; Killard, A. J.; Hanson C. J., ‘Optimisation and characterisation of biosensors based on polyaniline’ (2006) *Talanta* **68** pg 1591-1600.

Haghugh B.; Bozorgzadeh S., ‘Flow injection chemiluminescence determination of isoniazid using luminal and silver nanoparticles’ (2010) *Micrchemical Journal* **95** pg 192-197

Iwuoha E. I; Howel M; Wilson A., ‘Cytochrome P450_{2D6} (CYP2D6) Bioelectrode for Fluoxetine’ (2004) *Analytical Letters* **37** pg 933-939.

Koicha, M.; Parikh, S.C.; Patil, A.G., ‘Rifampicin: its biochemical and microbiological bioavailability in pulmonary tuberculosis patients (1983) *Indian Journal of Tuberculosis* **30** pg 63-65.

Loos U.; Musch E.; Mikus G.; Eichelbaum M., ‘Pharmacokinetics of oral and intravenous rifampicin during chronic administration’ (1986) *Journal of Molecular Medicine* **63** pg 1205-1207.

Mehmedagic A.; Verite P.; Menager S.; Andre D.; Lafont O., ‘Determination of pyrazinamide and its main metabolites in rat urine by high-performance liquid chromatography’ (1997) *Journal of Chromatography B: Biomedical Applications* **695** pg 365-372.

Rasoulzadeh F.; Jabary H.N., ‘Fluorescence quenching study of quercetin interaction with bovine milk xanthine oxidase’ (2009) *Spectrochimica Acta Part A: Molecular and Biomolecular Spectroscopy* **72** pg 190-191.

Shumyantseva V.V.; Bulko T.V.; Archakov A.I., 'Electrochemical reduction of Cytochrome P450 as an approach to the construction of biosensors and bioreactors' (2005) *Journal of Inorganic Biochemistry* **99** pg 1057-1058.

Spracklin D.K.; Hankins D. C., 'Cytochrome P450 2E1 is the Pricipal Catalyst of Human Oxidative Halothane Metabolism *in Vitro*' (1997) *The Journal of Pharmacology and Experimental Therapeutics* **1** pg 401-402.

Svobodova L.; Snejdarkova M.; Hianik T., 'Properties of glucose biosensors based on dendrimers layers. Effect of enzyme immobilization' (2002) *Analytical Bioanalytical Chemistry* **373** pg 737-738.

von Moltke L.L.; Greenbalt D.J.; Duan S.X.; Shader R.I., 'Human cytochromes mediating N-demethylation of fluoxetine in vitro' (1997) *Psychopharmacology* **132** pg 402-407.

Wu W-Y.; Yand J-Y.; Du L-M.; Wu H.; Li C-F., 'Determination of ethambutol by a sensitive fluorescent probe' (2011) *Spectrochimica Acta. Part A Molecular and Bimolecular Spectroscopy* **79** pg 418-422.

Yamamoto T.; Moriwaki Y.; Higashino K., 'Study of the metabolism of pyrazinamide using a high-performance liquid chromatographic analysis of urine samples' (1987) *Analytical Biochemistry* **160** pg 346-349.

Yamamoto T.; Kario K., 'A case of Xanthinuria: A study on the Metabolism of Pyrazinamide and Allopurinol' (1991) *Japan Journal of Medicine* **30** pg 430-431.

CHAPTER 7

Conclusions and Recommendations

Summary

This chapter revisits the specific objectives of the study to report whether the aims of this dissertation were achieved, and to give an overview of the success and shortcomings of the study. Also reported here is an indication of which areas of this study warrant further investigations in the future.

7.1 Conclusions:

For the first time this study has reported the successful development and application of CYP2E1 nanobiosensors for the detection of the tuberculosis treatment drugs; isoniazid, ethambutol, pyrazinamide and rifampicin. The first specific objective of this study was to electrosynthesize PANSA on gold electrode. Thorough characterization of PANSA showed that this polymer can be successfully coated on gold electrode to provide a platform for immobilization. Secondly, silver nanoparticles were synthesized through a soft solution technique in which polydispersed spherical nanoparticles were obtained. Dropcoating silver nanoparticles onto PANSA saw a highly electroactive PVP-AgNPs/ PANSA nanocomposite. Characterization of the nanocomposite using EIS, TEM, UV-Vis, AFM, CV, DPV and SWV indicated a stable platform for the immobilization of the enzyme CYP2E1 as well as the CYP2E1 modified forms; SA-CYP2E1 and EG-CYP2E1. The PVP-AgNPs/PANSA nanocomposite served as a point of attachment for the enzyme as well as an efficient electron mediator between the redox centre of CYP2E1 and the electrode surface. AFM and TEM displayed large and globular morphologies for the highly active nanobioelectrodes. The results obtained confirmed that the Au/PVP-AgNPs/PANSA/CYP2E1 nanobiosensors were successful in the reductive catalysis of the various TB drugs into respective water soluble and easy excretable metabolites. The resultant catalytic current responses were amperometrically monitored by steady state amperometric, cyclic, differential pulse and square wave voltammetric techniques where an increase in current was observed for the respective analytes namely; isoniazid, ethambutol, pyrazinamide and rifampicin.

From the calibration curves, linear ranges were established in which the sensitivities and the nanobiosensor detection limits were estimated. The sensitivities of the nanobiosensors (INH = 1.25 $\mu\text{A}/\mu\text{M}$; ETH = 1.13 $\mu\text{A}/\mu\text{M}$; PYR = 1.38 $\mu\text{A}/\mu\text{M}$ and RIF = 1.40 $\mu\text{A}/\mu\text{M}$) exhibited high sensitivities compared to previously reported studies involving the

biotransformation of these drugs. Michaelis-Menten kinetics was used to determine the values of K_M , K_M^{app} and I_{MAX} of the various nanobiosensor systems. The apparent Michaelis-Menten constants indicated the nanobiosensors to have high affinity for the respective drugs while the detection limits were found to be within the nanobiosensor linear range, thereby making the nanobiosensor systems suitable for the determination of the respective analytes in serum.

7.2 Recommendations for Future Study:

The following aspects of the nanobiosensors for the determination of tuberculosis treatment drugs presented in this work warrant further investigations.

1. More work needs to be done to improve the electroactivity of PANSA through copolymerization or the use of surfactants.
2. It is proposed that another procedure is required to develop the PANSA/PVP-AgNPs nanocomposite in order to improve electroactivity and to allow the nanocomposite to be able to immobilize various biological components.
3. It is also suggested that higher concentrations of the standard solutions of the tuberculosis treatment drugs be evaluated and to determine whether the detection limits can be further improved.
4. Inhibition of CYP2E1 by other TB treatments drugs or any other drugs is an important aspect of this study that also needs to be explored.
5. More research needs to be done to improve specificity and selectivity of the nanobiosensors in order to discriminate more efficiently between closely related forms of tuberculosis treatment drugs or other compounds which could be biotransformed using these systems.